

Methodologies for Low-Cost Testing and Self-Healing of RF Systems

A Dissertation
Presented to
The Academic Faculty

by

Abhilash Goyal

In Partial Fulfillment
of the Requirements for the Degree
Doctor of Philosophy in the
School of Electrical and Computer Engineering

Georgia Institute of Technology
August, 2011

Copyright 2011 by Abhilash Goyal

Methodologies for Low-Cost Testing and Self-Healing of RF Systems

Approved by:

Prof. Madhavan Swaminathan, Advisor
School of Electrical and Computer
Engineering
Georgia Institute of Technology

Prof. Abhijit Chatterjee
School of Electrical and Computer
Engineering
Georgia Institute of Technology

Prof. John D. Cressler
School of Electrical and Computer
Engineering
Georgia Institute of Technology

Prof. David C. Keezer
School of Electrical and Computer
Engineering
Georgia Institute of Technology

Prof. Suresh K. Sitaraman
The George W. Woodruff School of
Mechanical Engineering
Georgia Institute of Technology

To my loving family.....

Acknowledgements

First and foremost I would like to thank my advisor, Prof. Madhavan Swaminathan for his support, trust, encouragement, and guidance over the last five years. His way of guidance gave me a lot of freedom to work on different areas of my own interest.

My special thanks to Prof. Abhijit Chatterjee for this valuable support and guidance for my thesis. I am also very thankful to Prof. John D. Cressler for his time, support and for giving me access to the SiGe process to demonstrate the proposed self-healing methodology by designing an actual working chip.

I thank Prof. David C. Keezer, and Prof. Suresh K Sitaraman for being the part of my PhD committee and for their valuable time, constructive advice and feedback. I also thank Bob House and James at Georgia Tech for their support in fabricating and soldering PCB boards for my thesis.

I am specially thankful to all current and past Epsilon group members. I am also thankful to all team members of Prof. John D. Cressler and Prof. Abhijit Chatterjee research group. Also, I would like to extend my thanks to team members of PRC and School of ECE at Georgia Tech.

I am extremely thankful to Nithya Sankaran for her true friendship and support.

Finally, I would like to thank all my friends and my all family members. I specially thank my parents, Mr. Satya Deo Goyal and Mrs. Radha Goyal for their unconditional love and support. It is hard to express in words my gratitude to my elder brother, Ashish Goyal. I am very lucky to have an elder brother like him. I am also very thankful to my

wife, Mrs. Anubhuti for her support. My very special thanks to my spiritual Guru Shri. Shri Ravi Shankar for his blessings.

Table of Contents

Acknowledgements	IV
List of Tables	IX
List of Figures	X
Summary	XVI
Chapter 1	
Introduction	1
1.1 Typical Production Flow of the RF Systems	4
1.2 Previous Research Efforts to Test RF/Mixed-Signal Active Circuits	7
1.3 Previous Research Efforts to Post-Silicon Yield Enhancement of RF Circuits	12
1.4 Previous Research Efforts to Test Embedded Passives Circuits/Substrate Testing	14
1.4.1 Test Methodology Based on Passive-RF Resonator	15
1.4.2 Test Methodology using Sinusoidal Input Signals	26
1.5 Summary of Major Contributions of This Thesis	37
Chapter 2	
Oscillation Based Test of Embedded RF Filters	41
2.1 Prior Oscillation Based Test Methods	42
2.2 Proposed Methodology	43
2.3 Simulations Results	50
2.4 Measurement Results	54
2.5 Discussions	63
2.6 Summary	66
Chapter 3	
One-Port Resonance-Based Test Methodology	69
3.1 Proposed Methodology	70
3.2 Simulations Results	74
3.3 Proof of Concept	81
3.4 Testing Of Commercially Available RF substrate	86
3.5 Discussions	88
3.6 Summary	91

Chapter 4

Low-Cost Testing of RF Amplifier Circuits	93
4.1 Proposed Methodology	93
4.2 Simulation Results	100
4.3 Measurement Results	105
4.4 Discussions	109
4.5 Summary	113

Chapter 5

A Self-Healing Methodology for RF Amplifier Circuits	115
5.1 Proposed Self-Healing Methodology for RF Amplifiers	115
5.2 Simulation Results	126
5.2.1 Self-Healing SiGe HBT RF LNA	126
5.2.2 Self-Healing CMOS RF LNA	134
5.3 Hardware Prototype	140
5.4 Chip Prototype	143
5.5 Discussion	149
5.6 Summary	150

Chapter 6

A Self-Healing Methodology for Embedded RF Mixers	152
6.1 Proposed Self-Healing Methodology for RF Mixers	153
6.2 Simulation Results	160
6.3 Hardware Prototype	168
6.4 Summary	170

Chapter 7

RF Substrates Yield Improvement Using Package-Chip Co-Design and On-Chip Calibration	172
7.1 A Proposed Yield Improvement Methodology for RF substrates	173

7.2 Simulation Results	176
7.3 Measurement Results	180
7.4 Summary	182

Chapter 8

A Novel Variable Gain RF Amplifier for Self-Healing Systems **184**

8.1 Proposed design	184
8.2 Experimental Results	187
8.3 Summary	191

Chapter 9

Future Work and Papers Published **193**

References **197**

List of Tables

TABLE 2.1	Test Result For the RF High-Pass Filter Using The proposed oscillation based test method	53
TABLE 2.2	Estimated 3-dB Frequency For low-frequency output	54
TABLE 2.3	Test Results For The RF Band-Pass Filter Using the proposed oscillation based test method	55
TABLE 2.4	Estimated Centre Frequency of Band-Pass Filter from low-frequency test- setup output	56
TABLE 2.5	Summary of The Measurement For Panel-Level Testing of The Embedded filters by The proposed oscillation based test method	60
TABLE 2.6	Measured Oscillation frequency of the test setup (Fig. 2.13) over the duration of 21 hours at the panel-level testing for Sample 09	65
TABLE 3.1	Results to Test Open Defect In RF Interconnects	76
TABLE 3.2	Results to Test Open Defect In RF Interconnects	77
TABLE 3.3	Results to Test the RF Low-Pass Filter by The Proposed Resonance- Based Test (RBT) Method	79
TABLE 3.4	Cost Analysis of the proposed Test-setup	91
TABLE 4.1	Error in Prediction for Testing RF Amplifier	105
TABLE 4.2	Error in Prediction of Specifications form Measurements	108
TABLE 4.3	Summary of The Results for Repeatability Analysis in The Measurements (Sample B, Previous sub-Section).	111
TABLE 4.4	Cost Analysis of the proposed Test-setup	113
TABLE 5.1	Summary of Healing Results (Knob 1) SiGe HBT RF Amplifier	132
TABLE 5.2	Summary of Healing Results (Knobs 2) SiGe HBT RF Amplifier	132
TABLE 5.3	Summary of Healing Results (Both Knobs) SiGe HBT RF Amplifier	133
TABLE 5.4	Summary of CMOS Amplifier Healing Results (Knob 1)	137
TABLE 5.5	Summary of CMOS Amplifier Healing Results (Knobs 2)	138
TABLE 5.6	Summary of Healing Results (Both Knobs) CMOS RF Amplifier	139
TABLE 5.7	Summary of Calibration Results RF Amplifier	143
TABLE 6.1	Summary of Calibration Results (P1dB) of RF Mixer	166
TABLE 6.2	Summary of Calibration Results (Gain) of RF Mixer	166
TABLE 6.3	Summary of Calibration Results (Both Knobs) of RF Mixer	167
TABLE 7.1	Summary of Yield of RF substrate with RF Filter	179
TABLE 7.2	Summary of Measurements @ 1.20 GHz of RF System	182

List of Figures

Fig. 1	Thesis framework and scope of research	xvii
Fig. 1.1	Low yield because of widening gap in the performance	2
Fig. 1.2	RF substrate with embedded RF filters and mounted RF ICs and components	3
Fig. 1.3	A typical production flow of RF systems based on SOP/SIP packaging approach	5
Fig. 1.4	Illustration of the test cost and Defects-per-Million (DPM) in the shipped design	6
Fig. 1.5	Alternate test flow	9
Fig. 1.7	The proposed test-setup for testing embedded RF passive filters using passive	16
Fig. 1.8	The insertion loss of RF low-pass filter samples to demonstrate the test method based on passive resonator	18
Fig. 1.9	Simulation test-setup for testing RF filters based on passive resonator	19
Fig. 1.10	Test-setup output for different samples of RF low-pass filter	19
Fig. 1.11	Predicted high-frequency insertion loss of low-pass filters B, C and D	20
Fig. 1.12	Insertion loss profile of RF high-pass filters B, C and D	21
Fig. 1.13	Output of the proposed test setup for different samples of RF high-pass filter	21
Fig. 1.14	Predicted high-frequency insertion loss of high-pass filters B, C and D using the proposed methodology based on passive resonator	22
Fig. 1.15	Panel-level test setup of passive resonator based methodology for testing 102 embedded filters	23
Fig. 1.16	Measurement of 102 embedded low-pass filters based on proposed methodology using passive resonator	23
Fig. 1.17	Insertion loss of 102 embedded low-pass filters measured using a VNA	24
Fig. 1.18	One-port measurement of 102 embedded high-pass filters using passive-RF Resonator based method	24
Fig. 1.19	Insertion loss measurement of 102 embedded high-pass filters using VNAs	25
Fig. 1.20	The proposed test setup of the methodology using sinusoidal inputs	27
Fig. 1.21	The insertion loss of RF high-pass filter samples to demonstrate test methodology based on input sinusoidal signals	29
Fig. 1.22	Simulation setup for testing RF high-pass filters using test methodology based on input sinusoidal signals	29
Fig. 1.23	Simulated output for testing RF high-pass filters using method based on input sinusoidal signals	30

Fig 1.24	Predicted insertion loss of high-pass filter using method based on input sinusoidal Signals	31
Fig. 1.25	The insertion loss of RF low-pass filter samples to demonstrate the test method based on input sinusoidal signals	32
Fig. 1.26	Simulated output for testing RF low-pass filters using the test method based on input sinusoidal signals	32
Fig 1.27	Predicted insertion loss of low-pass filter using the test method based on input sinusoidal signals	33
Fig.1.28	A hardware test setup for testing embedded RF low-pass filter using the test method based on input sinusoidal signals	34
Fig. 1.29	Measured insertion loss of embedded RF low-pass filters to demonstrate the test method based on input sinusoidal signals	34
Fig. 1.30	Measured low-frequency output test signature of the proposed test method based on input sinusoidal signals	35
Fig. 1.31	Summary of the major contributions of the thesis	39
Fig. 2.1	Measurement test-setup of prior oscillation-based test (OBT) methods	42
Fig. 2.2	The proposed test-setup of two-port feedback based oscillation test methodology	44
Fig. 2.3	The closed-loop system with a calibration knob to calibrate oscillation frequency of the test-setup	45
Fig. 2.4	Effect of RF cable length on the forward transmission S-parameter of an RF Amplifier	46
Fig. 2.5	A proposed simulation test setup of two-port Feedback based test methodology	51
Fig. 2.6	Insertion loss of the RF high-pass filters	52
Fig. 2.7	Calibration of the oscillation frequency at the output of the RF using DC controlled knob	52
Fig. 2.8	Test-setup response vs. 3-dB frequency of the RF high-pass filter to derive prediction equation	54
Fig. 2.9	Modeling of RF band-pass filter	55
Fig. 2.10	A hardware test setup for a card-level testing of RF embedded filters by the two-port feedback based oscillation test method	57
Fig. 2.11	Measured insertion-loss of embedded RF low-pass filters	57
Fig. 2.12	Measurement result for the card-level testing of the embedded RF low-pass Filters	57
Fig. 2.13	A hardware test setup of the proposed method for a panel-level testing of integrated RF substrates	59
Fig. 2.14	Insertion loss of embedded RF low-pass filter samples at three different Locations of the panel of integrated RF substrate	59
Fig. 2.15	Tuning of the oscillation frequency at the output of the probe card using DC voltage at the calibration knob	60
Fig. 2.16	Measured response for a panel-level testing by two-port Feedback based Methodology	61
Fig. 2.17	3-dB frequency of embedded low-pass passive filters vs. output of the proposed test-setup to obtain a prediction equation	62

Fig. 2.18	Predicted vs. Actual 3-dB frequency of the embedded low-pass passive filters using 60 MHz test-setup output signal	62
Fig. 2.19	Oscillation frequency of the proposed test setup for 114 measurements to test Sample 09 at the panel-level testing	63
Fig. 3.1	The proposed test-setup of One-Port Resonance-Based Test (RBT) methodology	70
Fig. 3.2A	A modeling of an RF oscillator	71
Fig. 3.2B	check-A model for the change in loading from the RF filter due to fabrication Variations	71
Fig. 3.3 A	Simulation test-setup of the proposed resonance-based test methodology	74
Fig. 3.3 B	System modeling of the proposed resonance-based test methodology	74
Fig. 3.4 A	simulation model for RF interconnects with open defect	75
Fig. 3.5	Simulation model for RF interconnects with short defect	77
Fig. 3.6	Insertion loss of RF low-pass filters under test to demonstrate RBT Methodology	78
Fig. 3.7	3-dB frequency of the RF high-pass filters vs. test setup output	80
Fig. 3.8	A hardware prototype of the proposed resonance-based test method	81
Fig. 3.9	Insertion loss of SMD RF low-pass filters	82
Fig.3.10	Measurement results for testing SMD RF low-pass filter by the RBT methodology	82
Fig. 3.11	Insertion loss of RF high-pass filters under test	83
Fig. 3.12.	Measurement results for testing RF high-pass filter. Spectrum of the the RF Oscillator output	84
Fig. 3.13	Details for RF interconnect design using Roger's Substrate	85
Fig. 3.14	A hardware prototype to test RF interconnects by the RBT methodology	85
Fig. 3.15	Measurement results for testing RF Interconnects using RBT methodology	85
Fig. 3.16.	A hardware setup to test embedded RF passive filters at a panel level by the Proposed RBT methodology	86
Fig. 3.17.	Insertion loss of the RF low-pass filter samples embedded in RF substrate	87
Fig. 3.18	Measured output oscillation frequency of the proposed test setup vs 3-dB frequency of embedded RF low-pass filters in the RF substrate	88
Fig. 3.19	Test setup cost of the proposed resonance based test(RBT) method as compared to the conventional method	90
Fig. 4.1	The proposed test setup for testing RF LNA at low-cost	94
Fig. 4.2	Calibration knob to calibrate/tune the oscillations in the closed loop system (RF Amplifier with the Phase shifter)	95
Fig. 4.3	Performance prediction using non-liner mapping for testing RF amplifiers	99
Fig. 4.4	LNA in the feedback mode (simulation in ADS)	101
Fig. 4.5	Demonstration of tuning/calibration capability in the proposed test methodology for testing RF amplifiers	102
Fig. 4.6	Modeling of the system level simulation setup in MATLAB	102

Fig. 4.7	Test setup output (oscillation frequency) of the various LNA samples	103
Fig. 4.8	Simultaneous prediction of RF amplifier specifications at 1.2 GHz from the single 250 MHz test-signature using the proposed test methodology	104
Fig. 4.9	Hardware prototype of the proposed test setup for testing an RF amplifier	105
Fig. 4.10	Demonstration of tuning/calibration, measured oscillation frequency of the test setup for Sample A at output of the phase shifter	106
Fig. 4.11	Measured oscillation frequency of the test setup for different LNA samples	106
Fig. 4.12	Measured oscillation frequency of the test setup vs. measured Gain of the LNA Samples	107
Fig. 4.13 A	Predicted Gain of the LNA from low-frequency test-setup output	108
Fig. 4.13.B	Predicted NF (Noise Figure) of the LNA from low-frequency test-setup output	108
Fig. 4.13 C	Predicted P1dB of the LNA from low-frequency test-setup output	109
Fig. 4.14	Measured output oscillation frequency for over 14 hours using the proposed test setup to test RF amplifier	110
Fig. 4.15	Cost Analysis of the proposed test setup for testing RF amplifiers	112
Fig. 5.1	Proposed self-healing architecture of the RF amplifier	116
Fig. 5.2	Self-healing flow	117
Fig. 5.3	Proposed self-healing LNA architecture	118
Fig. 5.5	The performance curves of LNA for different calibration knobs	125
Fig. 5.6	Self-healing SiGe RF LNA modeling	128
Fig. 5.7	RF system modeling to demonstrate self-healing methodology for RF amplifiers	128
Fig. 5.8	Oscillation frequency of the various LNA samples	129
Fig. 5.9	SiGe RF amplifier analysis of parametric failures	130
Fig. 5.10	Performance curves: P1dB of LNA as a function of the tuning knobs	131
Fig. 5.11	Performance curves: gain of LNA as a function of the tuning knobs	131
Fig. 5.12	Specification distribution before and after healing using Knob1	132
Fig. 5.13	Specification distribution before and after healing using Knob2	133
Fig. 5.14	Specification distribution before and after healing using Knob1 and Knob2	134
Fig. 5.15	Self-healing CMOS RF LNA modeling	135
Fig. 5.16	Performance curves for 1.85 GHz CMOS LNA	136
Fig. 5.17	Specification distribution of CMOS LNA before and after healing using Knob1	138
Fig. 5.18	Specification distribution of CMOS LNA before and after healing using Knob2	139
Fig. 5.19	Specification distribution of CMOS LNA before and after healing using both Konbs	140
Fig. 5.20	A hardware prototype of the proposed self-healing RF amplifier	141
Fig. 5.21	Spectrum of the output after the feedback loop and after the RF down- conversion	141

Fig. 5.22	Gain vs. down-converted oscillation frequency of the LNA with feedback	142
Fig. 5.23	Performance curve: Gain of LNA1 as a function of the tuning knob	142
Fig. 5.24	A chip prototype of the self-healing SiGe LNA with self-generated test signature	144
Fig. 5.25	check - Improvement in the yield of X-band SiGe self-healing LNA	146
Fig. 5.26	Measurement results and the measurement setup of the RF LNA in self-healing Mode	147
Fig. 5.27	Measured and simulated gain of the X-band RF amplifier	148
Fig. 5.28	Measured gain of the RF LNA and the frequency of the self-generated sinusoidal signal from the LNA under self-healing mode	148
Fig. 5.29	Performance curve: gain of Sample 2 as a function of the tuning knob (I _{bias} , μ A)	148
Fig. 5.30	Power distribution before and after self healing of X-band SiGe LNA	150
Fig. 6.1	Proposed self-healing RF down-conversion mixer architecture	153
Fig. 6.2	Modeling of an RF down-conversion mixer	155
Fig. 6.3	Performance prediction of RF mixer using non-linear mapping	156
Fig. 6.4	Performance curves of mixer for different calibration knobs	159
Fig. 6.5	Schematic of self-healing RF down-conversion mixer	161
Fig. 6.6	Modeling of self-healing RF mixer architecture (System-level simulation)	161
Fig.6.7	Test-setup output (V _{test}) for different self-healing RF down-conversion mixer samples	162
Fig. 6.8	Prediction of Gain for the embedded RF down-conversion Mixer	163
Fig. 6.9	Prediction of P1dB for the embedded RF down-conversion Mixer	163
Fig. 6.10	Performance curve: P1dB of RF down-conversion mixer as a function of the calibration/tuning knobs	164
Fig. 6.11	Performance curve: Gain of RF down-conversion mixer as a function of the calibration/tuning knobs	165
Fig. 6.12	P1dB distribution before and after self-healing for parametric defects	165
Fig. 6.13	Gain distribution before and after self-healing for parametric defects	165
Fig. 6.14	Specification distribution before and after calibration using Knob1 and Knob2 for parametric defects	167
Fig. 6.15	A hardware prototype of the proposed self-healing RF Mixer	168
Fig. 6.16	Performance curve: Gain of RF down-conversion mixer as a function of the Tuning knob	169
Fig. 7.1	Model of RF system with embedded RF filters and surface mount RF IC	172
Fig. 7.2	The flow chat of the proposed yield improvement methodology for RF substrate	173
Fig. 7.3	A proposed RF receiver architecture for yield improvement of RF substrates	174
Fig. 7.4	The performance curves of LNA for Gain vs. Voltage at the tuning	176

	Knob	
Fig. 7.5	The insertion-loss profile and parametric yield of RF low-pass filter	177
Fig. 7.6	Design of RF amplifier (LNA) with one tuning knob	178
Fig. 7.7	Performance curves of LNA: Variation of Gain as a function of the tuning knob (V_{gs} voltage)	179
Fig. 7.8	The simulation model for on-chip calibration of RF amplifier (LNA) to increase the yield of RF substrates	179
Fig. 7.9	A hardware prototype of the proposed yield improvement methodology	181
Fig. 7.10	Measured insertion loss of the RF low-pass filters	181
Fig. 7.11	Performance curve: Gain of RF amplifier as a function of the tuning knob (V_{dd})	181
Fig.8.1	Schematic of the proposed variable-gain LNA	184
Fig.8.2	Small-signal equivalent schematic of the proposed variable-gain LNA	185
Fig.8.3	Layout of the 5.9 GHz LNA to demonstrate the proposed VGLNA.	188
Fig.8.4	Change in Magnitude of S_{21} at 5.92 GHz for different values of V_{ctrl}	188
Fig.8.5	Change in Magnitude of S_{22} at 5.92 GHz for different values of V_{ctrl}	189
Fig.8.6	Change in Magnitude of S_{11} at 5.92 GHz for different values of V_{ctrl}	189
Fig.8.7	Change in phase of S_{21} at 5.92 GHz for different values of V_{ctrl}	190
Fig.8.8	Chip prototype to demonstrate the proposed VGLNA	191
Fig.8.9	Measured change in magnitude of S_{21} of the VGLNA for different values of V_{ctrl}	191
Fig.8.10	Measured change in magnitude of S_{22} of the VGLNA for different values of V_{ctrl}	192
Fig.8.11	Measured change in magnitude of S_{11} of the VGLNA for different values of V_{ctrl}	192
Fig.8.12	Measured change in <i>phase</i> of S_{21} of the VGLNA for different values of V_{ctrl}	193
Fig. 9.1	Self-Healing Antenna Based on Resonance Test Method	195

SUMMARY

During the last decade, System-On-Chip (SOC) approach has emerged to integrate digital, analog and RF circuits on a single chip to miniaturize wireless communication systems. Although SOC approach is a promising solution for the miniaturization of RF systems, it is limited by low-Q passives and substrate coupling. As an alternative to the SOC approach, System-On-Package (SOP) and System-In-Package (SIP) approaches have shown potential to provide better integration of digital, analog and RF functionalities. Even though advances in these technologies have reduced many problems associated with manufacturing complex integrated RF systems, the manufacturing cost of RF systems is still a major concern for industry because of high test cost and yield issues of RF circuits.

This thesis proposes a multifaceted production test and post-manufacture yield enhancement framework for RF systems. This framework uses low-cost test and post-manufacture calibration/tuning techniques. Since the test cost and the yield of the RF circuits/sub-system directly contribute to the manufacturing cost of RF systems, the proposed framework minimizes overall RF systems' manufacturing cost by taking two approaches as shown in Fig.1. In the first approach, low-cost testing methodologies are proposed for RF amplifiers and integrated RF substrates with an embedded RF passive filter and interconnect. Techniques are developed to test RF circuits by the analysis of low-frequency signal of the order of few MHz and without using any external RF test-stimulus. Oscillation principles are used to enable testing of RF circuits without any external test-stimulus. In the second approach, to increase the yield of the RF circuits for

parametric defects, RF circuits are tuned to compensate for a performance loss during production test using on-board or on-chip resources. This approach includes a diagnosis algorithm to identify faulty circuits within the system, and performs a compensation process that adjusts tunable components to enhance the performance of the RF circuits. In the proposed yield improvement methodologies, the external test stimulus is not required because the stimulus is generated by the RF circuit itself with the help of additional circuitry and faulty circuits are detected using low-cost test methods developed in this research. As a result, the proposed research enables low-cost testing and self-healing of RF systems.

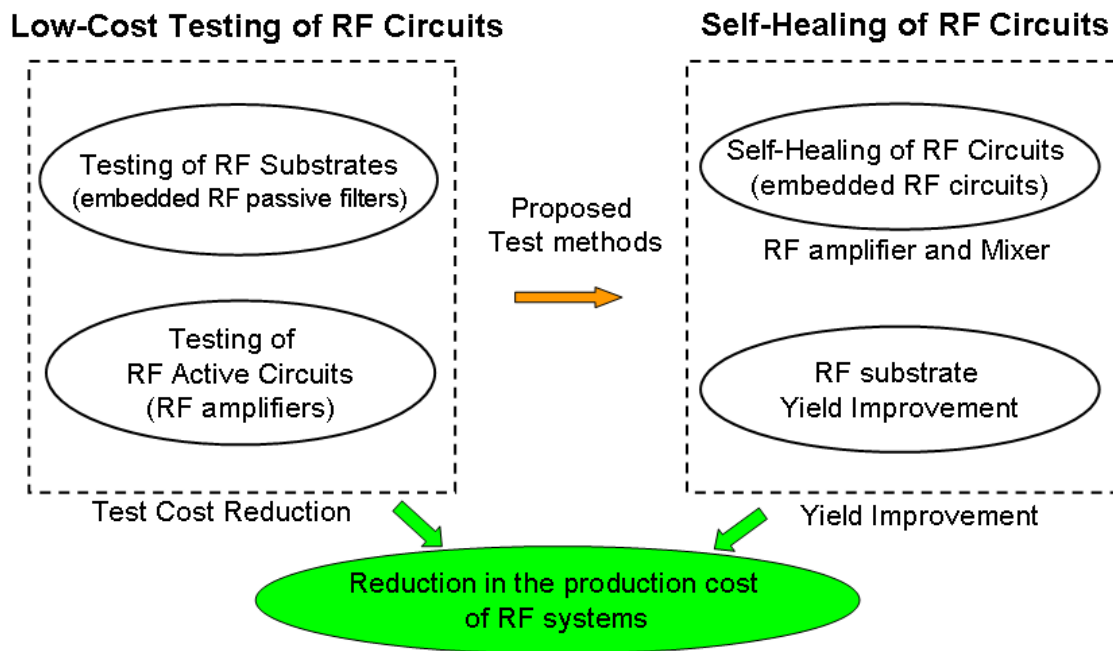


Fig. 1 Thesis framework and scope of research

Chapter 1 INTRODUCTION

With the revolutionary developments in the wireless communications technology, there is need for radio frequency (RF) front-end modules which can support different communication standards spanning diverse bandwidths. At the same time, it is expected that such RF modules should be compact, reliable and low cost.

During the past decade integrated circuit (IC) technology has progressed in accordance with Moore's law. These advances in IC technology have enabled the integration of RF front-ends with multiple analog and digital blocks on a single chip. For high speed operation, CMOS technology has evolved from 250 nm device feature size to 32 nm and now utilizes complicated strain engineering approaches. In addition, silicon BJT technology has evolved into silicon-germanium (SiGe) Heterojunction Bipolar Transistors (HBTs). However, there are discouraging predictions [1-4] regarding the effects of process variations on the yield in deep-submicron ICs processes. RF circuits, in particular, are expected to be increasingly prone to process variations, suffering from significant loss of parametric yield, as shown in Fig. 1.1. As a result, new post-manufacturing approaches must be developed to compensate RF circuits to increase their yield for low-cost RF systems. Also, testing of RF circuits for correct functionality will be necessary in the development of reliable RF devices.

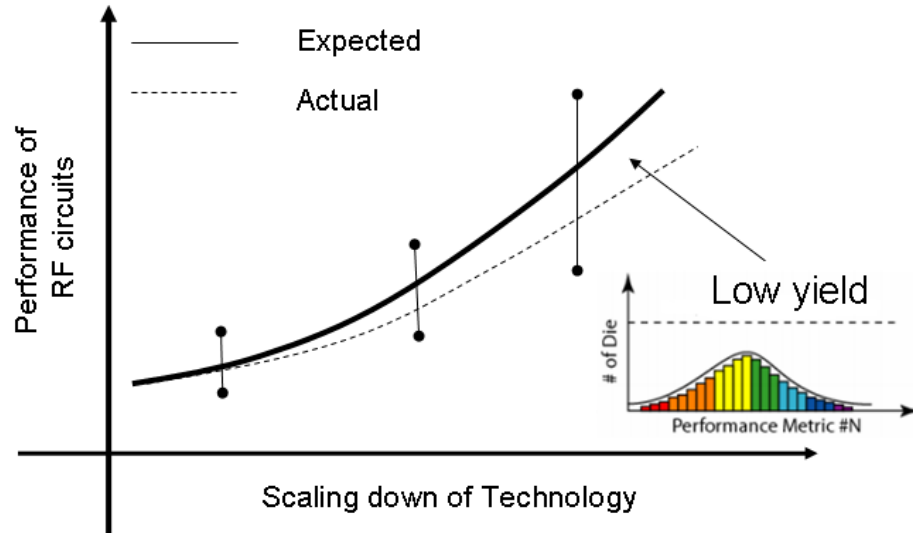


Fig. 1.1. Low yield because of widening gap in the performance [1].

The production-level test cost of RF circuits is significant mainly because of two reasons. First, the test-setup cost is high since RF circuit testing requires Automated-Test-Equipment (ATE) systems which are worth millions of dollars. Secondly, the test-time is high because the RF active circuit testing is performed in a sequential manner by a dedicated test-setup for different specifications. The test cost of RF circuits can account for upto 30% of their manufacturing cost [5–8]. As a result, low-cost techniques must be developed to reduce the test-cost of RF circuits and hence the overall cost of RF systems.

Current IC technologies can achieve very high density circuits, leading to size reduction of communication systems. However, these IC technologies are mainly silicon based and are limited by low-Q passives and substrate coupling. It is difficult to realize high quality integrated filters, duplexers, power amplifiers, and antennas using silicon based technology by itself.

To provide better integration of digital, analog and RF functionalities and for better performance of RF front-ends, several packaging technologies have been proposed in the last decade. Some of the proposed technologies include System-On-Package (SOP), System-In-Package (SIP) and Multi-Chip-Module (MCM). Among these packaging technologies, SOP has emerged as a promising technology for on-chip and package integration to miniaturize RF front-ends [8,9]. SOP technology not only enables embedding of passive components (inductor, capacitor or interconnect) but also enables the embedding of entire RF passive filters into the RF substrates as shown in Fig. 1.2. An RF substrate with embedded RF passives is called an integrated RF substrate.

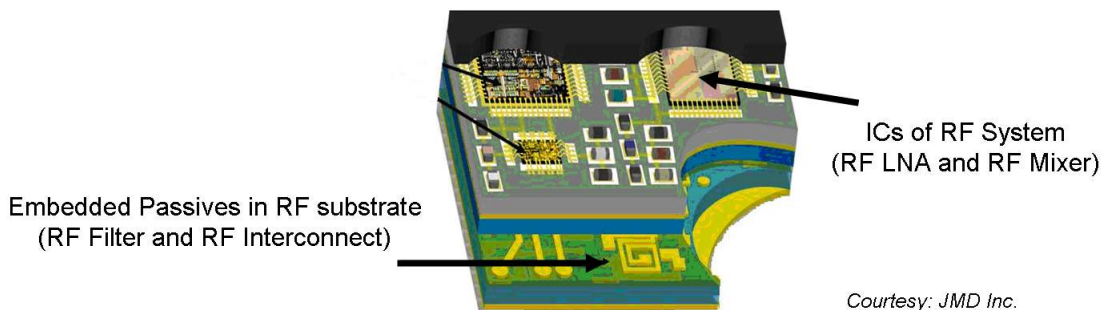


Fig. 1.2 RF substrate with embedded RF filters and mounted RF ICs and components

With the emergence of SOP technology, the recent years have seen the use of embedded RF passive filters instead of surface-mount filters for the miniaturization of RF front-end modules [8 -12]. However, this has created new challenges in the testing of integrated RF embedded passive filters. In most of the integrated RF substrates, only the input and output ports of embedded RF passive filters are accessible while the internal

nodes are inaccessible, such inaccessibility of internal nodes increases test challenges for these embedded RF circuits.

The performance of embedded passive filters is often different because of the process variations induced during fabrication. Hence, the testing of embedded RF filters in integrated RF substrates becomes essential. The total substrate test cost of integrated RF substrates is mostly contributed by the expensive instruments necessary for testing embedded RF passive circuitry. Expensive RF instruments such as Vector Network Analyzers (VNAs) and multiple RF probes are required for testing these embedded RF filters. To reduce the production cost of integrated RF substrates, new test approaches must be developed for testing such circuits.

1.1 Typical Production Flow for RF Systems

A typical production flow for RF sub-systems based on SIP/SOP approach can be broadly divided into six steps (Fig. 1.3), the first step includes designing of embedded RF passive circuits and RF active ICs/components, the second step includes prototype creation and measurements of these RF circuits/components, the third step includes high volume manufacturing of the RF circuits/components. The fourth step includes testing of integrated RF substrates and active components/ICs, the fifth step includes front-end assembly of good RF substrates with pre-tested ICs and in the final step, functional testing of assembled RF system is performed.

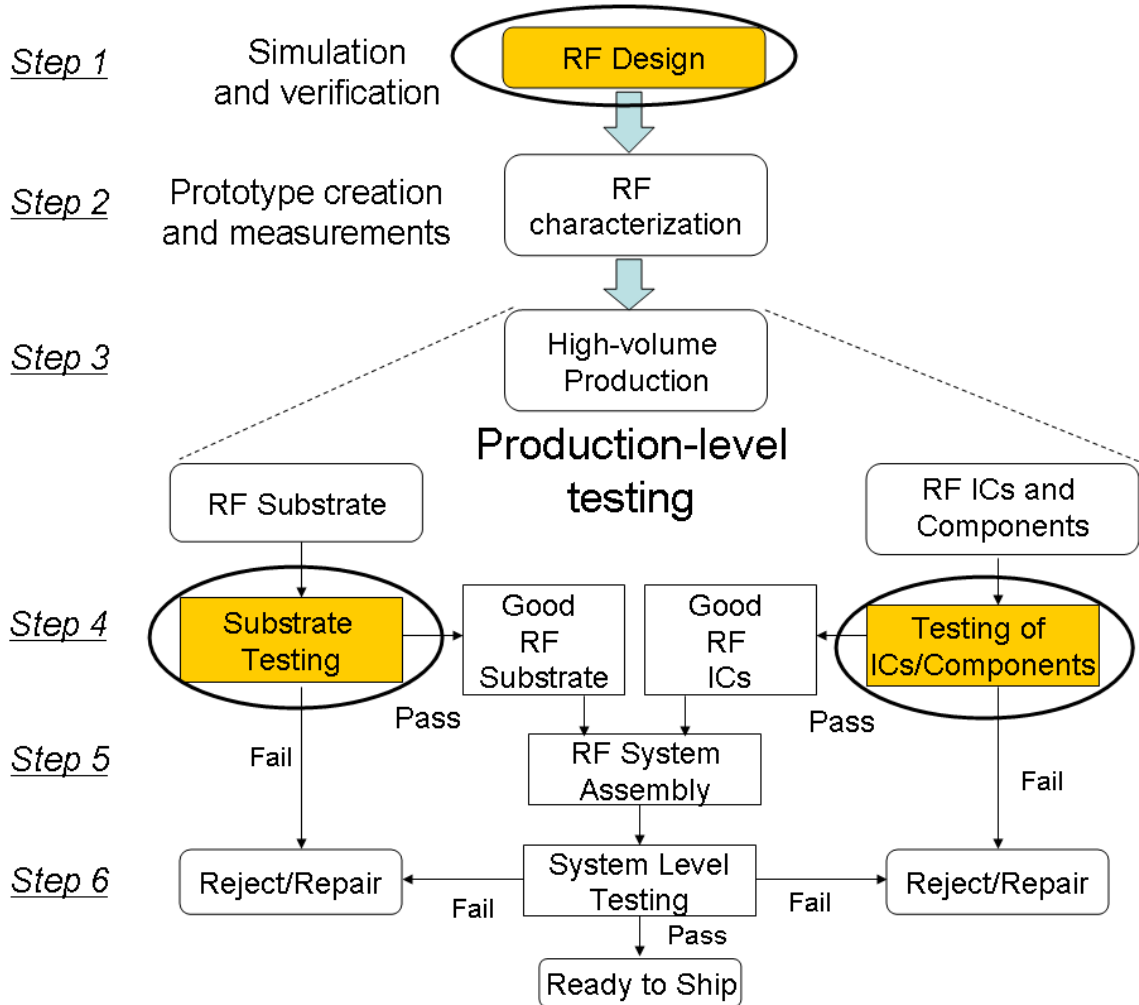


Fig. 1.3. A typical production flow of RF systems based on SOP/SIP packaging approach.

Depending on the application, the amount of production-level testing can vary from very rigorous to simple pass-or-fail testing. Typically, the test cost increases exponentially with improvement in Defects-Per-Million (DPM), as shown in Fig. 1.4 [4]. To minimize the test cost, test compaction [13, 14] is performed to identify a set of critical specifications and then circuits/modules are tested for those specifications. In general, if modules are integrated at the system level, then simple pass-or-fail testing is performed at the module level which is followed by system level functional testing.

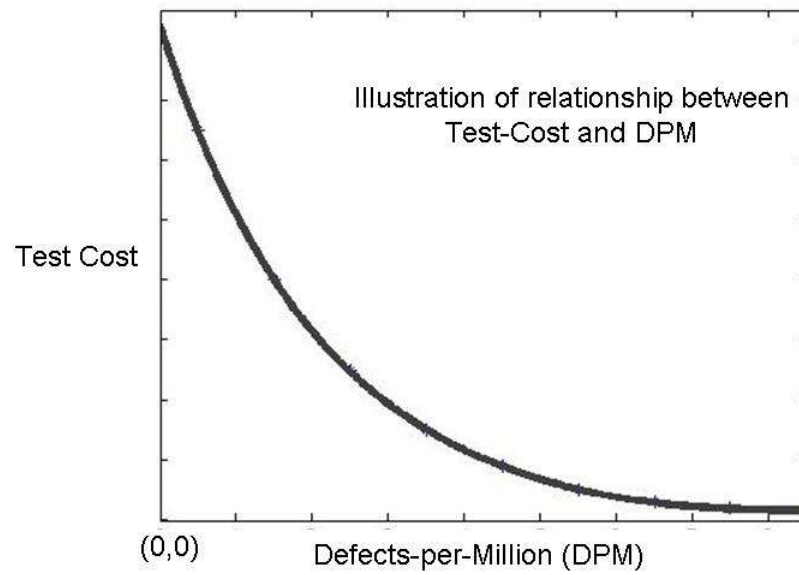


Fig. 1.4. Illustration of the test cost and Defects-per-Million (DPM) in the shipped design [4]

The testing of RF substrates prior to the attachment of surface-mounted devices (chips or components) is called substrate testing (Step 4, Fig. 1.3). Substrate testing is a screening process to ensure that integrated RF substrate is defect free, thus minimizing the wastage of expensive chips assembled on it. Testing of RF ICs/components could be a screening process or a very rigorous process to test RF ICs for each and every specification. In the proposed framework, it is assumed that testing of RF ICs includes screening process followed by the system-level functional testing of integrated RF sub-systems. **The proposed test methodologies in the present thesis focus on a low-cost production-level testing procedure that identifies defective devices rather than accurate RF characterization.**

Currently, failing (non-passing) RF substrates and RF active ICs/Components are simply discarded because the repairing of embedded RF circuits is very costly and difficult as it requires proper diagnoses and laser trimming of these designs. **In the**

present thesis, novel self-healing methodologies are proposed which enable post-manufacturing yield improvement of the RF circuits/systems without laser trimming.

The proposed production-level test methodologies as well as yield improvement methodologies are explained in detail in the following chapters.

1.2 Previous Research Efforts to Test RF/Mixed-Signal Active Circuits

With IC design becoming more complex, the problem of testing them is also becoming complex. To address this issue, significant research has been done to lower the cost of RF/Mixed-Signal active circuits by proposing several Built-Off Test (BOT), Built-In Test (BIT), Built-Off self-Test (BOST), Built-In Self-Test (BIST) approaches. In BOT approach, some of the functionalities of ATE are implemented on a load-board to prohibit the cost of a classical ATE. The load-board can have in-built capability of up-conversion, down-conversion, modulation or demodulation. The BIT approach is an aggressive version of BOT and it is more of a Design-For Test (DFT) methodology in which test functionalities are pushed closer to the Device-Under Test (DUT). In both BIT and BOT, load-board is a necessary component in the production test environment and typically routes the signal from (to) the external ATE to (from) the DUT. If BOT and BIT approaches are completely independent of any external ATE, they result in BOST and BIST approaches. With the emergence of SOC concept, BIT approaches can be implemented as BIST by using on-chip resources such as Digital Signal Processors (DSPs).

Boundary-scan standard, IEEE 1149.1 [15], is used in industry to access internal modules of digital ICs for testing static faults and testing of analog system is done by means of inserting additional test accesses around it [16, 17]. BIT/BITS is used widely in digital systems; its applicability to analog/RF systems is a subject of on-going research mainly because of difficulty in generating on-chip high-speed test stimulus, one-chip high-speed data acquisition, area overhead of additional circuitry, effect of additional circuitry on the performance of analog/RF circuits and degradation of high-speed signals due to input/output pads [18]. In [19] authors have demonstrated on-chip signal generator for mixed-signal BIST. The work presented in [20] shows the feasibility of using a BIT for measuring the performance of high-frequency embedded analog/RF blocks by measuring the spectral content of the test response using the direct down-conversion of RF test stimuli and test response waveforms. The authors of [21, 22] have developed a sub-sampling-based digitizer that can be used for capturing narrow-band RF waveforms. In [23], authors have demonstrated RF LNA design with integrated current and power sensors for RF BIST applications. Test approach based on BOT for testing high-speed digital circuits is demonstrated in [24, 25].

In traditional production-test approaches for testing of RF/mixed signal circuits, the functional specifications are measured using the same kind of test stimuli and configuration with respect to which the specifications are defined such as multi-tone signal generator for measuring distortion. In contrast to traditional production-test approaches, in “Alternate Test” methodology multiple specifications of analog/RF circuits are predicted from the test response of the DUT to a carefully crafted test stimulus, as shown in Fig. 1.4.

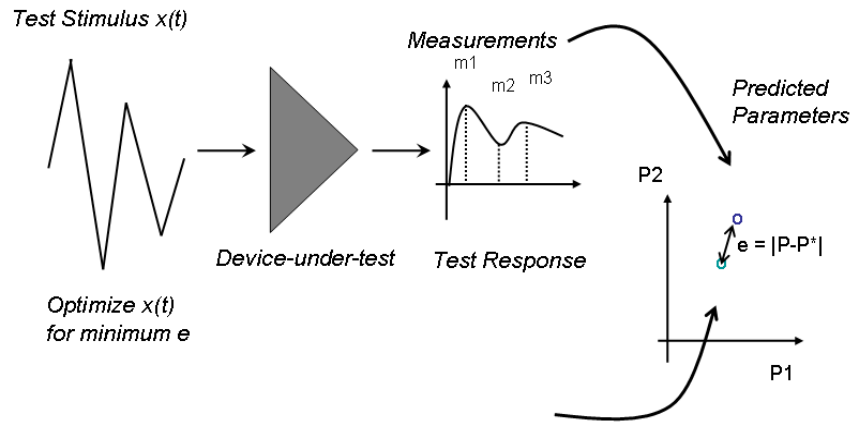


Fig. 1.5 Alternate test flow [26, 27].

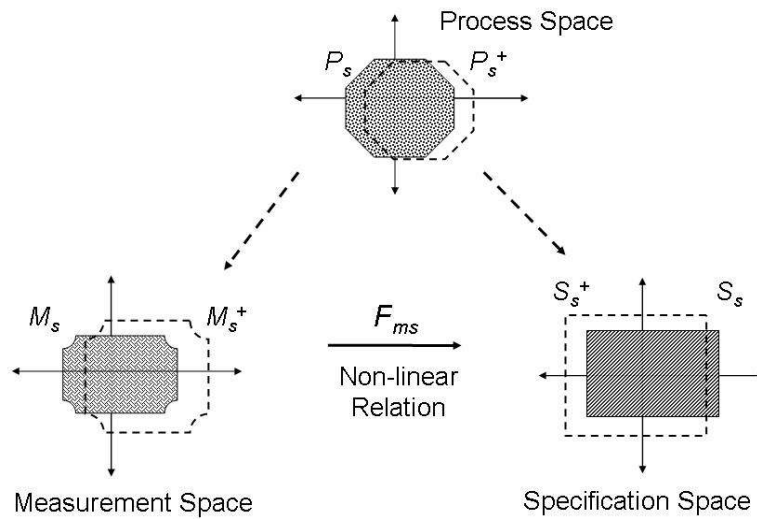


Fig. 1.6 Mapping concept of Alternate test flow [26, 27].

The concept of alternate test was proposed in [26, 27] and is shown in Fig. 1.5 and Fig. 1.6. It is explained in [26, 27] that the variation of any process or circuit parameters (P_s) affects the circuit specification (S_s) by a corresponding sensitivity factor. If M_s is the space of measurements made on the DUT, the variations in the parameters also affects the measurement data in M_s . For a given process space (P_s) a mapping function (non linear) can be computed on the specification space (S_s), $F_{ps}(P_s) : P_s \rightarrow S_s$.

Similarly, another mapping function (non linear) can be computed in M_s , $F_{pm}(P_s) : P_s \rightarrow M_s$. Therefore, for a region of acceptance in the circuit specifications, there exists a corresponding allowable “acceptable” region of variation in the parameter space. It is also shown in [26, 27] that a mapping function between M_s and S_s , $F_{ms}(m) : M_s \rightarrow S_s$ can be constructed using non-linear statistical multivariate regression. Thus, given the existence of the regression model for S_s , an unknown specification of a DUT can be predicted from the measured data (M_s). In [28-30], Multivariate Adaptive Regression Splines (MARS) [31] was used to construct non-linear regression models and specifications of the subsystem were predicted from the frequency spectrum of the test response.

Although concept of Alternate test methodology remains the same, recently this methodology has been applied to test RF active circuits. In [32], a BOT approach is taken to test RF LNA in which a load board is designed to alleviate the problem of bandwidth limitation of ATE cable by designing load-board with a modulator (that up-converts the low-frequency test signal sent from ATE) and a demodulator (that down-converts the RF test response to low frequency). A different BOT approach is reported in [33], where authors attempted to replace the need for using high-frequency testing by alternatively monitoring the transient change in the bias current of an RF power amplifier, and the information contained in such changes in bias current is measured to predict critical components specifications like gain and noise figure. In [34, 35], noise reference is presented to test RF circuits using alternate test methodology. Besides these, the alternate test methodology has been used for test RF circuits/sub-systems in [36-39].

In another kind of BIT approach, testing of active analog and mixed signal circuits has been proposed in [40, 41] based on Barkhausen criterion [42]. The method in [40, 41] is based on partitioning or reconfiguring the active analog circuits into an oscillator by adding or removing some extra components. This method is commonly known as Oscillation-Based Test (OBT). The modified OBT, referred to as Predictive Oscillation-Based Test (POBT) [43], predicts the performance of the original circuit by computing the correlation and measuring the oscillation frequency of the reconfigured analog active filter. OBT based method has been demonstrated for testing active circuits in digital, analog and mixed-signal domains in [44-48]. The method as described in these OBT based papers [40, 41, 43-48], cannot be applied for testing RF passive circuits embedded in integrated RF substrates because RF passive circuits have no active components. In the present work of this thesis, this inherent limitation of OBT methodology has been resolved and low-cost testing of integrated RF substrates with embedded RF passive filters is presented based on oscillation principles (Barkhausen criterion). Also, a low-frequency test methodology based on oscillation principles to test RF LNA is presented which enables the testing of the LNA without applying any external test stimulus. In the test mode, the test stimulus is self generated by the LNA with the help of external circuitry located on a load-board or on a probe card. It is also shown that multiple critical specifications of RF LNA like gain and linearity can be predicted by analyzing low-frequency signature of the proposed test setup.

The following section discusses the prior work in the area of post-silicon yield enhancement of RF circuits/systems.

1.3 Previous Research Efforts for Post-Silicon Yield Enhancement of RF Circuits/Systems

To increase the post-silicon yield, several methods have been presented in the literature for digital and analog circuits. These methods include calibration, compensation or self-correction, some of them are as follows: Self-correction techniques for digital circuitry have been presented in [49, 50]. In these methods, memory circuits employ redundant cells and test circuitry. After testing memory circuits by the embedded test circuitry, the faulty cells are replaced with redundant cells. In analog domain, self-correction techniques have been proposed for analog-to-digital and digital-to-analog circuits in [51, 52]. To reduce the device mismatches, these methods trim the reference voltage or capacitance. In [53], a technique was presented to compensate mismatch of transistors in current mirrors. However, application of similar techniques in RF domain is not yet explored because of high speed operations of RF circuits. A few compensation techniques for RF circuits have also been presented in literature. In [54], pre-distortion linearization has been employed to increase linearity of RF power amplifiers. To compensate RF front-end non-idealities (gain loss, in-phase/quadrature (IQ) gain mismatch, non-linear distortion and DC offset), calibration techniques based on DSP processing are presented in [55-58]. The calibration methods for increasing yield of RF sub-system namely embedded LNAs have been proposed in [59–61]. In all of these methods, an input stimulus is applied to calibrate the RF circuit and the output response is captured using embedded sensors. With the help of on-chip resources, the calibration knobs of the LNA are tuned to enhance its performance. Although the methods presented in [59-61] helps in improving the yield of the RF sub-system by calibrating the embedded LNA, these methods assume the availability of an RF-signal source. In

general, this requires the loop-back of the transmitter output which is cumbersome due to the need to send an RF signal from the RF transmitter to the input of the receiver (LNA). In addition, any source stimulus (RF transmitter) needs to be tested first, before testing the embedded RF amplifier (LNA). In the present research, a new self-healing methodology is presented to overcome the need for external RF input-test stimulus. This technique requires no external test stimulus for performing self-correction because the output-signature is generated by the DUT itself with the help of some additional circuitry. The performance of the DUT is enhanced by adjusting the control knobs after analyzing this self-generated output from the DUT using on-chip or on-board resources. Also, a novel self-healing methodology is proposed for RF mixers. This methodology eliminates the need for the generation of on-chip RF signals exclusively for self-calibration/self-correction of the RF mixers. In the present methodology, LO port signal is reused at the mixer RF port and no additional signal generation is required. In addition, in this thesis, a new yield improvement methodology is proposed for RF substrates. The proposed methodology introduces a concept of package-chip co-design and on-chip calibration of active circuitry for the yield improvement of passive embedded RF filters that are off-chip.

The following section discusses the prior work for testing embedded passive circuits and substrate testing.

1.4 Previous Research Efforts to Test Embedded Passives Circuits/Substrate Testing

The testing of RF substrates prior to the attachment of surface-mounted devices (chips or components) is called substrate testing as shown in Fig. 1.3. In the past,

numerous techniques to test interconnect in MCM substrates have been proposed to detect open or short defects. A net is defined as metal connection/transmission line between two ports in MCM substrates. Capacitance measurement method proposed in [62] measures the capacitance of net with respect to common ground. In another technique, a combination of capacitance measurement with the resistance measurement [63] between the extreme ends of a net has been proposed. To achieve contact-less testing of embedded nets, an electron-beam test technique has been proposed in [64]. Further, to detect latent opens in nets, IBM has proposed Electrical Module Test (EMT) [65]. The EMT technology is based on the application of alternate and direct currents through nets to detect latent electrical opens such as line narrowing, cracks or weak connections. Another method to detect latent open and short defects in nets for MCM substrate testing has been proposed in [66]. This method is based on the measurement in the shift in the resonance frequency of the RF-passive resonator due to the loading from the net under test. To test embedded passive filters, a method based on pole or zero analysis has been proposed in [67]. The method in [67] requires high-frequency instruments such as VNAs to measure S11 parameter. Since embedding of RF passive filters in the RF substrate is a new concept, not much prior research has been done for low-cost testing of integrated RF substrate with embedded RF passive filters. Currently, in practice, embedded RF passive filters are tested using high-frequency instruments such as VNAs. In the present research, low-cost test methods have been developed to reduce the test cost of RF passive filters embedded in RF substrates, thus reducing the overall production cost for integrated RF substrates.

As minor contributions of this present thesis, *for the first time*, testing using RF-passive resonator is extended for production-level testing of embedded RF filters using regression mapping. Also, “Alternate based test” method is extended for testing RF passive filters. These two methodologies are explained briefly in the following sections.

1.4.1 Test Methodology Based on Passive-RF Resonator

In this test approach, one-port measurement (S_{11}) is performed at lower frequency than the design frequency of the RF filter and insertion loss (S_{21}) is predicted by using the non-linear prediction models. To demonstrate this proposed approach, both simulation and measurement were performed and it is shown that the test frequency can be reduced by approximately 47% for a RF low-pass filter and 33% for a RF high-pass filter. Because of the one-port measurement at the reduced frequency, the proposed test-setup cost is less as compared to the conventional test method, which uses VNAs.

1.4.1.1 Proposed Methodology

The proposed test methodology is based on the change in the resonance frequency of a RF-passive resonator because of the loading effect from the RF filter. A RF-passive resonator has been employed to test interconnects in MCM technology [66]. The method in [66] uses shift in the resonance frequency of the resonator for pass or fail testing of interconnects. This proposed testing methodology is also based on a similar principle, but it has been applied to the embedded RF passive filters and shown that insertion loss (two-port measurement) at high frequency of RF passive filter can be predicted from one-port

measurement at low-frequency. Prediction of insertion loss at the design frequency from the low-frequency measurement is useful for large-resolution testing.

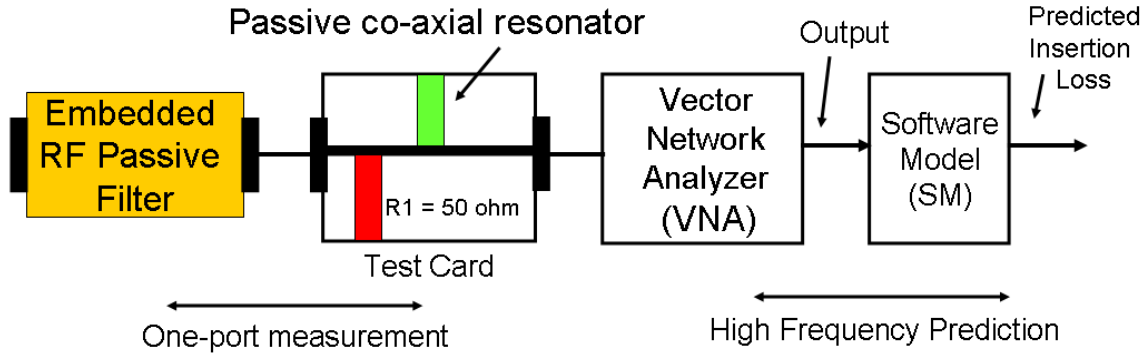


Fig. 1.7. The proposed test-setup for testing embedded RF passive filters using passive resonator.

Consider the test setup as shown in Fig. 1.7, it consists of embedded RF passive filter and a test card. The test card contains a passive co-axial resonator and a resistor. The resonance frequency of the co-axial resonator shifts because of the loading from an RF filter. Since different samples of the RF filters load the co-axial passive resonator differently, the testing of the RF filter is performed by careful analysis of the change in the response of the resonator. The purpose of the resistor on the test card is to increase the sensitivity to detect change in the resonance frequency. Resistor (R1) increases the sensitivity by providing approximately perfect match of 50 Ohm at the resonance frequency.

The presence of the test card enables the detection of the change in the admittance of the filters at much lower frequency than the design frequency of the RF filter, thus it enables the testing of the embedded RF filters at the lower frequency. The resonance frequency of the resonator should be chosen as low as possible but it should be large enough to capture the variations in filter's passive components at the design frequency of

the RF filters. Also, admittance of the RF filter should be differentiable in the vicinity of the resonance frequency of the test-setup with a golden filter. To increase the sensitivity of the test-card towards the loading from the RF filter, high quality factor (Q) resonators should be chosen.

In the proposed test methodology, testing is performed in two steps. The first step is a pass-or-fail testing, to differentiate very bad filters from good filters. In this step, RF filters are screened by defining allowable limits in the change in the resonance frequency of the test setup around the response of the test setup with a golden filter. The second step is high resolution testing, in which the insertion loss of the RF filter is predicted from the response of the test-setup. The prediction of insertion loss of the RF filter is performed by developing non-linear prediction model using MARS. This non-linear prediction model is referred as software model in this test approach.

An estimation of the maximum shift in the resonance frequency of the test setup and a development of the prediction model is performed by using a training set. The training set consists of a few calibrating RF filter samples with statistically likely parametric failures. These samples can be selected from different production lots or can be fabricated separately. In simulation, Monte Carlo simulations can be used to obtain such samples of the filter for constructing a training set.

1.4.1.2 Simulations Results

In this sub-section, the test methodology is demonstrated by modeling and testing of a RF low-pass (3-dB frequency of 1.39 GHz) and RF high-pass (3-dB frequency of 1.20 GHz) filters.

1.4.1.2.1 RF Low-Pass Filter Modeling

The testing of RF low-pass filter (3-dB frequency of 1.39 GHz) is considered in this sub-section. Let us consider five samples of the filter. The shift in the 3-dB frequency of the filter for variation in inductance (L_a) and capacitance (C_a) is shown Fig 1.8.

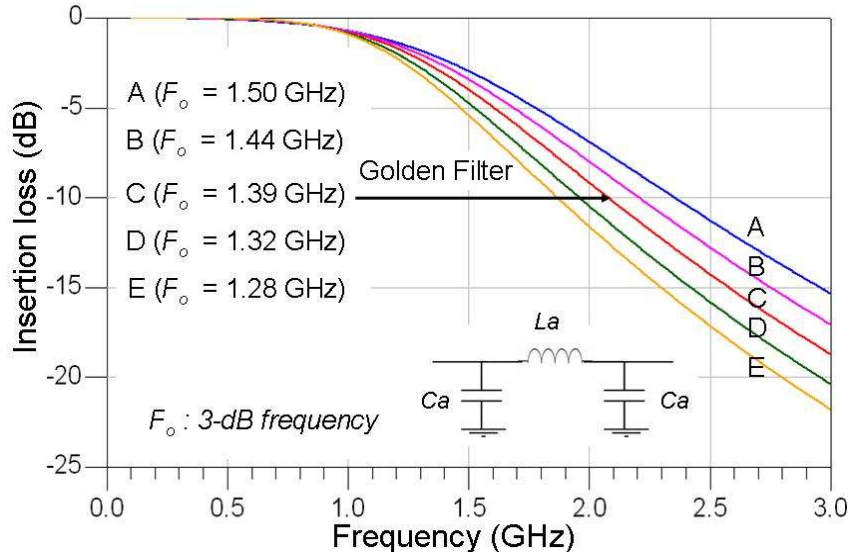


Fig. 1.8 The insertion loss of RF low-pass filter samples to demonstrate the test method based on passive resonator.

Let us assume that Sample C ($C_a = 2.0$ pF, $L_a = 12.2$ nH) is a golden filter and Sample B and Sample D are marginally good. In addition to this, assume that Sample A ($C_a = 1.6$ pF, $L_a = 11.8$ nH) and Sample E ($C_a = 2.4$ pF, $L_a = 12.6$ nH) are bad. Hence, the aim of this testing methodology is to distinguish among these filters. It is also assumed that pass-band of the RF low-pass filter is upto 1.60 GHz

When these filters were simulated with a test card using the setup shown in Fig. 1.9, correlated changes were observed in one-port S_{11} measurements at a low-frequency, as shown in Fig. 1.10.

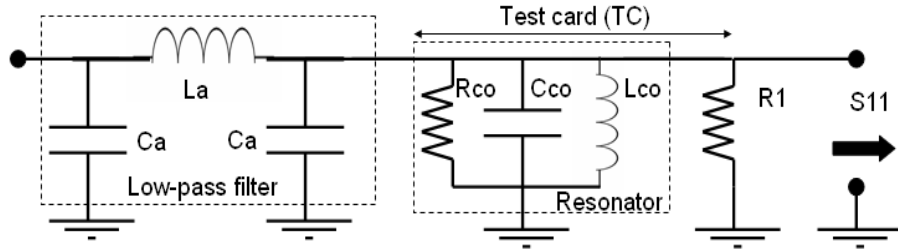


Fig. 1.9. Simulation test-setup for testing RF filters based on passive resonator.

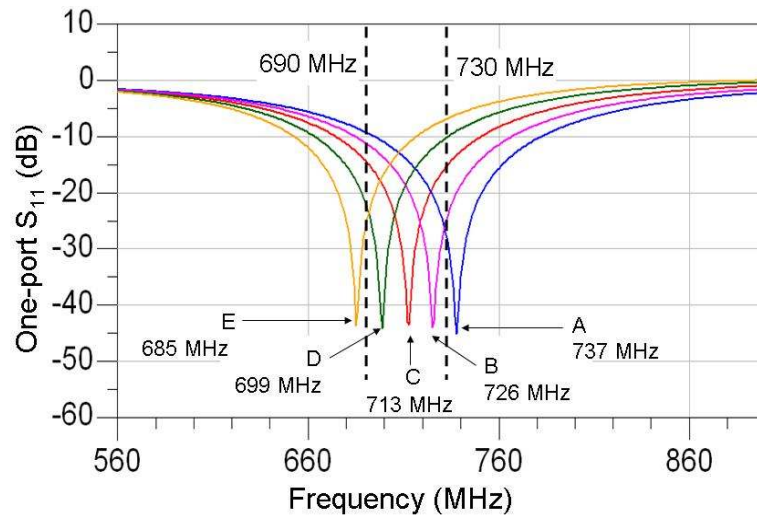


Fig. 1.10. Test-setup output for different samples of RF low-pass filter

It can be inferred from Fig. 1.10 that the response of the filters is either towards right or left of the golden filter response. Hence, a band of frequency can be defined for initial pass-or-fail testing of these filters. If a band from 690 MHz to 730 MHz is considered for good low-pass filters, filters A and E can be concluded as bad parts and filters B and D as marginally good parts.

To further demonstrate the high-resolution testing, prediction model (software model) was developed using 299 training samples for different values of L_a and C_a . Software model was developed from simulated S_{11} of the setup (Fig. 1.9). S_{11} parameters

from 500 MHz to 675 MHz have only been used to develop the prediction model. The predicted high-frequency insertion loss of filters B, C and D by the software model is shown in Fig. 1.11.

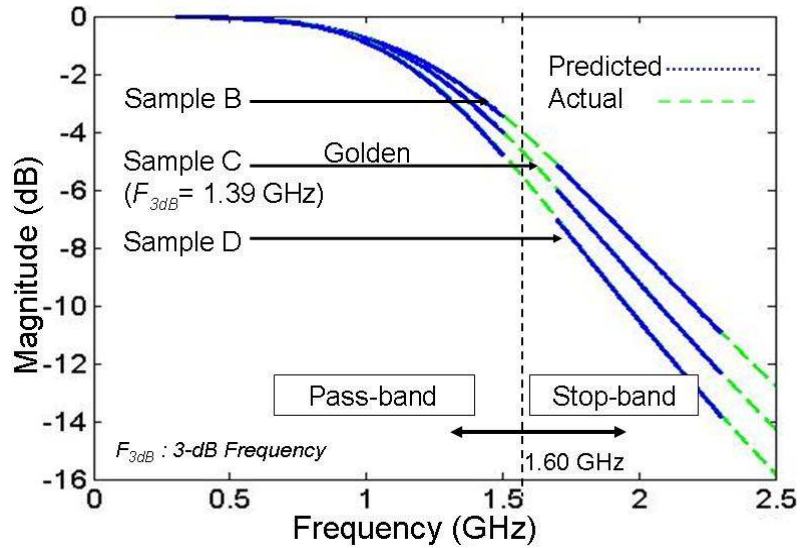


Fig. 1.11. Predicted high-frequency insertion loss of low-pass filters B, C and D.

1.4.1.2.2 RF High-Pass Filter Modeling

To further demonstrate this testing methodology, a RF high-pass filter (3-dB frequency of 1.20 GHz) is considered in this sub-section. Let us again consider five samples of the high-pass and assume that Samples A and E are bad, Samples B and D are marginally good, and Sample C is the golden filter. The insertion-loss profile of these high-pass filter samples is shown in Fig. 1.12. The setup similar to Fig. 1.19 is used for these simulations also and obtained test response is shown in Fig. 1.13.

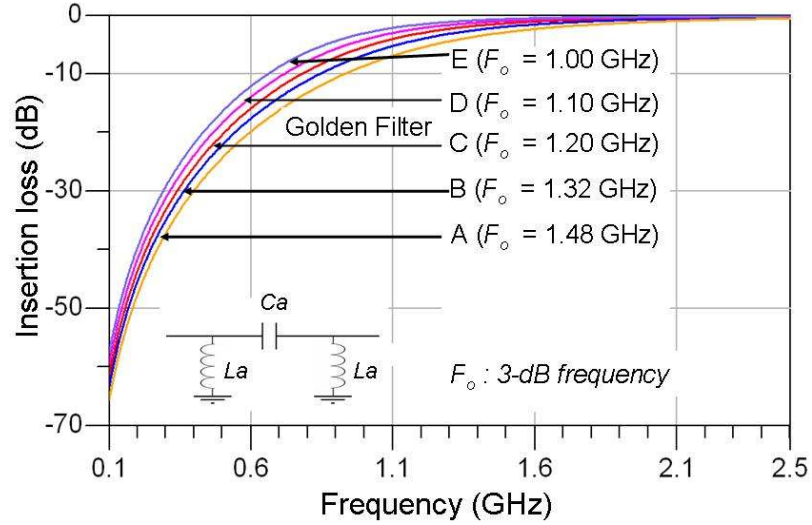


Fig. 1.12. Insertion loss profile of RF high-pass filters B, C and D.

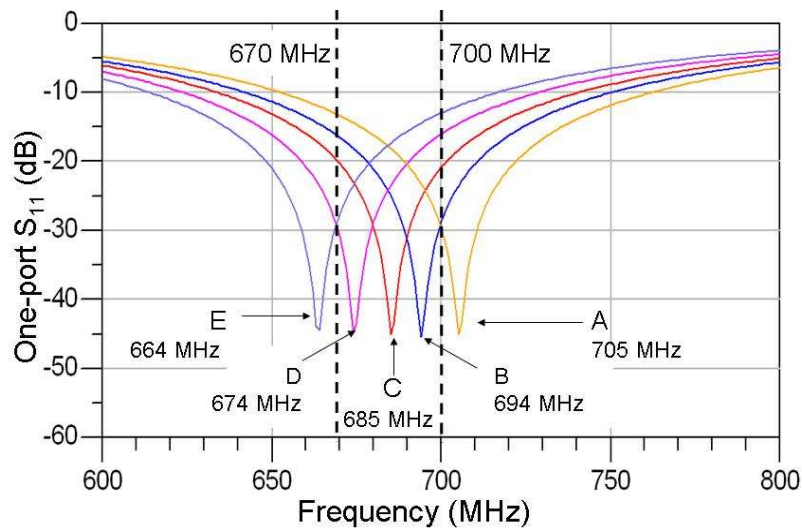


Fig. 1.13. Output of the proposed test setup for different samples of RF high-pass filter.

It can be inferred from Fig. 1.13 that by again defining a band of frequency around the response of golden high-pass filter Sample C, Samples A and E can be concluded as bad and Samples B and D as marginally good high-pass filters. For high-resolution testing, prediction model was developed similar to the previous sub-section using S_{11} from 500

MHz to 655 MHz of 299 calibrating high-pass filters. The predicted insertion-loss profile of Samples B, C and D are shown in Fig. 1.14.

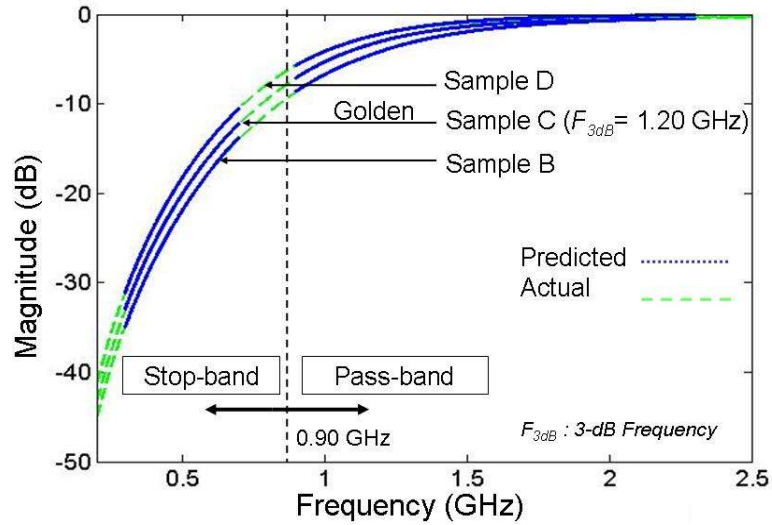


Fig. 1.14. Predicted high-frequency insertion loss of high-pass filters B, C and D using the proposed methodology based on passive resonator.

It is important to note that the responses in Fig. 1.10 and Fig 1.14 are at a much lower frequency than the design frequency. Thus, the proposed test setup shown in Fig. 1.7 reduces testing frequency by approximately 50% for these low-pass filters and approximately by 40% for these high-pass filters.

1.4.1.3 Measurement Results

In this section, the proposed test methodology is demonstrated at a panel-level. To enable panel-level testing, the test card was directly mounted on the RF probe as shown in Fig 1.15. The integrated RF substrate shown in this figure contains 102 embedded high-pass and low-pass filters.

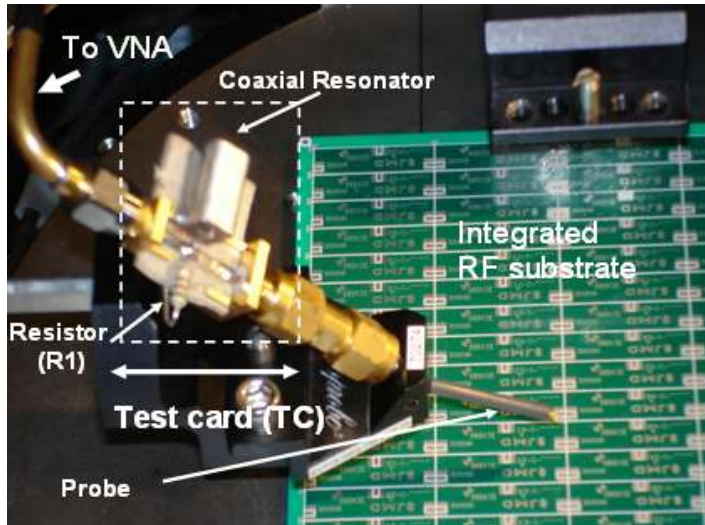


Fig 1.15. Panel-level test setup of passive resonator based methodology for testing 102 embedded filters.

One-port and low-frequency measurements for testing the embedded RF low-pass filters as proposed by this testing methodology are shown in Fig. 1.16. Insertion loss of these filters is shown in Fig. 1.17.

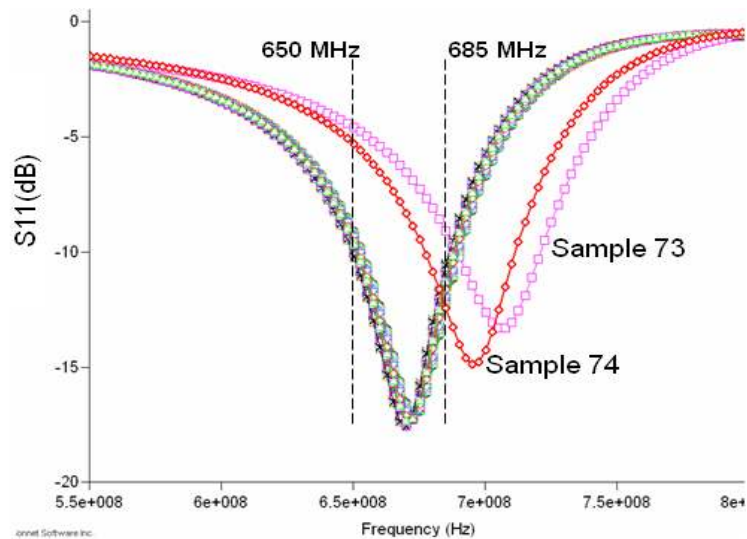


Fig. 1.16. Measurement of 102 embedded low-pass filters based on proposed methodology using passive resonator.

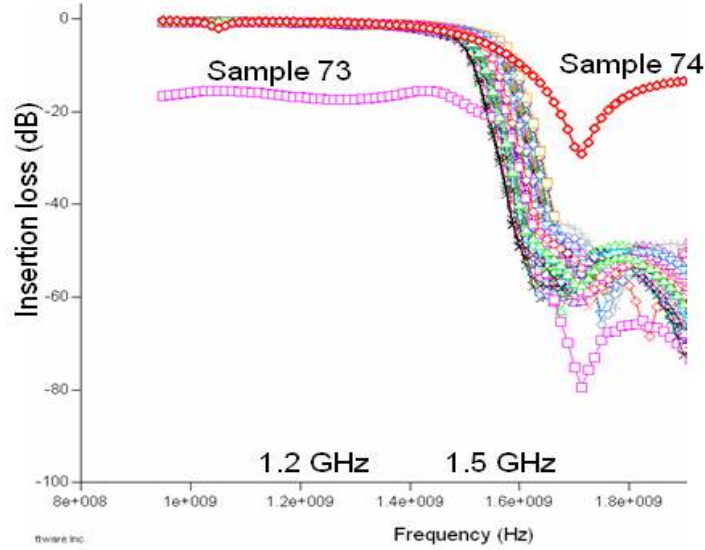


Fig. 1.17. Insertion loss of 102 embedded low-pass filters measured using aVNA.

It can be inferred from Fig. 1.17 that Samples 73 and 74 have bad low-pass filters, which is in agreement with the one-port and low-frequency measurements as shown in Fig. 1.16. Hence, based on the setup shown in Fig. 1.15, a pass-or-fail decision of embedded RF low-pass filter can be made after defining a band of frequency around golden filter response, such as from 650 MHz to 685 MHz in this case.

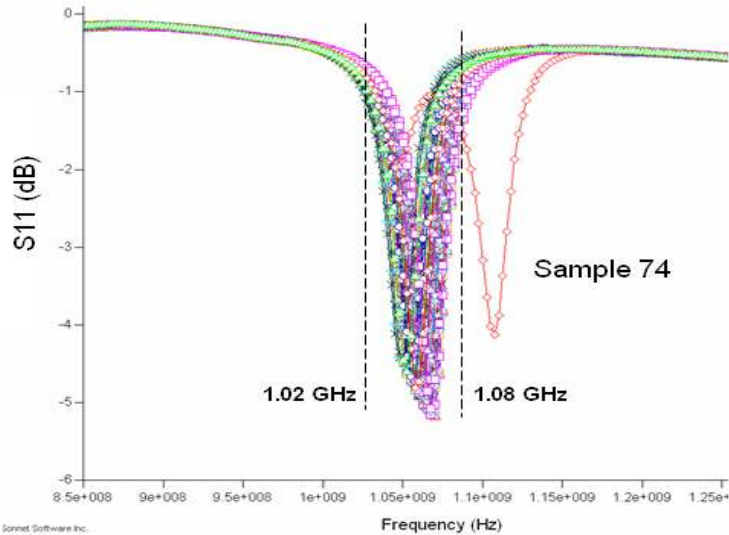


Fig. 1.18. One-port measurement of 102 embedded high-pass filters using passive-RF resonator based method.

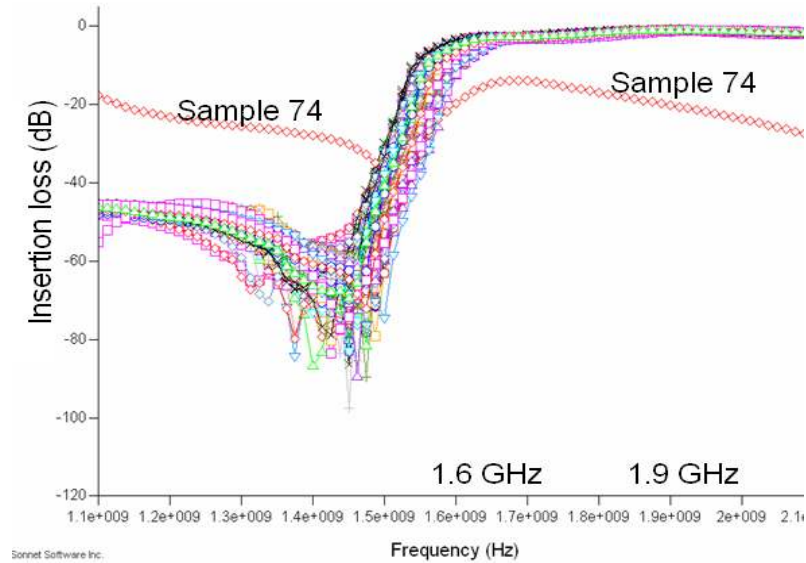


Fig. 1.19. Insertion loss measurement of 102 embedded high-pass filters using VNAs.

Fig. 1.18 shows one-port measurement for testing 102 embedded RF high-pass filters and Fig. 1.19 shows their insertion loss.

It can be concluded from Fig. 1.18 that Sample 74 is a bad high-pass filter. This conclusion is in agreement with the insertion loss measurement of high-pass filters as shown in Fig. 1.19. Hence, by the proposed methodology pass-or-fail testing can be done for high-pass filters as well. High-resolution testing of these RF low-pass and high-pass filters can be done by developing a prediction models as explained and shown in Section 1.4.1.2.

1.4.1.4 Concluding remarks

In this test methodology, only one-port measurement is performed using VNA at a lower frequency than the design frequency of the RF filters. The method has been demonstrated at panel/wafer level by testing 4th order embedded low-pass and high-pass

RF passive filters. It is shown that the testing frequency can be reduced by approximately 47% for the low-pass filter and 33% for the high-pass filter of the design frequency. Thus, in this method low-frequency VNAs can be used to reduce the test-setup cost.

Although this test methodology enables testing at lower frequencies, it still requires measurements using a VNA and RF input test stimulus. To enable testing without using a VNA at the production level, second approach is proposed which is based on Alternate test and is explained in the next section.

1.4.2 Test Methodology using Sinusoidal Input Signals

This test methodology eliminates the use of VNAs for production-level testing of RF filters. This methodology enables the testing of embedded RF filters by using sinusoidal input signals and regression analysis. Also, this methodology enables testing of these GHz passive filters at MHz frequencies. In this test method, insertion loss of a RF filter at design frequencies (in GHz range) is predicted from low-frequency time-domain response (in MHz range) using regression analysis. Thus, the test-setup cost reduces significantly. In past, the test approach based on regression analysis and using alternate test stimulus has been proposed and demonstrated for active circuits, as mentioned in Section 1.2. A similar approach has been taken in this sub-section as well, but for the first time “alternate-test” based approach is demonstrated for testing embedded RF passive circuits.

To demonstrate the proposed test methodology, simulation results are shown for testing a 1.18-GHz high-pass filter by analyzing low-frequency time-domain signal of the

order of 60 MHz. In addition, a hardware prototype to test embedded RF low-pass filter (3-dB frequency of 1.45-GHz) at MHz frequencies (of the order of 60 MHz) is illustrated.

1.4.2.1 Proposed Methodology

The proposed test setup is shown in Fig. 1.20. In this test setup a two-tone sinusoidal signal is used as an input for testing RF passive filters. The frequencies of the two tones are selected close to the 3-dB frequency of the filter or close to the most critical frequency of the filter’s performance. The output from the filter is down-converted to a lower frequency signal through a test board. The test board comprises a down-conversion RF mixer and a low-pass filter.

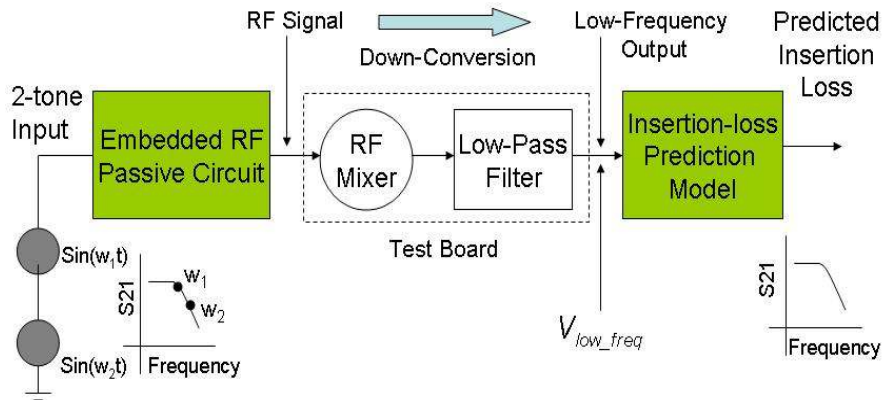


Fig 1.20 The proposed test setup of the methodology using sinusoidal inputs.

The low-frequency signal or test signature (V_{low_freq}) at the output of the test board is analyzed in the time-domain. The preliminary pass-or-fail test decision is performed by defining an allowable maximum and minimum amplitude variation (dV) of V_{low_freq} with respect to the response of the test-setup with a golden filter. Further, for high-resolution testing, the insertion loss over the frequency of operation of the RF filter is predicted using a prediction model. The prediction model is developed using regression analysis with the

help of a training set. In this method also, the training set consists of a few calibrating RF filter samples such that these samples represent variations in the manufacturing process of the embedded RF filters. It should be noted that the development of the prediction model is a one time effort and once it is developed, the insertion loss of the RF filters at GHz frequencies can be predicted from the low-frequency output ($V_{\text{low_freq}}$) of the proposed test-setup. Thus, this method enables production-level testing of RF passive filters without VNAs. In this test approach, MARS is used to develop the prediction model. The prediction model has been developed by mapping the test signature ($V_{\text{low_freq}}$, measurement space (M_s), Fig. 1.6) to the insertion loss of the RF filter (specification space (S_s)).

1.4.2.2 Simulations Results

This section demonstrates the testing of a RF low-pass filter (3-dB frequency of 1.30 GHz) and a RF high-pass filter (3-dB frequency of 1.18 GHz) at 60 MHz. All simulations have been performed in Advance Design System (ADS) and prediction model development was performed in MATLAB.

1.4.2.2.1 RF High-Pass Filter Modeling

Let us consider seven samples of 1.18-GHz RF high-pass filter. Shift in the insertion loss of these high-pass filters for variations in their capacitance (Ca) and inductance (La) is shown in Fig. 1.21. Among these filter samples, it is assumed that Filter F3 is a golden filter with $Ca = 1.22$ pF and $La = 8.6$ nH. Let us also assume that F2b ($Ca = 1.05$ pF, $La = 8.6$ nH), F2a ($Ca = 1.05$ pF, $La = 8.0$ nH), F4b ($Ca = 1.35$ pF, $La = 8.6$ nH) and F4a ($Ca = 1.35$ pF, $La = 9.2$ nH) are marginally good filter samples, while the bad filter

samples are F1 ($C_a = 0.9$ pF, $L_a = 7.5$ nH) and F5 ($C_a = 1.50$ pF, $L_a = 10.5$ nH). The aim of this testing methodology is to differentiate the good and bad samples of the filter.

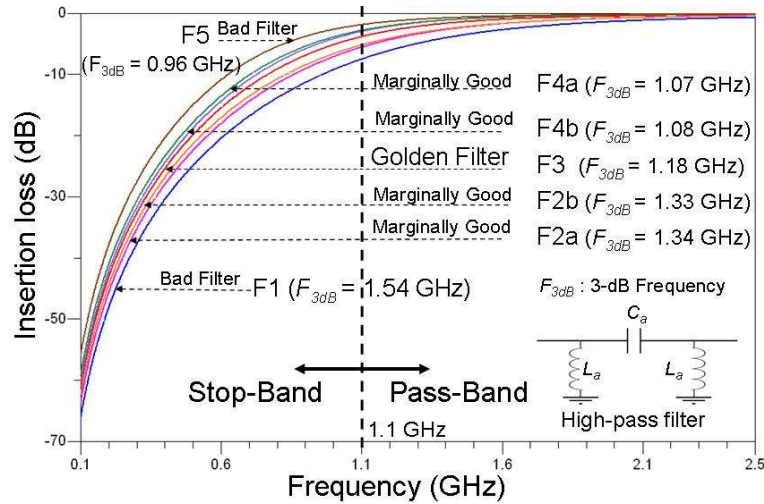


Fig. 1.21 The insertion loss of RF high-pass filter samples to demonstrate test methodology based on input sinusoidal signals.

The above RF filters were tested using the simulation setup, as shown in Fig. 1.22. In this simulation experiment, a two-tone input signal with frequencies 1.21 GHz and 1.23 GHz is used. The ADS’s down-conversion mixer model # MixerWithLo (local oscillator frequency = 1.17 GHz) and low-pass filter model # LPF_Butterworth (3-dB frequency = 80 MHz) were used to complete the simulation test setup.

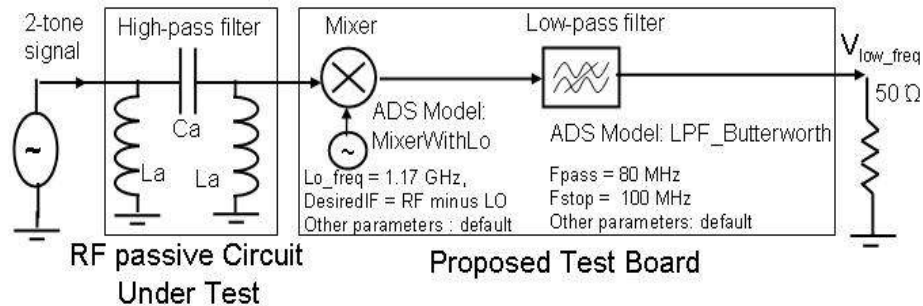


Fig. 1.22. Simulation setup for testing RF high-pass filters using test methodology based on input sinusoidal signals.

When the above RF filters (F1, F2a, F2b, F3, F4a, F4b and F5) were simulated with the proposed test setup, a correlated change in the amplitude of the test-setup response (V_{low_freq} , of the order of 60 MHz) was observed as shown in Fig. 1.23. It can be inferred from the results shown in Fig. 1.23 that the test-setup response for the different samples is around the response of the test-setup with the golden filter F3. Thus, a preliminary pass-or-fail testing of these RF filters is possible by defining the maximum and minimum allowable amplitude variations in V_{low_freq} with respect to the response of the test setup with Filter F3. For example, by considering allowable change in the amplitude (dV) from 350 mV to 510 mV around F3 response at 118 ns, the Filters F1 and F5 can be concluded as bad filters while the Filters F2a, F2b, F4a and F4b as marginally good filters.

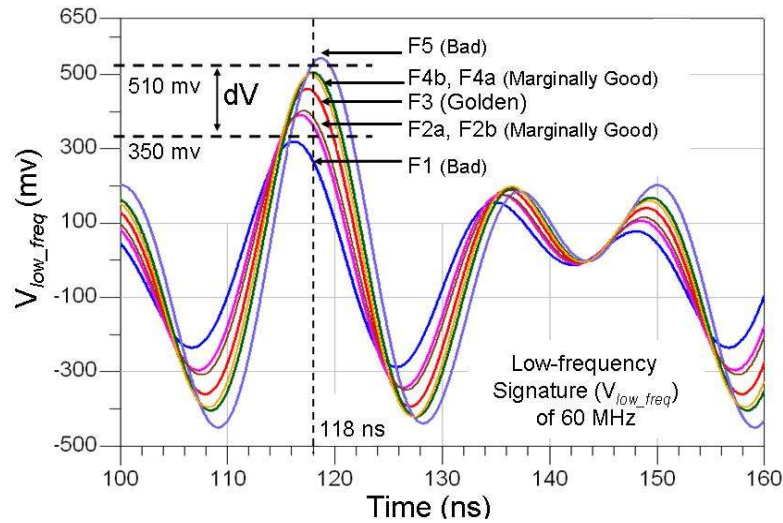


Fig. 1.23. Simulated output for testing RF high-pass filters using method based on input sinusoidal signals.

To demonstrate the high-resolution testing and to distinguish between the marginally good filters, a prediction model was developed using MARS from the responses of 299 calibrating filters. The predicted insertion loss from the 60 MHz time-domain signature

(V_{low_freq}) is shown in Fig. 1.24 for Filters F3, F2a, F2b, F4a and F4b. The average error in the predicted insertion-loss over the range of 0.50 GHz to 1.9 GHz (*stop-band and pass-band*) for all the filters is below 0.02 dB with maximum standard deviation of 0.067 dB. Thus, these results demonstrate that the insertion loss of RF filters can be predicted with good accuracy from the prediction model.

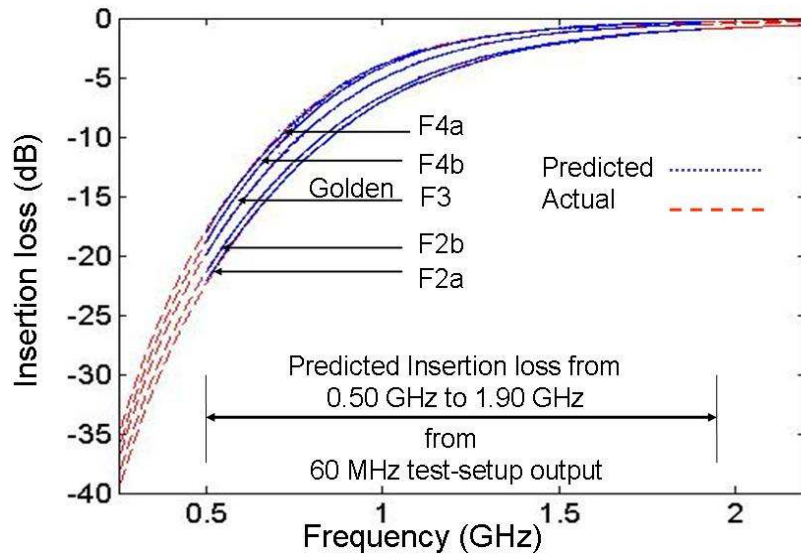


Fig 1.24. Predicted insertion loss of high-pass filter using method based on input sinusoidal signals.

1.4.2.2.2 RF Low-Pass Filter Modeling

To further demonstrate this test methodology, 1.30-GHz low-pass filter (Fig. 1.25) was modeled and tested by using the proposed method. In this example too, Filter F3 is assumed as a golden filter ($C_a = 2.4$ pF, $L_a = 12.4$ nH). While marginally good samples are assumed to be Filters F2b ($C_a = 2.3$ pF, $L_a = 12.3$ nH), F2a ($C_a = 2.2$ pF, $L_a = 12.2$ nH), F4a ($C_a = 2.6$ pF, $L_a = 12.4$ nH) and F4b ($C_a = 2.6$ pF, $L_a = 12.8$ nH). Additionally, it is assumed that Filters F1 ($C_a = 2.0$ pF, $L_a = 12.0$ nH) and F5 ($C_a = 2.8$ pF, $L_a = 12.8$ nH) are bad samples. The simulation test-setup similar to Fig. 1.22 is used to test these RF

low-pass filters as well. A two-tone input signal with frequencies 1.25 GHz and 1.28 GHz, a low-pass filter with 3-dB frequency of 90 MHz, and a local oscillator of frequency 1.22 GHz were used in this simulation experiment. The low-frequency time-domain output (V_{low_freq} of the order of 60 MHz) of the proposed test-setup is shown in Fig. 1.26.

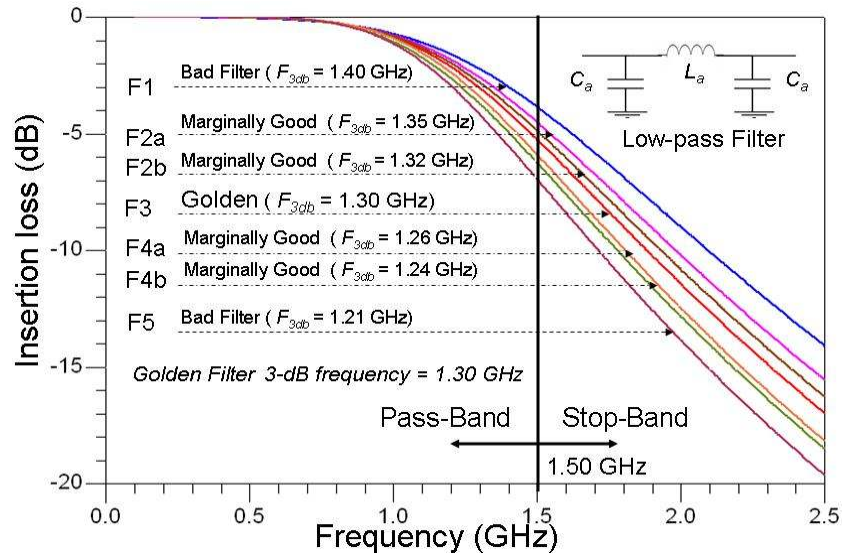


Fig. 1.25 The insertion loss of RF low-pass filter samples to demonstrate the test method based on input sinusoidal signals.

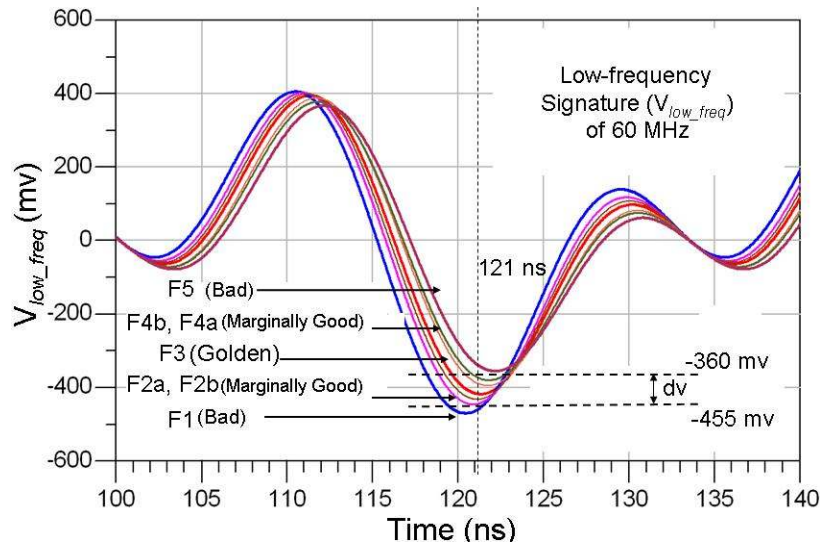


Fig. 1.26. Simulated output for testing RF low-pass filters using the test method based on input sinusoidal signals.

The simulation results (Fig. 1.26) suggest that preliminary pass-or-fail testing of these filters is again possible by defining maximum and minimum amplitude variations with respect to the golden filter (F3) response (dv from -360 mV to -455 mV at 121 ns).

For high resolution testing, prediction model was developed by using a total of 299 calibrating filters. The predicted insertion loss from the low-frequency test signature (V_{low_freq} of the order of 60 MHz) for the filters F2a, F2b, F3, F4a and F4b is shown in Fig. 1.27. The average maximum error in the prediction of the insertion loss within the frequency range of 0.50 GHz to 1.90 GHz (*pass-band and stop-band*) for all the filters is below 0.06 dB with maximum standard deviation of 0.045 dB.

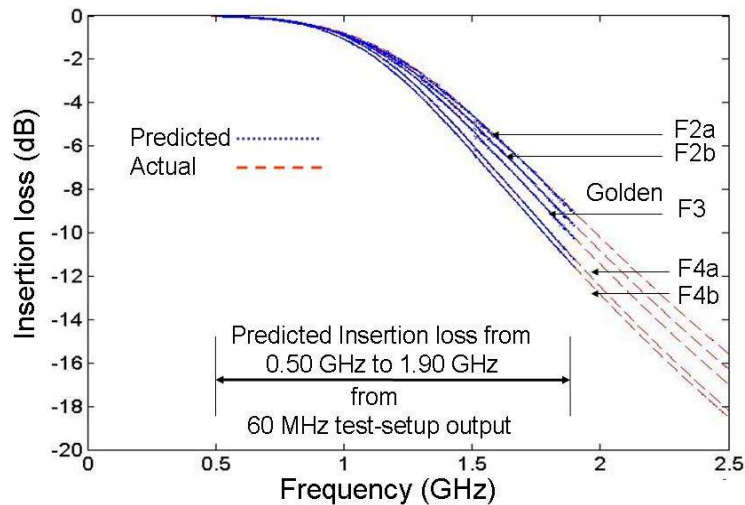


Fig 1.27. Predicted insertion loss of low-pass filter using the test method based on input sinusoidal signals.

1.4.2.3 Measurement Results

In this section, the test method is implemented for testing commercially-available embedded RF low-pass filter (3-dB frequency of 1.45 GHz) at 60 MHz. A hardware test setup is shown in Fig. 1.28. The test board comprises an RF down-conversion mixer

(RFMD # RF2411) and a low-pass filter (Mini-circuit SLP# 90). The input signal is composed of 2-tone sinusoidal signals at 1.46 GHz and 1.49 GHz. The local oscillator frequency of the RF mixer is chosen as 1.43 GHz.

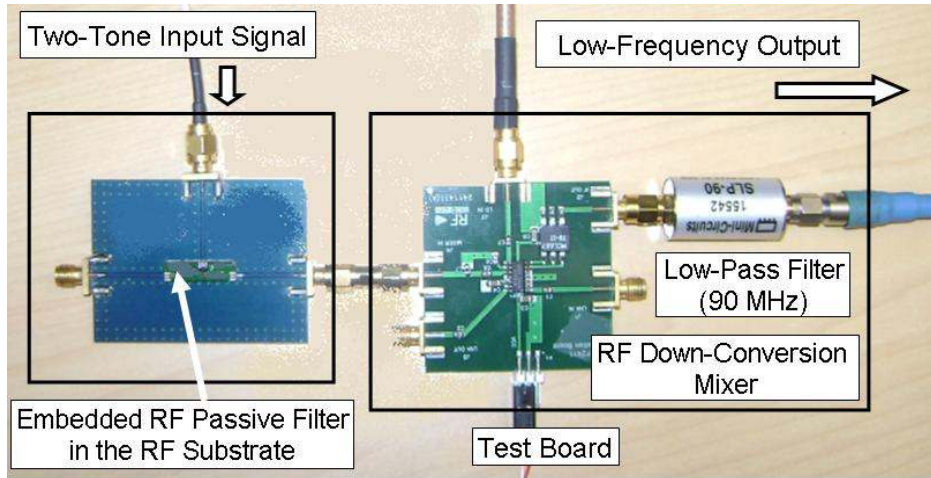


Fig.1.28. A hardware test setup for testing embedded RF low-pass filter using the test method based on input sinusoidal signals

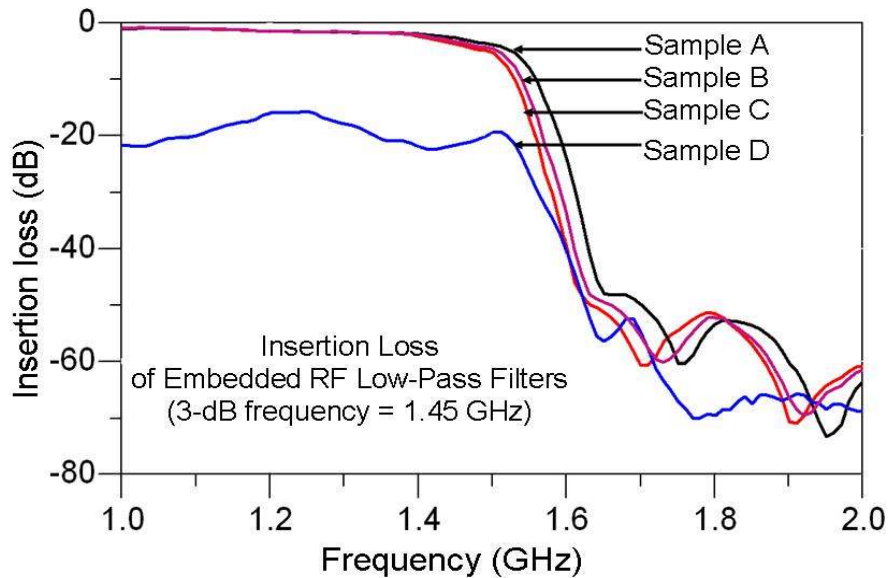


Fig. 1.29. Measured insertion loss of embedded RF low-pass filters to demonstrate the test method based on input sinusoidal signals.

The insertion losses of the embedded filter Samples A, B, C and D are shown in Fig. 1.29 and the measured low-frequency signal (V_{low_freq} of the order of 60 MHz) from the proposed test setup is shown in Fig. 1.30.

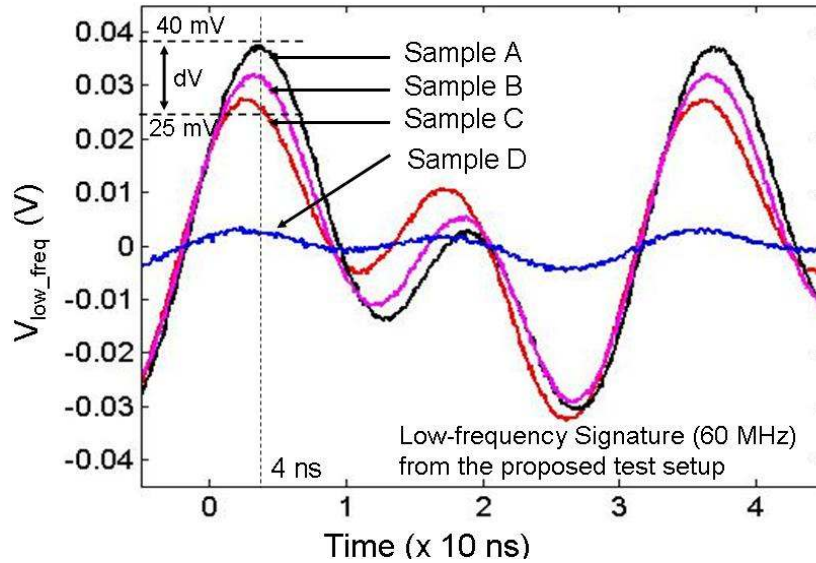


Fig. 1.30. Measured low-frequency output test signature of the proposed test method based on input sinusoidal signals.

It can be inferred from the insertion loss measurements (Fig. 1.29) that Sample D is a bad RF low-pass filter. A similar conclusion can be drawn from the low-frequency output (60 MHz) of the proposed test setup (Fig. 1.30). For example, the amplitude of the time-domain signature at 4 ns for Samples A, B, and C is around 35 mV, while the amplitude for sample D is only 5 mV. Therefore, by defining allowable amplitude variation around the response of the test setup with the golden filter, the pass-or-fail testing of these embedded filters is possible by the proposed test method. For high-resolution testing of these RF filters, prediction model as described in the previous section can be developed.

1.4.2.4 Concluding remarks

The test methodology to test embedded RF passive filters using sinusoidal input signals has been proposed. This methodology enables production-level testing without a VNA. The proposed method is demonstrated in simulations by testing a 1.30-GHz low-pass filter and a 1.18-GHz high-pass filter at low frequencies of the order of 60 MHz. Also, a hardware prototype of the proposed test-setup is demonstrated to test RF embedded low-pass filter (3-dB frequency of 1.45 GHz) at MHz frequencies (of the order of 60 MHz). Based on these experimental results, it is possible to conclude that the proposed methodology can be considered for low-cost testing of embedded RF passive filters.

This methodology eliminates use of a VNA for production-level testing, but it still requires an input RF source to inject test stimulus into the RF passive circuits. To eliminate the need of input sources and VNAs for testing embedded RF filters, third and fourth methodology is proposed. These methodologies are explained in detail in the next chapters.

1.5 SUMMARY OF MAJOR CONTRIBUTIONS OF THIS THESIS

This thesis proposes a multifaceted production test and post-manufacture yield enhancement framework for RF systems. This framework uses low-cost test and post-manufacture calibration/tuning techniques to drive down production test costs and increase the post manufacturing yield of RF circuits/systems. The key contributions of this thesis are as follows and summarized in Fig. 1.31

- 1) A low-cost test methodology based on oscillation principles (feedback) is proposed to test RF passive filters embedded in RF substrates. This methodology enables testing of RF passive filters by two-port measurement without any external input test stimulus. In addition, the testing is possible through low-frequency signal analysis.
- 2) A novel one-port *resonance based test* methodology to test RF passive filters and RF interconnect embedded in RF substrates is proposed. A core innovation is that the technique can detect defects in embedded passives/filters using only one port probe access and eliminates the need of an external RF input test stimulus. Also, in this methodology RF measurements are not required as testing is possible by low-frequency signal analysis.
- 3) A low-cost methodology to test RF active circuits, namely, RF LNA is presented. This methodology is also based on oscillation principles. The proposed method enables the testing of RF (GHz) amplifier by the analysis its low frequency signature (of the order of MHz) and enables their testing without applying any input test stimulus to these amplifiers.

- 4) A novel self-healing methodology is proposed for post-manufacturing yield improvement of RF amplifiers. The proposed methodology introduces the concept of *performance curves*. This methodology does not require the use of external test stimulus for performing self-healing because the stimulus is self-generated by the RF amplifier, with the help of additional circuitry and by using oscillation principles. Subsequently, calibration for the loss of RF amplifier performance due to process variations is performed by adjusting calibration/tuning knobs designed within the RF amplifier. Thus, the proposed methodology enables self-test and self-calibration/correction leading to truly self-healing RF systems.
- 5) For embedded RF mixer, a novel self-healing methodology is proposed. The proposed methodology eliminates the need for the generation of on-chip RF signals exclusively for testing and calibration/correction of RF mixers. In the present methodology, LO port signal is reused at the mixer RF port so that no extra signal generator is required.
- 6) A new yield improvement methodology is proposed for RF substrates with embedded RF passive circuitry. The proposed methodology introduces a concept of package-chip co-design and on-chip calibration of active circuitry for the yield improvement of passive embedded filters that are off-chip.
- 7) A novel variable-gain RF amplifier is proposed for self-healing systems. This amplifier can be used in multi-antenna systems as well. The proposed design of variable-gain amplifier maintains the relative phase (constant phase) of the signal and at the same time maintains the input and output matching of the RF amplifier.

Low cost testing of embedded passives

- Two-Port Oscillation Based (feedback) test for embedded RF passive filters (1).
- Novel One-Port Resonance Based test for Embedded RF passive filters and RF interconnects (2).

Post manufacturing yield improvement of RF Substrates

- Novel methodology that introduces a concept of package-chip co-design and on-chip calibration of active circuitry (6).

Self-healing of RF Systems

- Novel self-healing methodology for RF amplifiers that introduces the concept of performance curve. In this methodology, oscillation principles are used for self-healing (4).
- Self-testing of RF LNA by the analysis of low frequency signal based on oscillation principles (3).
- Novel self-healing methodology for RF mixers. In this methodology, LO signal is reused as RF signal for self-healing (5).
- Novel RF LNA design that enables variable gain while maintaining the constant phase of the signal and input/output matching (7).

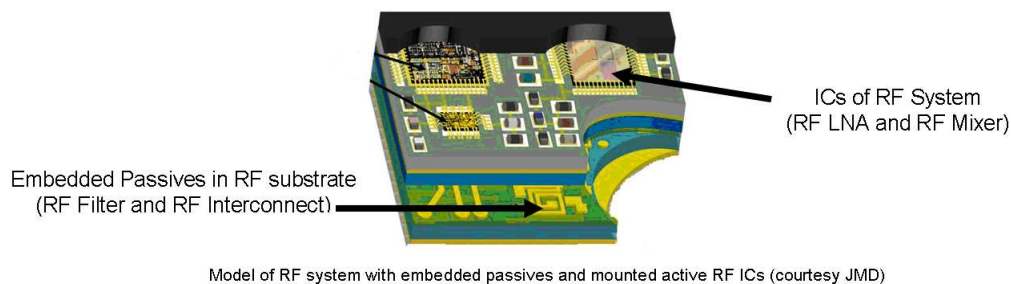


Fig. 1.31. Summary of the major contributions of the thesis

The contents of the thesis are organized as follows. Chapter 2 describes the proposed low-cost techniques for RF substrates with embedded RF passive filters based on oscillation principles. In Chapter 3, novel one-port resonance based low-frequency test methodology is proposed for embedded RF circuits. These test methodologies enable testing without any external test-stimulus. In Chapter 4, a low-cost testing of RF amplifier based on oscillation principle is described. Chapter 5 explains the proposed novel self-healing methodology for RF amplifiers. In Chapter 6, the proposed self-healing methodology for RF mixer is explained. Chapter 7 presents yield improvement methodology for RF substrates. In Chapter 8, novel variable-gain RF amplifier is proposed. Finally, Chapter 9 suggests future research topics consistent with the thesis.

(This page is intentionally left blank)

CHAPTER 2

OSCILLATION BASED TEST OF EMBEDDED RF FILTERS

In this chapter, a low-cost test methodology is proposed for testing integrated RF substrates with embedded RF passive filters. The proposed methodology enables the testing of embedded high-frequency GHz filters by the analysis of low-frequency signal (of the order of 100 MHz). In addition, it allows testing of RF filters without injecting any external test stimulus into the filters. Hence, significant reduction in the test cost is achieved by the proposed test method. The proposed test method relies on three core principles. First, the RF filter is made part of a feedback network of an external RF amplifier circuit located on the probe card, thereby causing the amplifier to oscillate. Second, the output spectrum of the amplifier (GHz) is down-converted to a lower frequency (MHz) to facilitate test response measurement. Third, RF (GHz) specifications of the filters are predicted by the analysis of the low-frequency (MHz) test-setup output. Both parametric and catastrophic failures in the embedded high-frequency (GHz) passive filter can be detected at low-frequency (MHz) by monitoring the change in the oscillation frequency of the proposed test setup. The test method is demonstrated with both simulations and measurements.

2.1 Prior Oscillation Based Test Methods

Test methods without using an input test stimulus based on oscillation (feedback) principle were proposed for analog active filters in [40, 41]. In all these methods, as shown

in Fig. 2.1, analog active filter is converted to an oscillator by either reconfiguring or partitioning using extra components to complete the feedback loop to produce the oscillations. The filters are tested by analyzing the output of the reconfigured active filter. The methods as described in [40, 41] can not be directly applied to test embedded RF passive filters mainly because of the absence of active components and inaccessibility of internal nodes in these passive filters. The test methods using oscillation principles have been demonstrated for testing several active circuits in digital, analog and mixed-signal domains [43-48]. However, the testing of embedded RF passive circuits/components based on oscillation (feedback) principle has not been explored before.

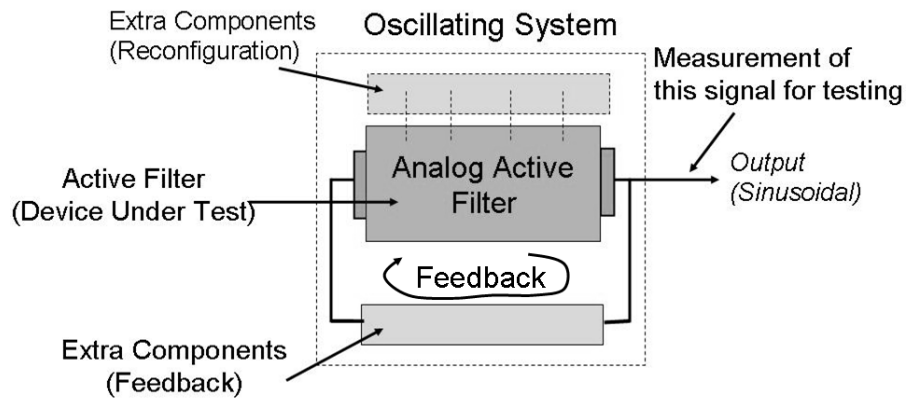


Fig. 2.1. Measurement test-setup of prior oscillation-based test (OBT) methods.

In this chapter, as shown in Fig. 2.2, a method based on oscillation principles (feedback) is proposed for testing RF passive filters, but in this method, the RF passive filter is made part of the feedback network of an external RF amplifier located on the probe card. This feedback causes the RF amplifier to become unstable thereby enabling self-generation of the test signal in the form of oscillations. Thus, this test approach eliminates the need for external RF test-signal generator to inject test stimulus in RF

passive filters for testing purposes. As compared to the prior oscillation-based test-setups (as in Fig. 2.1), a calibration adjustment is introduced in the proposed test setup to enable calibration capability in the RF test environment and to efficiently implement the test method for panel-level testing. In addition, output of the oscillating system (RF amplifier with the RF filter in its feedback) is down converted such that GHz filters can be tested by the analysis of low-frequency signals and with a higher resolution. In the proposed method, it is shown that it is possible to predict RF specifications of these GHz filters from the low-frequency output of the proposed test-setup.

As compared to the aforementioned methods to test embedded RF filters at the production floor, the proposed method eliminates measurements at RF frequencies, injection of any external RF-input test stimulus to the RF filters and the need of RF instruments such as a VNA.

2.2 Proposed Methodology

The proposed test methodology is based on three core principles. First, the RF filter is configured to be a part of the feedback network of an external RF amplifier circuit located on a probe card, thereby generating test signature by forcing the amplifier to oscillate around a frequency that is a statistical function of the RF filter characteristics. Second, the output response of the RF (GHz) amplifier is down-converted to a lower frequency of the order of 100 MHz to enable low-frequency testing and to increase sensitivity towards parametric failures. Third, GHz specification of the filters is predicted by the analysis of the low-frequency (MHz) test-setup output. In the proposed test setup, a calibration

adjustment is also introduced to account for unknown parasitics at RF frequencies and to ease the design of the probe card.

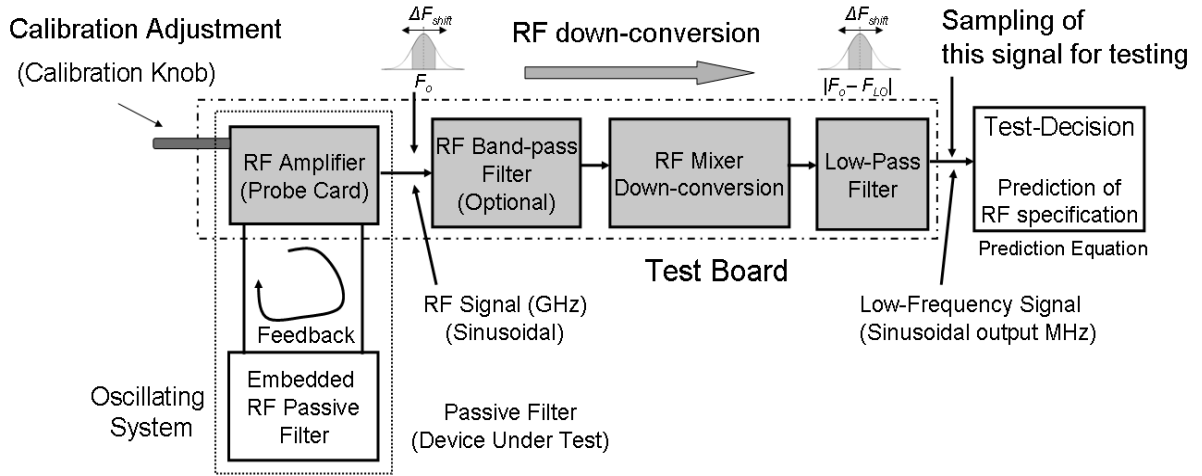


Fig. 2.2. The proposed test-setup of two-port feedback based oscillation test methodology.

2.2.1 Test Setup Design

The first step towards designing the proposed setup involves designing a closed-loop system that comprises the RF amplifier and RF passive filter under test (DUT). This closed-loop system is designed such that the presence of the DUT in the feedback of the RF amplifier, forces the amplifier to become unstable and it generates oscillations. Oscillations in a feedback network are governed by the well known Barkhausen criterion. According to this criterion, the signal must traverse the feedback loop with no phase shift and with no attenuation for the system to oscillate. The oscillation requirement for the matched load and unilateral amplifier using S-parameters can be represented by Equation (2.1) as given in [68]:

$$S_{21A} \cdot S_{21R} = 1 \quad (2.1)$$

where S_{21A} is the amplifier forward transmission S-parameter and S_{21R} is the feedback network forward transmission S-parameter.

In the proposed test approach, the feedback network is the embedded RF passive filter (DUT), thus in Equation (2.1), S_{21R} is replaced by insertion-loss of the RF filter (S_{21F} , forward transmission S-parameter). Because of the process variations the performance of the RF filter changes and thus the closed-loop feedback also changes which causes change in the oscillation frequency of the test-setup.

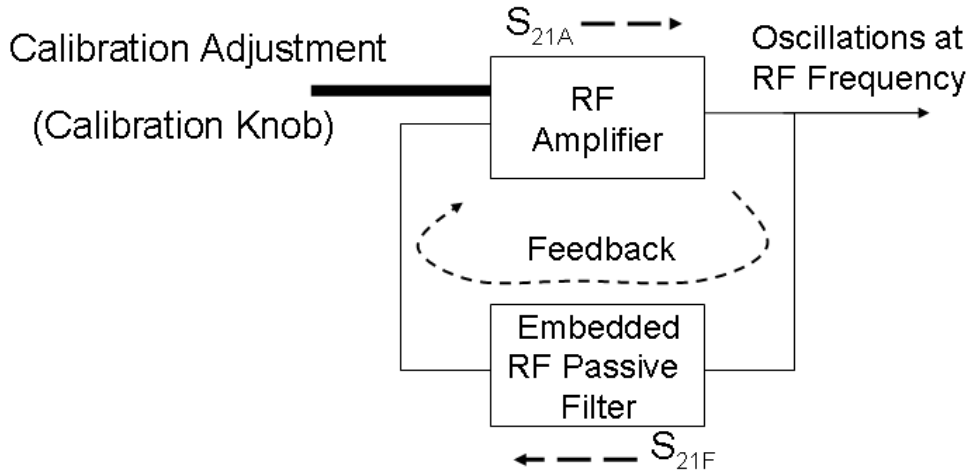


Fig. 2.3. The closed-loop system with a calibration knob to calibrate oscillation frequency of the test-setup.

Designing an RF closed-loop system to oscillate at the desired frequency is quite challenging [68,69] mainly because of unknown RF parasitics. At RF frequencies, even the lengths of the cables used in the measurement set-up affect the oscillation condition. To illustrate the effect of the lengths of the RF cables, consider that RF filter is connected to the RF amplifier as shown in Fig. 2.4 by using a loss-less RF cable of length “ L_{RF} ”. Since S-parameters depend on the selection of the reference plane, the forward

transmission S-parameter (S_{21A}) of the RF amplifier is no longer S_{21A} , but changes to S_{21A}^m as given by Equation (2.2) and changes the oscillation condition of the closed-loop system. Equation (2.2) can be derived using theory of shift in reference plane as given in [70].

$$S_{21A}^m = e^{-jQ_1} e^{-jQ_2} S_{21A} \quad (2.2)$$

where, S_{21A} is original forward transmission S-parameter coefficient of RF amplifier and S_{21A}^m is translated forward transmission S-parameter coefficient. Also, Q_1 or $Q_2 = \beta \cdot L_{RF}$ is the electrical length of RF cables, where L_{RF} is the physical length of the RF cables and β is the propagation constant.

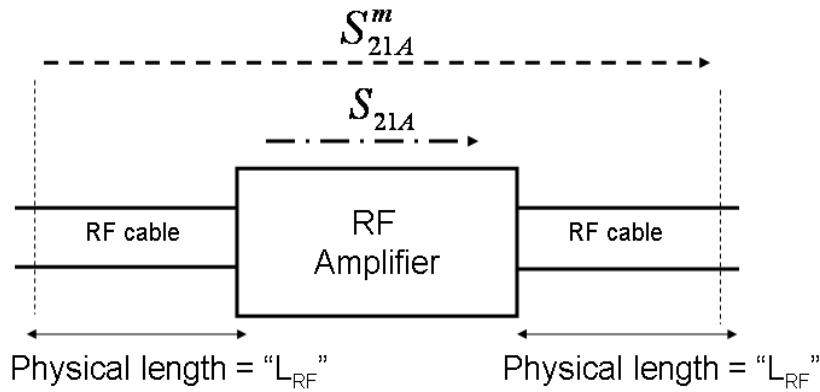


Fig. 2.4. Effect of RF cable length on the forward transmission S-parameter of an RF amplifier.

In addition to the RF cable length, RF parasitics such as capacitive or inductive coupling also changes the oscillation condition. The modeling of these RF parasitics on the production floor is not a simple task. Thus, to ease the design of the test-setup and to account for the effect of RF parasitics and RF cable length, a calibration/tuning adjustment is proposed in the test-setup, as shown in Fig. 2.3 and Fig. 2.4.

This calibration adjustment is implemented in the test setup by designing a calibration knob, which provides a mechanism to calibrate the oscillation frequency of the closed-loop system (RF amplifier with RF filter). The calibration knob is designed in the RF amplifier and it is controlled by a DC voltage such that it changes the oscillation frequency of the test-setup as DC voltage changes. This knob can be implemented considering the complete closed-loop system as a voltage-controlled oscillator. For demonstration purposes, we have implemented the calibration knob using a varactor. The varactor can be attached to one of the nodes of the RF amplifier which controls the amplifier's gain.

In this test method, the RF amplifier with calibration adjustment is designed in a manner that:

- 1) It can oscillate at the desired test frequency after incorporating the embedded RF passive filter. The oscillation frequency can be fine-tuned using a calibration knob. The oscillation frequency can be chosen close to the frequency that is a statistical function of the RF filter characteristics.

- 2) The oscillation frequency of the test board changes based on good and faulty filter samples and the oscillation frequency is measurable using low-cost measurement instruments. The RF amplifier can be designed such that catastrophic failures in the embedded filter cause no oscillations to occur while parametric faults in the embedded filter cause a shift in the oscillation frequency around the response of the golden filter.

An estimation of the maximum allowable shift in the oscillation frequency is performed by using a few calibrating filter samples. In practice, such calibrating filter samples are selected from different production lots and across a large number of panels such that they

represent the variations in the performance of the filters due to the fabrication process. For simulations, a statistical analysis like Monte Carlo can be used to obtain such filter samples.

Once the external feedback circuit is designed and an estimation of shift in the oscillation frequency due to parametric defects has been made, the test board can be designed with RF band-pass filter, RF down-conversion mixer and low-pass filter. The design procedure should ensure that the oscillation frequency of the test board has immunity to the power supply variations as described in [42, 68]. The RF band-pass filter is optional and it is used to restrict the band of frequencies at the input of RF mixer to avoid image problems [69]. The local oscillator frequency of the RF mixer can be chosen according to Equation (2.3) and the cut-off frequency of the low-pass filter can be chosen according to Equation (2.4).

$$F_{LO} < F_{\min} \quad (2.3)$$

$$F_{low_pass} > F_{LO} - F_{\max} \quad (2.4)$$

In the above equations (2.3) and (2.4), F_{\min} and F_{\max} are the estimated minimum and maximum oscillation frequencies of the closed-loop system due to manufacturing defects, F_{LO} is local oscillator frequency of the RF mixer, and F_{low_pass} is the cut-off frequency of the low-pass filter.

The resolution (R_m) to measure the shift in the oscillation frequency of the test setup can be defined by equation (2.5):

$$R_m = \Delta F_{shift} / F_{golden} \quad (2.5)$$

where F_{golden} is the oscillation frequency of the test-setup with the golden filter, and ΔF_{shift} is the shift in the oscillation frequency of the test-setup relative to the response of the test setup with the golden filter. In this method, the down-conversion of the RF amplifier output preserves the shift in the oscillation frequency (ΔF_{shift}), but reduces the frequency of the measurement from the GHz range ($F_{golden} = F_0$) to the MHz range ($F_{golden} = |F_0 - F_{LO}|$). Hence, the resolution (R_m) for detecting ΔF_{shift} increases.

2.2.2 Test Decision

In this method, good filter samples are differentiated from faulty filter samples by careful analysis of the shift in the oscillation frequency of the test setup with respect to its response with the golden filter. For preliminary pass-or-fail testing, an allowable shift in the oscillation frequency of the test-setup is defined by using Monte Carlo simulations or by using few calibrating filter samples.

Sensitivity (S_{sen}) of the proposed test setup towards the change in the performance of the RF filter is defined as:

$$S_{sen} = \Delta f_{spec} / \Delta f_{osc} \quad (2.6)$$

where Δf_{osc} is the change in the oscillation frequency of the test-setup and Δf_{spec} is the change in the specification of the RF filter. Δf_{spec} can be the change in 3-dB frequency for low-pass and a high-pass filter, or centre frequency for band-pass filter. Depending on the

resolution of testing, S_{sen} can be increased or decreased by appropriately designing the RF amplifier.

By this method, prediction of RF specification (f_{spec}) of the passive filters can be performed using low-frequency output of the test-setup by proper design of the RF amplifier. This prediction can be used for high-resolution specification-based testing. Since the change in the oscillation frequency of the amplifier is related to the change in the performance of the RF filter and down-conversion of the RF amplifier preserves this change in the oscillation frequency, the estimation of RF specification (f_{spec}) becomes possible by the oscillation frequency of the test setup. The estimation of f_{spec} is done by integrating (2.7):

$$f_{spec} = \int S_{sen} * df_{osc} \quad (2.7)$$

$$f_{spec} = (S_{sen}) * f_{osc} + K \quad (2.8)$$

where K is a constant and S_{sen} is the sensitivity of the test-setup, f_{spec} is RF specification and f_{osc} is the frequency of the sinusoidal output of the test setup. Equation (2.8) can be found by plotting f_{osc} and f_{spec} and then using linear curve fitting. Response of few calibrating filters which can represent parametric variations should be used to derive equation (2.8). This equation will be referred as the “prediction equation” in this chapter.

2.3 Simulations Results

In this section, the test strategy is demonstrated by testing and modeling RF high-pass and band-pass filters.

2.3.1 RF High-Pass Filter Modeling

In this sub-section, RF high-pass filter (3-dB frequency of 1.24 GHz) was modeled, seven filter samples were considered and simulation setup as shown in Fig. 2.5 was used. The insertion loss of RF filters for the different values of inductance (L_a) and capacitance (C_a) is shown in Fig. 2.6. It is assumed that H4 is the golden filter ($C_a = 1.20$ pF, $L_a = 7.50$ nH), filters H2, H3, H5, H6 are marginally good filters, and H1 ($C_a = 1.10$ pF, $L_a = 7.20$ nH) and H7 ($C_a = 1.31$ pF, $L_a = 7.81$ nH) are bad high-pass filters.

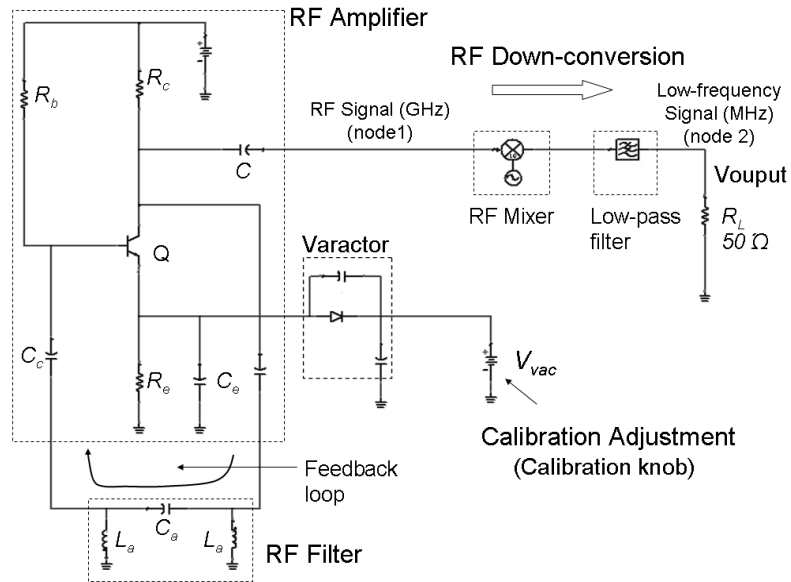


Fig. 2.5. A proposed simulation test setup of two-port Feedback based test methodology.

To demonstrate the calibration adjustment in the test-setup, voltage at the calibration knob (V_{vac}) was changed and the variation in the oscillation frequency at the output of the RF amplifier (node 1, Fig. 2.5) for golden Sample H4 is shown in Fig. 2.6. It can be inferred from this result that the oscillation frequency of RF amplifier with RF filter in its feedback can be fine tuned by varying V_{vac} .

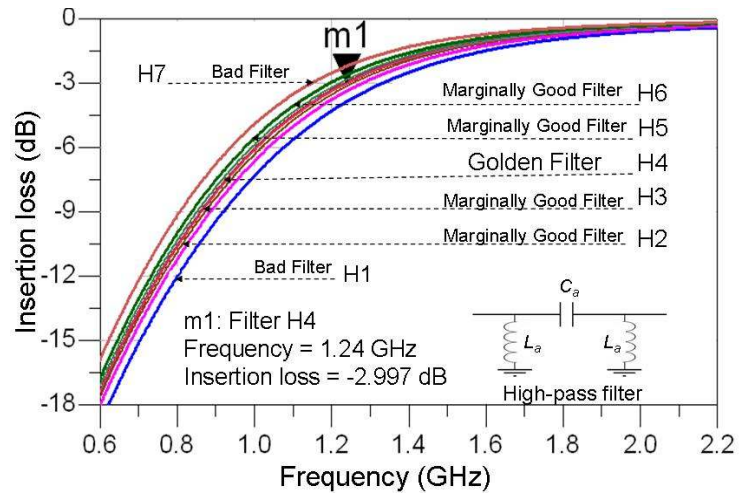


Fig. 2.6. Insertion loss of the RF high-pass filters.

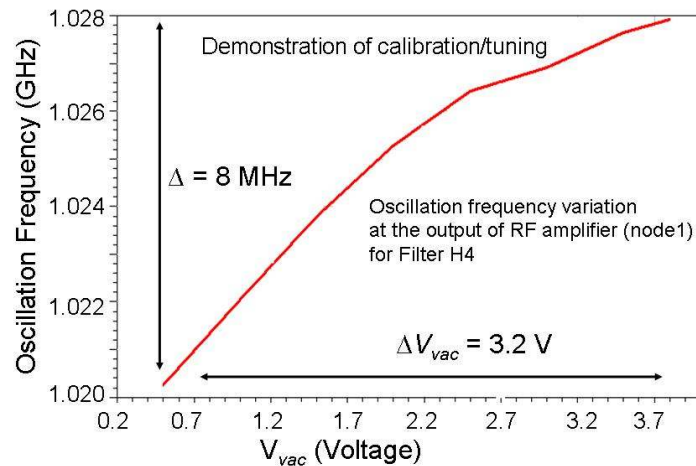


Fig. 2.7. Calibration of the oscillation frequency at the output of the RF amplifier (node1, Fig. 3.5) using DC controlled knob.

When all the samples of RF high-pass filter were simulated as shown in Fig. 2.5, a corresponding change in the oscillation frequency at the output of the test setup was observed. The obtained results are summarized in Table 2.1, where it can be inferred that the oscillation frequency of the test setup is around the response of the golden high-pass filter, H4. Thus, pass-or-fail testing is possible for these RF high-pass filters by defining an allowable shift in the oscillation frequency around the response of the golden filter. For

example, for the allowable shift of ΔF_{shift} from + 25 MHz to – 25 MHz around 63.82 MHz, Filters H1 and H7 can be differentiated as bad samples and H2, H3, H5 and H6 as marginally good RF high-pass filter samples. It can also be noted from Table 2.1 that the resolution (R_m) to measure ΔF_{shift} at the RF amplifier's output is 0.05 ($\Delta F_{shift}/F_{0_amp} = 50$ MHz/1.02 GHz) while R_m at the output of the proposed test setup is 0.78 ($\Delta F_{shift}/F_{0_oput} = 50$ MHz /63.82 MHz). Hence, the resolution to measure the shift in oscillation frequency is increased by a factor of approximately 15 as a result of down-converting the output of the RF amplifier.

Table 2.1: Test Result For the RF High-Pass Filter Using The proposed oscillation based test method

RF filter	Filter's 3-dB frequency (f_{spec})	Filter's Classification	RF amplifier's output frequency (node 1)	Output Frequency of the test-setup (f_{osc})
H1	1.33 GHz	Bad	1.08 GHz	119.70 MHz
H2	1.28 GHz	Marginally Good	1.05 GHz	87.30 MHz
H3	1.26 GHz	Marginally Good	1.03 GHz	73.76 MHz
H4	1.24 GHz	Golden Filter	1.02 GHz (F_{0_amp})	63.82 MHz (F_{0_oput})
H5	1.22 GHz	Marginally Good	1.01 GHz	54.11 MHz
H6	1.20 GHz	Marginally Good	1.00 GHz	41.62 MHz
H7	1.15 GHz	Bad	0.97 GHz	10.80 MHz

To estimate the 3-dB frequency (f_{spec}) of the good filters from the test-setup output (f_{osc}), the responses of filters H1, H2, H6 and H7 were used and a prediction equation was derived, which is shown in Fig. 2.8. The estimated 3-dB frequencies of the filters H3, H4 and H5 are given in Table 2.2 and it can be noticed that the predicted 3-dB frequency from the MHz signal is quite accurate as the error in the prediction is less than 1%.

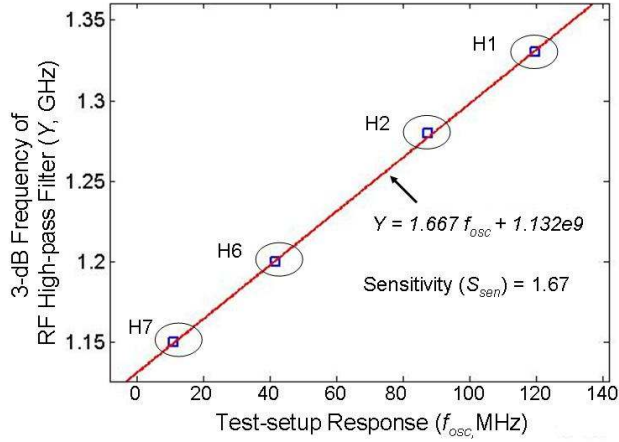


Fig. 2.8. Test-setup response vs 3-dB frequency of the RF high-pass filter to derive prediction equation

Table 2.2: Estimated 3-dB Frequency For low-frequency output

RF High-pass filter	Filter's (3-dB frequency) (f_{spec})	Test-setup Oscillation Output (f_{osc})	Estimated or Predicted $Y = 1.667 * f_{osc} + 1.132e9$	
			3-dB frequency (Y)	% error in Estimation $(f_{spec} - Y) / f_{spec} \%$
H3	1.26 GHz	73.76 MHz	1.255 GHz	0.4%
H4	1.24 GHz	63.82 MHz	1.238 GHz	0.2%
H5	1.22 GHz	54.11 MHz	1.222 GHz	-0.2%

2.3.2 RF Band-Pass Filter Modeling

The testing methodology is further demonstrated by modeling and testing of RF band-pass filter (center frequency = 1.80 GHz and band-width = 300 MHz). In this example, seven samples of RF filters were considered using the topology shown in Fig. 2.9. The test-setup similar to Fig. 2.5 is used and the results obtained are summarized in Table 2.3 and Table 2.4. It is assumed that B4 is a golden filter ($C_a = 2.2$ pF, $L_a = 2.5$ nH, $C_c = 0.7$ pF, $C_f = 0.4$ pF). Filters B2, B3, B5 and B6 are marginally good filters. The bad band-pass

filters are B1 ($C_a = 2.12$ pF, $L_a = 2.42$ nH, $C_c = 0.67$ pF, $C_f = 0.38$ pF) and B7 ($C_a = 2.28$ pF, $L_a = 2.58$ nH, $C_c = 0.72$ pF, $C_f = 0.41$ pF).

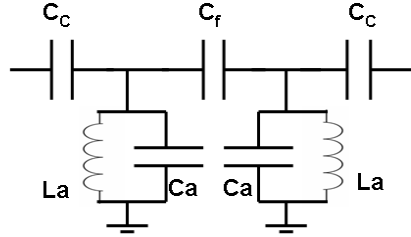


Fig. 2.9. Modeling of RF band-pass filter.

It can be deduced from the results shown in Table 2.3 that the oscillation frequency of the simulation test setup is again around the response of the golden filter, B4. Hence, for allowable ΔF_{shift} from + 40 MHz to - 40 MHz, the RF band-pass filters can be categorized as bad or marginally good. It can again be noticed that the resolution (R_m) to measure the shift in the oscillation frequency of the test setup increases by down-converting the RF amplifier's output. Similar to the previous sub-section, Samples B1, B2, B6 and B7 were used to drive the prediction equation and the estimated center frequency for Samples B3, B4 and B5 is given in Table 2.4.

Table 2.3 Results to Test RF Band-Pass Filter by The Proposed Method

RF filter	Filter's centre frequency (f_{spec})	Filter's Classification	RF amplifier's output frequency (node 1)	Output Frequency of the test-setup (node 2)
B1	1.85 GHz	Bad	1.80 GHz	122.10 MHz
B2	1.84 GHz	Marginally Good	1.78 GHz	96.37 MHz
B3	1.82 GHz	Marginally Good	1.75 GHz	73.38 MHz
B4	1.80 GHz	Golden Filter	1.74 GHz (F_o_{amp})	58.99 MHz (F_o_{oput})
B5	1.78 GHz	Marginally Good	1.73 GHz	45.35 MHz
B6	1.75 GHz	Marginally Good	1.70 GHz	23.18 MHz
B7	1.73 GHz	Bad	1.68 GHz	4.20 MHz

Table 2.4: Estimated Centre Frequency of Band-Pass Filter from low-frequency test- setup output

RF filter	Filter's (Centre frequency) (f_{spec})	Test-setup Oscillation Output (f_{osc})	Estimated or Predicted $Y = 1.074 * f_{osc} + 1.727e9$	
			Centre frequency (Y)	% error in Estimation $(f_{spec} - Y) / f_{spec} \%$
B3	1.82 GHz	73.38 MHz	1.806 GHz	0.8%
B4	1.80 GHz	58.99 MHz	1.790 GHz	0.6%
B5	1.78 GHz	45.35 MHz	1.776 GHz	0.2%

2.4 Measurement Results

In this sub-section, the test method is implemented for testing commercially-available integrated RF substrates with embedded 4th-order 1.45-GHz RF passive low-pass filters. The samples of integrated RF substrates were provided by JMD Inc (Atlanta). The test method is demonstrated at both card level and panel/wafer level. For panel-level testing, a hardware prototype with a provision for calibration adjustment has been demonstrated. By this experiment, it is demonstrated that testing of GHz passive filters is possible by the analysis of low-frequency signal of the order of 60 MHz. It is also demonstrated that the sensitivity to detect faulty embedded filters increases by down-converting the output of the RF amplifier.

2.4.1 Testing at Card Level

Card-level testing of the RF filter is demonstrated by four samples (A, B, C, and D). The hardware test setup similar to Fig. 2.10 is used in this section as well. The insertion-loss profile of the embedded filter samples is shown in Fig. 2.11 and the response of the test setup for these RF filter samples is shown in Fig. 2.12.

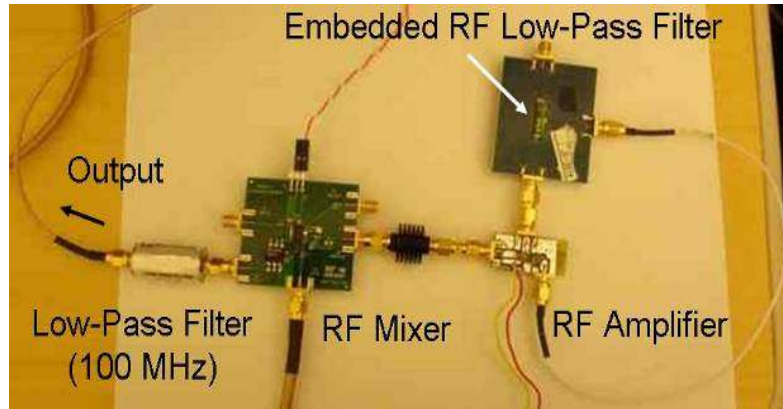


Fig. 2.10. A hardware test setup for a card-level testing of RF embedded filters by the two-port feedback based oscillation test method.

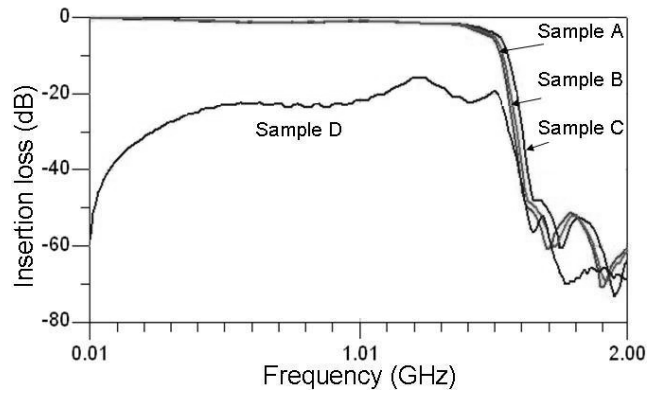


Fig. 2.11. Measured insertion-loss of embedded RF low-pass filters.

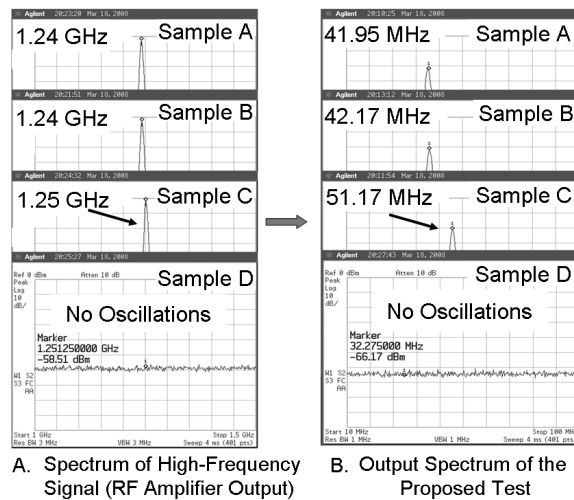


Fig. 2.12. Measurement result for the card-level testing of the embedded RF low-pass filters.

From the insertion-loss profile of the different filter samples (Fig. 2.11), it can be concluded that Sample D has a catastrophic failure and is a faulty RF low-pass filter. A similar conclusion can be drawn using the proposed test method as no oscillation occurs at the output of the test setup for Sample D (Fig. 2.12). In addition, it can be inferred from the results shown in Fig. 2.11 and Fig. 2.12 that it is possible to test these filters since the oscillation frequency of the proposed test setup changes with variations in the insertion-loss profile of the filter.

2.4.2 Testing at Panel/Wafer Level

A test-setup with a calibration adjustment is demonstrated and prediction of 3-dB frequency of GHz low-pass filters from a low-frequency (MHz) test-setup output is also shown. In this test setup, an RF amplifier with a calibration knob was assembled on a probe card and it was directly mounted on RF probes as shown in Fig. 2.13.

The samples of the embedded RF low-pass filter were randomly probed at different locations of the fabricated panel as shown in Fig. 2.14. This figure also shows insertion loss of these samples. The panel of integrated RF substrate has 102 samples of embedded RF low-pass filter. The measured output oscillation frequencies of the test setup for different samples of the embedded filter are shown in Fig. 2.16. and the summary is given in Table 2.5.

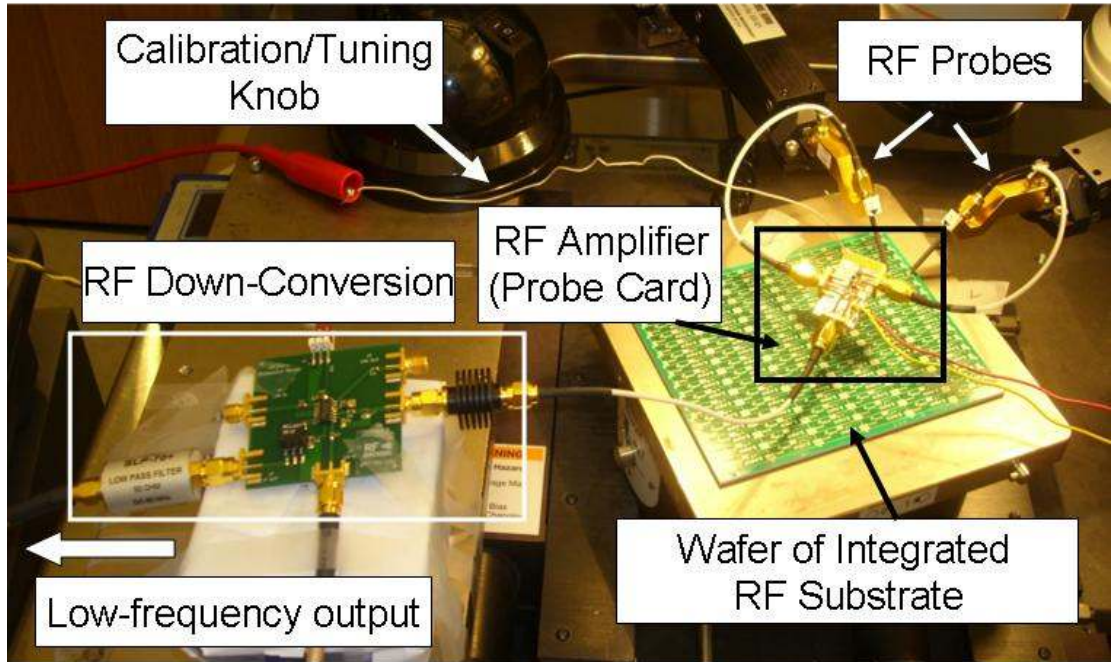


Fig. 2.13. A hardware test setup of the proposed method for a panel-level testing of integrated RF substrates.

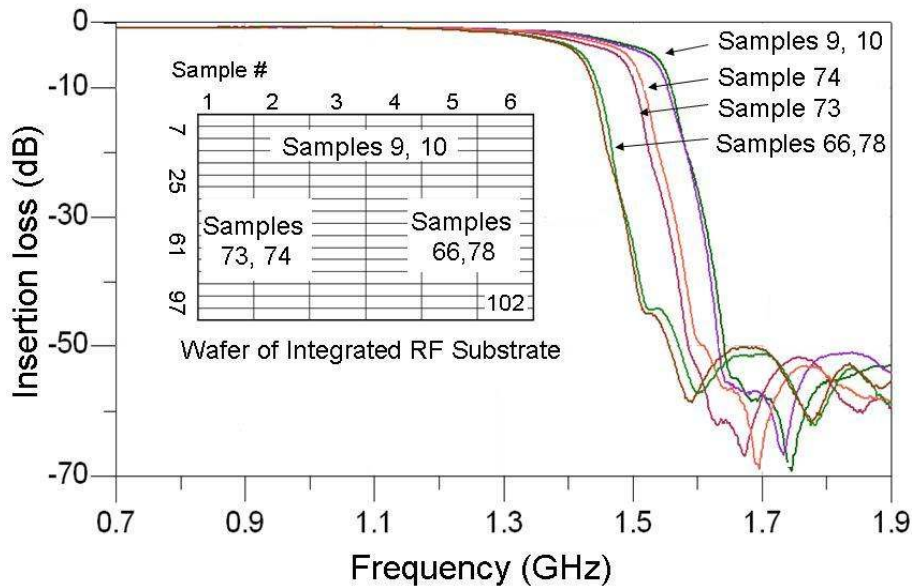


Fig. 2.14. Insertion loss of embedded RF low-pass filter samples at three different locations of the panel of integrated RF substrate.

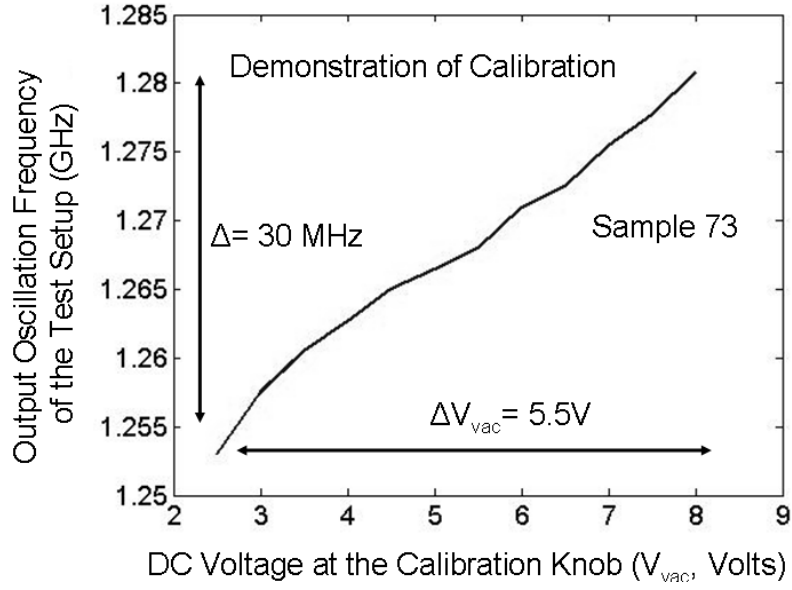


Fig. 2.15. Tuning of the oscillation frequency at the output of the probe card using DC voltage at the calibration knob.

To demonstrate the calibration in the test setup, the probing of filter Sample 73 was considered. The DC voltage at the calibration knob (Fig 2.13) was varied and the corresponding oscillation frequency at the output of the RF amplifier was obtained as shown in Fig. 2.15. It can be inferred from this experimental result that it is possible to fine tune the oscillation frequency of the probe-card using the proposed calibration adjustment.

Table 2.5 Summary of The Measurement For Panel-Level Testing of The Embedded filters by The proposed oscillation based test method

RF Low-pass filter	Filter's Specification (3-dB Frequency) (f_{spec})	Proposed Test Setup	
		Output of the oscillating RF amplifier	Output of the proposed test-setup (f_{osc})
Sample 09	1.50 GHz	1.29 GHz	49.60 MHz
Sample 10	1.49 GHz	1.29 GHz	48.00 MHz
Sample 73	1.44 GHz	1.27 GHz	33.20 MHz
Sample 74	1.46 GHz	1.28 GHz	37.00 MHz
Sample 78	1.41 GHz	1.26 GHz	18.00 MHz
Sample 66	1.40 GHz	1.26 GHz	16.40 MHz

It can be inferred from the Table 2.5 and Fig. 2.14 that the test setup has almost the same output oscillation frequency for the samples which have similar insertion loss profiles. Also, the test method gives different output oscillation frequencies if the insertion loss profile differs. For example, the output oscillation frequency for Samples 09 and 10 is around 50 MHz, while for Samples 78 and 66 the output oscillation frequency is around 17 MHz. Also, it can be noticed that Samples 09 and 10 cannot be distinguished by the analysis of the output of the oscillating RF amplifier, but these samples can be distinguished after down-converting the RF amplifier output. Thus, testing of the GHz filters by low-frequency signal analysis provides higher resolution to the test.

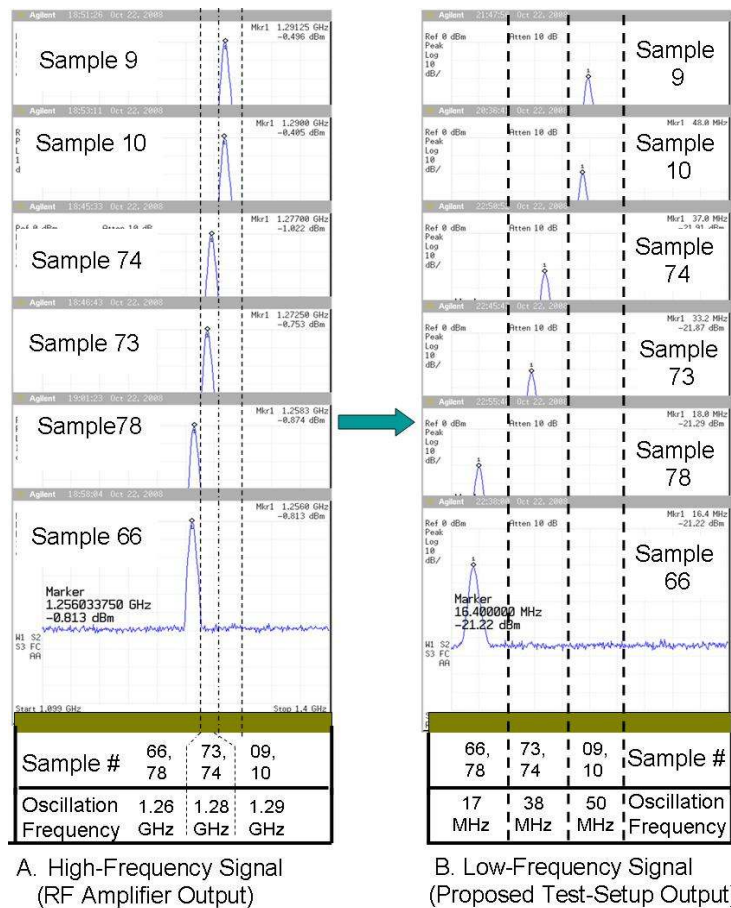


Fig. 2.16. Measured response for a panel-level testing by two-port Feedback based methodology.

To demonstrate the prediction of 3-dB frequency of the filters from the low-frequency sinusoidal output of the test-setup, measurements of all the 102 samples of the embedded RF filters were performed. Out of the 102 samples, 51 samples were selected as calibrating filters and used to obtain prediction equation ($f_{spec} = 3.376 * f_{osc} + 1.341e09$, Fig. 3.17) while the remaining 51 samples were used to validate the proposed approach. The predicted 3-dB frequency (GHz) from the low-frequency test-setup output (60 MHz) is shown in Fig. 2.18. The mean percentage error in the prediction is 0.26% with a standard deviation of 0.24% which shows reasonable accuracy in the predictions.

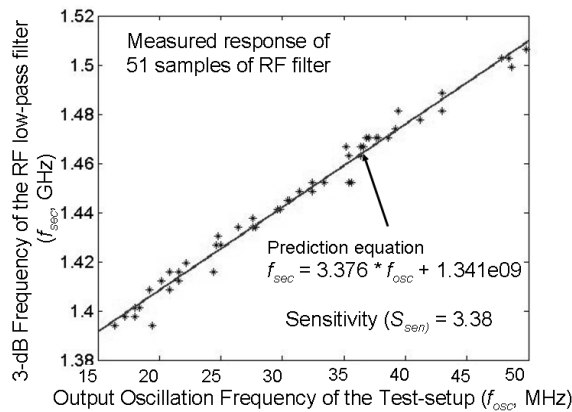


Fig. 2.17. 3-dB frequency of embedded low-pass passive filters vs. output of the proposed test-setup to obtain a prediction equation.

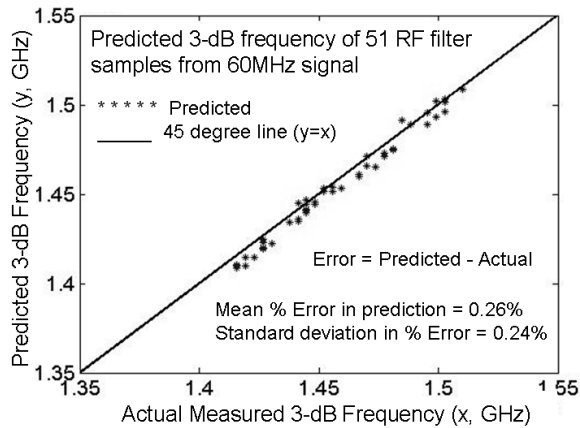


Fig. 2.18. Predicted vs. Actual 3-dB frequency of the embedded low-pass passive filters using 60 MHz test-setup output signal.

2.5 Discussions

In this section some practical considerations and guidelines are discussed for successful and efficient implementation of the proposed test method for production-level testing. Also, this section compares the proposed test-setup cost/capability as compared to the conventional test-setup that uses VNA, studies measurement noise (repeatability), and stability of the proposed test setup.

2.5.1 Measurement noise or repeatability of the test results

To estimate the measurement noise or repeatability of results, the following experiment was conducted. In this experiment, a mechanical RF probe station (Cascade # 9000) was used and 114 measurements were conducted for Sample 09 during panel-level testing. The oscillation frequency of the test setup for these measurements and summary of the results are shown in Fig. 2.19.

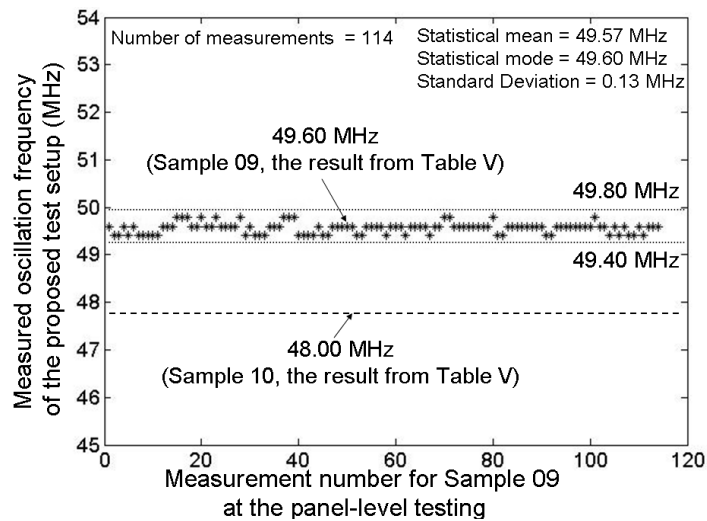


Fig. 2.19. Oscillation frequency of the proposed test setup (Fig. 2.13) for 114 measurements to test Sample 09 at the panel-level testing.

The statistical mode of the measurements is 49.60 MHz, and the statistical mean is 49.57 MHz, both of which are approximately the same when compared to the measurement results shown in Section 2.4.2, Table 2.5 (oscillation frequency = 49.60 MHz). Hence, it can be concluded from this experiment that the results obtained by the proposed setup are repeatable. Moreover, it should be noted that even by considering a maximum deviation of 0.40 MHz in the oscillation frequency of the test setup due to the variable parasitics or system noise at the panel-level testing, Sample 09 and Sample 10 can be distinguished by using this test method.

2.5.2 Test-setup stability

For efficient implementation of this test method, a test board should be designed such that its oscillation frequency should not drift inherently over the testing time of embedded filters, otherwise, the test setup will require recalibration (which will require power up or calibration using the proposed calibration adjustment). A small inherent drift of the oscillation frequency is acceptable, provided this drift is within the resolution limit of the measurement setup, or, it is within the resolution threshold that distinguishes the good RF filters from those that are faulty. To demonstrate the stability of the proposed test setup, a 21-hour long experiment was performed in normal ambient conditions during panel-level testing for the embedded RF passive filter, Sample 09 (Section 2.4.2). Measurements were performed using a spectrum analyzer (HP # E4407B) with ref level = 0 dBm, sweep = 4 ms, start frequency = 10 MHz, end frequency = 90 MHz, number of points = 401 and resolution bandwidth of 1 MHz. As shown in Table. 2.6, the oscillation frequency of the

test-setup (Fig. 2.13) does not drift from 49.60 MHz during the first 9 hrs of the experiment and even after 21 hrs the oscillation frequency is drifted by only 0.2 MHz. It can be inferred from the results shown in the previous sub-section (Section 2.5.1) that this inherent drift of 0.2 MHz after 21 hrs is still within the limit of measurement noise of 0.4 MHz. Hence, it can be concluded that the test setup used in this experiment is stable and immune to the inherent drifts in the oscillation frequency.

Table 2.6: Measured Oscillation frequency of the test setup (Fig. 2.13) over the duration of 21 hours at the panel-level testing for Sample 09

Start (Time = 0 Hrs)	Intermediate (Time = 9 Hrs)	End (Time = 21 Hrs)
49.60 MHz	49.60 MHz	49.80 MHz

2.5.3 Comparison to the conventional test/measurement approach that uses VNA.

2.5.3.1 Limitations of the proposed approach

During the production-level testing “test compaction” is performed and circuits are tested by comparing their response with that of the golden circuit (Known-Golden-Die test methodology). The proposed methodology is an alternate test solution for testing embedded RF passive filters, but it should not be considered as a replacement of RF measurements during the characterization phase of the RF filters. Using this methodology, it is shown that both catastrophic and parametric failures in the embedded passive filter can be detected, but if for a certain product all the specifications need to be measured as it

is performed during RF characterization, then VNA based testing/measurement setup should be used.

2.5.3.2 Test-setup cost

An approximate test-setup cost analysis can be done as follows. A typical RF probe costs around \$800, a VNA that can work up to 3.0 GHz costs around \$21,000 and a VNA that can work up to 6.0 GHz costs around \$42,000. Since a conventional method requires RF instruments such as a VNA, the test setup cost for a 3.0 GHz measurement system will be around \$21,000 and around \$42,000 for a 6.0 GHz system. However, the proposed method uses *low frequency measurements/analysis, consequently the test-setup cost is reduced substantially*. The custom design of an RF amplifier, RF Mixer and a low-pass filter with down-conversion capability will cost only around \$3,000 at 3.0 GHz or 6.0 GHz. As a result, the proposed test method *reduces the test-setup cost by about 75%*. In this cost analysis, the cost of instruments is taken from [71-73] and cost of a custom board is assumed to be approximately \$1100.

2.6 Summary

The proposed test methodology in this section enables the testing of high-frequency (GHz) filters at a low-frequency (MHz). Also, it enables testing without a vector network analyzer and without injecting any other external test stimulus to passive filters. In It also enables prediction of RF specifications from low-frequency test-setup output. The test method is demonstrated by card and panel/wafer level testing of commercially-available

integrated RF substrate with embedded 1.45-GHz RF low-pass passive filters at 60 MHz. Stability analysis, repeatability analysis and test-setup cost analyses of the test method were also performed and the results suggest that the proposed method is promising solution for low-cost testing of integrated RF substrates.

Although this test method significantly reduces test-setup cost, it still requires two-port probing and measurement. To further reduce the test-setup cost, one-port probing methodology is proposed in the next section.

(This page is intentionally left blank)

Chapter 3

ONE-PORT RESONANCE-BASED TEST METHODOLOGY

In this chapter, one-port test approach is proposed for testing high-frequency (RF) interconnects as well as RF passive filters embedded in RF substrates. The proposed technique relies on the use of an RF oscillator that is coupled to the embedded interconnect/filter via a probe card. Shifts in the RF oscillation frequency (referred to as *resonance based testing*) are used for defect detection and is different from prior oscillation based test techniques that configure the device under test (DUT) itself into an oscillator. A core innovation is that the technique can detect defects in embedded passives/filters using only one port probe access and eliminates the need of an external RF input test stimulus. Such one-port probing causes a shift in the oscillation frequency of the external oscillator because of the loading from the embedded RF passive circuit. To facilitate test response measurement, the output of the external RF oscillator (GHz signal) is down-converted to lower frequencies (MHz). The proposed test method is demonstrated through both simulations and measurements. Additionally, panel-level testing of RF substrates is illustrated.

The proposed methodology focuses on a low-cost production-level testing procedure that identifies defective devices rather than accurate RF characterization which is required for design validation/verification.

3.1 Proposed Methodology

In the proposed Resonance-Based Test (RBT) methodology (Fig. 3.1), the shift in the oscillation frequency of the test setup is used to detect failures in the DUT without reconfiguring or converting the DUT into an oscillator as is typically performed in aforementioned conventional oscillation-based test techniques. In the proposed method, the DUT is included in the existing oscillating system, and the presence of the DUT causes a shift in the oscillation frequency of the system. The testing of the DUT is accomplished by careful analysis of this shift in the oscillation frequency.

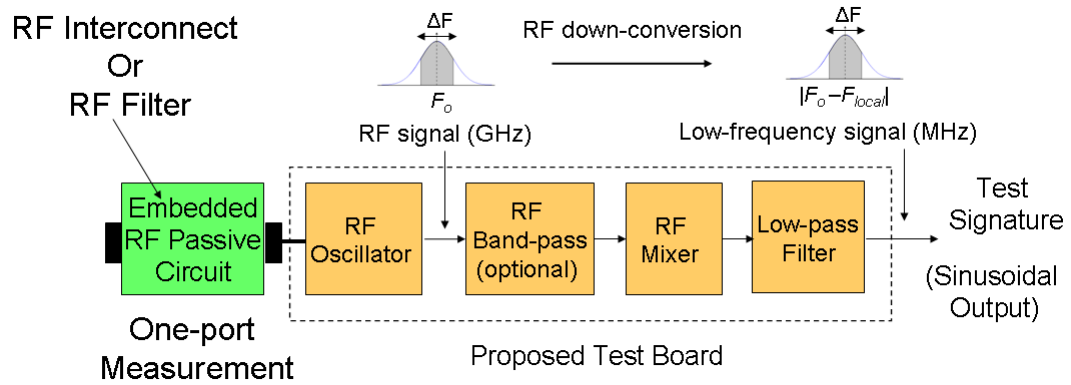


Fig. 3.1. The proposed test-setup of One-Port Resonance-Based Test (RBT) methodology

3.1.1 Test Concepts

In Fig. 3.2A, the canonical RF circuit for a negative-resistance oscillator is shown, where $Z_{in}(w) = R_{in} + j X_{in}$ is the input impedance of the active circuitry of the RF oscillator and $Z_L(w)$ is load impedance. Oscillation occurs when Equation (3.1) is satisfied [70].

$$Z_{in}(w) + Z_L(w) = 0 \quad (3.1)$$

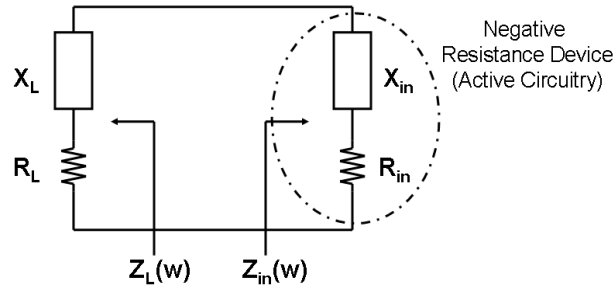


Fig. 3.2A. A modeling of an RF oscillator.

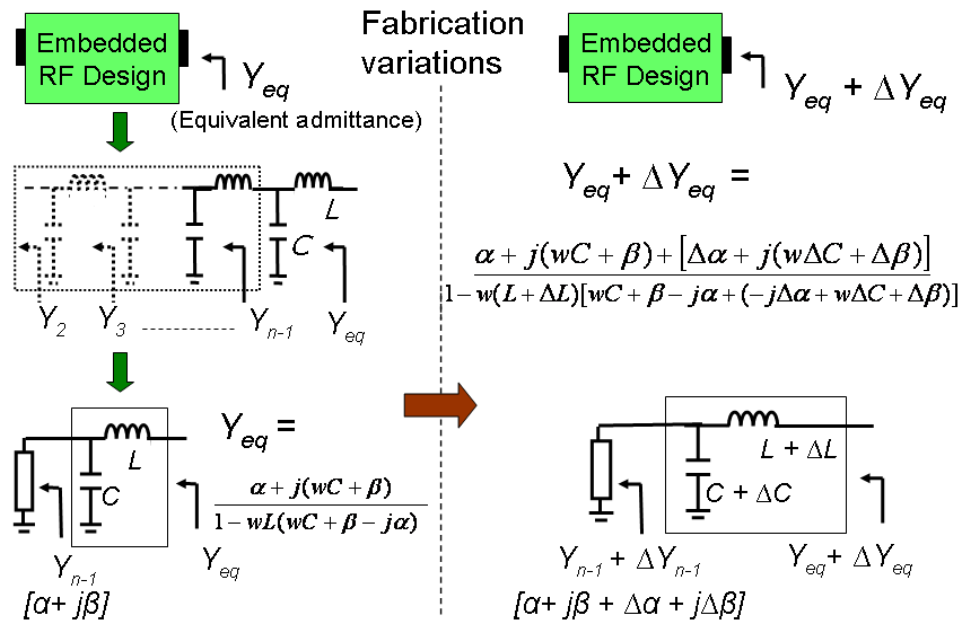


Fig. 3.2B. A model for the change in loading from the RF filter due to fabrication variations.

Consider the embedded RF passive circuit (DUT) as shown in Fig. 3.2B. Because of the fabrication process, the admittance (Y_{eq}) of the DUT changes to $Y_{eq} + \Delta Y_{eq}$ and if this DUT is connected to the active circuitry in the RF oscillator of Fig 7, then Z_{in} will change to $Z_{in} + \Delta Z_{in}$. As a result of this, the condition for oscillation will be affected and defects in the DUT will manifest themselves as changes in the oscillation frequency of the RF oscillator. By the careful analysis of the change in the oscillation frequency of the RF oscillator, a good DUT can be differentiated from a defective DUT either by defining an

allowable shift (ΔF) in the oscillation frequency or by using non-linear decision boundaries [74].

To enable low-frequency testing and to facilitate test response measurement, the output of the external RF oscillator (GHz signal) is down-converted to a lower frequency (MHz). In this methodology, the down-conversion of the RF oscillator output preserves the shift in the oscillation frequency (ΔF) of the test setup, but reduces the frequency of the measurement from the GHz range ($F_{golden} = F_0$) to the MHz range ($F_{golden} = |F_0 - F_{local}|$). Hence, the sensitivity (R_m) for detecting ΔF increases and testing is enabled by low-frequency one-port measurement without a VNA or injecting external test stimulus into the DUT.

3.1.2 Test Setup Design

The first step in the proposed setup involves designing an RF oscillator. For designing RF oscillator, one-port negative-resistance approach can be used [68, 70]. Negative-resistance approach is useful in designing this test setup because it models the RF oscillator as shown in Fig. 3.2.

The RF oscillator is designed in such a way that

- 1) It oscillates at a desired test frequency (F_o) after inclusion of the DUT (i.e. the DUT is connected to the RF oscillator through the *single* port)
- 2) The oscillation frequency of the RF oscillator changes when the known-good DUT is replaced by a defective DUT
- 3) The change in the oscillation frequency (ΔF) is measured using low-cost equipment.

By using a few RF substrate samples for calibration and from the known statistical distribution of the fabrication process for the relevant embedded passives, the shift in the oscillation frequency of the RF oscillator is determined. In practice, the RF substrates used for calibration are selected from different manufacturing production lots such that they represent realistic variations in the fabrication processes.

Once the RF oscillator is designed and an estimation of the shift in the oscillation frequency due to parametric defects has been made, the test board is designed with a RF band-pass filter, RF down-conversion mixer and a low-pass filter. The center frequency of the RF band-pass filter can be chosen according to Equation (3.2) and its band width can be chosen according to Equation (3.3). The local oscillator frequency of the RF mixer can be chosen according to Equation (3.4) and the cut-off frequency of the low-pass filter can be chosen according to Equation (3.5). The RF band-pass filter is optional and is used to restrict the band of frequencies at the input of the RF mixer to avoid the image problem.

$$F_{band_pass_center} = F_0 \quad (3.2)$$

$$F_{band_pass_bandwidth} = F_{max} - F_{min} \quad (3.3)$$

$$F_{local} < F_{min} \quad (3.4)$$

$$F_{low_pass} > F_{max} - F_{local} \quad (3.5)$$

In the above Equations (3.2)-(3.5), F_0 is the desired test frequency of the RF oscillator, F_{min} and F_{max} are the estimated minimum and maximum oscillation frequencies due to manufacturing defects, $F_{band_pass_center}$ is the center frequency of the RF band-pass filter,

$F_{band_pass_bandwidth}$ is the bandwidth of the RF band-pass filter, F_{local} is the local oscillator frequency of the mixer and F_{low_pass} is the cut-off frequency of the RF low-pass filter.

3.2 Simulation Results

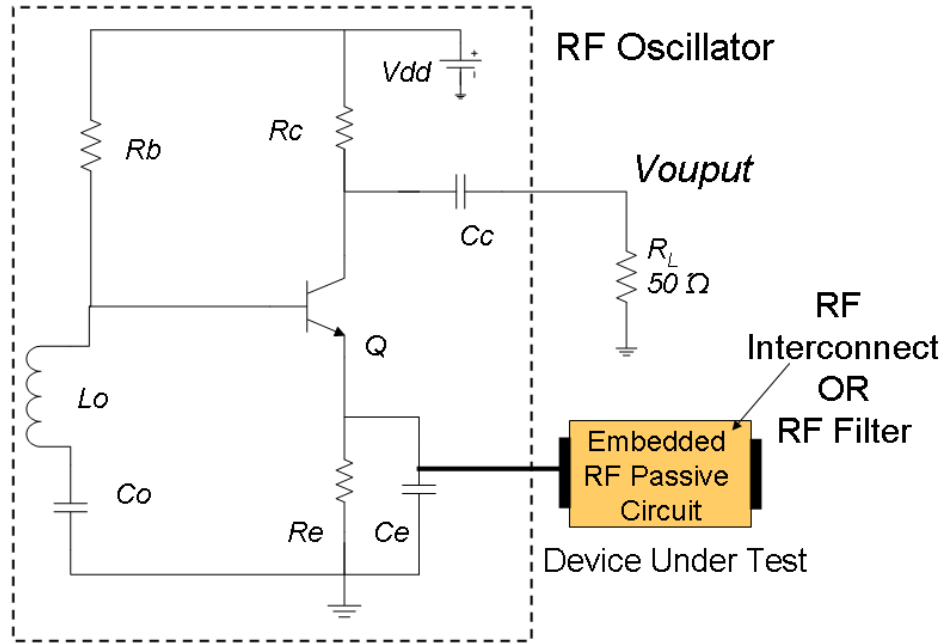


Fig. 3.3. A). Simulation test-setup of the proposed resonance-based test methodology.

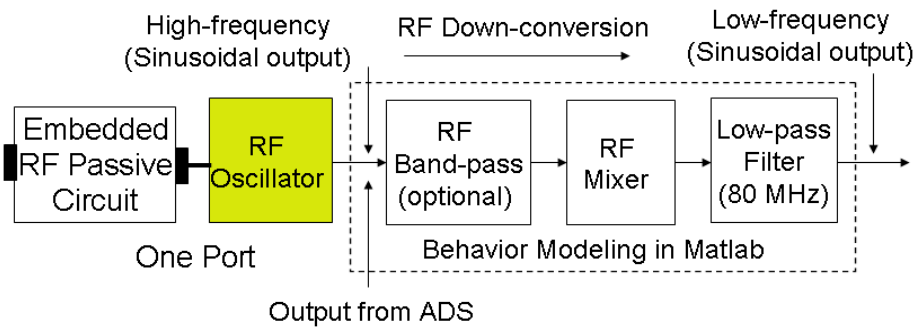


Fig. 3.3. B). System modeling of the proposed resonance-based test methodology.

In this section, the proposed resonance-based test methodology is demonstrated by testing both RF filters and RF interconnects. All simulations are done using the Advance

Design System (ADS) as shown in Fig. 3.3A and the RF down-conversion is modeled in MATLAB as shown as in Fig. 3.3B.

3.2.1 RF interconnect testing

3.2.1.1 Open Test

Test of interconnects containing defects that lead to a complete break or near break of interconnect is called open test. To demonstrate the RF interconnect testing for open defects, 50 ohms RF interconnects of length 8mm are considered, and RF oscillator was designed as shown in Fig. 3.3. Open defects in the RF interconnects are modeled as shown in Fig. 3.4 [66]. In this model, near-open/complete-open defect because of the constriction in the interconnect width manifests itself as an increase in resistance (R_d) at the defect location. Larger the value of R_d indicates more constriction, which implies an open.

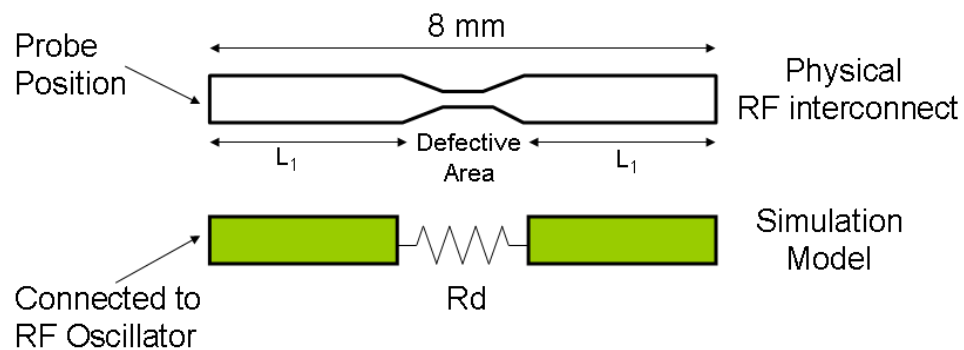


Fig. 3.4. A simulation model for RF interconnects with open defect [66].

Table 3.1 Results to Test Open Defect in RF Interconnects.

Interconnect Sample	Defect resolution (Rd)	RF Oscillator frequency	Test-Setup output frequency
Sample O1 (Golden)	Rd = 0 Ohms	1.210 GHz	55 MHz
Sample O2	Rd = 20 Ohms	1.215 GHz	60 MHz
Sample O3 (near open)	Rd = 100 Ohms	1.220 GHz	65 MHz
Sample O4	Rd = 200 Ohms	1.230 GHz	75 MHz
Sample O5 (open)	Rd = 2K Ohms	1.240 GHz	85 MHz

The shift in the oscillation frequency of the test-step for varying defect sizes (Rd) is summarized in Table 3.1. It can be inferred from these results that as size of the open defect increases the shift in the oscillation frequency of the test-setup also increases. Thus, the open defects can be tested by the analysis in the shift of the oscillation frequency of the proposed test setup.

3.2.1.2 Short Test

Testing of interconnects containing defects leading to a connection or a near connection of two individual interconnections is called the shorts test. To demonstrate the short test, the model as shown in Fig. 3.5 [66] is used. The short-defect manifests itself through the flaring of lines due to process variations or through process defects, leading to an increase in capacitance (Cs) at the defect location. A large capacitance defect represents a complete short with smaller values representing a near-short.

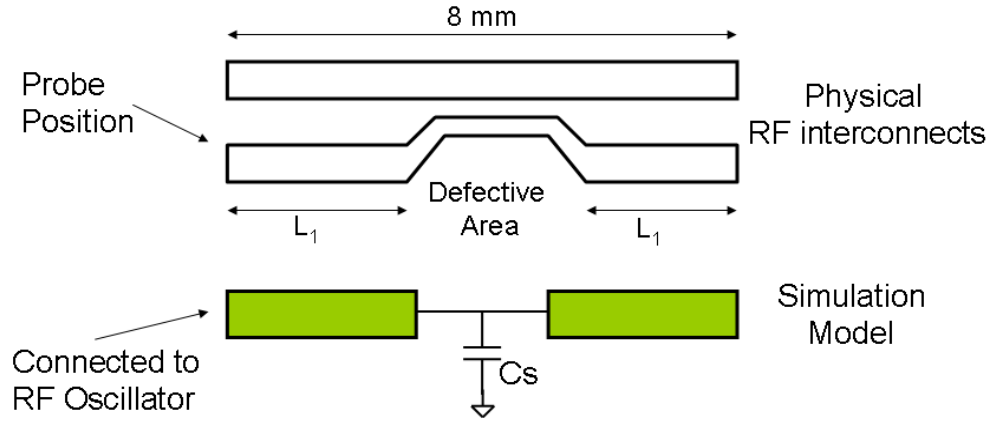


Fig. 3.5. Simulation model for RF interconnects with short defect [66].

Table 3.2 Results to Test Open Defect in RF Interconnects

Interconnect Sample	Defect resolution (C_s)	RF Oscillator frequency	Test-Setup output frequency
Sample S1 (Golden)	$C_s = 0$ F	1.210 GHz	55 MHz
Sample S2	$C_s = 100$ fF	1.205 GHz	50 MHz
Sample S3 (near short)	$C_s = 200$ fF	1.200 GHz	45 MHz
Sample S4	$C_s = 0.5$ pF	1.1850 GHz	30 MHz
Sample S5 (short)	$C_s = 1.0$ pF	1.1650 GHz	10 MHz

As a previous sub-section, RF interconnects of length 8mm is considered and same test-setup is used for testing short defects as well. The response of the test-setup, for varying defect sizes (C_s) is summarized in Table 3.2. It can be inferred from these results that as size of the short defect increases the shift in the oscillation frequency of the test-setup also increases and this shift is in the opposite direction as compared to the open defects. Thus, short defect can also be tested by the proposed method.

3.2.2 RF Filter Testing

3.2.2.1 Low-pass filter testing

An RF low-pass filter (3-dB frequency of 1.54 GHz) is modeled and seven samples of the RF low-pass filter are considered to demonstrate the test technique. The insertion loss of these filters for the different values of inductance (L_a) and capacitance (C_a) is shown in Fig. 3.6. It is assumed that the low-pass filter L4 is a golden filter with $C_a = 2.0$ pF, $L_a = 10.50$ nH. Filters L2 ($C_a = 1.9$ pF, $L_a = 9.98$ nH), L3, L5 and L6 ($C_a = 2.1$ pF, $L_a = 11.03$ nH) are marginally good, and filters L1 ($C_a = 1.84$ pF, $L_a = 9.66$ nH) and L7 ($C_a = 2.16$ pF, $L_a = 11.34$ nH) are bad. A simulation test setup as shown in Fig. 3.3 is used and the summary of the simulation results with RF down-conversion response is given in Table 3.3.

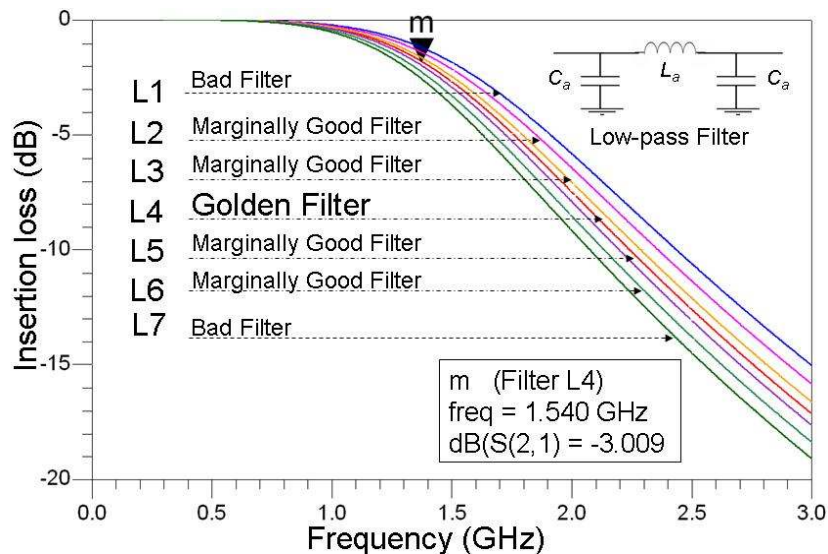


Fig. 3.6. Insertion loss of RF low-pass filters under test to demonstrate RBT methodology.

Table 3.3 Results to Test the RF Low-Pass Filter by The Proposed Resonance- Based Test (RBT) Method

RF filter	3-dB frequency	Filter's classification	RF oscillator output frequency	Test-setup output frequency
L1	1.67 GHz	Bad	1.41 GHz	125 MHz
L2	1.62 GHz	Marginally Good	1.38 GHz	95 MHz
L3	1.57 GHz	Marginally Good	1.36 GHz	75 MHz
L4	1.54 GHz	Golden Filter	1.34 GHz	55 MHz
L5	1.51 GHz	Marginally Good	1.33 GHz	45 MHz
L6	1.47 GHz	Marginally Good	1.31 GHz	25 MHz
L7	1.43 GHz	Bad	1.29 GHz	5 MHz

Based on the results shown in Table 3.3, it can be inferred that the oscillation frequency of the test setup is around the response of the golden low-pass filter, L4. Therefore, for allowable shift in the oscillation frequency around the response of the golden filter, these RF filters can be distinguished as bad and marginally good. For example, for Δf from +45 MHz to -35 MHz around 55 MHz, Filters L1 and L7 can be concluded as bad samples, and L2, L3, L5 and L6 as marginally good samples. It can also be noted from Table 3.3 that the resolution (R_m) to measure ΔF at the RF oscillator's output is 0.06 ($\Delta F/F_0 = 80$ MHz/1.34 GHz) while R_m at the output of the proposed test setup is 1.7 ($\Delta F/(F_0 - F_{local}) = 80$ MHz /45 MHz). Hence, the resolution to measure the shift in oscillation frequency is increased by a factor of approximately 28 as a result of down-converting the output of the RF oscillator and testing is possible by the analysis of a low-frequency signal.

3.2.2.2 High-pass filter testing

To further demonstrate this test method, the testing of a RF high-pass filter (3-dB frequency of 1.30 GHz, Fig. 3.7) is shown in this sub-section. In this example also seven samples of the RF filter are considered. It is assumed that the golden filter is H4 (Ca =

1.20 pF, $L_a = 6.40$ nH), filters H2 ($C_a = 1.14$ pF, $L_a = 6.08$ nH), H3, H5, H6 ($C_a = 1.26$ pF, $L_a = 6.72$ nH) are marginally good filters, and H1 ($C_a = 1.05$ pF, $L_a = 5.63$ nH) and H7 ($C_a = 1.34$ pF, $L_a = 7.17$ nH) are bad high-pass filters. When these filters were simulated with the RF oscillator (Fig. 3.3), a corresponding change in the oscillation frequency of the RF oscillator was observed for the different filters. The obtained oscillation frequencies vs 3-dB frequencies of the filters are plotted in Fig. 3.7.

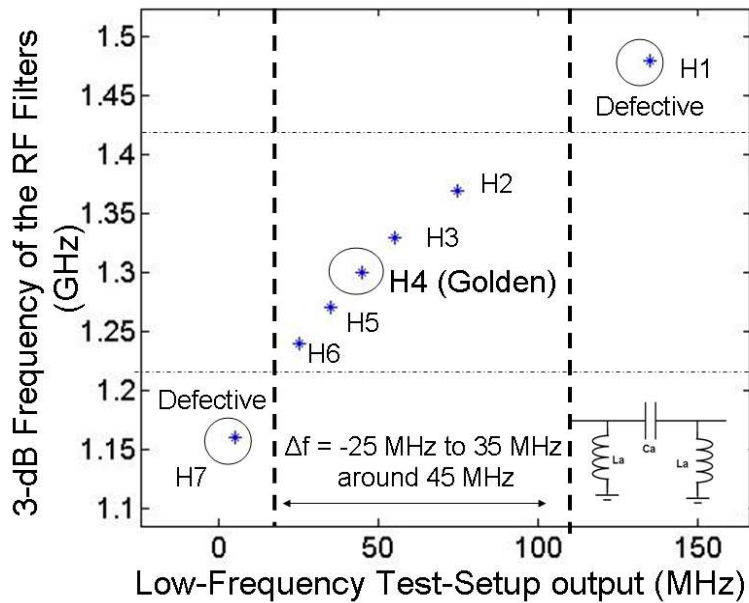


Fig. 3.7. 3-dB frequency of the RF high-pass filters vs test setup output.

In this example as well, it is evident from Fig. 3.7 that again the oscillation frequency of the test setup is around the response of the golden filter, H4. Hence, the testing of these high-pass filters is possible by defining an allowable shift in the oscillation frequency around the response of the golden filter. For example, for the allowable shift of $\Delta F + 35$ MHz to -25 MHz around 45 MHz, filters H1 and H7 can be concluded as bad RF high-pass filters and H2, H3, H5 and H6 as marginally good filters.

3.3 Proof of Concept

3.3.1 RF low-pass filter testing

As a proof of concept, a hardware prototype of the proposed test setup was made and is shown in Fig. 3.8. A low-pass filter (3-dB frequency = 1.54 GHz) was designed and assembled for the topology shown in the previous section using different SMD capacitors and inductors. Among these filters, sample L2 is (capacitor = 2.4 pF, inductor = 8.2 nH) while sample L1 (capacitor = 2.0 pF, inductor = 6.8 nH) and sample L3 (capacitor = 2.7 pF, inductor = 8.7 nH) are its variants. To test these filters, an RF oscillator was designed and commercially available RF down-conversion mixer, low-pass filter (100MHz) were used. The RF attenuator was used to avoid non-linearity in the RF mixer because of high-power output from the RF oscillator. The insertion loss profiles of the RF low-pass filters are shown in Fig. 3.9, and measurement results of the proposed test setup are shown in Fig. 3.10.

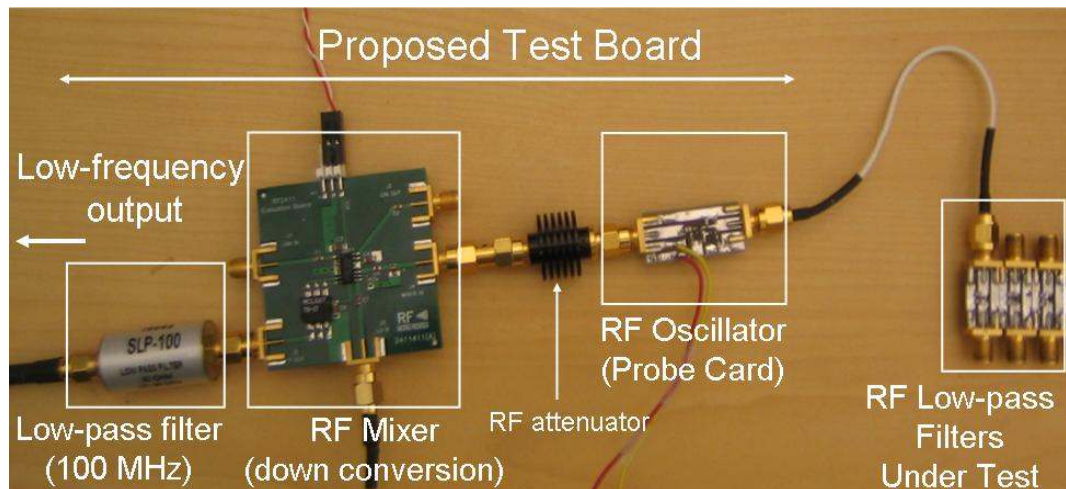


Fig. 3.8. A hardware prototype of the proposed resonance-based test method.

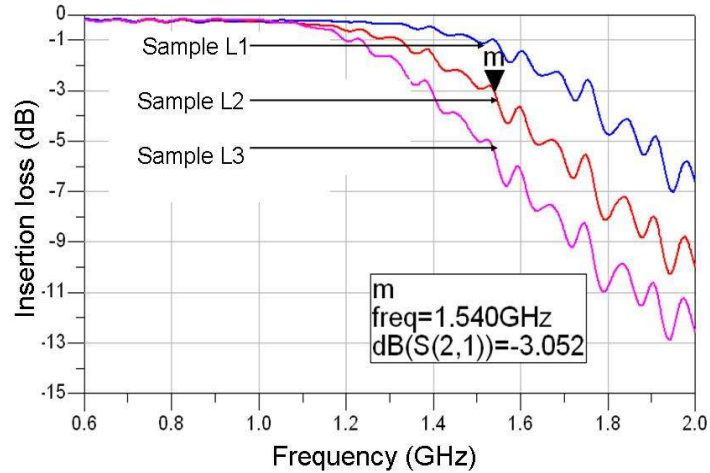


Fig. 3.9. Insertion loss of SMD RF low-pass filters.

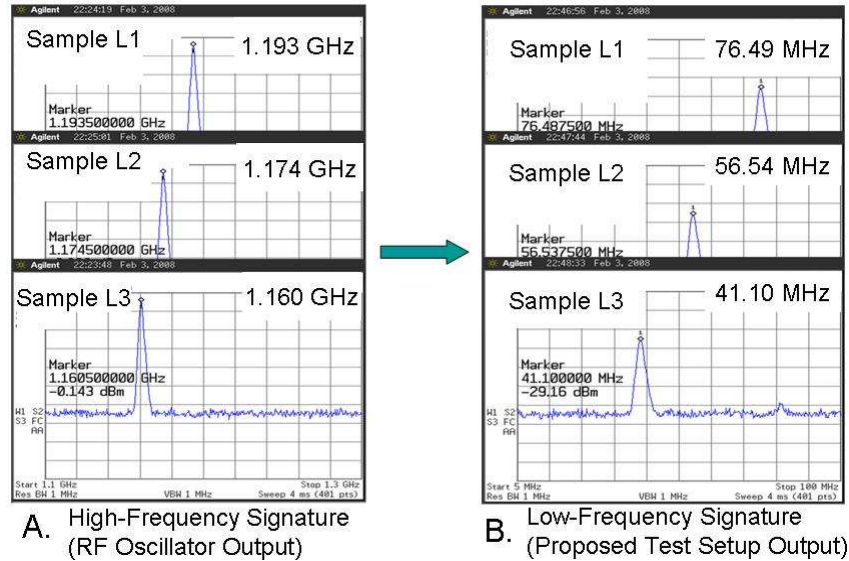


Fig.3.10 Measurement results for testing SMD RF low-pass filter by the RBT methodology.

It can be observed from the above measurement results that the RF oscillator frequency changes for the different RF low-pass filters. Hence, by comparing the shift in the oscillation frequency around the response of Filter L2 (golden filter), testing of these is possible by the analysis of low-frequency signal of the order of 80 MHz.

3.3.2 RF high-pass filter testing

A 1.13-GHz high-pass filter was designed and assembled for the topology shown in the previous section by using different surface-mount capacitors and inductors. Among these filters, it is assumed that Filter B is a golden filter (capacitor = 1.20 pF, inductor = 8.2 nH) while its variants are Filter A (capacitor = 1.50 pF, inductor = 10.0 nH) and Filter C (capacitor = 0.60 pF, inductor = 6.8 nH). The insertion loss profile of these RF high-pass filters is shown in Fig. 3.11, and measurement results using the proposed one-port test method are shown in Fig. 3.12.

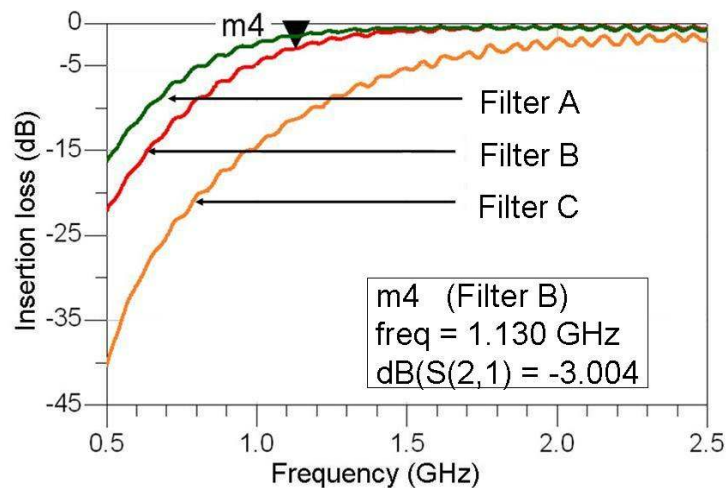


Fig. 3.11. Insertion loss of RF high-pass filters under test.

It can be again observed from the above measurement results that the RF oscillator frequency changes for the different RF filters. Hence, again by comparing the shift in the oscillation frequency around the response of Filter B (golden filter), testing of these RF passive filters is possible by the analysis of low-frequency signal of the order of 80 MHz.

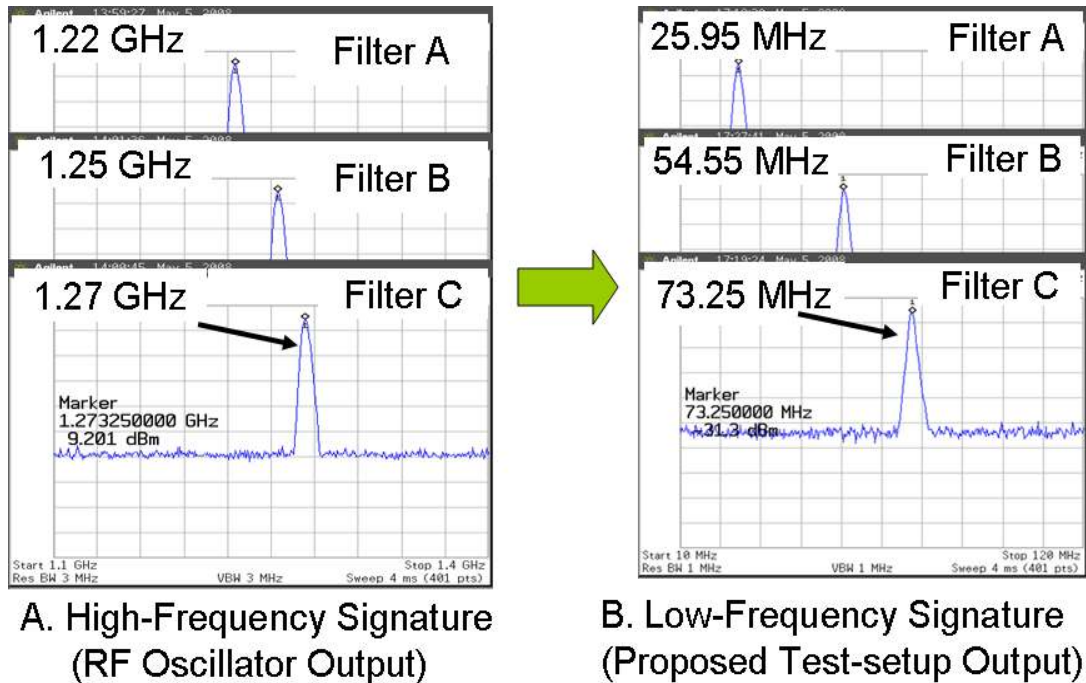


Fig. 3.12. Measurement results for testing RF high-pass filter. Spectrum of the the RF oscillator output.

3.3.3 RF interconnect testing

To demonstrate the RF interconnect testing, RF interconnect of 8 mm interconnect was designed on two-metal layer Roger’s 6000 RF substrate. The dimension of interconnect was chosen to meet 50 ohms characteristic impedance using the microwave solver “line-cal” in ADS. Both the open and short defects are designed, and the results obtained are shown in Fig. 3.15. The setup similar to Fig. 3.8 is used in this test as well, and it is shown in Fig. 3.14.

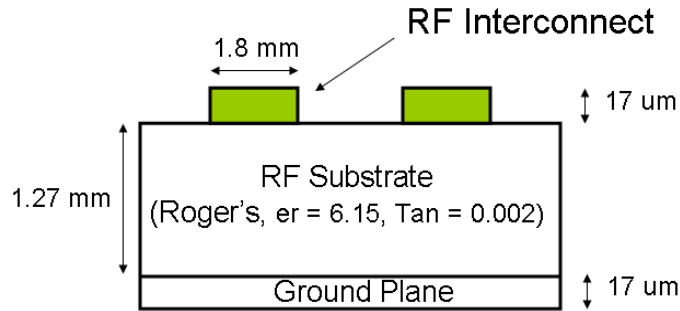


Fig. 3.13. Details for RF interconnect design using Roger's Substrate.

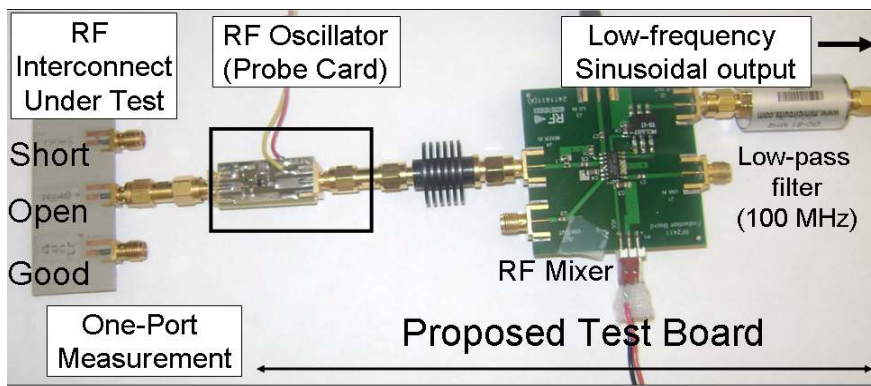


Fig. 3.14. A hardware prototype to test RF interconnects by the RBT methodology.

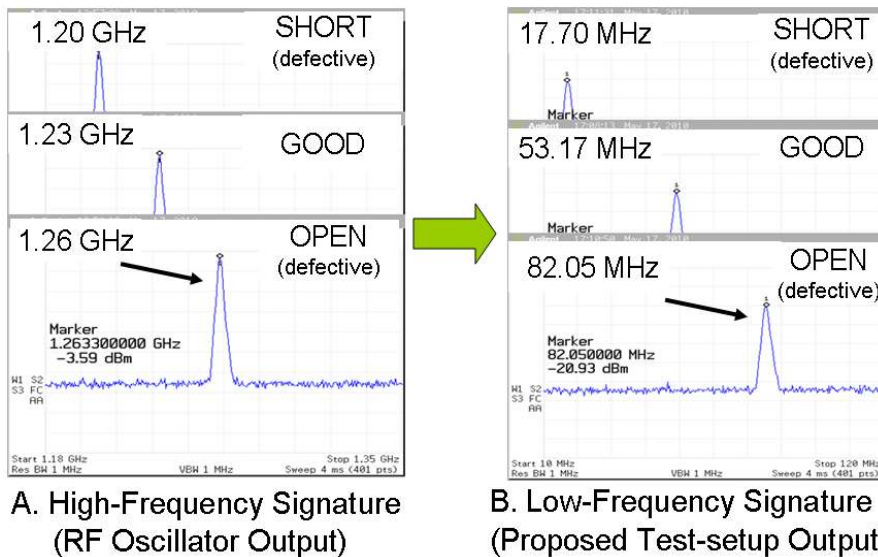


Fig. 3.15 Measurement results for testing RF Interconnects using RBT methodology.

In this RF interconnect testing also, it can be observed from the above measurement results that the defects in the RF interconnect manifest themselves as a shift in the test setup oscillation frequency. For the open defect, the shift in the oscillation frequency is towards the right of the defect-free interconnect, while for the short defect the shift in the oscillation frequency is towards the left. Thus, by comparing the shift in the oscillation frequency around the golden interconnect, testing of these RF interconnects is possible by the proposed method.

3.4 Testing Of Commercially Available RF substrate

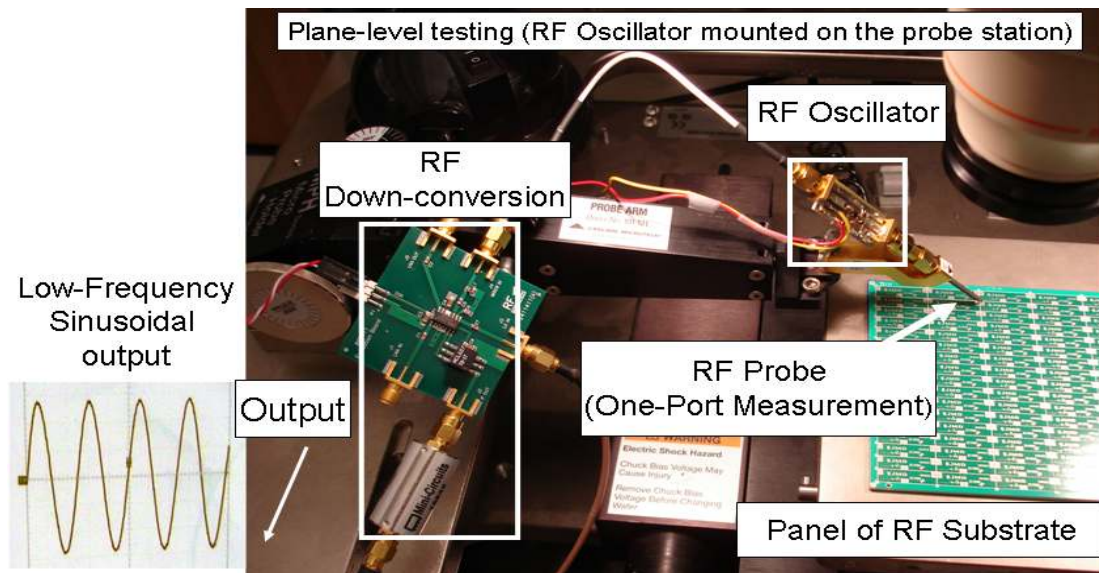


Fig. 3.16. A hardware setup to test embedded RF passive filters at a panel level by the proposed RBT methodology

In this section, this RBT test technique is demonstrated at the panel level for testing commercially-available unpopulated RF substrates with embedded RF low-pass passive

filters (3-dB frequency of 1.45 GHz, 4th order). Again, these samples of embedded filters were provided by JMD Inc, Atlanta. Test setup as shown in Fig. 3.16 was used and samples of the RF substrate were randomly probed at three different locations of the fabricated wafer as shown in Fig. 3.17. Fig. 3.17 also shows insertion-loss profile of the RF filters embedded in the RF substrate. Measured output oscillation frequency of the proposed test technique vs 3-dB frequency for the different RF filter samples are plotted in Fig. 3.18. This experiment was performed on the cascade's probe station # EC3008.

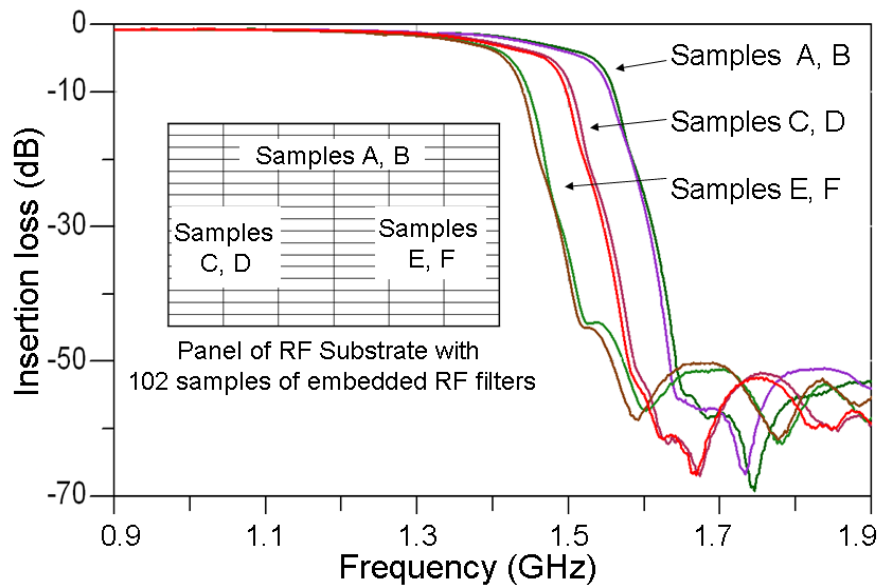


Fig. 3.17. Insertion loss of the RF low-pass filter samples embedded in RF substrate.

It can be noticed from the measurement results shown in Fig. 3.17 and Fig. 3.18 that the test setup (Fig. 3.16) has almost the same output oscillation frequency for the samples with similar insertion loss profiles. Also, the test method gives different output oscillation frequencies if the performance of the filters changes. For example, the output oscillation frequency for Samples E and F is around 34 MHz, while for Samples A and B the output

oscillation frequency is around 75 MHz. Hence, it is possible to distinguish these embedded filters by the proposed RBT method.

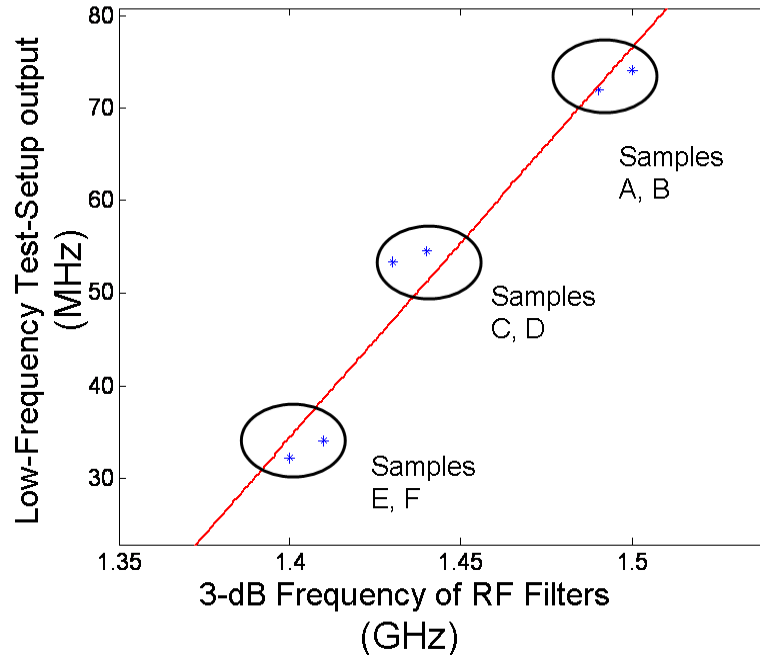


Fig. 3.18. Measured output oscillation frequency of the proposed test setup vs 3-dB frequency of embedded RF low-pass filters in the RF substrate.

3.5 Discussion

This section discusses the stability of the proposed test setup and compares the proposed test-setup cost/capability to the conventional test-setup that uses VNA.

3.5.1 Measurement Stability Analysis

To implement this test method efficiently, the test setup should be designed such that its oscillation frequency should not drift inherently over the test time of embedded circuits otherwise the test setup will require recalibration. A little inherent drift in the oscillation

frequency is acceptable provided such drift is within the resolution limit of the measurement setup, or, it is within the resolution threshold that distinguishes the good embedded RF circuits from those that are faulty. To demonstrate the stability of the proposed test setup, a *40-hour* long experiment was performed during the testing of RF interconnect (Section 3.3.3, with open defect). Measurements were performed using a spectrum analyzer (HP # E4407B) with start frequency = 10 MHz, end frequency = 120 MHz, ref level = 0 dBm, number of points = 401 and resolution bandwidth of 1 MHz. The oscillation frequency of the test-setup has not drifted from 82.05 MHz over the duration of 20 hrs and even after 40 hrs of the experiment, it drifted only by 0.17 MHz (or 0.2%). Hence, it can be concluded that the test setup in this experiment is stable and immune to the inherent drifts in the oscillation frequency.

3.5.2 Key Contributions Test Setup Cost

During production-level testing, “test compaction” is performed and circuits are tested by comparing their response with that of the golden circuit (Known-Golden-Die test methodology). The proposed test technique is a manufacturing test solution for embedded RF interconnects and filters, and is not meant to replace RF characterization during chip design and product development. It is ideally suited for detecting the effects of large manufacturing process variations. In this method, one-port measurement is used, and it is shown that it is possible to detect defects in RF interconnect and RF filters by the analysis of low-frequency signal. Also, the proposed method eliminates the use of external RF input test stimulus

An approximate test-setup cost analysis can be done as follows. The conventional method depends on S-parameter measurements and uses two RF probes and a VNA for testing RF substrates, but the proposed method uses *just one RF probe and low frequency measurement*. For production-level testing, the low-frequency sinusoidal output (MHz) of the proposed test-setup can be obtained with custom design of the RF oscillator, RF Mixer and low-pass filter. The output of the test setup can be sampled by an ADC, and then FFT of the sampled signal can be taken to determine the frequency of the sinusoidal signal. Therefore, test-setup cost reduces substantially. Summary of the cost analysis is given in Table 3.4 and shown in Fig 3.19. which show that the proposed test method reduces the test-setup cost by about 80%. It is also important to note that as test frequency increases the proposed test setup become more cost effective.

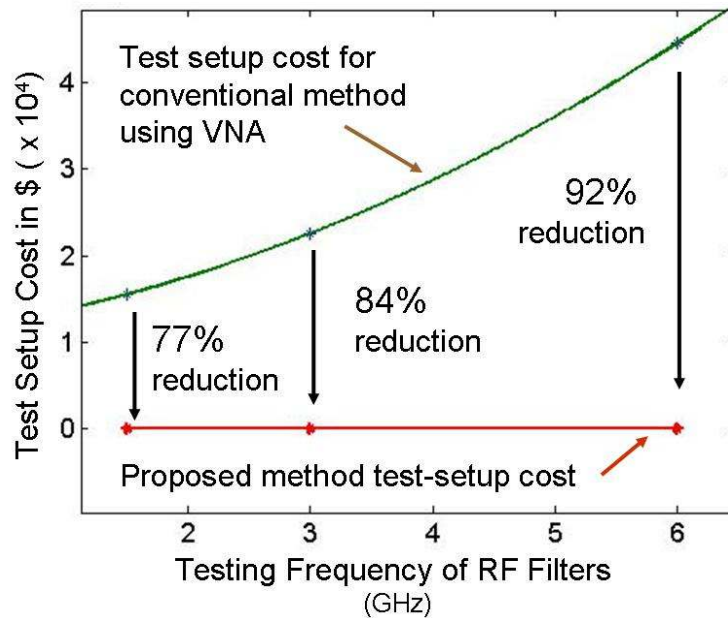


Fig. 3.19. Test setup cost of the proposed *resonance based test(RBT)* method as compared to the conventional method

Table 3.4 Cost Analysis of the proposed Test-setup

Test Frequency	Test Setup cost		
Maximum Frequency of Testing	Conventional Method (VNA + 2 RF Probes) (X)	Proposed Method (RF oscillator+ RF down-conversion setup) (Y)	Reduction in Test-Setup Cost $Z = (X-Y)/X\%$
1.50 GHz	\$15,600	\$2,900	85.0%
3.0 GHz	\$22,600	\$2,900	87.0%
6.0 GHz	\$44,600	\$2,900	93.0%

*Cost of instruments is taken from [71-73] for reference purpose only.

*Cost of Custom Board with ADC is assumed to be \$1100

3.6 Summary

A new test methodology is proposed, which involves one-port measurement and enables testing of embedded RF interconnect and filters without a vector network analyzer or any external test stimulus. Also, it enables testing of these RF components with low-frequency analysis. The method is demonstrated by simulations and measurements. Obtained results suggest that the proposed method can be considered as an alternate production-level test technique which does not require high-frequency measurements for testing RF substrates.

(This page is intentionally left blank)

Chapter 4

LOW-COST TESTING OF RF AMPLIFIER CIRCUITS

In this chapter, a low-cost approach for testing high frequency (GHz) RF amplifiers is proposed. It is demonstrated for the first time that those RF amplifiers can be tested for their specifications using oscillation principles. In the test mode, the RF test signal is “self generated” by the amplifier with the help of additional external circuitry which forces the amplifier to oscillate (Barkhausen criterion) around its characteristic frequency. The RF sinusoidal output from the oscillating RF amplifier is down-converted to a lower frequency enabling low frequency test response analysis as well as increased sensitivity to parametric deviations. In addition to the detection of catastrophic failures, it is shown that multiple RF specifications (Gain, P1dB, and IIP3) can be predicted via analysis of the frequency of the down-converted response. To account for RF parasitics on the production floor, a calibration technique is proposed in the test-setup. Thus, the proposed method reduces test cost significantly by reducing the cost of test setup (by as much as 80%) and significantly reducing test time. The viability of the proposed test method is demonstrated both by simulation experiments and measurement.

4.1 Proposed Methodology

Consider the test setup as shown in Fig. 4.1. In the test mode, a closed-loop feedback is applied to the LNA such that this feedback causes the LNA to become unstable and forces it to oscillate around its characteristic frequency according to the well known Barkhausen

criterion. The defects in the LNA changes the closed-loop feedback of the test setup, hence the oscillation frequency of the system changes around the oscillation frequency of the “golden” LNA. The oscillation frequency of the test-setup is considered as a test signature for testing LNA. The testing of the LNA is performed by careful analysis of the change in the oscillation frequency of the test setup. In this test-method, pass-or-fail testing is performed by defining allowable deviation in the oscillation frequency of the test setup around “golden” LNA response, and high-resolution testing is performed using regression prediction model after predicting specifications of the LNA.

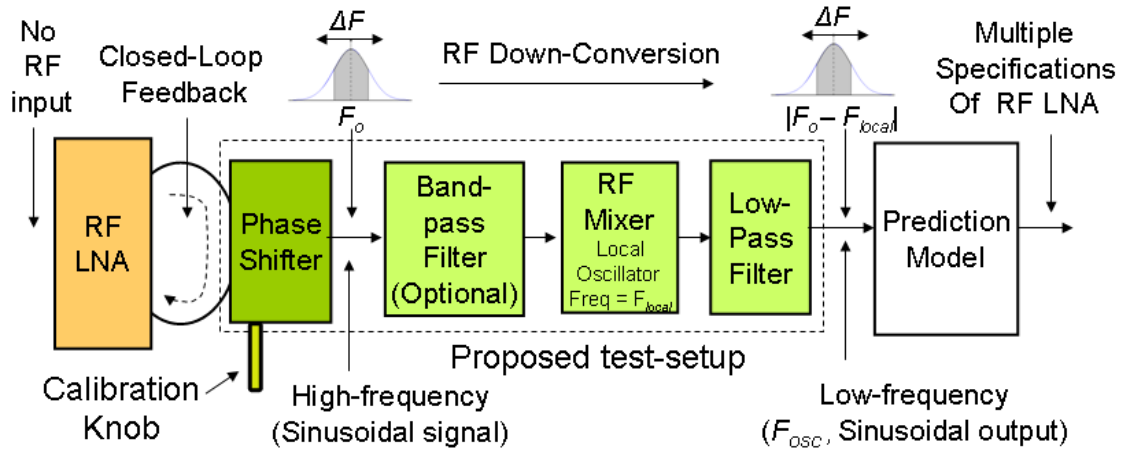


Fig. 4.1. The proposed test setup for testing RF LNA at low-cost.

4.1.1 Test Board Design

In the closed loop system as shown in Fig. 4.2, the oscillation condition is governed by Barkhausen criterion, according to Equation (4.1). According to this criterion, the signal must traverse the feedback loop with no phase shift and no attenuation for the system to oscillate.

$$1 - \alpha \beta = 0 \quad (4.1)$$

where, α is gain factor of the amplifier and β is feedback factor of the phase shifter (feedback network).

Designing an RF closed loop system to oscillate at the desired frequency is quite challenging mainly because of unknown RF parasitics. At RF frequencies, even the lengths of the cables used in the measurement setup affect the oscillation frequency. Not only that, RF parasitics such as coupling capacitors also cause deviation in the oscillations. The modeling of these RF parasitics on the production floor is not a simple task. Thus, to ease the design of the test setup and to account the effect of RF parasitics, a *calibration knob* is proposed in the test setup as shown in Fig 4.2. This knob provides a calibration mechanism as it enables the tuning of oscillation frequency of the test-setup.

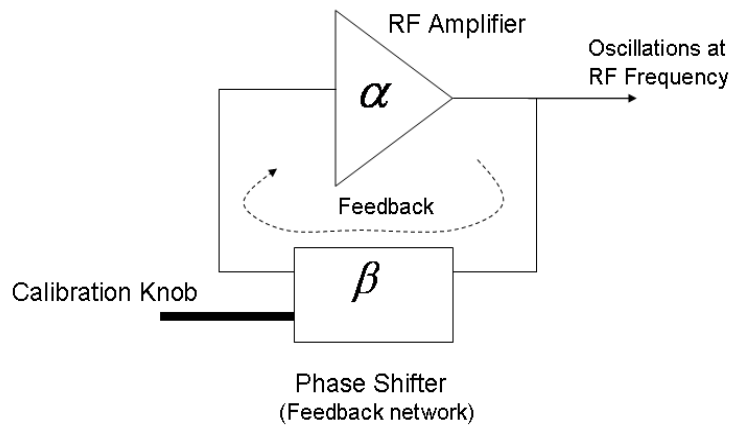


Fig. 4.2. Calibration knob to calibrate/tune the oscillations in the closed loop system (RF Amplifier with the Phase shifter).

In the proposed test setup, the calibration knob is controlled by a DC voltage and it is a part of an external feedback network called the phase shifter. The calibration knob can be implemented considering the RF amplifier with phase shifter as a voltage-controlled

oscillator. For demonstration purposes, we have implemented the calibration knob by using a varactor in the phase shifter.

In this test method, an external feedback circuit (phase shifter) is designed in such a manner that

(a) After its inclusion, the LNA oscillates around the desired test frequency (F_o). This external feedback circuit can be designed such that catastrophic faults in the LNA cause no oscillations to occur, while the parametric faults in the LNA cause a shift in the oscillation frequency around the response of the golden LNA.

(b) The change in the oscillation frequency due to the parametric defects is measurable by low-cost measurement instruments.

Estimation of the maximum (F_{max}) and minimum (F_{min}) change in the oscillation frequency due to parametric defects around the desired testing frequency (F_o) is performed using a few LNA samples. In practice, these LNA samples are selected from different manufacturing production lots such that they represent the variations in the fabrication process. For simulations, a statistical analysis like Monte Carlo can be used to obtain such LNA samples.

Once the external feedback circuit is designed and an estimation of shift in the oscillation frequency due to parametric defects is completed, the test board is designed with a RF band-pass filter, RF down-conversion mixer and a low-pass filter. The design procedure should ensure that the oscillation frequency of the test board has immunity to the power supply variations or system noise. The RF band-pass filter is optional and is used to restrict the band of frequencies at the input of the RF mixer to avoid image problems.

The center frequency of the RF band-pass filter can be chosen according to Equation (4.2) and its band width can be chosen according to Equation (4.3). The local oscillator frequency of the RF mixer can be chosen according to Equation (4.4) and the cut-off frequency of the low-pass filter can be chosen according to Equation (4.5).

$$F_{band_pass_center} = F_0 \quad (4.2)$$

$$F_{band_pass_bandwidth} = F_{max} - F_{min} \quad (4.3)$$

$$F_{local} < F_{min} \quad (4.4)$$

$$F_{low_pass} > F_{max} - F_{local} \quad (4.5)$$

In the above Equations (4.2)-(4.5), F_0 is the desired test frequency of the RF LNA, F_{min} and F_{max} are the estimated minimum and maximum oscillation frequencies due to manufacturing defects, $F_{band_pass_center}$ is the center frequency of the RF band-pass filter, $F_{band_pass_bandwidth}$ is the bandwidth of the RF band-pass filter, F_{local} is the local oscillator frequency of the mixer and F_{low_pass} is the cut-off frequency of the RF low-pass filter.

In the proposed test method, oscillation frequency of the test setup is the test signature and it is measured around “golden” LNA response for testing. Thus, sensitivity to measure the test signature can be defined by below Equation (4.6).

$$R_m = \Delta F / F_{golden} \quad (4.6)$$

where, F_{golden} is the oscillation frequency of the test-setup with the golden filter, and ΔF is the shift in the oscillation frequency of the test-setup relative to the response of the test setup with the golden filter.

In this method, the down-conversion of the RF phase-shifter output preserves the shift in the oscillation frequency (ΔF) of the test board, but reduces the frequency of the measurement from GHz range ($F_{golden} = F_0$) to MHz range ($F_{golden} = |F_0 - F_{local}|$). Hence,

the sensitivity (R_m) for detecting ΔF increases by the proposed test-setup (Fig. 4.1) as compared to the prior oscillation-based test setup (Fig. 2.1).

4.1.2 Prediction Model Development

In RF design, specifications are interdependent due to which change in one specification causes change in the other. Let us assume that the non-linearity of the amplifier is upto third order as given by Equation (4.7), then P1dB of the amplifier can be approximated as Equation (4.8), IIP3 as Equation (4.9) and NF can be approximated as Equation (4.10). It is can be inferred from these equations that P1dB, IIP3 and NF are dependent on Gain (α_1) of the LNA which show interdependency of different specifications. In addition, at circuit level, components that contribute to one specification also contribute to the other specifications to some extent. This increases the interdependency of RF specifications on each other.

$$V_{out} = \alpha_1 V_{in} + \alpha_2 V_{in}^2 + \alpha_3 V_{in}^3 \quad (4.7)$$

$$P1dB = 10 \log(0.145 \alpha_1 / \alpha_3) \quad (4.8)$$

$$IIP3 = 10 \log(1.33 \alpha_1 / \alpha_3) \quad (4.9)$$

$$NF = 10 \log(1 + V_n^2 / (4kTR \alpha_1^2)) \quad (4.10)$$

In equations (4.7)-(4.10), k is the Boltzmann constant, T is temperature and R is load resistance (typically 50 ohms), α_1 is the gain of the amplifier; α_2 and α_3 are non-linearity coefficients and V_n^2 is noise contribution from the LNA.

Further, assume that because of process variations, α_1 changes to $\alpha_1(p_p)$, α_2 to $\alpha_2(p_p)$, α_3 to $\alpha_3(p_p)$, V_n^2 to $V_n^2(p_p)$. Hence, Gain, P1dB, IIP3 and NF become function of process

variations such as Gain (p_p), P1dB(p_p), IIP3(p_p) and NF(p_p) as shown in Fig. 4.3. For oscillations to start, closed-loop gain of the system has to be greater than one. As oscillations build up, non-linearity of the system causes these oscillations to become stable at a particular frequency. Thus, in our proposed test setup, oscillation frequency also shifts because of the change in the performance of the RF LNA. Since this shift in oscillation frequency is preserved during RF down-conversion, there exists a finite possibility to derive non-linear analytical expressions which compute the relationship between the LNA specifications and the response of the test setup. However, derivation of such analytical expressions could be very hard, and if LNA has higher order of non-linearity (greater than 3), then derivation of such analytical equations can become even harder. But, development of a non-linear model to predict specifications of RF LNA can be easily done by using successive-learning processes such as Multivariate Adaptive Regression Splines (MARS) and Artificial Neural Networks (ANN).

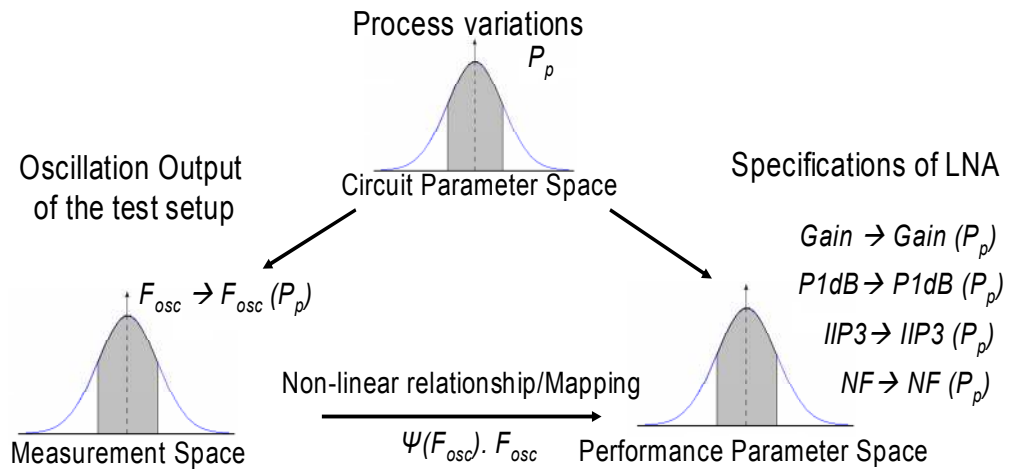


Fig. 4.3. Performance prediction using non-linear mapping for testing RF amplifiers.

In our proposed method, for demonstration, a nonlinear prediction model based on

MARS has been used. The specifications of the RF LNA are predicted using a non-linear prediction model that maps the observed change in the oscillation frequency (F_{osc}) of the test-setup to changes in performance specifications of the RF LNA. The development of a prediction model using MARS is a supervised learning process and it requires a “training set” of LNAs with statistically likely failures. The training set used to estimate the maximum (F_{max}) and minimum (F_{min}) change in the oscillation frequency due to parametric defects around the desired testing frequency (F_0) can be used for the development of the prediction models. The oscillation frequency is used as a test-signature (F_{osc}) to predict the performance of the LNA (S_s) according to Equation (4.11):

$$S_s = \Psi(F_{osc}). F_{osc} \quad (4.11)$$

where, S_s refers to LNA specifications such as Gain, P1dB, IIP3 and NF. $\Psi(F_{osc})$ is a non-linear regression function of the weighted sum of basis functions made of splines. MARS uses an initial recursive partitioning during training to gradually add basis functions using forward stepwise placement; then, a backward procedure is applied and the basis functions associated with the smallest increase in the least squares fit are removed. More details regarding MARS can be found in [31].

4.2 Simulation Results

In this section, by using the proposed approach, the testing of 1.20 GHz LNA is demonstrated by the analysis of low- frequency test signature of the order of 250 MHz. The cascode LNA with source degeneration was designed for CMOS 0.18 um process (Gain = 11.0 dB, P1dB = -5 dBm, IIP3 = 4.3 dBm, NF = 1.7 dB).

For illustration, 10 single-catastrophic failures (5 open and 5 short) were introduced at 5 nodes (Fig. 4.4) of the LNA and 100 parametric instances of the LNA were generated

by *simultaneous random perturbation* of various components of the LNA including inductors, capacitors and transconductance of the transistors (Gaussian distribution of 3-sigma = 5%) using Monte Carlo simulations. It is assumed that each type of component has similar variations, but they are independent of each other's variations. For example, all capacitors are assumed to have similar variations, but their variations are independent from those of transistors and inductors. Fig. 4.4 shows simulation setup in which the feedback is applied to the LNA using a phase shifter so that it becomes unstable and starts oscillating around 1.20 GHz.

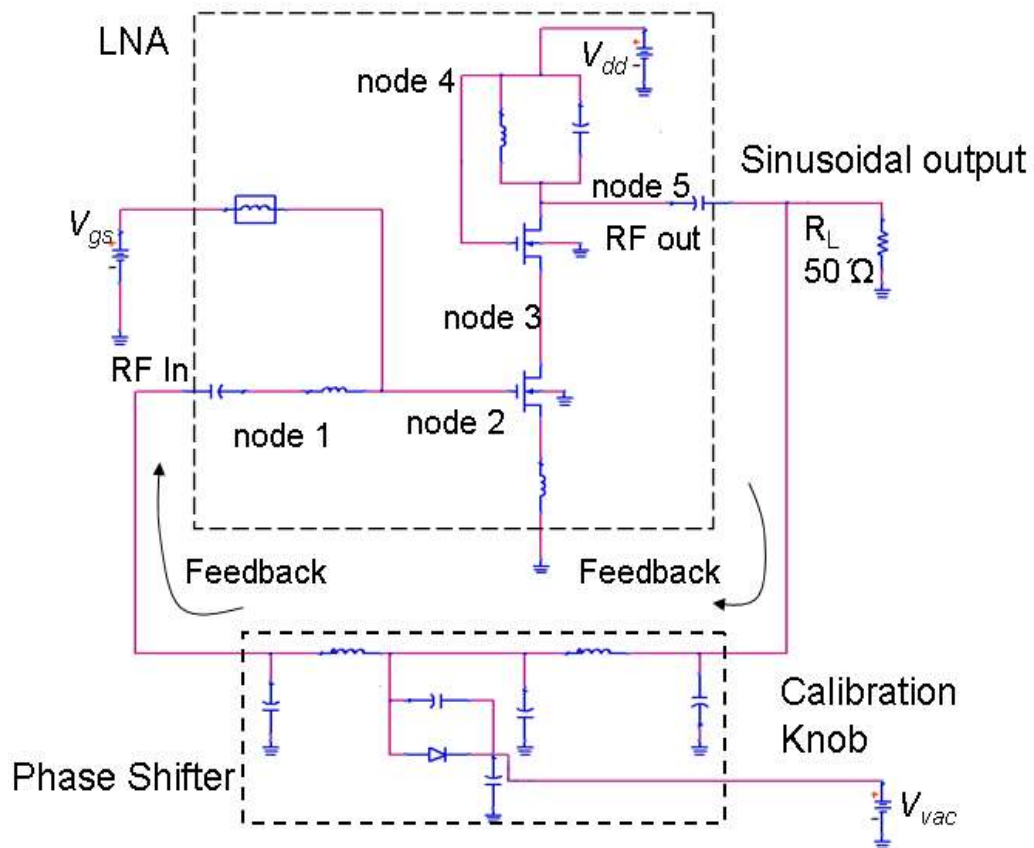


Fig. 4.4 LNA in the feedback mode (simulation in ADS).

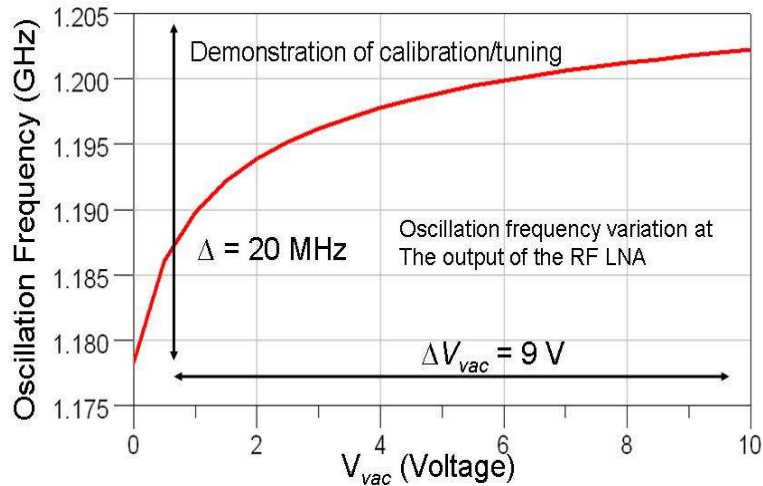


Fig. 4.5. Demonstration of tuning/calibration capability in the proposed test methodology for testing RF amplifiers.

In this test-setup, the phase shifter is designed such that no oscillation occurs for catastrophic failures while oscillation frequency shifts for parametric failures around the response of the golden LNA. In this phase shifter, calibration knob is introduced using a varactor. To demonstrate the tuning/calibration capability in the test-setup, voltage at the calibration knob is varied and results are shown in Fig. 4.5. These simulations were done in Advance Design System (ADS) tool and the sinusoidal signal at the output of the LNA was down-converted using the behavioral model of RF band-pass filter, RF-mixer and low-pass filter in MATLAB, as shown in Fig. 4.6.

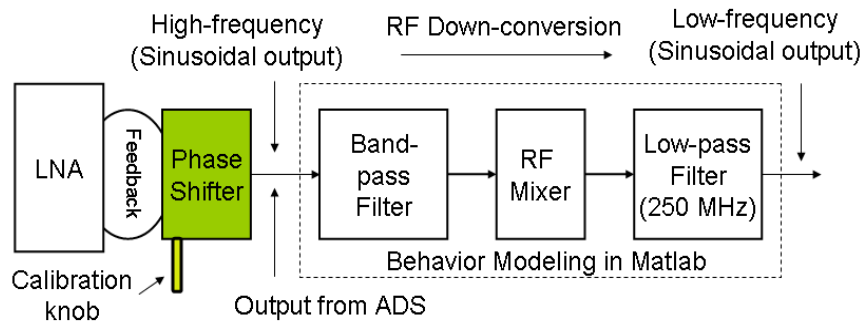


Fig. 4.6. Modeling of the system level simulation setup in MATLAB.

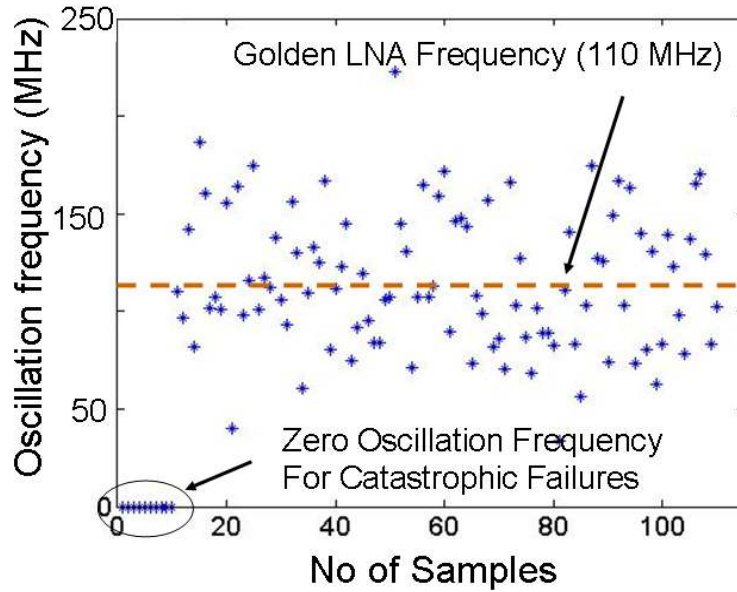


Fig. 4.7. Test setup output (oscillation frequency) of the various LNA samples.

In Fig. 4.7, the down-converted oscillation frequency of all the 110 samples of the LNA (with 100 parametric and 10 catastrophic defects) is shown. It can be inferred from Fig. 4.7 that no oscillation has occurred for the LNAs with catastrophic defects while oscillation frequency has shifted for LNAs with parametric variations. Also, the oscillation frequency for other LNA with parametric failures is around the response of the golden LNA.

To demonstrate prediction of RF specifications, the non-linear models that predict the Gain, IIP3, NF and P1dB of the LNA were developed using 300 samples and validated using the above 100 samples. All these samples were obtained by simultaneously perturbing the LNA components using Monte Carlo simulations. The predicted Gain, P1dB, IIP3, and NF are shown in Fig 4.8. The summary of the prediction statistic is given in Table 4.1 which shows that multiple specifications of the LNA can be predicted with reasonable accuracy from the response of the proposed test-setup.

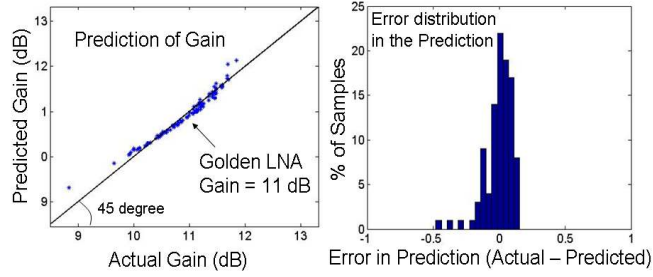


Fig. 4.8 (a). Prediction of Gain and error in prediction

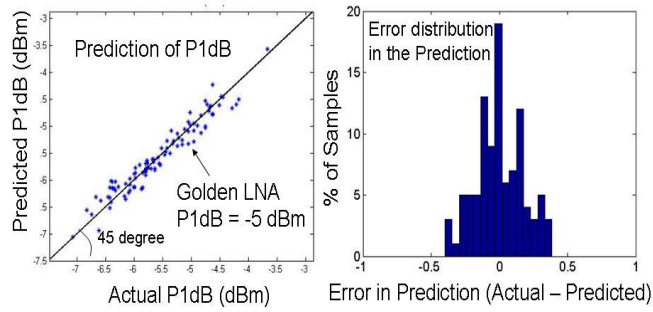


Fig. 4.8 (b). Prediction of P1dB and error in prediction

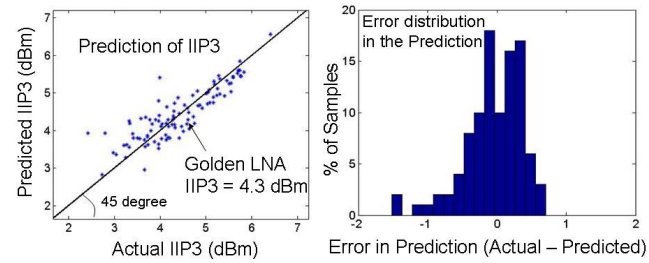


Fig. 4.8 (c). Prediction of IIP3 and error in prediction

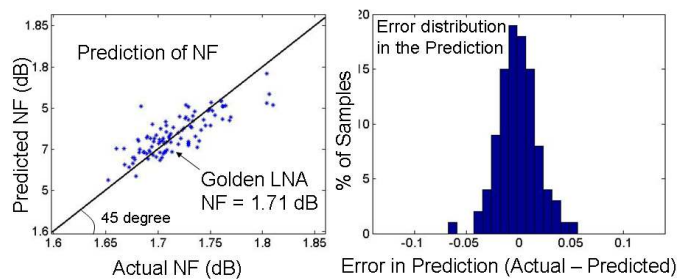


Fig. 4.8 (d). Prediction of NF and error in prediction

Fig. 4.8. Simultaneous prediction of RF amplifier specifications at 1.2 GHz from the single 250 MHz test-signature using the proposed test approach.

Table 4.1: Error in Prediction for Testing RF Amplifier

Error → Specification	Mean	Standard Deviation	Median	Min	Max
Gain (dB)	0.000	0.106	-0.015	-0.480	0.156
IIP3 (dBm)	-0.036	0.414	-0.005	-1.513	0.706
P1dB (dBm)	0.002	0.175	-0.003	-0.399	0.3870
NF (dB)	0.000	0.019	-0.001	-0.068	0.057

4.3 Measurement Results

As proof of concept, a hardware prototype of the proposed test setup is shown in Fig. 4.9 and demonstrated by testing commercially available LNA. Using this hardware prototype it is demonstrated that Gain, NF and P1dB of the LNA can be predicted simultaneously from the single test-signature output of the proposed test setup. In the test-setup of Fig. 4.9, three evaluation boards (Samples A, B and C) were used and it is assumed that Sample A is the golden LNA. To demonstrate the tuning/calibration capability of oscillation frequency at the output of the phase-shifter, voltage at the calibration knob was varied and measured results are shown in Fig. 4.10. Response of the test-setup for the above LNAs after the phase shifter and RF down-conversion is shown in Fig. 4.11.

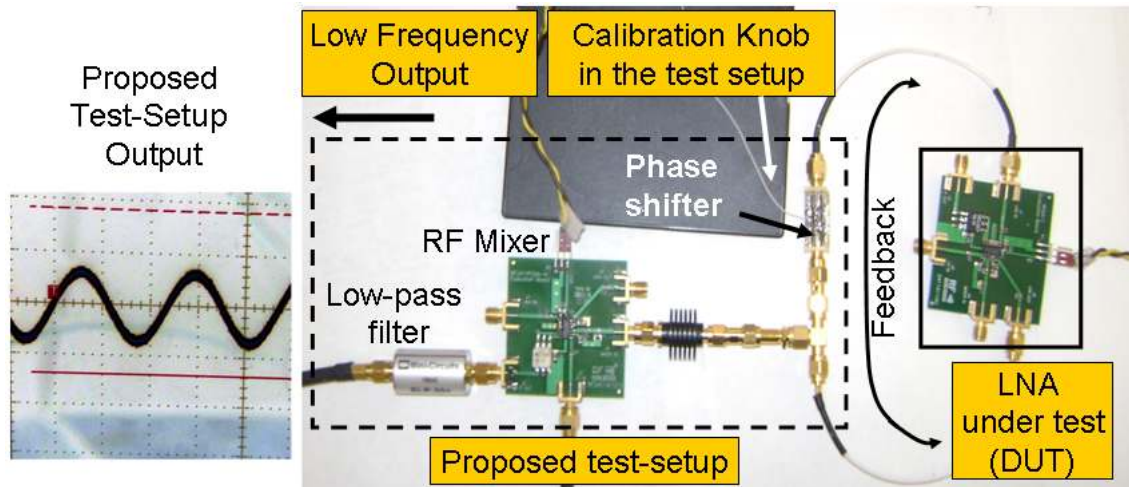


Fig. 4.9. Hardware prototype of the proposed test setup for testing an RF amplifier.

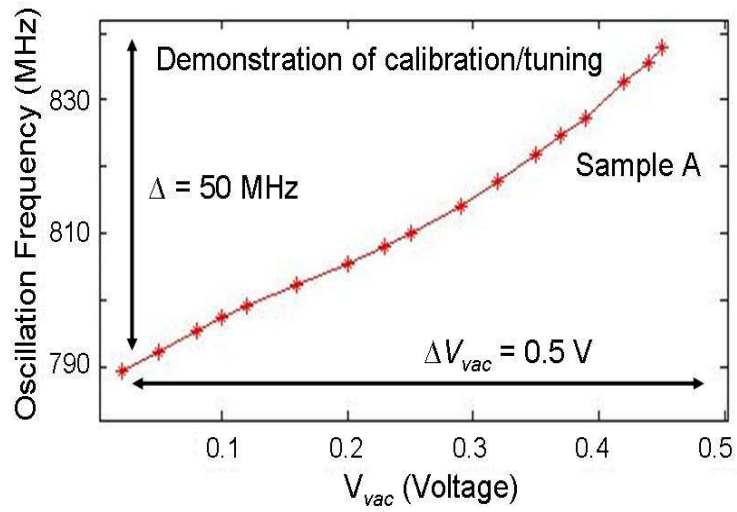


Fig. 4.10. Demonstration of tuning/calibration, measured oscillation frequency of the test setup for Sample A at output of the phase shifter.

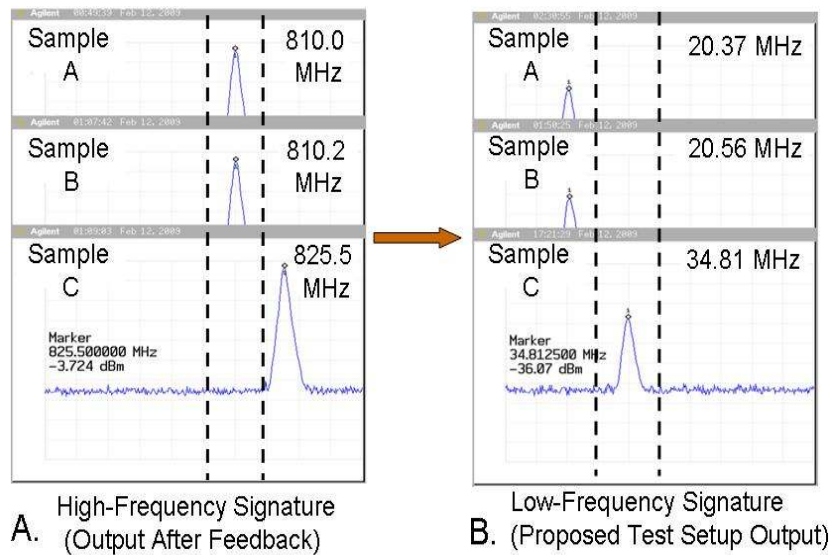


Fig.4.11. Measured oscillation frequency of the test setup for different LNA samples.

The measured gain (@ 810 MHz) of the LNAs vs. output oscillation frequency of the test setup is shown in Fig. 4.12. It can be inferred from these measurement results that the

oscillation frequency of the proposed test setup changes with the performance of the LNA. Hence, by defining allowable band around the golden LNA, initial pass-or-fail testing of the LNAs can be performed..

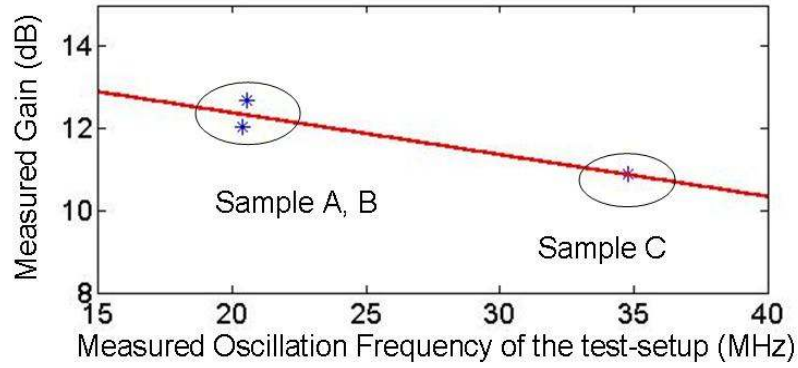


Fig. 4.12. Measured oscillation frequency of the test setup vs. measured Gain of the LNA samples.

Further, as proof of concept for high-resolution testing, prediction models for predicting Gain, NF and P1dB of the LNAs were developed. To make multiple instances as well as performance deviations expected due to process variations, the power supply of the above LNA Samples A and B was changed from 2.6 V to 5.0 V to obtain 65 instances of the RF LNA. Although this experiment scheme does not fully emulate the variations expected in a real production, it can show feasibility of the proposed method along with the simulations as described in the previous section. A similar approach to obtain multiple instances of the design under test by varying power supply has been used in [75]. Among abovementioned 65 instances, 35 samples were chosen for training set and the prediction model was developed using MARS for Gain, NF and P1dB. The prediction model was evaluated using 30 samples and their predicted Gain, NF and P1dB are shown in Fig. 4.13.a, Fig 4.13.b, and Fig 4.13.c. Summary of the error in prediction is given in Table 4.2.

Table 4.2: Error in Prediction of Specifications form Measurements

Error (Actual – Predicted) → Specification	Mean	Standard Deviation	Median	Min	Max
Gain (dB)	-0.018	0.264	-0.041	-0.522	0.471
P1dB (dBm)	-0.057	0.242	-0.105	-0.358	0.442
NF (dB)	-0.013	0.044	-0.022	-0.093	0.068

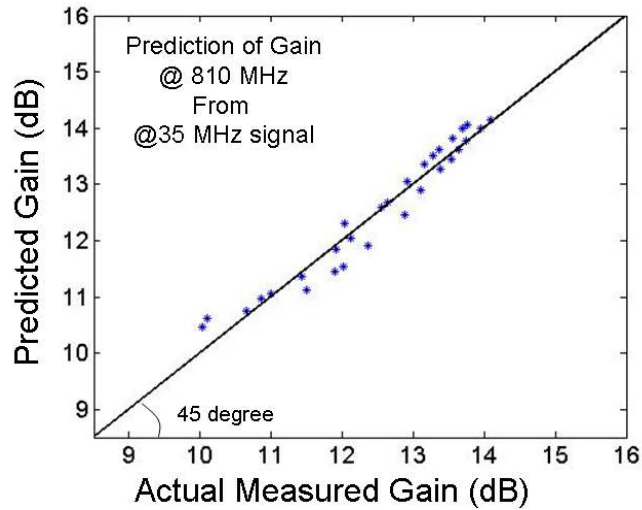


Fig. 4.13.a. Predicted Gain of the LNA from low-frequency test-setup output.

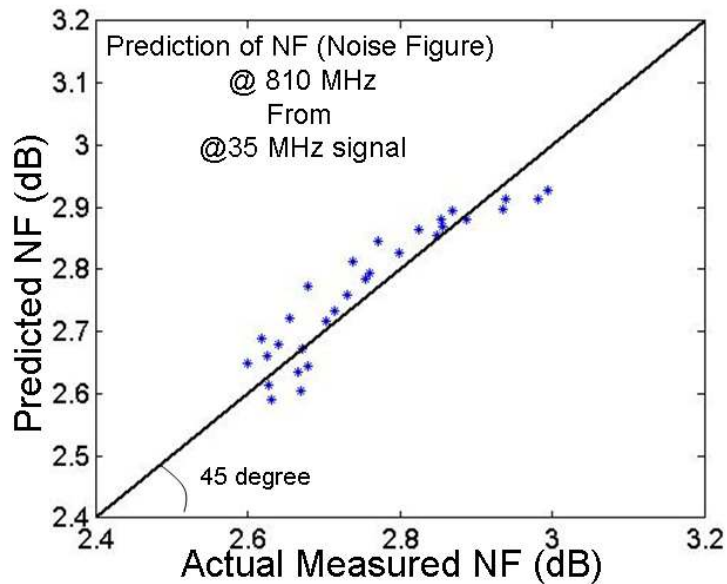


Fig. 4.13. b. Predicted NF (Noise Figure) of the LNA from low-frequency test-setup output

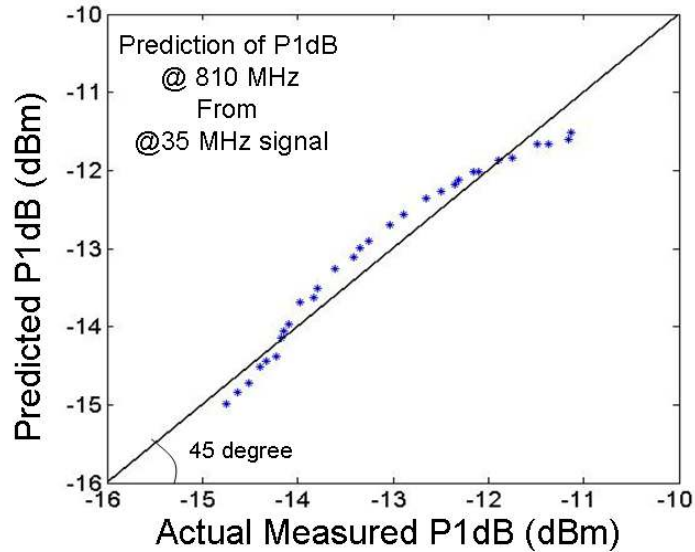


Fig. 4.13.c. Predicted P1dB of the LNA from low-frequency test-setup output

Fig. 4.13. Predicted vs Actual Measured Gain, NF, P1dB of RF Amplifier using the proposed test approach. Gain, NF, P1dB are predicted simultaneously from the single test-setup output

Based on the above results we conclude that the proposed method can be used for testing of RF LNAs by the analysis of low-frequency signal of the order of a few MHz and by simultaneous prediction of multiple RF specifications using a single test-signature output of the test-setup.

4.4 Discussions

This section discusses practical considerations, advantages and guidelines for efficient implementation of the proposed method for a production-level testing.

4.4.1 Stability Analysis

To implement this test method efficiently, the test setup should be designed such that its oscillation frequency should not drift inherently over the test time of the RF circuits, otherwise the test setup will require recalibration (which will require re-start of test setup or calibration using the proposed calibration knob). A slight inherent drift in the oscillation frequency is acceptable provided such drift is within the resolution limit of the measurement setup, or, it is within the resolution threshold that distinguishes the good RF LNAs from those that are faulty. To demonstrate the stability of the proposed test setup, a 14-hour long experiment was performed during the testing of Sample A. Measurements were taken using a spectrum analyzer (HP # E4407B) with start frequency = 5 MHz, end frequency = 80 MHz, ref level = -8 dBm, sweep = 4 ms (401 points), and resolution bandwidth of 1 MHz. As shown in Fig. 4.14, the oscillation frequency of the test-setup (Fig. 4.9) did not drift from 20.37 MHz over the duration of the experiment. Hence, it can be concluded that the proposed test setup is stable and is immune to the inherent drifts in the oscillation frequency.

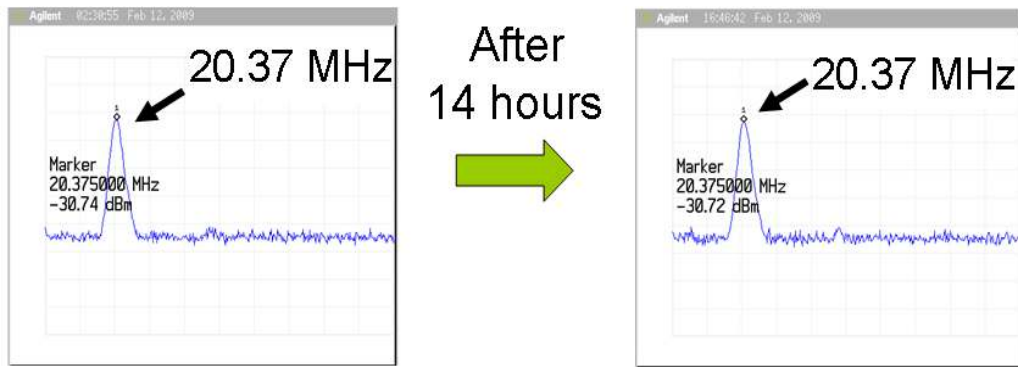


Fig. 4.14. Measured output oscillation frequency for over 14 hours using the proposed test setup to test RF amplifier.

4.4.2 Measurement noise or repeatability of the test results

To estimate the measurement noise or repeatability of the test results, 65 measurements were conducted for Sample B (previous sub-section). The summary of results is given in Table 4.3.

Table 4.3: Summary of The Results for Repeatability Analysis in The Measurements (Sample B, Previous sub-Section).

No of Measurements	Mode (MHz)	Mean (MHz)	Standard Deviation (MHz)	Maximum frequency (MHz)	Minimum frequency (MHz)
65	20.56	20.57	0.116	20.75	20.18

The statistical “mode” of the measurements is 20.56 MHz, and the statistical “mean” is 20.57 MHz, both of which are approximately the same when compared to the measurement results shown in previous sub-sections, Fig. 4.11 (oscillation frequency = 20.56 MHz). Moreover, standard deviation in these measurements is only 0.116 MHz. Hence, it can be concluded from this experiment that the results obtained by the proposed setup are repeatable and with proper design of the test setup, system noise will not be an issue in implementing this test method.

4.4.3 Cost Analysis

The test cost of the RF active circuits is mainly contributed by two factors, test-setup cost and test time. In the proposed method, same test-setup is used for simultaneously testing of multiple RF specifications using a single test signature output as shown in previous sub-sections, thus it is obvious that the proposed method will reduce test time. In addition to this, the proposed test setup also minimizes test-setup cost. For

production-level testing, the low-frequency sinusoidal output (MHz) of the proposed test-setup can be obtained with custom design of the phase-shifter, and output of the test setup can be sampled by a ADC, and then FFT of the sampled signal can be taken to determine the frequency of the sinusoidal signal. Therefore, *no RF measurements are required and test-setup cost reduces substantially*. Conventional methods need RF instruments such as RF input test signal generators and RF spectrum analyzer to measure Gain, IIP3, P1dB and NF. Although Gain and P1dB are typically measured by using Vector Network Analyzer (VNA), but for low-cost testing, signal generator and spectrum analyzer can also be used. Thus, for the comparison purpose we have compared proposed test-setup cost with the spectrum analyzer based test setup. Summary of the cost analysis is given in Table 4.4 and plotted in Fig. 4.15, which shows that the proposed test method reduces the test-setup cost by about 80%. It is also important to note that as test frequency increases the proposed test setup becomes more cost effective.

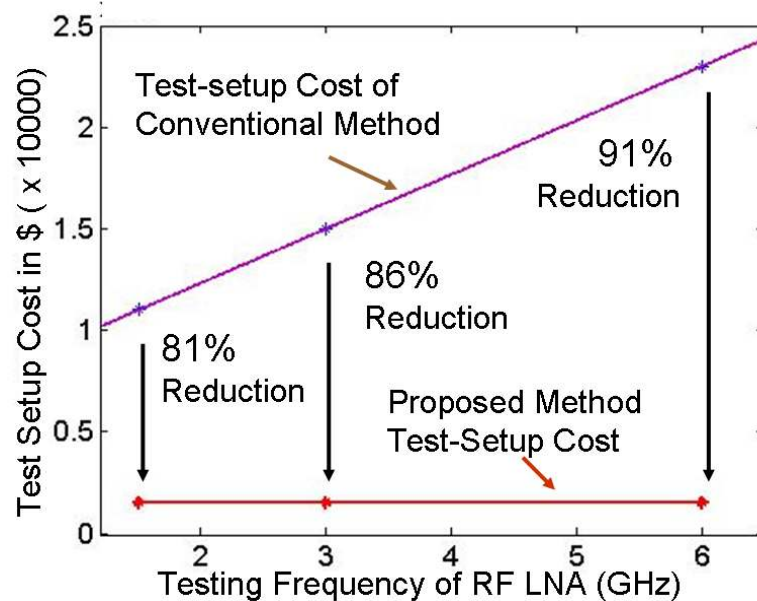


Fig. 4.15. Cost Analysis of the proposed test setup for testing RF amplifiers.

Table 4.4: Cost Analysis of the proposed Test-setup

Test Frequency	Test Setup cost		Reduction in Test-Setup Cost $Z = \frac{(X-Y)}{X}\%$
	Conventional Method (Spectrum Analyzer + RF test input signal generators) (X)	Proposed Method (Custom Board with ADC + RF down-conversion setup) (Y)	
1.50 GHz	\$11,000	\$2,100	81.0%
3.0 GHz	\$15,000	\$2,100	86.0%
6.0 GHz	\$23,000	\$2,100	91.0%

*Cost of instruments is taken from [71-73] for reference purpose only.

*Cost of Custom Board with ADC is assumed to be \$1100

4.5 Summary

In this chapter, a low-cost test methodology for testing RF amplifiers is proposed. The proposed approach enables testing of RF amplifiers by the analysis of low-frequency signature of the order of few MHz without applying any input test stimulus to the RF amplifiers. The test signature is self generated by the amplifier in the test mode. The method is demonstrated by testing commercially available 810-MHz LNA at 35 MHz. The cost analysis and stability analysis of the proposed test method were also performed and results show that the proposed test-setup is stable and can be used for low-cost testing of RF amplifiers.

(This page is intentionally left blank)

CHAPTER 5

A SELF-HEALING METHODOLOGY FOR RF AMPLIFIER CIRCUITS

This chapter proposes a new self-healing methodology for embedded RF Amplifiers in RF sub-systems. *The final goal of the self-healing is to increase the post-manufacturing yield for parametric defects.* The proposed methodology is based on oscillation principles in which the Device-Under-Test (DUT) itself generates the output test signature with the help of additional circuitry. In the proposed methodology, the self-generated test signature from the DUT is analyzed by using on-chip resources for testing the DUT and controlling its calibration knobs to compensate for multi-parameter variations in the DUT's manufacturing process. Thus, the proposed methodology enables self-test and self-calibration/correction of RF amplifiers without the need for external test stimulus, enabling self-healing RF designs. The proposed methodology is demonstrated through simulations as well as measurements performed on an RF LNA, which were designed in commercially-available 6 metal layers, 0.18 μm , 120 GHz SiGe BiCMOS process technology.

5.1 Proposed Self-Healing Methodology for RF Amplifiers

As shown in Fig. 5.1, the proposed technique does not require the use of external test stimulus for performing self-healing because the stimulus is generated by the Device-Under-Test (DUT) itself, with the help of additional circuitry and by using oscillation

principles. This stimulus is used to assess the impact of process variations on the performance of the DUT. Subsequently, compensation for loss of DUT performance due to process variations is performed by adjusting calibration/tuning knobs designed into the DUT. This tuning knob manipulation is driven by analysis of the self-generated output (referred to as the DUT *signature*) from the DUT, as shown in Fig. 5.1. The output signature of the DUT is analyzed with available on-chip resources (RF mixer, ADC, PMU and DSP). Thus, the proposed methodology enables self-test as well as self-calibration/correction of the embedded LNA, leading to *truly self-healing* RF designs. In the past, oscillations based testing has been proposed for analog/mixed-signal/RF circuits in [43-48, 76]. The proposed methodology in the present chapter is also based on oscillation principles, but for the first time, a self-healing methodology for the yield improvement of active RF circuits such as an embedded RF LNAs has been proposed. Also, to achieve the yield improvement, the concept of *performance curves* is proposed.

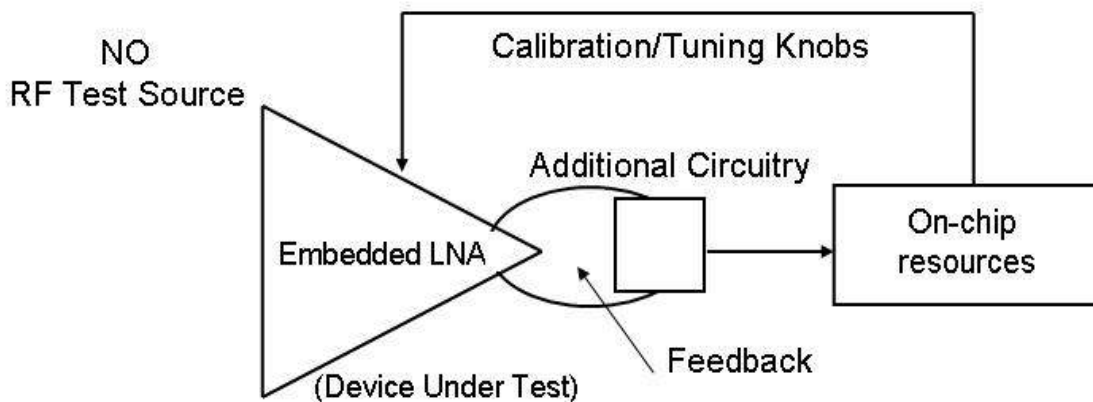


Fig. 5.1. Proposed self-healing architecture of the RF amplifier.

5.1.1 Self-Healing Flow

Fig. 5.2 shows the overall self-healing procedure, which includes both self-testing and self-calibration/correction. After fabrication, the LNA is tested to identify those LNAs with catastrophic vs. parametric defects. The proposed self-calibration/correction is exercised only if the LNA is determined to be free of catastrophic faults.

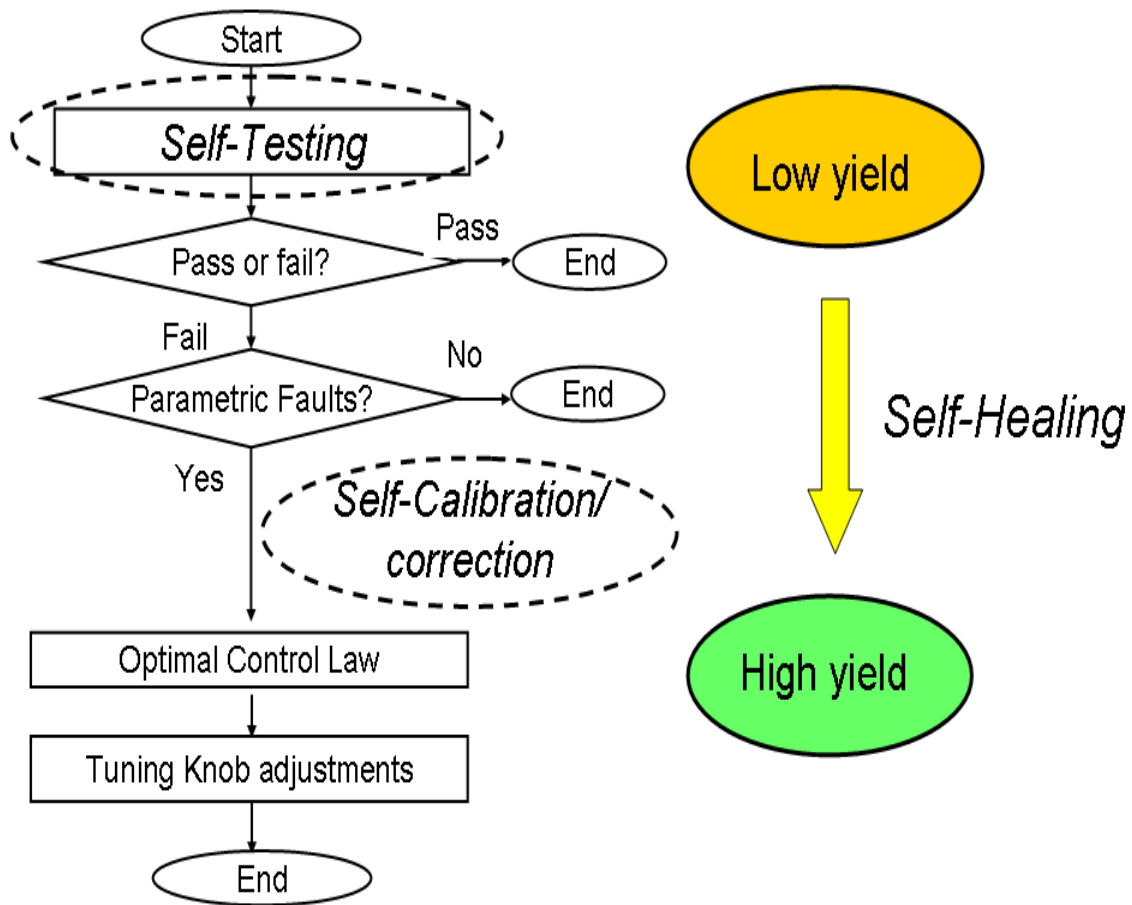


Fig. 5.2. Self-healing flow.

5.1.2 Self-Healing Architecture

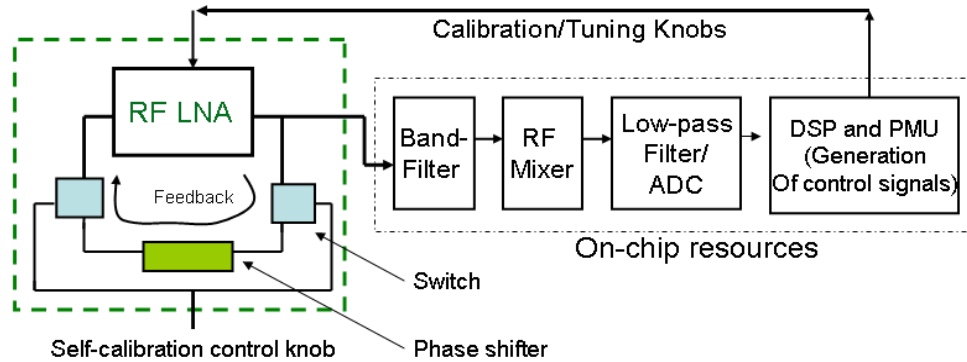


Fig. 5.3. Proposed self-healing LNA architecture.

Consider the proposed self-healing architecture of the embedded LNA, as shown in Fig. 5.3. In the self-healing mode, external feedback is enabled across the LNA such that this feedback causes the LNA to oscillate and produce a sinusoidal signal for testing and calibration purposes. The feedback network is a simple phase shifter and can be implemented on-chip or off-chip on the circuit board. The phase-shifter is connected to the input and output ports of the LNA by RF switches to complete the feedback loop. The sinusoidal signature from the LNA output is down-converted and the FFT of the down-converted signal is computed in the base-band DSP to determine the oscillation frequency of the LNA with the enabled feedback. It can be seen from Fig. 5.3 that all of the above can actually be accomplished *without the use of any external RF test stimulus*. Self-healing of the LNA in the presence of process variations is achieved by adjusting the LNA's tuning "knobs" from on-chip power management unit (PMU), using the on-chip RF mixer, ADC, low-pass filter, image reject filter, and DSP, resources that are necessary for performing normal wireless communications functions.

In the proposed architecture, a phase shifter is designed in such a manner that:

(a) After inclusion of the external feedback, the LNA oscillates around the desired operating or testing frequency.

(b) The oscillation frequency of the LNA with the included external feedback is sensitive to process variations and differs significantly for the golden LNA and LNAs with parametric failures.

(c). The phase shifter design is robust to manufacturing process variations and may be located on the circuit outside the chip (allowing its performance to be controlled accurately). In the present chapter, the self-healing methodology is demonstrated assuming *on-chip phase-shifter* and it is subjected to the same process variation as of the RF LNA.

(d). The change in the oscillation frequency due to parametric defects in the LNA is measurable by the receiver chain (must lie within the bandwidth of the receiver chain and be detectable using the on-chip ADC's sampling speed and resolution).

In our experiments, estimation of the maximum (F_{max}) and minimum (F_{min}) change in the oscillation frequency due to parametric defects around the desired testing frequency (F_0) is performed using Monte Carlo simulations. In practice, oscillation frequency measurements made on LNA samples selected from different production lots and across a large number of wafers should be used to determine the values of F_{max} and F_{min} . The presence of a band-pass filter after the LNA works as an image-reject filter and helps to avoid misclassification of a faulty LNA as a good LNA because of the down-conversion of the output signal of the LNA.

5.1.3 Classification of Catastrophic and Parametric Failures

In the proposed healing methodology, the detection of failures is performed using predictive oscillation-based testing [43, 47, 76]. In the present thesis, predictive oscillation-based testing is extended for on-chip testing of RF amplifiers (RF BIST for RF amplifiers) and show that the detection of faults is possible because of the non-linear mapping between test signature and specifications of the LNA. In addition, as mentioned earlier, this thesis for the first time proposes the yield improvement using oscillations principles for active RF circuits, which is explained in detail in the following sections.

In an RF design, the RF performance/specifications are dependent on the functional behavior of the RF passive components (inductors and capacitors) at the desired operating frequency. In addition, as mentioned in the earlier chapter, RF specifications are interdependent since a change in one specification causes a change in the other. Let us assume that the non-linearity of the amplifier is up to third order, as given by Equation (5.1), then P1dB of the amplifier can be approximated by Equation (5.2). It can be inferred from these equations that P1dB is dependent on gain (α_1) of the LNA, which shows interdependency of different specifications. In addition, at the circuit level, components that contribute to one specification also contribute to the other specifications to some extent. This increases the interdependency of RF specifications on each other.

$$V_{out} = \alpha_1 V_{in} + \alpha_2 V_{in}^2 + \alpha_3 V_{in}^3 \quad (5.1)$$

$$P1dB = 10 \log(0.145 \alpha_1 / \alpha_3) \quad (5.2)$$

In Equations (5.1) and (5.2), α_1 is the gain of the amplifier; α_2 and α_3 are non-linearity coefficients.

Furthermore, in active circuit design, some of the ac characteristics such as the transistor's transconductance (g_m) is dependent on DC biasing. As shown in Equations (5.3) and (5.4), respectively, the g_m of the BJT and CMOS depends on the bias current to first order. Thus, the gain (α_1) of the RF amplifier is dependent on the bias current as well, which shows interdependency of RF specifications on biasing.

$$g_m = \frac{I_c}{V_t} = \beta \frac{I_b}{V_t} \quad (5.3)$$

$$g_m = \sqrt{2(W/L)\mu C_{ox}I_d} \quad (5.4)$$

In Equations (5.3) and (5.4), β is the beta or current gain of the BJT, I_b is the base current of the BJT, $V_t = kT/q$, W is the width of the MOS transistor, L is length of the MOS transistor, μ is the mobility of the transistor, C_{ox} is the gate capacitance of the transistor, I_d is the drain current of a MOS transistor and I_c is the collector current of the BJT.

Because of process variations, assume that g_m changes to $g_m(p_p)$, α_1 changes to $\alpha_1(p_p)$, α_2 to $\alpha_2(p_p)$, α_3 to $\alpha_3(p_p)$, Hence, the RF amplifier's gain and P1dB become a function of process variations such as gain (p_p), P1dB(p_p) as shown in Fig. 5.4. For oscillations to initiate, the closed-loop gain of the system has to be greater than unity and satisfy the Barkhausen criterion. As oscillations build up, non-linearity of the system causes these oscillations to become stable. Thus, in our methodology, the oscillation frequency also shifts because of the change in the performance of the RF amplifier.

Since this shift in oscillation frequency is preserved during RF down-conversion, there exists a finite possibility to derive non-linear analytical expressions which compute the relationship among the amplifier specifications, the oscillation frequency and the bias current of the amplifier. However, derivation of such analytical expressions is difficult, and if the amplifier has higher order non-linearities (greater than 3), then derivation of such analytical equations can become intractable. However, development of a non-linear model to predict specifications of RF amplifier can be easily accomplished by using successive-learning processes such as Multivariate Adaptive Regression Splines (MARS) and Artificial Neural Networks (ANN). This concept of performance prediction has been previously applied for mixed-signal/RF testing based on alternate testing and predictive oscillation testing in [32, 43, 76]. In addition, in [47, 77] it is shown that accuracy of prediction depends on the choice of the successive-learning processes and number of test signature variables (such as number of sinusoidal input tones, oscillation frequency and dc current).

In our approach, the phase shifter is designed in such a way that catastrophic defects in the LNA cause no oscillations to occur, while parametric defects lead to a change in the oscillation frequency of the LNA (with feedback) around the response of the golden LNA. The information about the DC power consumed by the RF amplifier is assumed to be available from on-chip power-management unit (PMU). The specifications of the embedded LNA are predicted from the non-linear prediction model that maps its performance specifications to the observed change in the oscillation frequency and DC current supplied by the PMU to the LNA. A nonlinear prediction model based on Multivariate Adaptive Regression Splines (MARS) has been used in the present thesis.

MARS uses an initial recursive partitioning during training to gradually add basis functions using forward stepwise placement; next, a backward procedure is applied and the basis functions associated with the smallest increase in the least squares fit are removed. More details regarding MARS can be found in [31].

The development of a non-linear prediction model using MARS is a one time effort which requires a “training set” of RF amplifiers with statistically likely parametric failures. The training set used to estimate the maximum (F_{max}) and minimum (F_{min}) change in the oscillation frequency due to parametric defects around the desired testing frequency (F_0) is used for the development of the prediction models. As discussed earlier, RF amplifiers for which oscillations do not occur are considered to have catastrophic failures, while amplifier samples which result in oscillations are assumed to have parametric failures. Self-correction/calibration of the amplifier (with parametric failures) is performed by adjusting the tuning knobs designed in the amplifier according to the procedure described below.

5.1.4 Self-Calibration Procedure and Tuning Knob Selection

Self-healing RF circuits require design with “calibration/tuning knobs” through which their performance can be controlled post-manufacture by adjusting the tuning knob values. Calibration/tuning knob control algorithms must also be devised that allow the performance specifications of RF circuits to be compensated to the maximum extent possible using such post-manufacture tuning knob control. In the best case scenario, the design of tuning knobs that can control the specifications of a DUT *independent* of other specifications is desired. This allows all specifications to be controlled independently post-

manufacture, allowing maximum yield recovery. However, in analog/RF circuits, different performance metrics of the circuits are *interdependent*, thereby making it nearly impossible to find tuning knobs which satisfy the above property. For particular applications, certain specifications of the RF circuits in question are important, while others are not. For example, a gain specification of the LNA can be stringent in certain applications, while other specifications (such as P1dB and noise figure) have sufficient performance margins. In this case, a tuning knob can be introduced to vary the gain of the LNA with less concern for P1dB and noise figure. For multi-specification designs, multiple tuning knobs may be necessary and optimal tuning solutions should be found to meet the required yield criteria.

The calibration/correction procedure can be a one-time or iterative. In the iterative procedure, the calibration/tuning knobs are adjusted and measurements are made at each iteration until the required specifications of the DUT are achieved. This procedure gives high yield recovery but is time consuming. In the one-time calibration procedure, after analyzing the response of the DUT, the tuning knobs are programmed only once.

In the present chapter, a one-time calibration procedure is proposed, which works as follows. After the specifications of the DUT are predicted using the non-linear prediction model, the DUT calibration/tuning knobs are adjusted using the *performance curves* of the DUT and Equation (5.5). The *performance curves* of the DUT reveal the changes in the specifications of the DUT as functions of the DUT tuning knob values (one function for each DUT specification) and are obtained by changing the tuning knob values of the golden DUT and observing how its performance specifications are affected. To estimate the change in each specification of the DUT, the weighted sum of the effect of each DUT

tuning knob is computed according to Equation (5.5). Equation (5.5) is a first-order linear approximation of the effect of multiple tuning knob perturbations on each specification of the DUT. For multi-specification optimization, a set of such linear simultaneous equation can be solved.

$$\Delta S_j = \sum w_i \Delta K_i \quad (5.5)$$

where, ΔS_j is required compensation in the specification “j”

w_i is weight associated with the change in the tuning knob (ΔK_i).

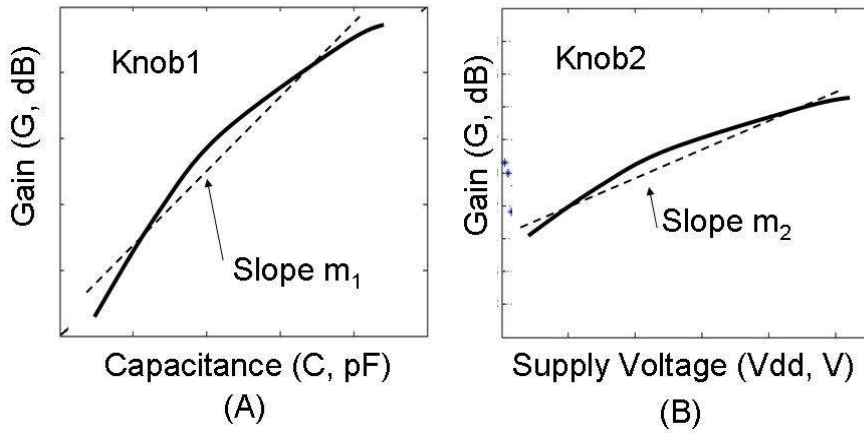


Fig.5.5.The performance curves of LNA for different calibration knobs.

To illustrate, let us consider embedded RF amplifier with two knobs, Knob1 and Knob2. Knob1 tunes a capacitance in the amplifier and Knob2 tunes power supply of the amplifier. The change in the gain of the amplifier because of the change in power supply and capacitance is shown in Fig. 5.5. Then, the calibration in the gain (ΔG) can be performed vs Equation (5.6).

$$\Delta G = m_1 \cdot \Delta C + m_2 \cdot \Delta Vdd \quad (5.6)$$

where, m_1 and m_2 can be approximated by the slope of the line in performance curves in Fig. 5.5A and Fig. 5.5B, respectively.

For efficient functioning of this calibration procedure, the tuning knobs should be chosen so that the specifications of the DUT vary almost linearly with the tuning knob values (even in the presence of nonlinearities in the DUT, the linear assumption gives yield improvement as shown in the following sections). Furthermore, as stated earlier, the tuning knobs can be chosen such that each DUT specification is largely dependent on only one knob. In that case, Equation (5.5) reduces to $\Delta S_I = w_I \Delta K_I$.

5.2 Simulation Results

To demonstrate the proposed self-healing methodology, SiGe HBT and CMOS RF LNAs have been designed in SiGe BiCMOS platform. For these designs, the actual simulation models provided by the foundry are used. In addition, each phase-shifter, RF switches and RF LNA were subjected to the same process variations using Monte Carlo analysis and for this simulation; models as provided by the foundry were again used.

5.2.1 Self-Healing SiGe HBT RF LNA

In this 2.80 GHz RF LNA (Gain = 22.09 dB, P1dB = -19.81 dBm), two tuning knobs have been introduced, one to change the bias current (I_{bias}) and other to change the

capacitance in the LC tank. The change in the capacitance is achieved by changing the voltage on the varactor, V_{cap} . Fig. 5.6 shows the simulation setup in which the feedback is applied to the LNA using an on-chip phase shifter such that the LNA becomes unstable and begins oscillations. This enables the self generation of a test signature without any input test stimulus. In this test-setup the phase-shifter is designed such that no oscillation occurs for catastrophic failures while oscillation frequency shifts for the parametric failures around the response of the golden LNA.

For illustration, 10 single-catastrophic failures (5 open and 5 short) were introduced at 5 nodes (Fig. 5.6) of the LNA and 100 parametric instances of the LNA were generated using Monte-Carlo simulations. Simulations were performed in Cadence Spectra using Advance Design System (ADS) dynamic link tools and the sinusoidal signal at the output of the LNA was down-converted using a behavioral model of a RF-mixer, a low-pass filter and a band-pass filter in Matlab, as shown in Fig. 5.7. In addition, all DSP processing was implemented in Matlab.

The down-converted oscillation frequency of all the 110 samples of the LNA (with 100 parametric and 10 catastrophic defects) is shown in Fig. 5.8. It can be inferred from the Fig. 5.8 that for some of the LNAs no-oscillations have occurred, while for others the oscillation frequency is around the response of the golden LNA. It is important to note that no oscillation has occurred for the LNA with catastrophic defects. Thus, depending on the occurrence of the oscillation, the LNA with parametric variations can be easily separated from LNAs with catastrophic defects.

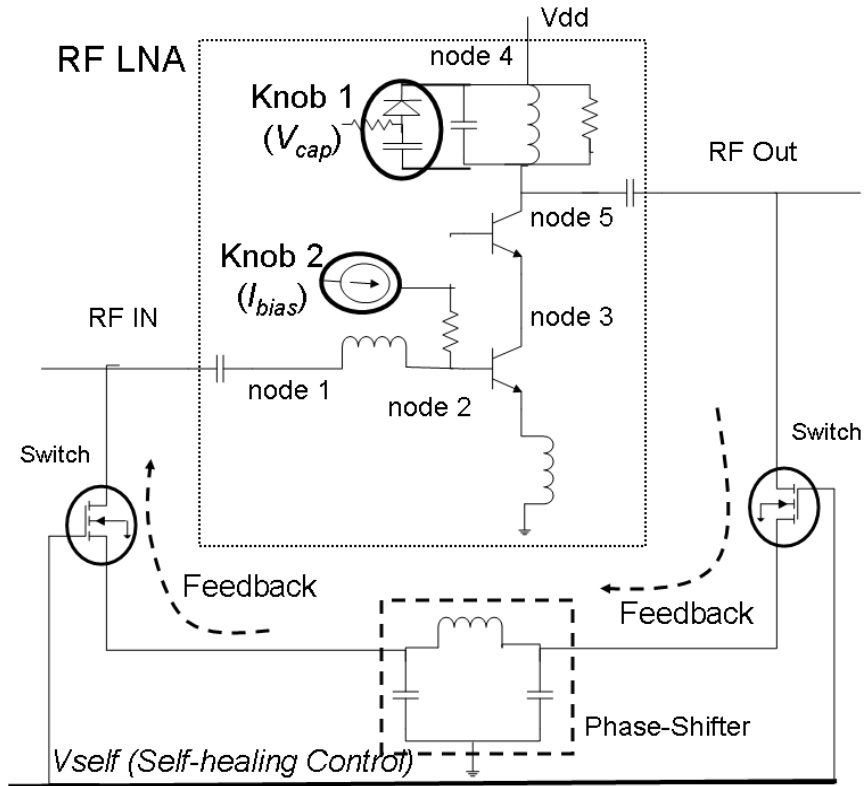


Fig.5.6. Self-healing SiGe RF LNA modeling.

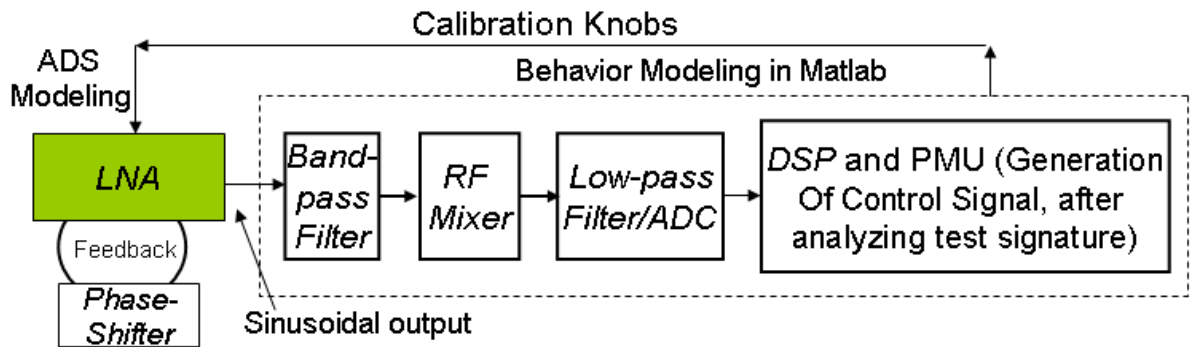


Fig.5.7. RF system modeling to demonstrate self-healing methodology for RF amplifiers.

To determine which samples of the LNAs should be chosen for the self-calibration/correction, using MARS, a non-linear prediction model to predict the forward

small signal transmission gain (Gain, dB) and 1-dB compression point (P1dB, dBm) was developed from the response of the training set, which had 300 LNAs. These 300 LNAs were obtained by Monte Carlo simulation. The prediction model was used to find the specifications and the predicted gain and P1dB of the 100 samples of the LNA is shown in Fig. 5.9A and Fig. 5.9B, respectively.

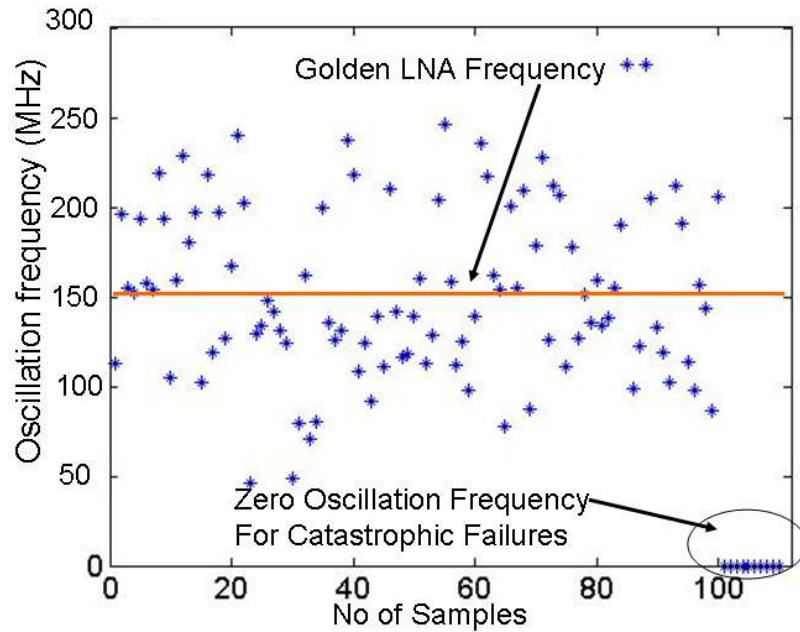


Fig.5.8. Oscillation frequency of the various LNA samples.

It can be seen from the results shown in Fig. 5.9 that the predicted performance of the LNA from the self-generated test signature is quite accurate. Thus, this methodology can be used for on-chip self-testing of the LNAs. Let us assume that the allowable performance specification of the gain is from 21.0 dB to 23.0 dB and P1dB should be greater than -21.0 dBm. Considering an error in the prediction at the boundary of the allowable specifications, 29 samples were selected for calibration/correction to meet the gain specification and 21 samples to meet P1dB specification.

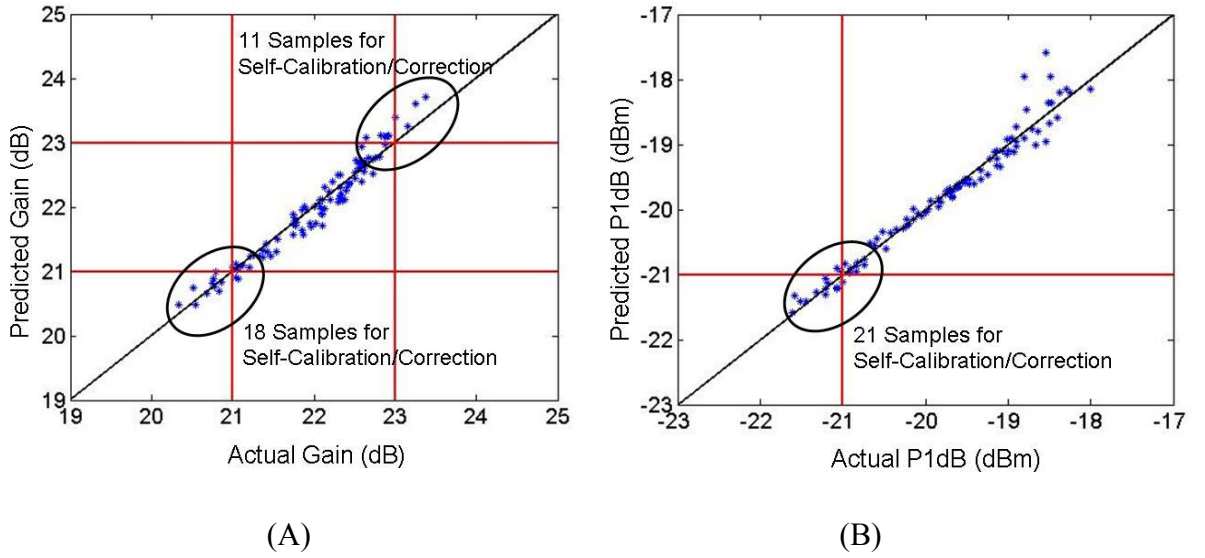


Fig. 5.9 SiGe RF amplifier analysis of parametric failures (a) Prediction of gain of SiGe RF amplifier, (b) Prediction of P1dB of SiGe RF amplifier

The self-calibration/correction was performed with the help of two tuning knobs. The first tuning knob (Knob1) changes the varactor voltage (V_{cap}) in the LC tank of the LNA, while the second tuning knob (Knob2) changes the bias current (I_{bias}) of the LNA (Fig. 5.6). The performance curves of the LNA with respect to these two tuning knobs, Knob1 and Knob2, are shown in Fig. 5.10 and Fig. 5.11. The obtained equations are:

$$\Delta G = 0.32 * \Delta V_{cap} + 0.05 * \Delta I_{bias}, \quad (5.7)$$

$$\Delta P1dB = -0.02 * \Delta V_{cap} + 0.09 * \Delta I_{bias} \quad (5.8)$$

where, ΔG in dB, $\Delta P1dB$ in dBm, ΔI_{bias} in μA , and ΔV_{cap} in V.

For yield improvement, the change in tuning knobs was calculated using above equations and the predicted value of the specifications from the non-linear prediction

model was used to calculate ΔG and $\Delta P1dB$. For all the calibrations/corrections, the ΔV_{cap} is in the range of ± 2.25 V and the change in ΔI_{bias} is below $12.10 \mu A$.

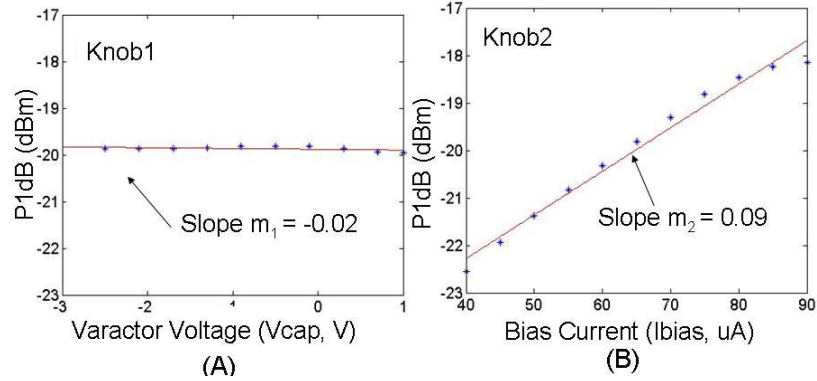


Fig. 5.10. Performance curves: P1dB of LNA as a function of the tuning knobs

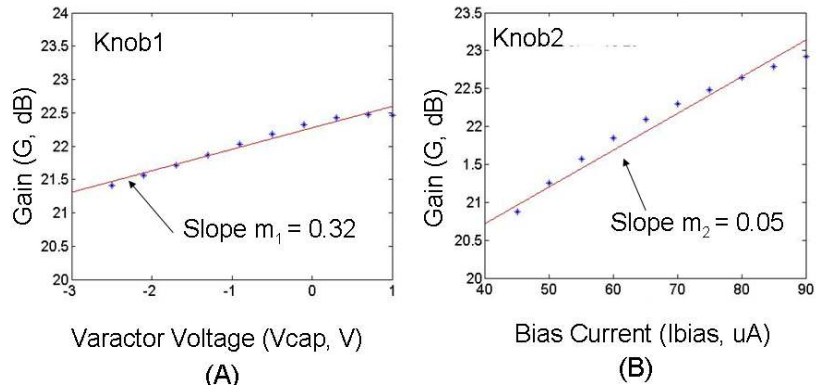


Fig. 5.11 Performance curves: gain of LNA as a function of the tuning knobs

5.2.1.1 SiGe LNA Calibration using a single Knob for P1dB

In this sub-section, the proposed calibration procedure was applied to 21 samples of the LNA to increase their P1dB above -21.0 dBm. Only one tuning knob, Knob2, was used. The specification distribution before and after healing is given in Fig. 5.12 and the summary of the results is given in Table 5.1. It can be inferred from the results obtained

that all of the LNAs began meeting the P1dB specification. However, the distribution for gain has not improved much. To increase the number of LNA samples with an allowable tolerance of the gain, the calibration for the gain is explored in the next sub-section.

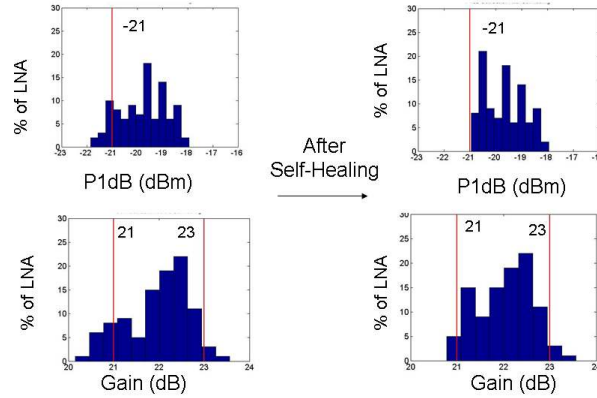


Fig. 5.12. Specification distribution before and after healing using Knob1.

Table 5.1: Summary of Healing Results (Knob 1)
SiGe HBT RF Amplifier

SiGe HBT RF Amplifier	% of LNAs with Gain (21.0 – 23.0 dB)	% of LNA with P1dB (> -21 dBm)	Yield of LNA (Gain and P1dB)
Before Healing	87%	87%	83%
After Healing	93%	100%	93%

5.2.1.2 SiGe LNA Calibration using a Single Knob for Gain

In this sub-section, the SiGe LNA samples were calibrated using Knob1, with focus on improving the yield of gain. The obtained results are shown in Fig.5.13 and are summarized in Table 5.2.

Table 5.2: Summary of Healing Results (Knobs 2)
SiGe HBT RF Amplifier

SiGe HBT RF Amplifier	% of LNAs with Gain (21.0 – 23.0 dB)	% of LNA with P1dB (> -21 dBm)	Yield of LNA (Gain and P1dB)
Before Healing	87%	87%	83%
After Healing	97%	91%	91%

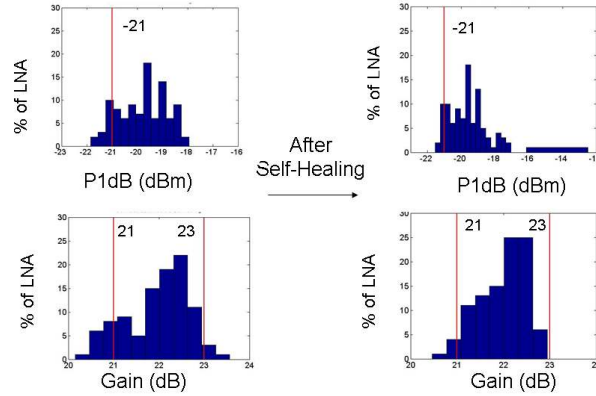


Fig. 5.13. Specification distribution before and after healing using Knob2.

The above results show an improvement in gain yield to 100%, but P1dB yield only to 91%. Hence, to get better yield of the LNA, calibration was performed using both of the knobs.

5.2.1.3 SiGe LNA Calibration using both the Knobs

In this calibration procedure both knobs were used and obtained results are shown in Fig. 5.14 and summarized in Table 5.3. Samples which did not meet both gain and P1dB specifications were calibrated using both the knobs, and the change in the calibration knobs was calculated by solving two equations $\Delta G = 0.32 * \Delta V_{cap} + 0.05 * \Delta I_{bias}$, $\Delta P1dB = -0.02 * \Delta V_{cap} + 0.09 * \Delta I_{bias}$. Samples which were not meeting P1dB alone were calibrated using Knob2, and Knob1 was used for calibrating samples which were not meeting gain alone.

Table 5.3: Summary of Healing Results (Both Knobs) SiGe HBT RF Amplifier

SiGe HBT RF Amplifier	% of LNAs with Gain (21.0 – 23.0 dB)	% of LNA with P1dB (> -21 dBm)	Yield of LNA (Gain and P1dB)
Before Healing	87%	87%	83%
After Healing	100%	100%	100%

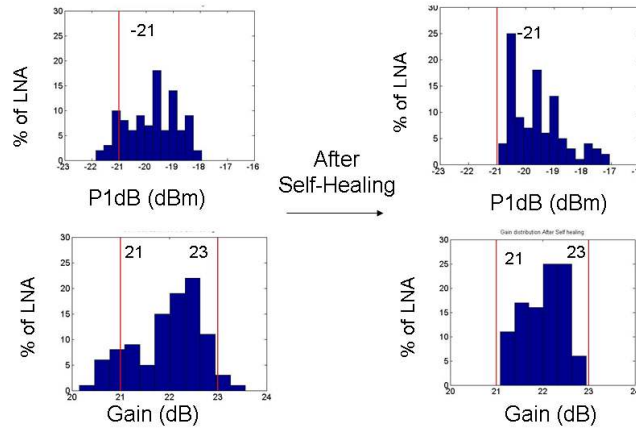


Fig. 5.14. Specification distribution before and after healing using Knob1 and Knob2.

Based on above the results it can be concluded that the yield of the LNA has increased by the proposed self-healing methodology, which includes self-testing and self-calibration/correction.

5.2.2 Self-Healing CMOS RF LNA

To further demonstrate the self-healing methodology, a 1.85 GHz CMOS LNA was designed which a gain = 16.80 dB, and P1dB = -10.71 dBm. In this LNA, as shown in Fig. 5.15, two tuning knobs have been introduced, one to change the bias voltage (V_g) and the other to change the power supply (V_{dd}). Again, in this design, the phase-shifter is designed such that no oscillation occurs for catastrophic failures, while the oscillation frequency shifts for the parametric failures around the response of the golden LNA. For illustration, 10 single-catastrophic failures (5 open and 5 short) were introduced at 5 nodes of the LNA (Fig. 5.15) and 100 parametric instances of the LNA were generated by Monte-Carlo

simulations. Simulations were performed in Cadence Spectra using Advance Design System (ADS) dynamic link.

Similar to the results of the previous section, the analysis showed that for the LNAs with catastrophic failures no oscillations occurred, while for others the oscillation frequency was around the response of the golden LNA. Thus, depending on the occurrence of the oscillation, the LNA with parametric variations can be separated from LNAs with catastrophic defects. To determine which samples of LNAs should be selected for self-calibration/correction, a non-linear prediction model using MARS was developed to predict the forward transmission gain and P1dB. The prediction model was developed using the training set which had 300 LNAs, which were again obtained using Monte Carlo simulations. The gain and P1dB specification was predicted using the non-linear prediction model and self-calibration/correction was performed by the calibration produce described in the previous sections.

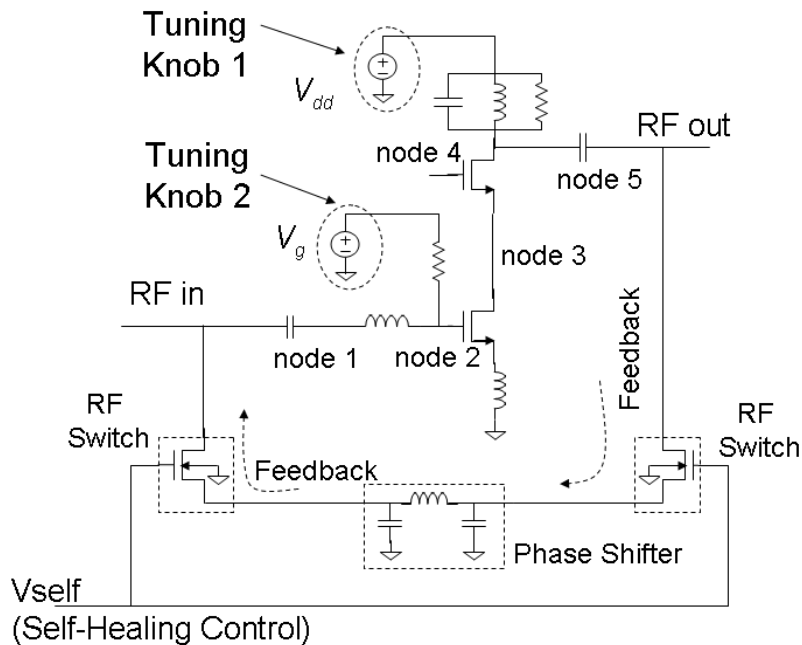


Fig. 5.15. Self-healing CMOS RF LNA modeling.

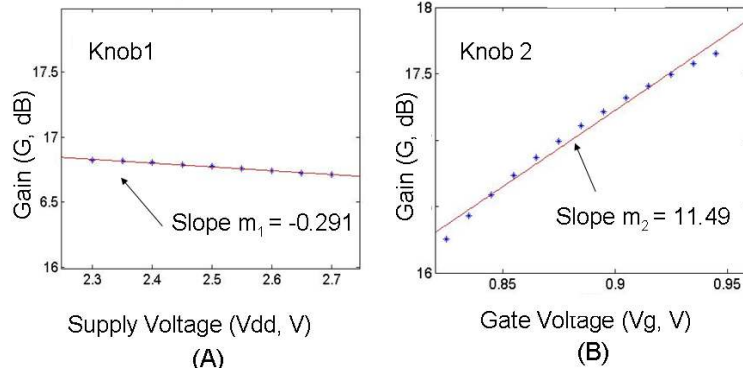


Fig. 5.16 A). gain of the CMOS LNA as a function of the tuning knobs.

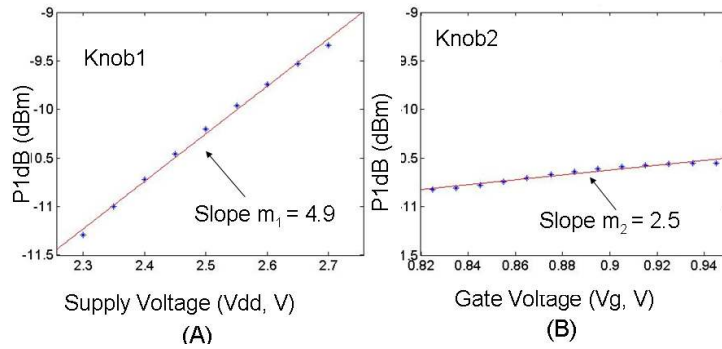


Fig. 5.16 B). P1dB of the CMOS LNA as a function of the tuning knobs.

Fig. 5.16. Performance curves for 1.85 GHz CMOS LNA.

The self-calibration/correction was performed with the help of the two tuning knobs designed for the LNA. The performance curves of the LNA with respect to these two tuning knobs, Knob1 and Knob2, are shown in Fig. 5.16. The obtained equations of the form of Equation (5.5) are:

$$\Delta G = -0.291 * \Delta V_{dd} + 11.49 * \Delta V_g \quad (5.9)$$

$$\Delta P1dB = 4.9 * \Delta V_{dd} + 2.5 * \Delta V_g \quad (5.10)$$

where, ΔG in dB, $\Delta P1dB$ in dBm, ΔV_{dd} in V, and ΔV_g in V.

For yield improvement, above equations were used and 30 samples were selected for calibration to meet the gain specification and 28 samples to meet the P1dB specification. In this experiment, it is assumed that the allowable performance specification of gain is from 15.20 dB to 17.80 dB and P1dB should be greater than -11.40 dBm. The obtained results of the calibration are shown below. For all these calibrations/corrections, the change in bias voltage (ΔV_g) is in the range of + 0.072 V to -0.154 V and the change in power supply (ΔV_{dd}) is below 0.420 V.

5.2.2.1 CMOS LNA Calibration using a Single Knob for P1dB

In this sub-section, the proposed calibration procedure was applied to 28 samples of the CMOS LNA to increase their P1dB above -11.40 dBm. Only one calibration knob, Knob1, was used. The summary of specification distribution before and after calibration is shown in Fig. 5.17 and given in Table 5.4.

The obtained results show that after calibration only 2% of the samples are not meeting the P1dB specification. However, the distribution for the gain has not improved. To increase number of LNA samples with in allowable tolerance of the gain, the calibration for the gain is explored in the next sub-section.

Table 5.4: Summary of CMOS Amplifier Healing Results (Knob 1)

CMOS RF Amplifier	% of LNAs with Gain (15.20– 17.80 dB)	% of LNA with P1dB (> -11.40 dBm)	Yield of LNA (Gain and P1dB)
Before Healing	87%	91%	81%
After Healing	87%	98%	85%

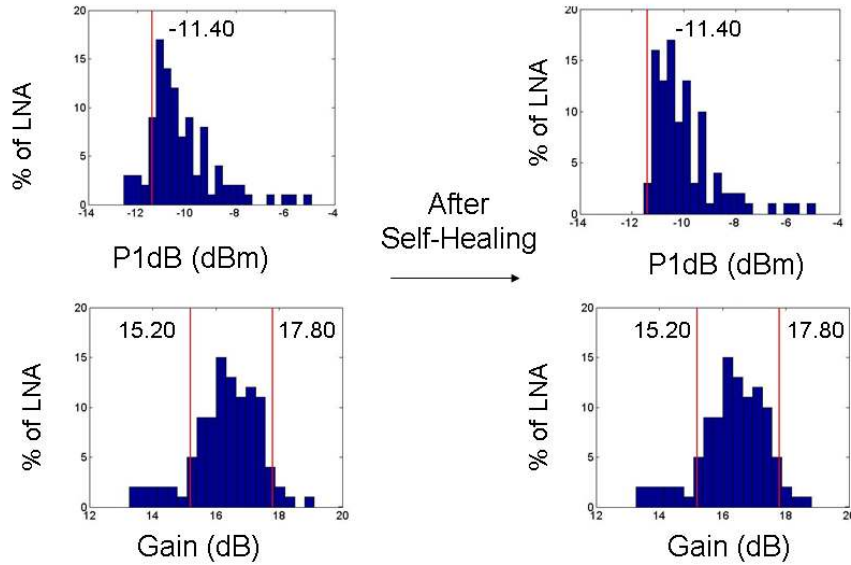


Fig. 5.17. Specification distribution of CMOS LNA before and after healing using Knob1.

5.2.2.2 CMOS LNA Calibration using a Single Knob for Gain

In this sub-section, the LNA samples were calibrated using Knob2 with focus on improving yield of the gain. The obtained results are summarized in Table 5.5 and shown in Fig. 5.18.

The above results show improvement in gain yield to 96%, but the P1dB yield is still 91%. Hence, to obtain better yield for the LNA, calibration was performed using both the knobs.

Table 5.5: Summary of CMOS Amplifier Healing Results (Knobs 2)

CMOS RF Amplifier	% of LNAs with Gain (15.20 – 17.80 dB)	% of LNA with P1dB (> -11.40 dBm)	Yield of LNA (Gain and P1dB)
Before Healing	87%	91%	81%
After Healing	96%	91%	87%

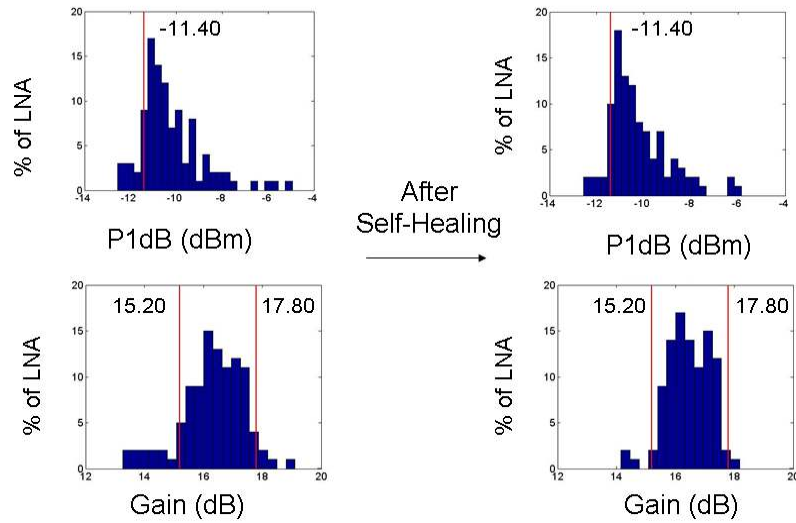


Fig. 5.18. Specification distribution of CMOS LNA before and after healing using Knob2.

5.2.2.3 CMOS LNA Calibration using both the Knobs

In this calibration procedure both knobs were used and the obtained results are given in Table 5.6 and shown in Fig. 5.19. Samples which were not meeting both gain and P1dB specifications were calibrated/corrected using both knobs and the change in the calibration knobs was calculated by solving Equations (5.9) and (5.10). Samples which were not meeting P1dB alone were calibrated using Knob1, and Knob2 was used for calibrating samples which were not meeting the gain alone.

Table 5.6: Summary of Healing Results (Both Knobs) CMOS RF Amplifier

CMOS RF Amplifier	% of LNAs with Gain (15.20 – 17.80 dB)	% of LNA with P1dB (> -11.40 dBm)	Yield of LNA (Gain and P1dB)
Before Healing	87%	91%	81%
After Healing	96%	98%	94%

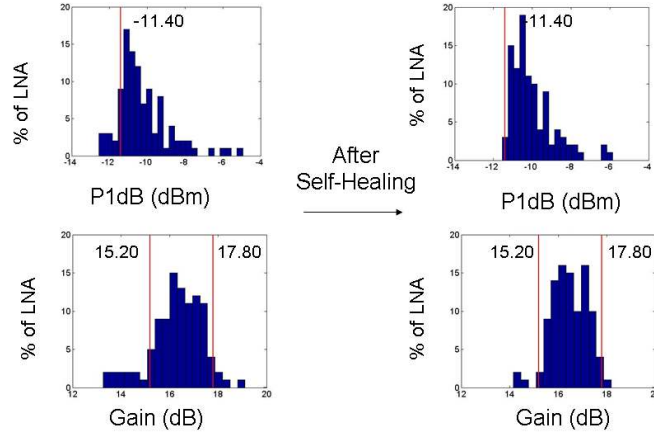


Fig. 5.19. Specification distribution of CMOS LNA before and after healing using both Konbs.

Based on the results shown in Table 5.6, it can be concluded that the yield of the CMOS RF amplifier has increased from 81% to 94% by the proposed self-healing methodology.

5.3 Hardware Prototype

As a proof of concept, a hardware prototype of the proposed self-healing RF amplifier has been made using commercially available LNA, as shown in Fig. 5.20. To change the performance of the LNA, a single tuning knob that varies the power supply (V_{dd}) was used. Three samples of the LNA were considered and it was assumed that the golden sample was LNA1. In addition, it is assumed that the allowable performance specification of the gain (@875 MHz) is from 10.50 dB to 12.50 dB. The performance curve of the LNA (Gain vs V_{dd}) is shown in Fig. 5.23. The output oscillation frequency of the hardware prototype is shown in Fig. 5.21 at $V_{dd} = 3.5$ V. The measured gain for LNA3 is 10.43 dB, LNA2 is 11.77 dB and LNA1 is 11.56 dB. The measured gain of the LNAs vs. output

oscillation frequency of LNAs in the feedback mode after down-conversion is shown in Fig. 5.22. It can be inferred from these measurement results that the oscillation frequency of the proposed self-healing LNA changes with the performance of the LNA.

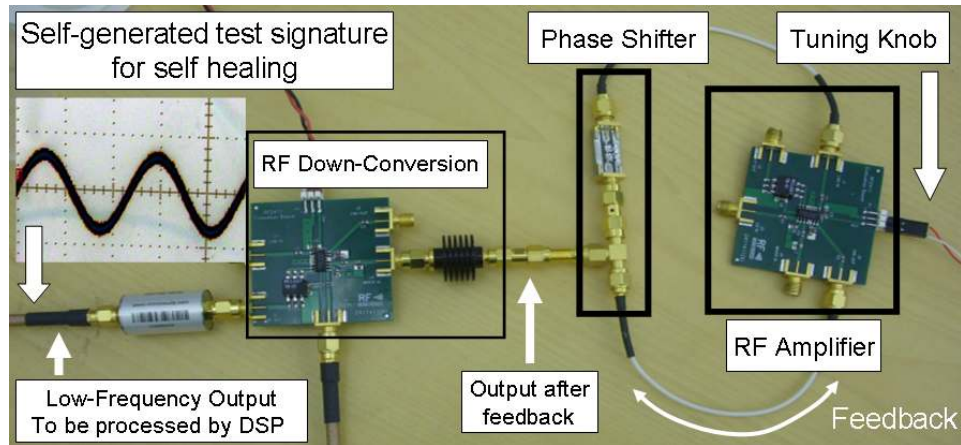


Fig. 5.20. A hardware prototype of the proposed self-healing RF amplifier.

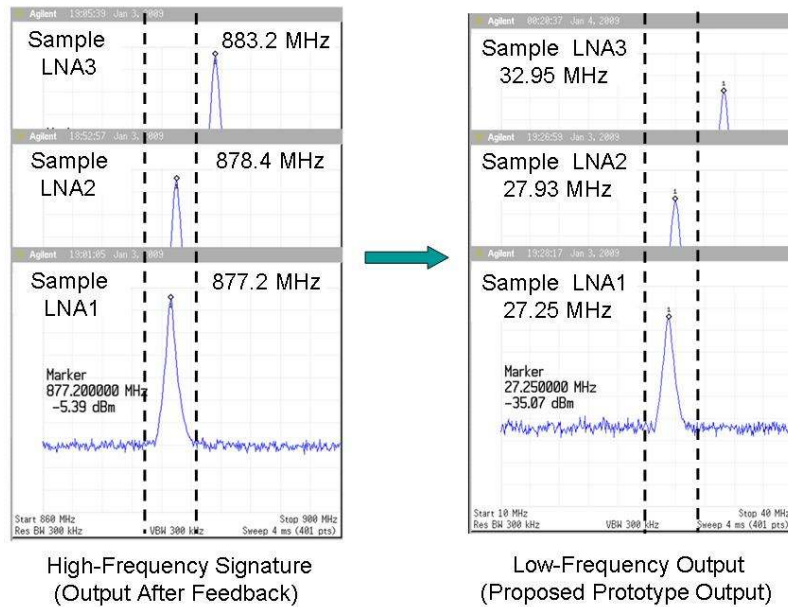


Fig. 5.21. Spectrum of the output after the feedback loop and after the RF down-conversion.

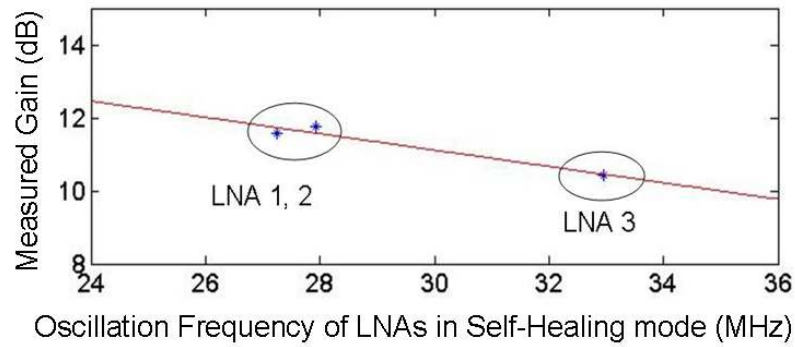


Fig. 5.22. Gain vs. down-converted oscillation frequency of the LNA with feedback.

Let us assume that the prediction model to predict the gain of the LNAs is made as explained in Section 5.1 and the predicted gain for LNA2 and LNA3 is 11.00 dB and 10.00 dB, respectively. Hence, by the proposed methodology, the power supply (V_{dd}) voltage that needs to be changed will be given by

$$\Delta G = 1.0 * \Delta V_{dd} \quad (5.11)$$

Where, $m = 1.0$ (Fig. 5.23). Let the target value of the gain for which both the LNAs need to be calibrated be 11.5 dB. Then tuning knob for LNA2 should be changed by 0.5 V and for LNA3 should be changed by 1.5 V.

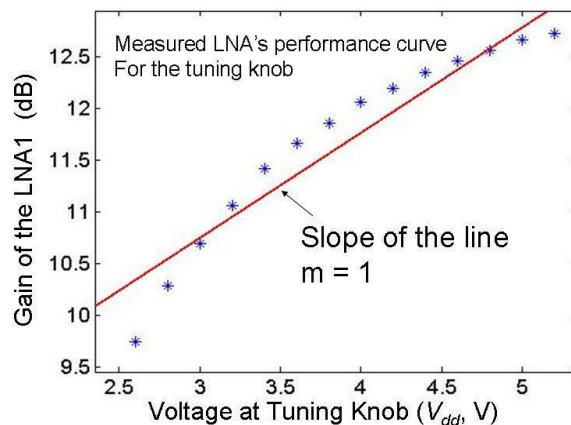


Fig. 5.23. Performance curve: Gain of LNA1 as a function of the tuning knob.

Table 5.7: Summary of Calibration Results
RF Amplifier

Allowable Band (10.5 – 12.5 dB) @875 MHz	Gain Before Calibration	Gain After Calibration
LNA 1 (Golden)	11.56 dB	11.56 dB
LNA 2	11.77 dB	12.25 dB
LNA 3	10.43 dB	11.49 dB

After tuning/calibration, the gain of LNA2 was measured to be 12.25 dB and that of LNA3 was measured to be 11.49 dB (Table 5.7), which are in range of allowed values of the LNAs gain. Hence, this experiment demonstrates that by tuning this self-healing LNA, the performance of the LNA can be changed and thus it can be used to increase their manufacturing yield.

5.4 Chip Prototype

5.4.1 Simulation Results

To further demonstrate our self-healing methodology concept, a cascode X-band SiGe LNA was designed as a chip prototype. In this SiGe LNA, small-signal gain is the targeted specification to be self-healed. The LNA has a gain of 15.00 dB at 9 GHz. To achieve self-healing, an on-chip phase-shifter is designed as shown in Fig. 5.24 and the bias current (I_{bias}) is used as a tuning knob for calibration purposes. The die size of the LNA is $1.1 \mu\text{m} \times 0.8 \mu\text{m}$ and the overhead of the additional required circuitry for self-healing is around $0.4 \mu\text{m} \times 0.275 \mu\text{m}$, which is about 12% of the total area. In this calculation, area of RF and DC pads are not included.

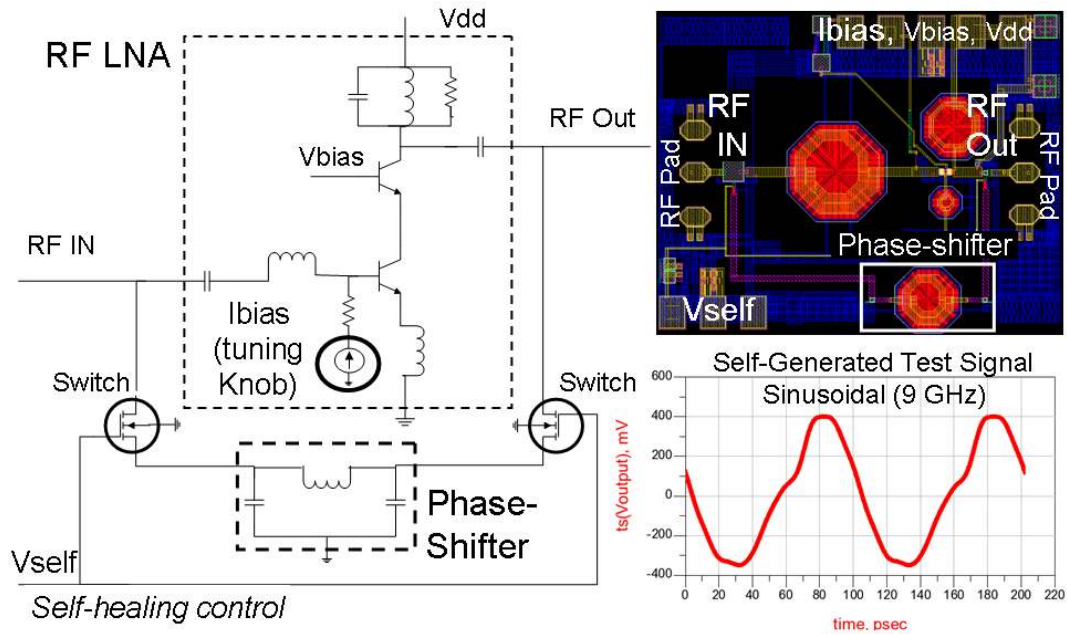


Fig. 5.24. A chip prototype of the self-healing SiGe LNA with self-generated test signature.

To demonstrate the self-healing methodology, 100 samples of the LNA were obtained using Monte Carlo simulations which include process variations in both RF amplifier as well as in extra circuitry (RF switches and phase-shifter). It is assumed that the allowable range in gain variation is from 13.50 dB to 16.50 dB. To show that yield improvement is possible, as described in the previous sections, the following steps were followed. It is important to note that for this experiment the *post layout extracted netlist of SiGe LNA was used*. Thus, this experiment is very close to the healing of actual ICs.

Step 1

LNA was forced to oscillate by providing feedback through the phase shifter. The phase shifter was made a part of the feedback loop by changing the voltage from 0.0 V to 3.3 V at self-healing control knob, Vself (Fig. 5.24). This completes the feedback and the

LNA begins oscillating, thereby generating a sinusoidal test signal output, as shown in Fig. 5.24.

Step 2

This self-generated test signature is used to assess the impact of process variations on the performance of the LNA. The prediction of gain was performed using a non-linear prediction model similar to that described in the Section 5.1 and 5.2. The non-linear prediction model was developed using MARS and response of 300 samples of LNA was used to develop this model. Again, these 300 samples were obtained using Monte Carlo simulations.

Step 3

To determine which samples of the LNAs should be chosen for self-calibration/correction, the gain of the LNAs was predicted using a non-linear prediction model (similar to that in Section 5.1 and Section 5.2) and 16 samples were selected for self-calibration/correction.

Step 4

The performance curve (*Gain vs I_{bias}*) was used to obtain the dependency between gain (G) and the tuning knob (I_{bias}) and the resulting equation of the form of Equation (5.5) is :

$$\Delta G = 0.0136 * \Delta I_{bias} \quad (5.12)$$

where, ΔG in dB and ΔI_{bias} is in μA .

Step 5

For yield improvement, the change in the tuning knob (bias current) was calculated using Equation (51.2). Subsequently, the tuning knob value was adjusted and the yield improvement, as shown in Fig. 5.25 was achieved.

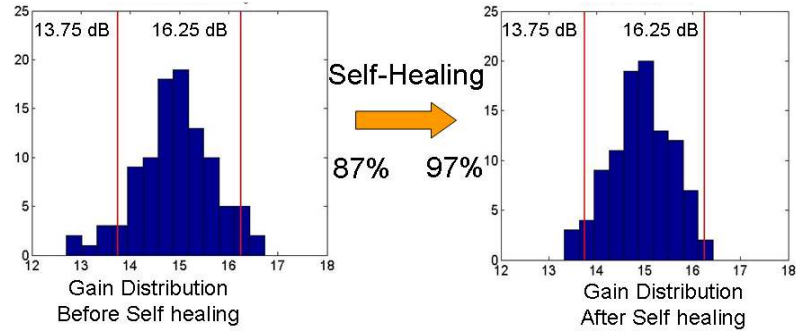


Fig. 5.25. Improvement in the yield of X-band SiGe self-healing LNA.

Based on the results shown above in Fig 5.25, it can be concluded that the yield of this X-band amplifier has increased from 87% to 97% by the proposed self-healing methodology.

5.4.2 Measurement Results

To demonstrate the self-healing mode, the measurement setup as shown in Fig. 5.26 was used. In this setup, no RF input was applied to the RF LNA and only one RF probe was used for sensing self-generated sinusoidal RF signal. The RF sinusoidal signal was generated when a voltage = 3.3 V was applied at self-healing control (V_{self}). The self-generated sinusoidal signal of 8.0 GHz from the RF amplifier is shown in Fig. 5.26. The deviation in the measured oscillation frequency from that of simulated value of 9.0 GHz, is mainly because of the shift in the performance of the amplifier vs. simulations, as

shown in Fig. 5.27. A similar gain reduction/variation was noticed in the other designs sent for this fabrication run as well. To demonstrate that as the performance of the RF amplifier changes, the oscillation frequency of the amplifier in the self-healing mode also changes, the measurement results of three RF amplifiers is plotted in Fig. 5.28, which shows their gain vs. oscillation frequency of the self-generated signal. The gain of the RF amplifier was measured using a conventional VNA setup. During this VNA setup, the self-healing control (V_{self}) was equal to 0 V and the RF LNAs were stable (the measured stability factors [78], $\mu(S)$ and $\mu'(S)$, are greater than 1 and no oscillations were observed). To demonstrate the calibration capability in this RF LNA, the measured performance curve of the RF amplifier (Gain vs I_{bias}) is shown in Fig. 5.29.

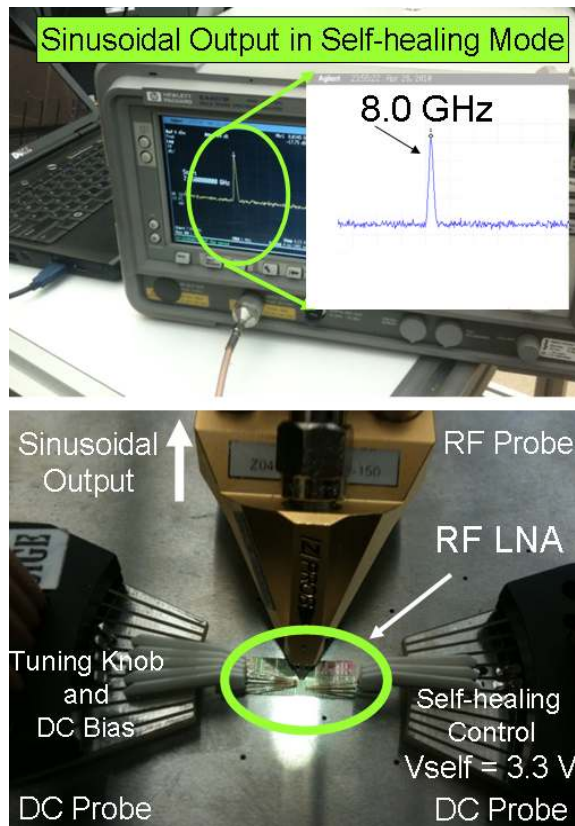


Fig. 5.26. Measurement results and the measurement setup of the RF LNA in self-healing mode.

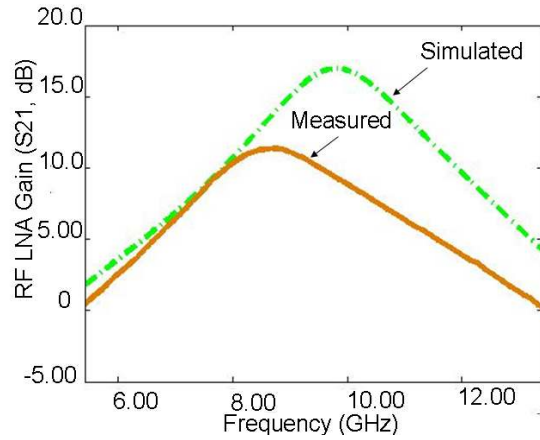


Fig. 5.27. Measured and simulated gain of the X-band RF amplifier.

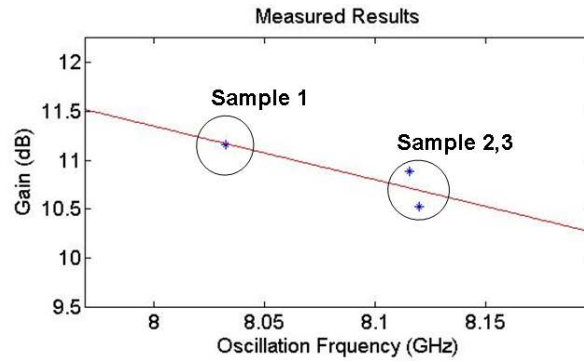


Fig. 5.28. Measured gain of the RF LNA and the frequency of the self-generated sinusoidal signal from the LNA under self-healing mode.

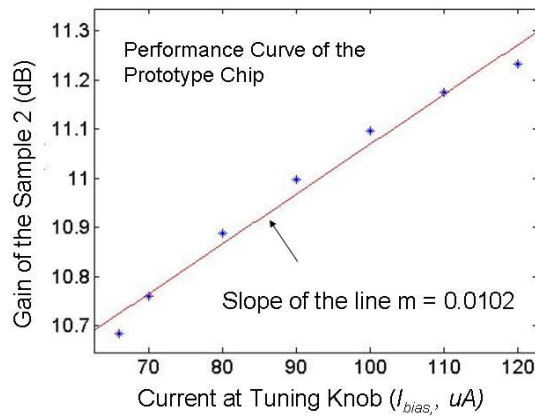


Fig. 5.29. Performance curve: gain of Sample 2 as a function of the tuning knob (I_{bias} , μA).

This experiment demonstrates that it is possible to generate on-chip oscillations by providing on-chip feedback to the RF amplifier. In addition, as RF amplifier's performance varies, the oscillation frequency also varies. Further, the performance of the amplifier can be changed by designing tuning knob in the amplifier as shown in the performance curve (Fig. 5.29). Thus, by developing non-linear prediction/regression model (such as using MARS) from large set of samples, the manufacturing yield of the RF amplifier can be increased using the performance curves and equations of the form Equation (5.5), as explained in the previous sections.

5.5 Discussion

It can be inferred from the above results that the proposed methodology provides yield improvement; the trade-off is the extra area required for implementing the RF switches, the phase-shifter and the tuning knobs. In addition to the extra area, at RF frequencies loading effects of this extra circuitry need to be taken into consideration in the RF design. The SiGe 2.8 GHz RF of Section 5.3 has a gain of 22.17 dB and P1dB of -19.93 dBm without feedback (without RF switch and phase shifter). In contrast, it has a gain of 22.09 dB and P1dB of -19.81 dBm after adding the required extra circuitry. This shows that performance of RF amplifier changes due to the extra circuitry, but it is important to note that the change in performance is not very large and it can overcome with some extra design effort.

In addition, while using active tuning knobs (changing bias voltage/current), the average power consumption can change. To illustrate the change in profile of power consumption, the power consumption of the X-Band SiGe RF amplifier (Section 5.4)

before and after healing is shown in Fig. 5.30 and results are summarized in Table 5.8. The mean of the power consumption is almost the same before and after self-healing/yield improvement because after healing some of the RF amplifiers started consuming less power while other started consuming more power. From these results, it can be concluded that the average power consumption change is very small, but it should be accounted for in certain low-power applications.

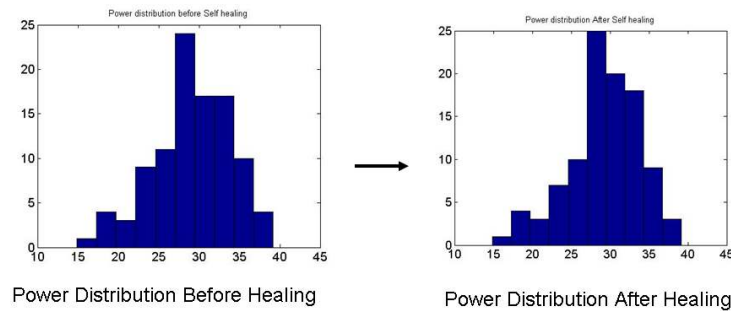


Fig. 5.30. Power distribution before and after self healing of X-band SiGe LNA.

5.6 Summary

In this chapter, a new self-healing methodology has been proposed for RF amplifier circuits. The methodology has been demonstrated on an embedded RF LNA in the RF front-end systems. It has been shown through simulations that a significant yield improvement of the RF amplifier can be achieved by using this methodology. Both a board-level prototype and a chip-level prototype of the self-healing LNA have also been demonstrated. Results from the experiments performed are quite encouraging and it can be concluded that the proposed methodology can be considered an alternate solution for the development of future self-healing systems.

(This page is intentionally left blank)

CHAPTER 6

A SELF-HEALING METHODOLOGY FOR EMBEDDED RF MIXERS

In this chapter, a new self-healing methodology for embedded RF down-conversion mixers is proposed. In the proposed methodology, the output of the RF mixer is analyzed by using on-chip resources for testing and the mixer performs self-calibration/correction for parametric defects using tuning knobs. The tuning knobs enable the RF mixer to self-calibrate/correct for multi-parameter variations induced due to process variability. The proposed methodology eliminates the need for generation of on-chip RF signals exclusively for testing and calibration/correction of the RF mixers. In this methodology, during the self-healing mode, LO port signal of the mixer is reused at the RF port so that no extra signal generator is required. Thus, the proposed approach enables self-testing of embedded RF down-conversion mixers even in RF systems that do not have transmission capabilities. During the self-calibration/correction, the output of the RF down-conversion mixer is used to assess the impact of process variations on the performance of the mixer through prediction of multiple specifications. Subsequently, calibration for loss of mixer performance due to process variations is performed by adjusting calibration/tuning knobs designed in the RF mixer. The output signature of the mixer is analyzed with resources available on-chip (Low-pass filter, ADC and DSP). Thus, the proposed methodology enables self-testing and self-calibration/correction of embedded RF down-conversion mixers.

In the following sections, the proposed self-healing methodology is discussed. Also, the self-healing RF mixer architecture and generation of calibration control signals for the yield improvement is described. Simulation and measurement experiments are then presented, which are followed by summary.

6.1 Proposed Self-Healing Methodology for RF Mixers

6.1.1 Self-Healing Flow

The self-healing methodology flow for RF down-conversion mixers is similar to the self-healing flow of the RF amplifier as discussed in the previous chapter (Fig. 5.2). The first step in the present methodology is to test RF mixer to identify the mixers with catastrophic vs. parametric defects. The proposed self-calibration/correction procedure is exercised only if the RF down-conversion mixer is determined to be free of catastrophic faults. The final goal of the self-healing is to increase the post-manufacturing yield for parametric defects.

6.1.2 Self-Healing RF Down-Conversion Mixer Architecture

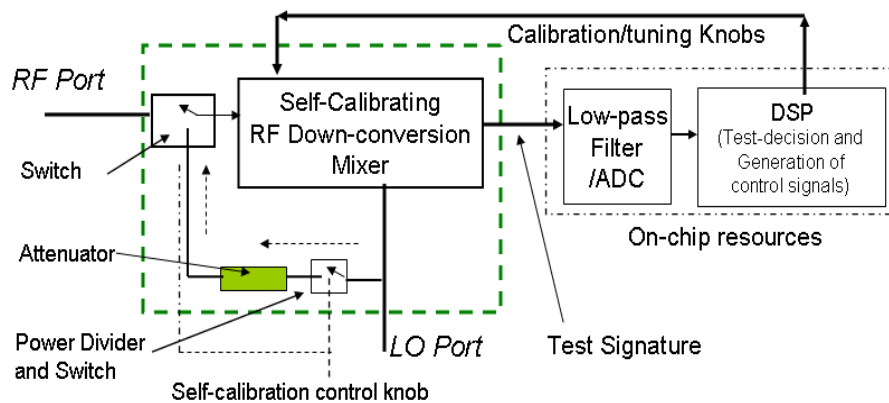


Fig. 6.1. Proposed self-healing RF down-conversion mixer architecture.

Consider the proposed self-healing architecture of the embedded RF down-conversion mixer as shown in Fig. 6.1. In the self-healing mode, local oscillator signal from the LO Port is reused with the help of switches, power-divider and attenuator. The attenuator is proposed in this architecture so that high-power signal from LO Port does not completely saturate the RF Port. The higher order harmonics from the output of the RF mixer are removed using on-chip low-pass filter and an ultra low-frequency signal is obtained for testing the RF down-conversion mixer. The generation of this ultra low-frequency signal is explained in the next sub-section. The output of the low-pass filter is sampled using an on-chip ADC and analyzed with a base-band DSP for testing. The calibration/correction of the RF down-conversion mixer in the presence of process variations is achieved by adjusting the “calibration/tuning knobs” designed in the mixer. It can be seen from Fig. 6.1 that all of the above can actually be accomplished using chip resources. Test-signal generation is achieved by reusing signal at Local oscillator (LO port) and analysis is performed using on-chip resources such as low-pass filter, ADC and DSP that are necessary for performing normal wireless communication functions.

6.1.3 Self-Testing of RF mixers

In this sub-section, the generation of test signature, V_{test} , is explained. As mentioned earlier, in the proposed methodology, LO signal (LO Port) is reused to drive the RF port as shown in Fig. 6.1. Consider the behavioral model [79] of RF mixer as shown in Fig. 6.2. In this model, the mixer is modeled as a non-linear transfer function followed by an ideal multiplier. Let us assume that the input at the RF port of the mixer is $x(t)$ and non-linearity of the transfer function is of the 3rd order, then the output of the non-linear

transfer function will be given by Equation (6.1) and output of the mixer will be given by Equation (6.2).

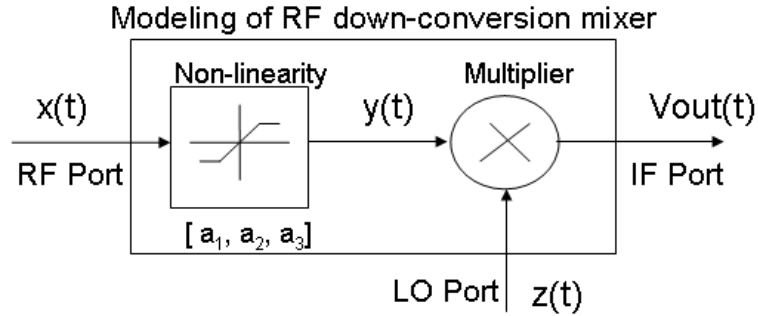


Fig. 6.2. Modeling of an RF down-conversion mixer [79].

In the above model,

$$y(t) = a_1 x(t) + a_2 x^2(t) + a_3 x^3(t) \quad (6.1)$$

$$V_{out}(t) = y(t).z(t). \quad (6.2)$$

where, a_1 = small signal gain of the mixer

a_2, a_3 = non-linearity coefficients

$x(t)$ = RF input signal (input at RF port)

$y(t)$ = output after non-linear block

$z(t)$ = Local oscillator signal (input at LO port)

$V_{out}(t)$ = Output of the mixer

if $x(t) = A \cos(\omega t)$ and $z(t) = B \cos(\omega t)$, then

$$y(t) = a_1 A \cos(\omega t) + a_2 A^2 \cos^2(\omega t) + a_3 A^3 \cos^3(\omega t) \quad (6.3)$$

$$y(t) = a_2 A^2 / 2 + (a_1 A + 3a_3 A^3 / 4) \cos(\omega t) + a_2 A^2 / 2 \cos(2\omega t) + a_3 A^3 / 4 \cos(3\omega t) \quad (6.4)$$

$$V_{out}(t) = (a_1 AB / 2 + 3a_3 A^3 B / 8) + 3a_2 A^2 B / 4 \cos(\omega t) + (a_1 AB / 2 + a_3 A^3 B / 2) \cos(2\omega t)$$

$$+ a_2 A^2 B/4 \cos(3wt) + a_3 A^3 B/8 \cos(4wt) \quad (6.5)$$

$$V_{out}(t) = V_{test} + V_{highfrequency}(t) \quad (6.6)$$

where,

$$V_{test} = a_1 AB/2 + 3a_3 A^3 B/8 \quad (6.7)$$

$$V_{highfrequency}(t) = 3a_2 A^2 B/4 \cos(wt) + (a_1 AB/2 + a_3 A^3 B/2)\cos(2wt) + a_2 A^2 B/4 \cos(3wt) + a_3 A^3 B/8 \cos(4wt) \quad (6.8)$$

It can be inferred from the above Equation (6.7) that if the RF port and LO port of the RF down-conversion mixer are driven with the same frequency signal ($\cos(wt)$), then it is possible to get an ultra low-frequency signal (V_{test} , DC Voltage) that contains the gain and non-linearity information of the down-conversion mixer. Since the Gain and P1dB of the RF down-conversion mixer are functions of a_1 and a_3 coefficient, V_{test} can be used for testing RF down-conversion mixer. In the present work, we have used this V_{test} as a test signature for self-healing of RF down-conversion mixers.

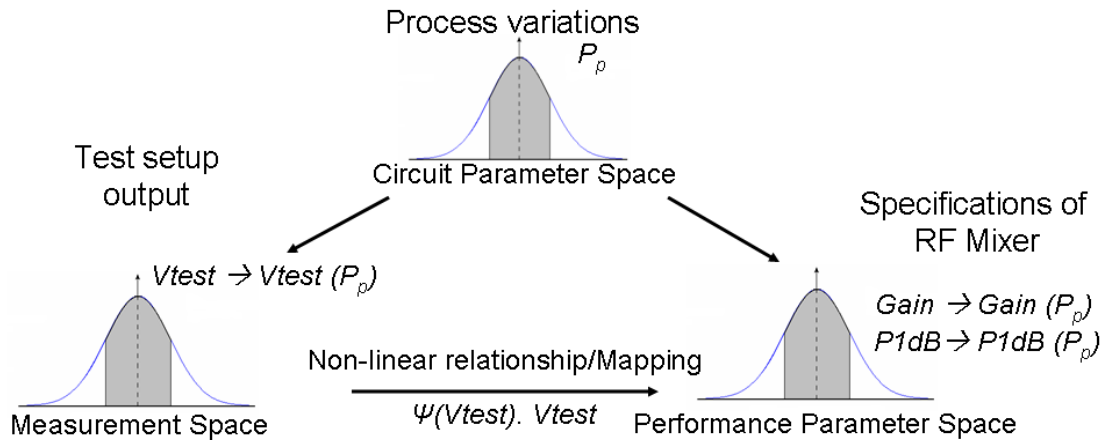


Fig. 6.3. Performance prediction of RF mixer using non-linear mapping.

Let us assume that because of the process variation (p_p), a_1 changes to $a_1(p_p)$ and a_3 to $a_3(p_p)$. Hence, V_{test} , and RF mixer's Gain/P1dB becomes function of process variations such as $V_{test}(p_p)$, $Gain(p_p)$ and $P1dB(p_p)$, respectively and as shown in Fig. 6.3. Also, at circuit level in RF design, components contribute to or influence more than one specification. Thus, there exists a finite possibility to derive a non-linear analytical expression which can show the relationship between the mixer specifications and the response of the test setup (V_{test}). However, the derivation of such an analytical expression could be very hard, and if the RF mixer has an order of non-linearity (greater than 3), then derivation of such analytical equations can become intractable. However, development of a non-linear model to predict specifications of RF mixer can be easily done by using successive learning methods such as Multivariate Adaptive Regression Splines (MARS) and Artificial Neural Networks (ANN). In this chapter, a non-linear prediction model based on MARS is used similar to the one discussed in previous chapter. As explained in the previous chapter, the development of a prediction model using MARS is a supervised learning process. This requires a "training set" of mixers with statistically likely parametric failures. In practice, measurements made on RF mixer samples selected from different production lots and across a large number of wafers are used to develop prediction model.

In the present methodology, the ultra low-frequency signal, V_{test} , is used as a test-signature to predict the performance of the RF mixer (S_i) according to Equation (6.9):

$$S_s = \Psi(V_{test}). V_{test} \quad (6.9)$$

where S_s is RF down-conversion mixer specifications (Gain, P1dB) and $\Psi(V_{test})$ is non-linear regression function of the weighted sum of basis functions made of splines.

In below experiments, to distinguish among parametric and catastrophic defects, an estimation of the allowable maximum (V_{max}) and minimum (V_{min}) voltage changes around the response of the golden RF mixer (V_{test}) is performed using Monte Carlo simulations. The training set used to develop the prediction model can also be used to estimate V_{max} and V_{min} .

6.1.4 Self-Calibration/Correction of RF mixers

In the present self-healing methodology, similar to that of the previous chapter (Section 5.1), one-time calibration/tuning procedure is proposed, which works as follows. After the specifications of the mixer are predicted using the non-linear prediction model, the mixer tuning knobs are adjusted using the *performance curves* and Equation (6.10). As explained in the previous chapter (Section 5.1), the *performance curves* of the DUT show the changes in the specifications of the DUT as functions of the DUT tuning knob values (one function for each DUT specification) and are obtained by changing the tuning knob values of the golden DUT and observing how its performance specifications are affected. To estimate the change in each specification of the DUT, the weighted sum of the effect of each DUT tuning knob is computed according to Equation (6.10). Equation (6.10) is a first-order linear approximation of the effect of multiple tuning knob perturbations on each specification of the DUT. For multi-specification optimization, a set of such linear simultaneous equation can be solved.

$$\Delta S_j = \sum w_i \Delta K_i \quad (6.10)$$

where

ΔS_j is required calibration in the specification “j”

w_i is weight associated with the change in the tuning knob, ΔK_i .

To illustrate, let us consider embedded RF mixer with two knobs, Knob1 and Knob2. Knob1 tunes bias current (I_{bias}) of the RF mixer and Knob2 tunes an inductor (L_s) in the mixer. The change in the P1dB of the mixer because of the change in the bias current and inductance is shown in Fig. 6.4. Then, the calibration/correction for the P1dB ($\Delta P1dB$) can be performed using Equation (6.11).

$$\Delta P1dB = m_1 \cdot \Delta I_{bias} + m_2 \cdot \Delta L_s \quad (6.11)$$

where,

m_1 and m_2 can be approximated to the slope of the performance curves in Fig. 6.4A and Fig. 6.4B, respectively.

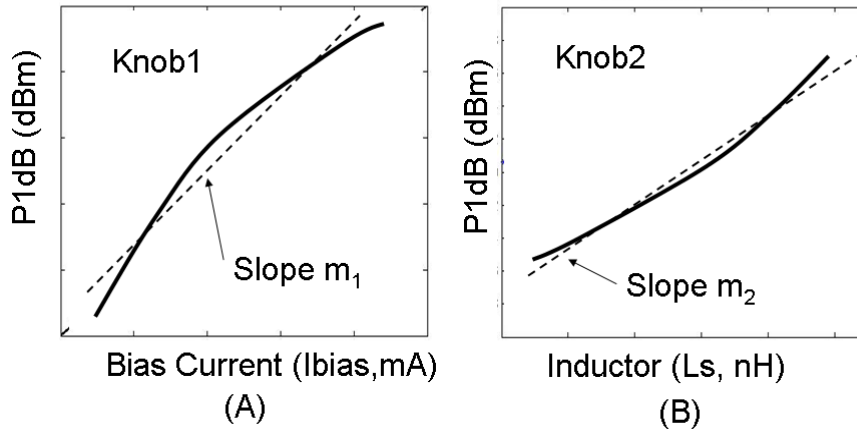


Fig. 6.4. Performance curves of mixer for different calibration knobs.

For efficient working of this calibration/correction procedure, the tuning knobs should be chosen so that the specifications of the mixer vary almost linearly with the tuning knob values (even in the presence of nonlinearities in the mixer, the linear assumption gives yield improvement as shown in the following sections).

6.2 Simulation Results

To demonstrate the proposed self-healing methodology, a 900 MHz down-conversion differential Gilbert mixer was designed in CMOS 0.18 μm process with Gain = 2.7 dB and P1dB = -10.3 dBm. Fig. 6.5 shows the schematic of the differential Gilbert mixer. In this mixer, two tuning knobs have been introduced. First is to change the bias current (I_{bias}) and second is to change the inductor (L_s) in the source degeneration part of the mixer.

For illustration, 8 single-catastrophic failures (4 open and 4 short) were introduced at 4 internal nodes (Fig 6.5) of the RF mixer and 100 parametric instances of the mixer were generated by simultaneously perturbing the various parameters of the RF mixer components including inductors, resistors and transconductance of the transistors using Monte Carlo simulations (total 2 inductors, 2 resistors, 8 transistors). It is assumed that all the components follow Gaussian distribution (3-sigma = 10%) and also that the variations in each type of component are similar, but independent from the variations in other types of components. For example, all inductors are assumed to have similar variations, but their variations are independent from those of transistors and resistors. System-level simulation setup is shown in Fig. 6.6. RF down-conversion mixer simulations were performed using Advance Design System (ADS) tool. The low-pass filter modeling was also performed using ADS while DSP processing and generation of prediction model were performed using MATLAB.

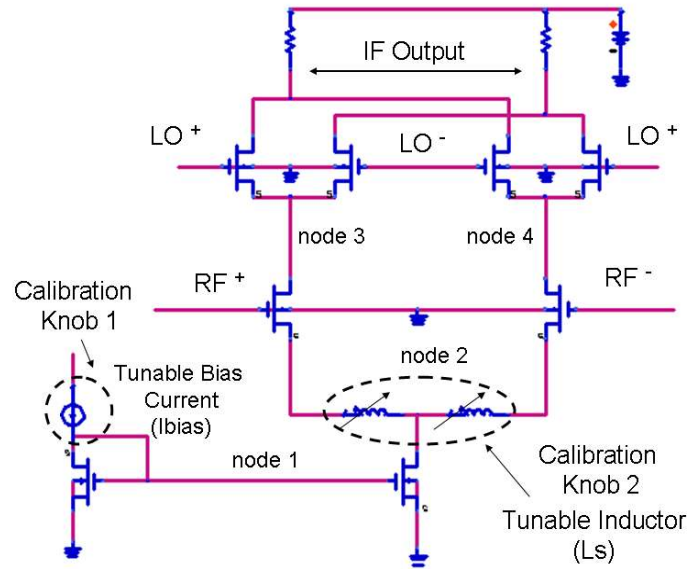


Fig. 6.5. Schematic of self-healing RF down-conversion mixer.

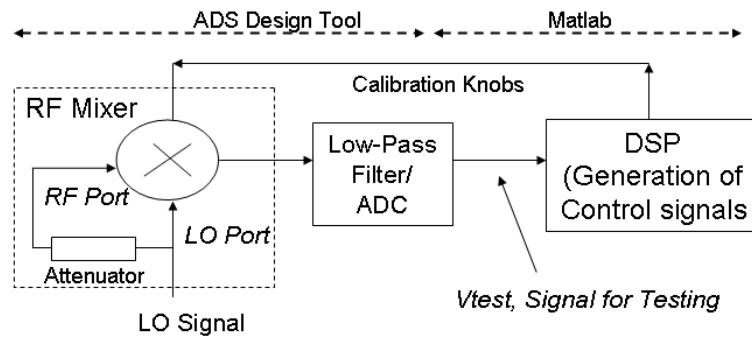


Fig. 6.6. Modeling of self-healing RF mixer architecture (System-level simulation).

Fig. 6.7 shows the ultra low-frequency test signature, V_{test} , for all the 108 samples of the RF mixer (with 100 parametric and 8 catastrophic defects). It can be inferred from Fig. 6.7 that by defining allowable voltage (V_{max} , V_{min}) around the response of the golden RF down-conversion mixer, the samples with parametric variations can be separated from samples with catastrophic defects.

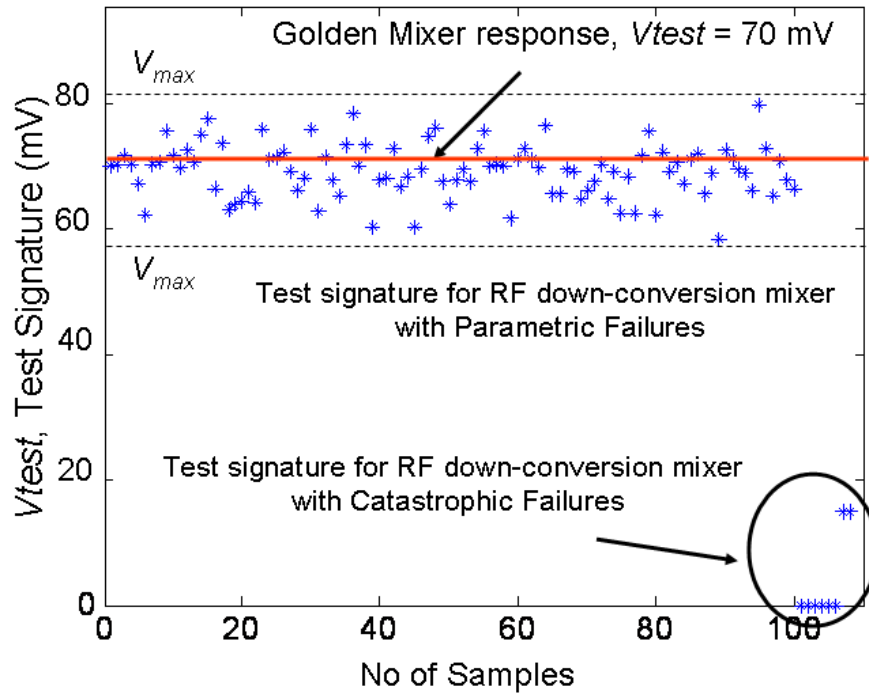


Fig.6.7. Test-setup output (V_{test}) for different self-healing RF down-conversion mixer samples.

To choose the mixer samples for calibration/correction, a non-linear prediction model to predict the gain (Gain, dB) and 1-dB compression point (P1dB, dBm) was developed using MARS. The prediction model was developed using a training set which had 125 RF down-conversion mixers. These 125 mixers were obtained by simultaneously perturbing the mixer components using Monte Carlo simulations. The predicted Gain and P1dB of the 100 samples of the RF down-conversion mixer are shown in Fig. 6.8 and Fig. 6.9, respectively.

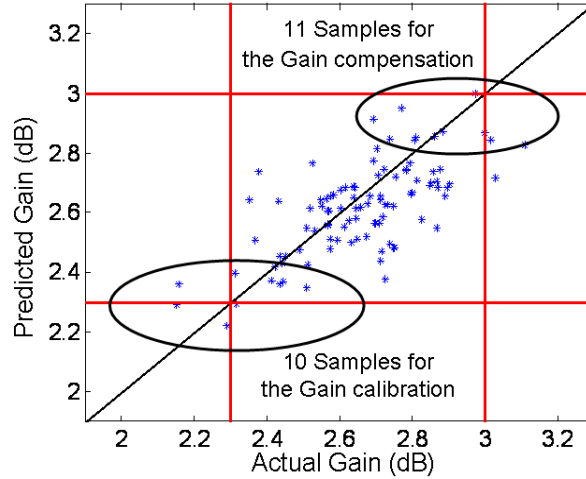


Fig. 6.8. Prediction of Gain for the embedded RF down-conversion Mixer

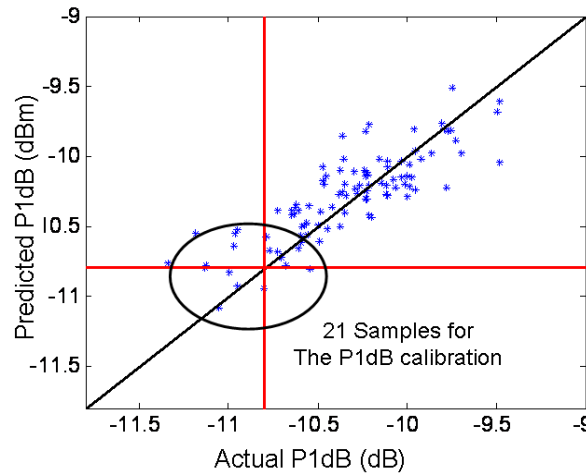


Fig. 6.9. Prediction of P1dB for the embedded RF down-conversion Mixer

It can be seen from the results shown in Fig. 6.8 and Fig. 6.9 that the predicted performance of the RF mixer from the DC test signature (V_{test}) is reliably accurate. Thus this method can be used for the testing of RF down-conversion mixers. Let us assume that the allowable performance specification of Gain is from 2.3 dB to 3.0 dB and P1dB should be more than -10.8 dBm. Considering an error in the prediction at the boundary of the allowable specifications, 21 samples were considered for calibration/correction to meet Gain specification and 21 samples to meet P1dB specification.

The self-calibration/correction is performed with the help of two tuning knobs. The first tuning knob (Knob1) changes the bias current (I_{bias}) of the mixer and the second tuning knob (Knob2) changes the inductance (L_s) in the source degeneration part of the mixer. The variable inductance can be implemented choosing inductors from a bank of embedded inductors or using active inductors [80]. Also, variable current source can be implemented using switchable current mirrors [81]. As a proof of concept, it is shown that the performance of the RF mixer can be varied by changing the inductor (L_s) in its source degeneration part and the bias current (I_{bias}).

The performance curves of the RF down-conversion mixer with respect to these two tuning knobs, Knob1 and Knob2, are shown in Fig. 6.10 and Fig 6.11. For yield improvement, the change in tuning knobs was calculated using Equation (6.10) and the predicted value of the specification from the regression model is used for calculating ΔS_j . For all the calibration, the change in inductor (ΔL_s) is in the range of ± 0.80 nH and the change in bias current (ΔI_{bias}) is in the range of -0.65 mA to 0.93 mA.

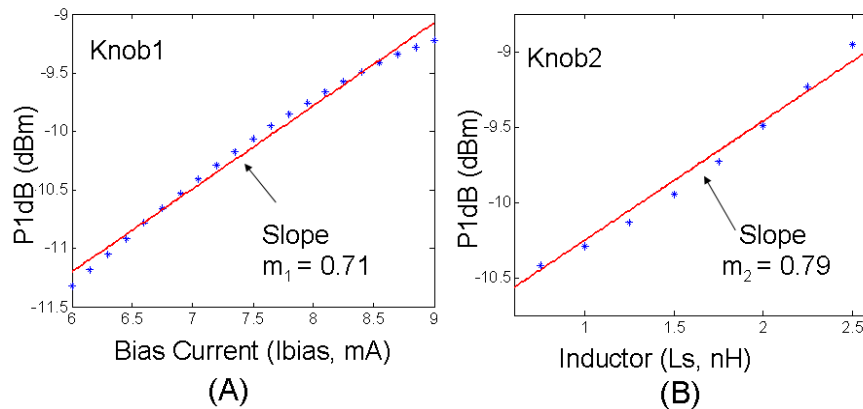


Fig. 6.10. Performance curve: P1dB of RF down-conversion mixer as a function of the calibration/tuning knobs.

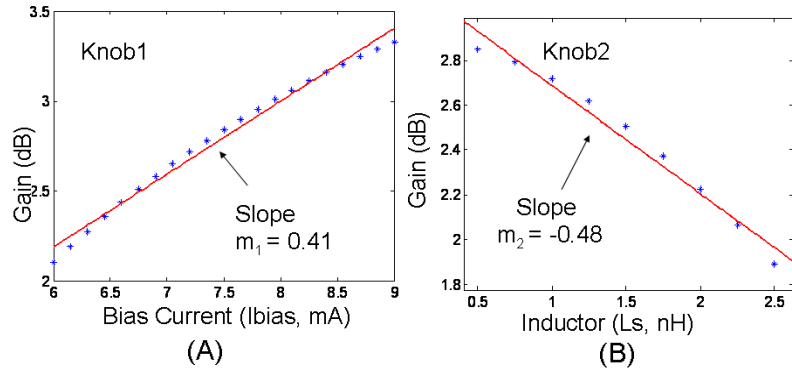


Fig. 6.11. Performance curve: Gain of RF down-conversion mixer as a function of the calibration/tuning knobs.

6.2.1 Calibration/Correction for P1dB

In this sub-section, the proposed methodology was applied to 21 samples of the RF mixer to increase their P1dB above -10.8 dBm and only one calibration knob, Knob2, was used for this purpose. The specification distribution before and after calibration/correction is given in Fig. 6.12 and the summary of the results is given in Table 6.1. It can be inferred from these results that RF mixers with P1dB greater than -10.8 dBm has increased from 88% to 97% after the calibration/correction.



Fig. 6.12. P1dB distribution before and after self-healing for parametric defects.

Table 6.1: Summary of Calibration Results
(P1dB) of RF Mixer

	% of RF mixer with P1dB (> -10.8 dBm)	Yield of Mixer (Considering only P1dB)
Before self-healing	88%	88%
After self-healing	97%	97%

6.2.2 Calibration/Correction for Gain

In this sub-section, the mixer samples were calibrated/corrected using Knob1 with focus on improving Gain within the range of 2.3 dB to 3.0 dB. The obtained results are shown in Fig. 6.13 and summarized in Table 6.2. The obtained results show improvement in Gain yield from 91% to 98%.

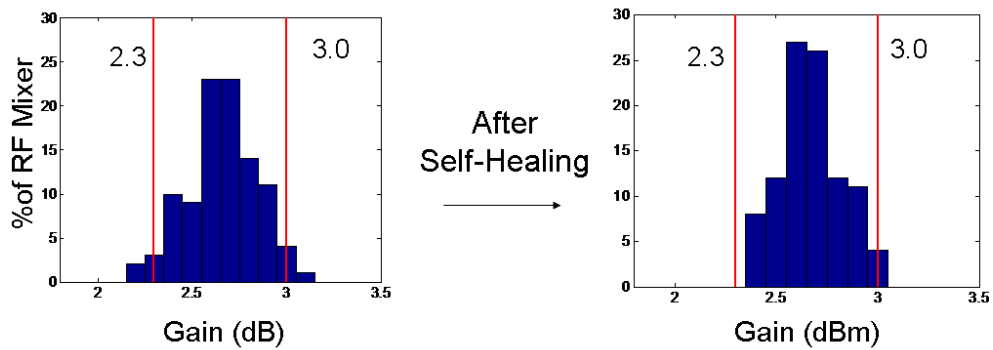


Fig. 6.13. Gain distribution before and after self-healing for parametric defects.

Table 6.2: Summary of Calibration Results (Gain) of
RF Mixer

	% of RF mixer with Gain (2.3 – 3.0 dB)	Yield of Mixer (Considering only Gain)
Before self-healing	91%	91%
After self-healing	98%	98%

6.2.3 Simultaneous Calibration/Correction for Gain and P1dB

In this calibration/correction process, RF down-conversion mixers were compensated for both the specifications; Gain and P1dB, using both the knobs, Knob 1 and Knob 2. The changes in the calibration knobs were calculated by solving two equations ($\Delta G = 0.41 * \Delta I_{bias} - 0.48 * \Delta L_s$, $\Delta P1dB = 0.71 * \Delta I_{bias} + 0.79 * \Delta L_s$). The specification distributions of the Gain and P1dB are given in Fig. 6.14 and the summary of yield improvement is given Table 6.3.

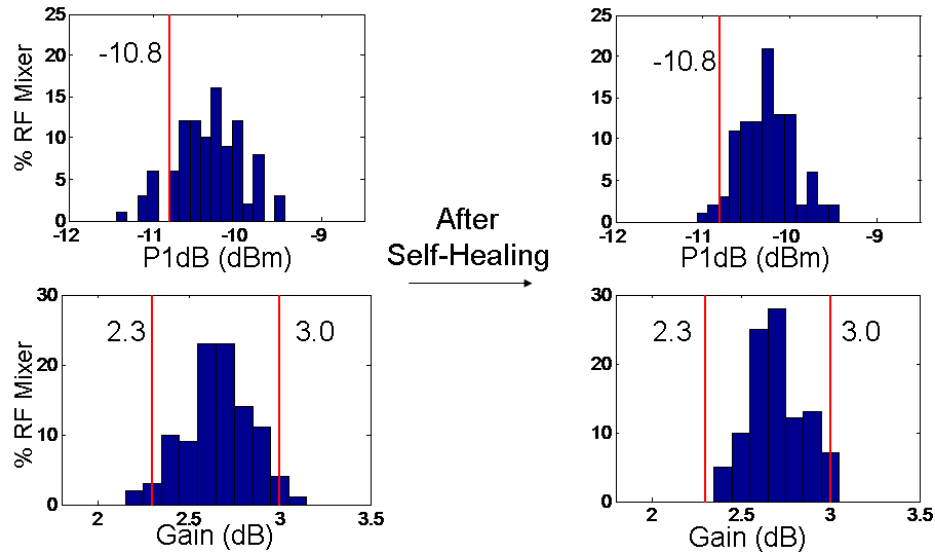


Fig. 6.14. Specification distribution before and after calibration using Knob1 and Knob2 for parametric defects.

Table 6.3: Summary of Calibration Results (Both Knobs) of RF Mixer

	% of Mixer having P1dB (> -10.8 dBm)	% of Mixer Gain in (2.3 – 3.0 dB)	Yield of RF Mixer (Gain and P1dB)
Before self-healing	88%	91%	83%
After self-healing	97%	99%	96%

Based on the results shown in Table 6.3, it can be concluded that the combined yield (Gain and P1dB) of the RF down-conversion mixer has increased from 83% to 96% by the proposed methodology.

6.3 Hardware Prototype

As a proof of concept, a hardware prototype of the proposed self-healing RF down-conversion mixer has been made using commercially available RF mixer as shown in Fig. 6.15. This figure shows the configuration of the mixer in the self-healing mode. Let us assume that the allowable performance specification of the Gain of the mixer (@1800 MHz) is from 5.0 dB to 7.5 dB. In the self-healing mode, the RF port is driven by the Local oscillator (LO) signal after power-divider and attenuator of -30 dBm. The level of LO signal is 10 dBm and input level at RF port is -25.7 dBm.

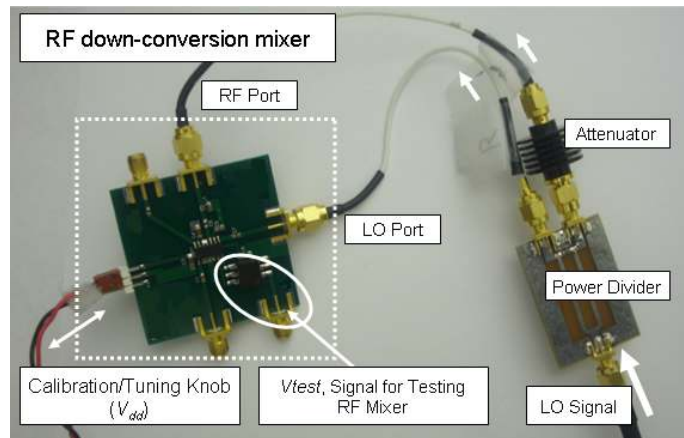


Fig. 6.15. A hardware prototype of the proposed self-healing RF Mixer.

To enable calibration/correction in the mixer, a single calibration/tuning knob that varies the power supply (V_{dd}) was used. This tuning knob was used to tune the Gain of the

RF mixer. The measured variation in the Gain (@1800 MHz) with respect to the V_{dd} is shown in Fig. 6.16. This figure can also be considered as a *performance curve* of the RF mixer with respect to the tuning knob, V_{dd} . For calibration to be performed as discussed in the previous section, slope of the line is approximated as $m = 2.1$.

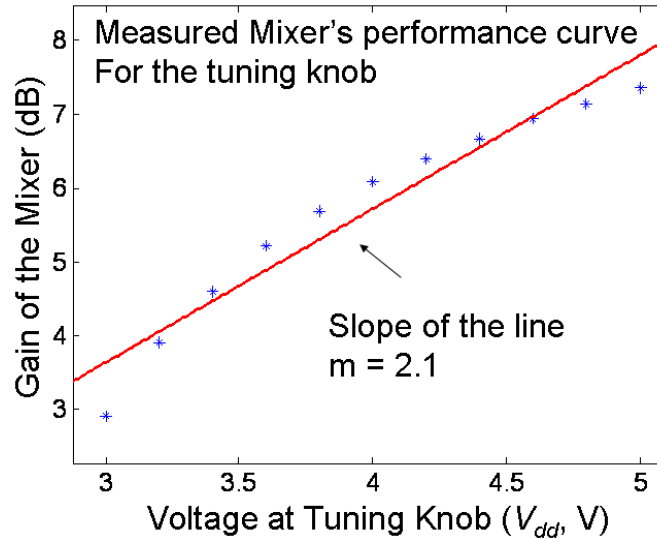


Fig. 6.16. Performance curve: Gain of RF down-conversion mixer as a function of the tuning knob.

To demonstrate calibration, one more sample of RF down-conversion mixer was considered. Let us assume that the prediction model to predict the Gain of the mixers is made as explained in Section 6.1 and the predicted gain for this mixer using the prediction model is 7.30 dB. Although gain of 7.30 dB is acceptable, to account for error in prediction model, self-calibration/correction should be performed. The power supply (V_{dd}) voltage that needs to be changed was given by the below equation using the proposed method.

$$\Delta G = 2.1 * \Delta V_{dd} \tag{6.12}$$

where, $m = 2.1$ (Fig. 6.16). Let the target value of the Gain for which the mixer needs to be compensated is 6 dB. Then, the tuning knob for the mixer should be changed by 0.62 V.

After calibration/correction, the Gain of this mixer was measured as 5.5 dB which is within the acceptable range of the mixer's Gain. Hence, this experiment demonstrates that by tuning the knob of this self-healing RF down-conversion mixer, the performance of the mixer can be changed and it can be used to increase the manufacturing yield.

6.4 Summary

In this chapter, a new self-healing methodology has been proposed for embedded RF down-conversion mixers. Experimental results have shown that significant yield improvement of the mixers can be achieved by using this methodology. It is demonstrated that performance compensation of RF down-conversion mixers can be performed simultaneously for critical specifications such as Gain and 1-dB compression point (P1dB).

(This page is intentionally left blank)

CHAPTER 7

RF SUBSTRATES YIELD IMPROVEMENT USING PACKAGE-CHIP CO-DESIGN AND ON-CHIP CALIBRATION

In this chapter, yield improvement methodology is proposed for RF substrates with embedded RF passive circuitry. The proposed methodology introduces a concept of package-chip co-design and on-chip calibration of active circuitry for the yield improvement of off-chip passive embedded RF filters. RF receiver architecture for the package-chip co-design and on-chip calibration technique is presented. The proposed methodology is demonstrated through simulations and measurements. The methodology is explained in detail in the next section and the model of RF system with an embedded RF filter and a surface mounted active Integrated Circuit (IC) is shown in Fig. 7.1.

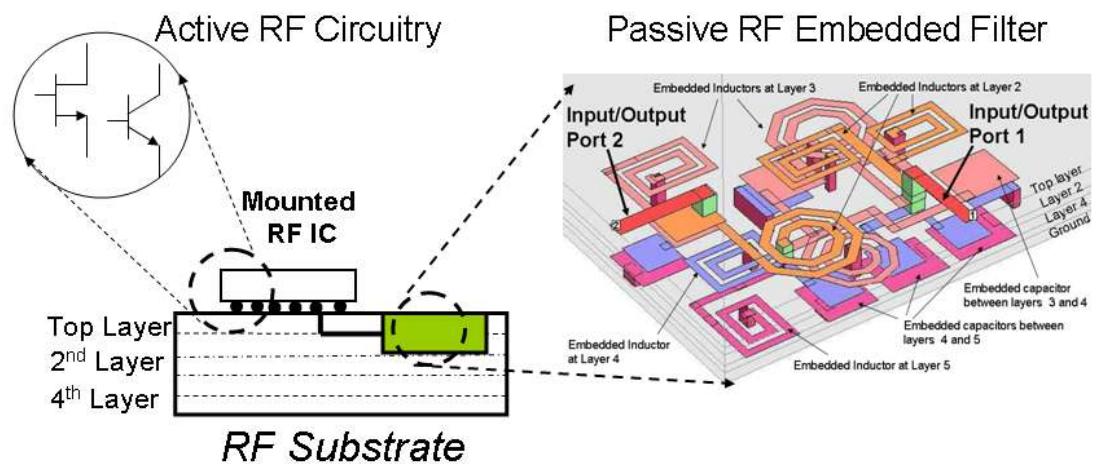


Fig. 7.1 Model of RF system with embedded RF filters and surface mount RF IC.

7.1 A Proposed Yield Improvement Methodology for RF substrates

7.1.1 Yield improvement flow

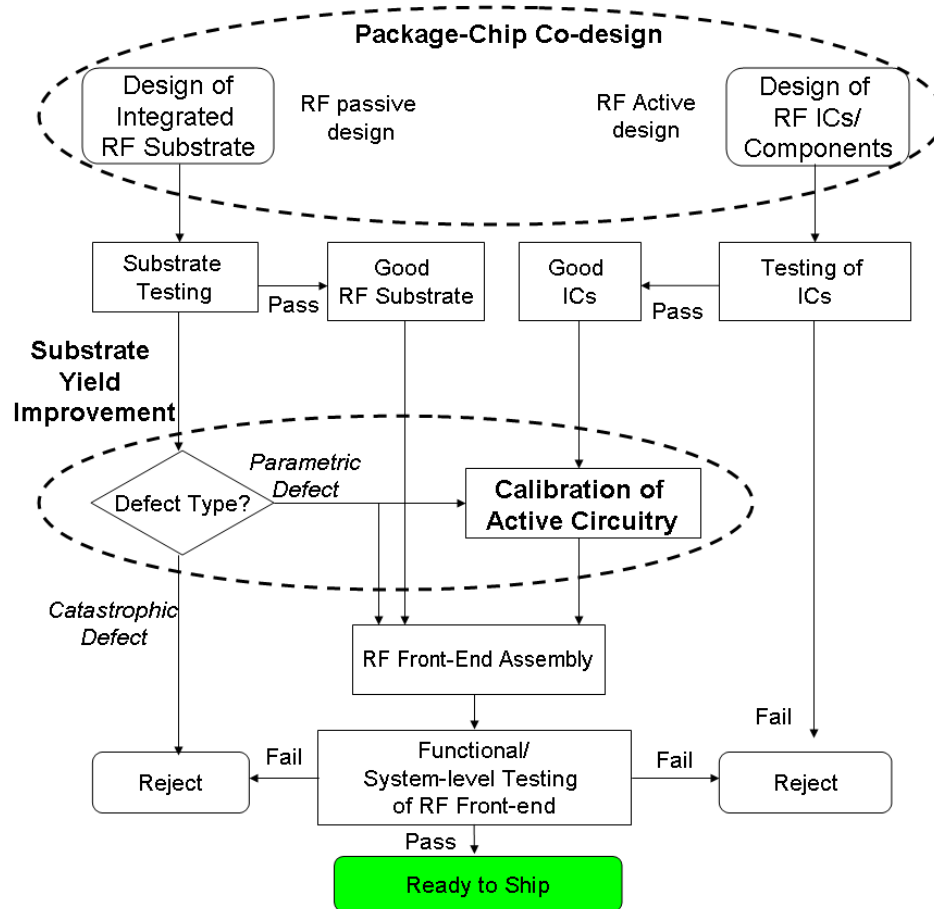


Fig. 7.2. The flow chat of the proposed yield improvement methodology for RF substrate.

The proposed yield improvement methodology is targeted for parametric defects. In this yield improvement methodology as shown in Fig 7.2, the package-chip co-design is performed such that the on-chip RF active circuitry is designed with calibration/tuning capability to account for the performance loss of RF passive circuits embedded in the RF

substrates. After the substrate testing, the RF substrates with catastrophic defects are simply discarded, but the substrates with parametric defects are measured and they are still used for RF front-end assembly. Finally, the on-chip calibration of RF active circuitry is performed to compensate the loss in the performance of RF system due to the parametric defects in integrated RF substrate. As a result, yield of the integrated RF substrates increases because after the substrate testing the non-passing RF substrates can still be used for building a functional RF system.

7.1.2 RF front-end architecture and on-chip calibration

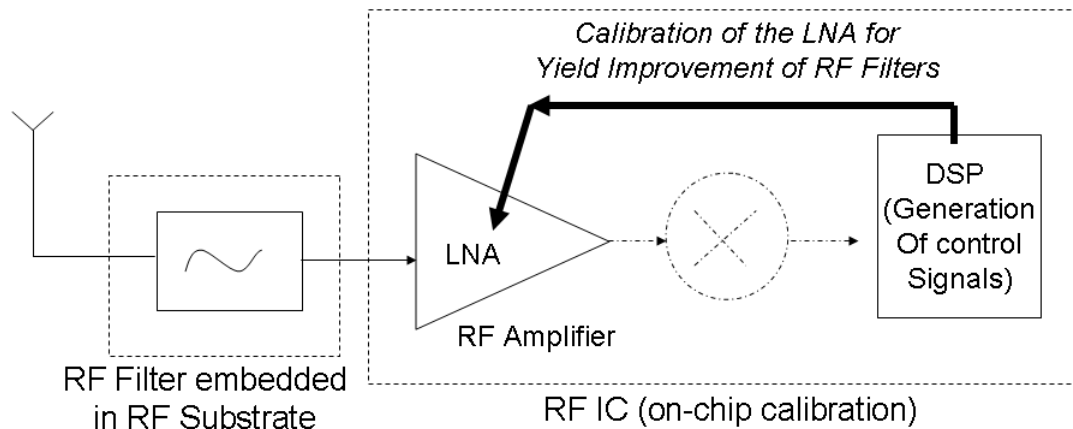


Fig. 7.3. A proposed RF receiver architecture for yield improvement of RF substrates

The proposed RF receiver architecture for RF substrate yield improvement is shown in Fig.7.3. In this architecture, RF amplifier (LNA) is designed with tuning knobs to enable calibration/tuning capability such that the loss in the performance of the RF filter is

compensated by applying control signals to these tuning knobs. These control signals are generated from the on-chip digital signal processor (DSP) such that the output of the LNA is acceptable for the proper functioning of the RF receiver.

The on-chip calibration procedure can be either one-time or iterative. In the iterative procedure, the tuning knobs are adjusted and measurements are made at each iteration until the required performance is achieved. This procedure gives high yield recovery but it is time consuming. In the one-time calibration procedure, the tuning knobs of LNA are programmed only once.

In this methodology, one-time calibration procedure is used, which works as described below. After the performance deviation in the insertion-loss of the embedded RF filter is known from the substrate testing (Fig. 7.2), the LNA Gain-tuning control knob is adjusted using the performance curve of the LNA and Equation (1). The concept of the performance curve of the design was introduced in the previous chapter, this curve shows the variation in the specification of the design as a function of the tuning knob value as shown in Fig. 7.4.

$$\Delta G = M_{cal} \Delta V_{cal} \quad (7.1)$$

Where,

M_{cal} can be approximated to the slope of the performance curve in Fig. 7.4 and ΔG is a deviation in the insertion-loss of the embedded RF passive filters from the designed specification at the operating frequency.

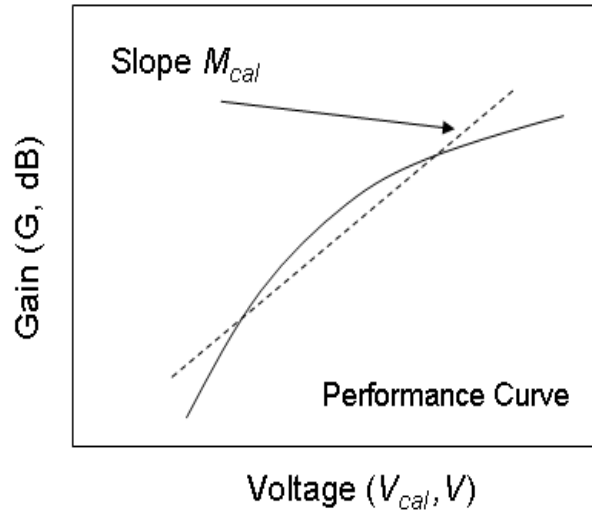


Fig. 7.4. The performance curves of LNA for Gain vs. Voltage at the tuning Knob

For the efficient working of the proposed calibration procedure, the LNA's performance curve should be as linear as possible. Equation (7.1) is a first-order linear approximation of the performance curve of the LNA, but even in the presence of nonlinearities, the linear assumption of Equation (7.1) gives yield improvement as shown in the following sections.

7.2 Simulation Results

To demonstrate the proposed yield improvement methodology, a RF low-pass filter with 3-dB frequency of 1.50 GHz is designed for the topology shown in Fig. 7.5 with $L_a = 8.5$ nH and $C_a = 3$ pF. Although in the literature, the quality factor (Q factor) of more than 50 has been reported for embedded inductors and 80 for embedded capacitors in RF substrates, in this example Q factor of 20 for inductors and 50 for capacitors is used. Let

us assume that this RF filter will be integrated with 1.20 GHz RF receiver which is composed of a RF low-pass filter and an RF amplifier. The RF low-pass filter is embedded in an RF substrate and the RF amplifier is on-chip active circuitry. The maximum allowable insertion loss of the RF low-pass filter at 1.2 GHz is 1.5 dB while system gain of the receiver (ratio of the signal at the input of the RF filter to the output of the RF amplifier) should be in between 12 dB to 10 dB.

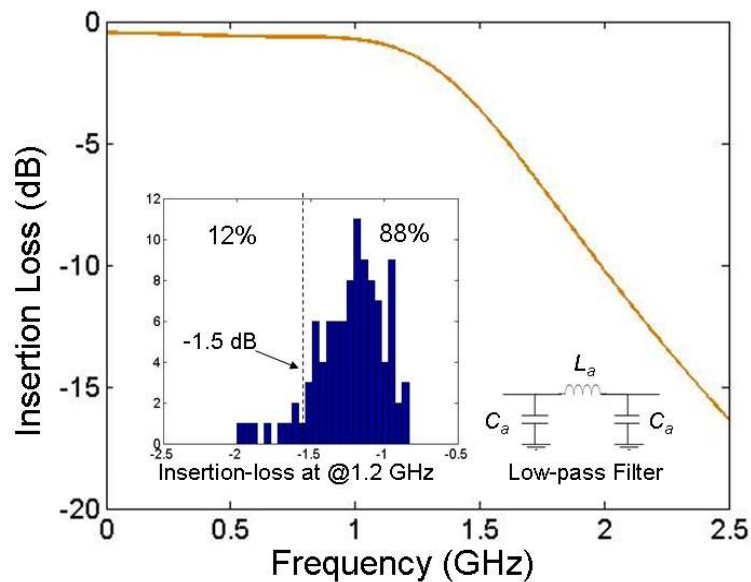


Fig. 7.5. The insertion-loss profile and parametric yield of RF low-pass filter.

For illustration, 100 parametric instances of the RF low-pass filter were generated by randomly perturbing inductor and capacitors using Monte Carlo simulations. In Monte Carlo simulation, Gaussian distribution of 3-sigma = 5.0 % is used and capacitors are varied independently from that of inductor. The Monte Carlo simulation results are shown in Fig. 7.5 and it can be deduced from these results that some of the RF low-pass filters are meeting the specifications of insertion loss at 1.2 GHz while some are not meeting the

specifications. There are 12% such filters which are not meeting the specifications at 1.2 GHz. Thus, the current yield of the RF substrate with embedded filter is 88%.

To demonstrate the increase in the yield of the RF substrates and to meet the RF receiver system requirement, a cascode source degenerated LNA (Fig. 7.6) was designed in CMOS 0.18 μm process. The LNA was designed for the gain of 11.50 dB at 1.2 GHz. This amplifier was not designed for the higher gain because in the practical scenario, the LNA will have process variations and that may cause the system gain to exceed the system specifications. In this LNA, one tuning knob was designed such that its Gain can be varied by changing gate-source voltage (V_{gs}) of the input transistor. The performance curve of the LNA with respect to the tuning knob, V_{gs} , is shown in Fig. 7.7.

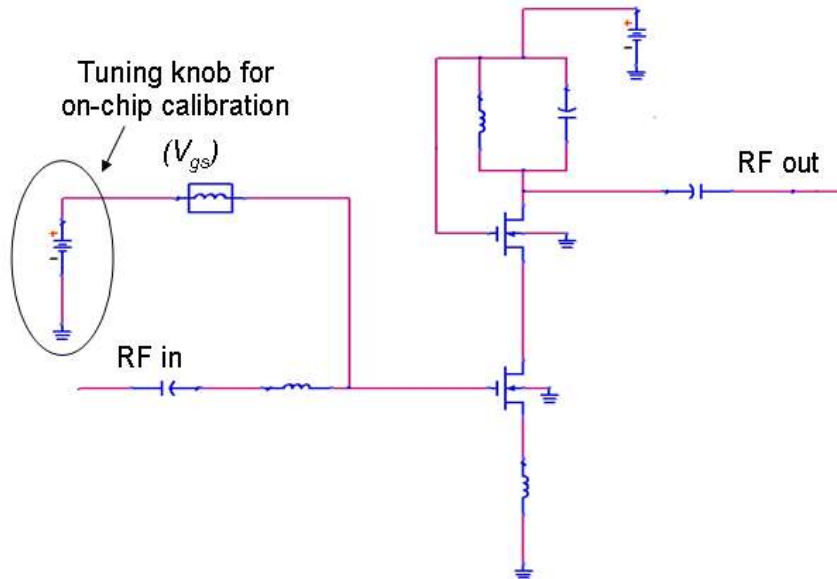


Fig. 7.6. Design of RF amplifier (LNA) with one tuning knob.

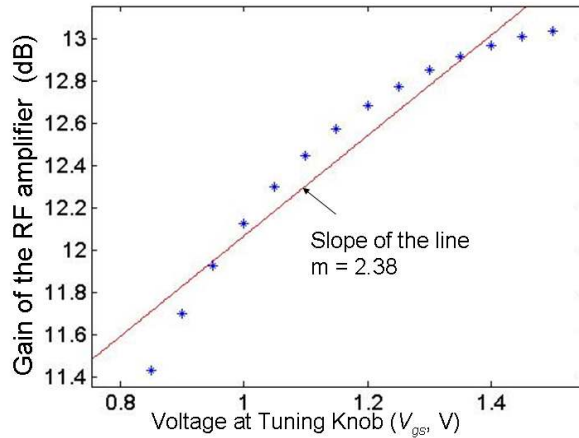


Fig. 7.7. Performance curves of LNA: Variation of Gain as a function of the tuning knob (V_{gs} voltage).

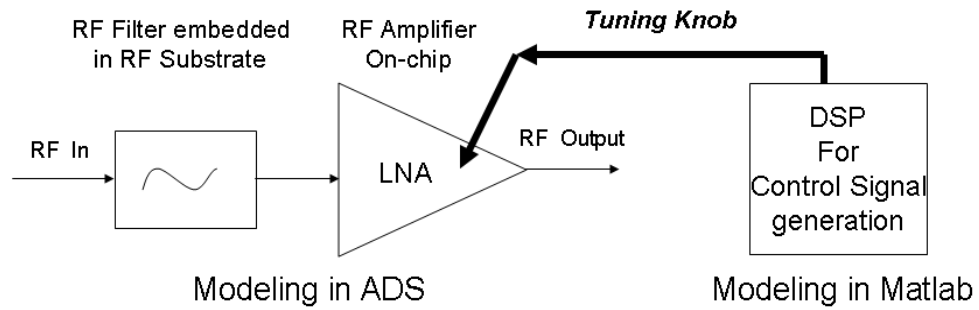


Fig. 7.8. The simulation model of on-chip calibration of RF amplifier (LNA) to increase the yield of RF substrates.

Table 7.1: Summary of Yield of RF substrate with RF Filter

	Before On-Chip Calibration	After On-Chip Calibration
Yield of RF substrates with Embedded RF low-pass filter	88%	98%

To increase the yield of the RF substrates, the calibration of the RF amplifier was performed as explained in the previous section and using the Equation (7.1) along with

performance curve (Fig. 7.7). Matlab and ADS tools were used to model the on-chip calibration of RF amplifier as shown in Fig. 7.8. As a result of this calibration, some of the defective RF filters were assembled with RF amplifier to meet the system requirement of the RF receiver and therefore, the yield of RF substrates increased. The obtained result in the yield improvement is summarized in Table 7.1, which shows that the yield of RF substrates with embedded RF low-pass filter is increased from 88 % to 98 %. For this experiment, V_{gs} of the RF LNA was varied in the range from 0.06 V to 0.22V.

7.3 Measurement Results

As a proof of concept, a hardware prototype of the 1.20 GHz receiver with RF low-pass filter and RF amplifier is shown in Fig. 7.9. Three different samples of RF low-pass filter (3-dB frequency of 1.54 GHz) were assembled using surface-mount capacitors and inductor for the topology shown in the previous section. The insertion loss of these RF low-pass filters is shown in Fig. 7.10. The commercially available RF amplifier (LNA) is used to complete this hardware prototype. For illustration of on-line calibration, a tuning knob that varies the power supply (V_{dd}) of the RF amplifier is used. The performance curve of the LNA (Gain vs V_{dd}) is shown in Fig. 7.11. It is assumed that the allowable performance specification of the system gain (from input of the filter to the output the RF amplifier) @ 1.20 GHz is from 10.25 dB to 11.25 dB and maximum allowable insertion loss of the RF filter is 0.75 dB.

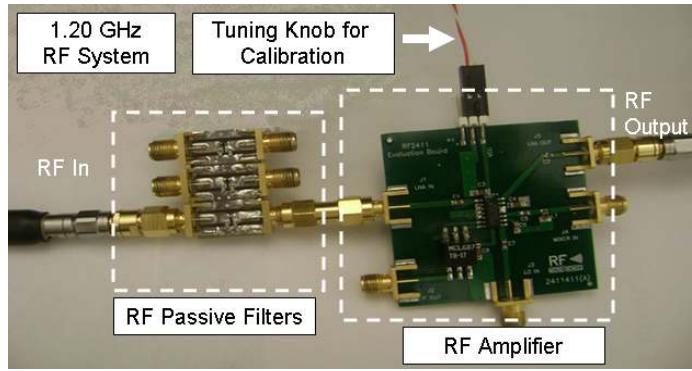


Fig. 7.9. A hardware prototype of the proposed yield improvement methodology.

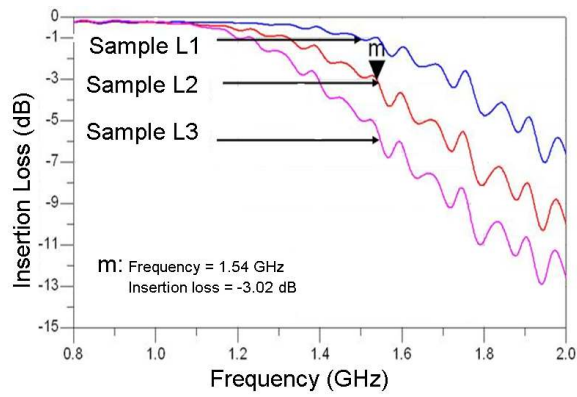


Fig. 7.10. Measured insertion loss of the RF low-pass filters.

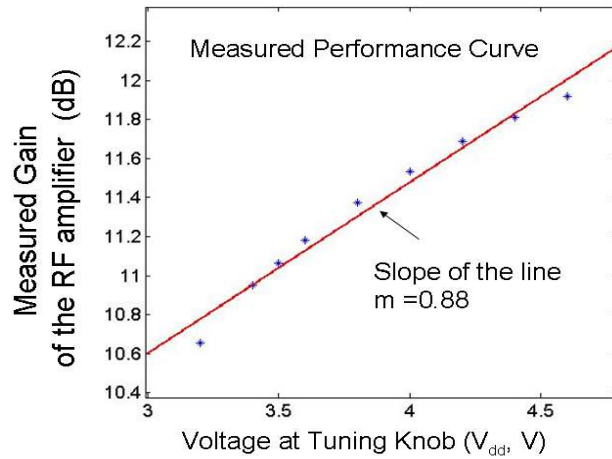


Fig. 7.11. Performance curve: Gain of RF amplifier as a function of the tuning knob (V_{dd}).

Table 7.2 Summary of Measurements @ 1.20 GHz
of RF System

Filter Sample	Insertion Loss of RF Filters (dB)	Before On-Chip Calibration System Gain (dB)	After On-Chip Calibration System Gain (dB)
L1	0.25 (Good)	10.75	No calibration is required
L2	0.59 (Good)	10.57	No calibration is required
L3	0.96 (Defective)	10.16	10.81

It can be inferred from the Table 7.2 that filter Samples L1 and L2 meet the insertion loss specification, but L3 does not meet the insertion loss specification. Also, it can be inferred that the system gain (RF filter with RF LNA) is not within 10.25 to 11.25 dB. But, after the calibration of the RF amplifier, it can be deduced from the Table 7.2 that the system gain with the filter Sample L3 is between 10.25 to 11.25 dB, thus Sample L3 can be used to build this RF system. Therefore, from this experiment, it can be concluded that the proposed methodology can be used to increase the yield of these RF filters.

7.4 Summary

In this chapter, yield improvement methodology has been proposed for RF substrates with embedded RF passive filters. In this methodology, on-chip calibration of the RF active circuitry is performed to increase the yield of off-chip passive embedded RF circuits in the RF substrates. The methodology is demonstrated through simulations and hardware prototype. Based on the obtained results, it can be concluded that it is possible to increase the yield of the RF substrates by this methodology.

(This page is intentionally left blank)

CHAPTER 8

A NOVEL VARIABLE GAIN RF AMPLIFIER FOR SELF-HEALING SYSTEMS

This chapter proposes a novel variable gain RF amplifier (LNA) for building self-healing RF systems. This amplifier can also be used for building multiple antenna systems in which the relative constant phase of the signal has to be maintained. The variable gain capability of the LNA is useful for increasing the yield of RF substrates or RF sub-systems as explained in the previous chapters.

8.1 Proposed design

(This part of the chapter is under review)

Fig.8.1. Schematic of the proposed variable-gain LNA

(This part of the chapter is under review)

Fig.8.2. Small-signal equivalent schematic of the proposed variable-gain LNA.

(This part of the chapter is under review)

8.2 Experimental Results

8.2.1 Simulations Results

For demonstration, 5.9 GHz LNA was designed for the topology shown in Fig. 8.1. This LNA was designed in commercially available SiGe BiCMOS process and all the components, including inductors, were designed on chip. For this experiment, actual models as provided by the foundry were used and extracted post-layout netlist is considered of the layout as shown in Fig. 8. 3. The obtained results are shown in Fig. 8.4 – 8.7. The magnitude of S21 (dB) at 5.92 GHz is shown in Fig. 8.4. The S11 (dB) and S22 (dB) are shown in Fig. 8.5 and 8.6, while phase of S21 (degree) is shown in Fig. 8.7.

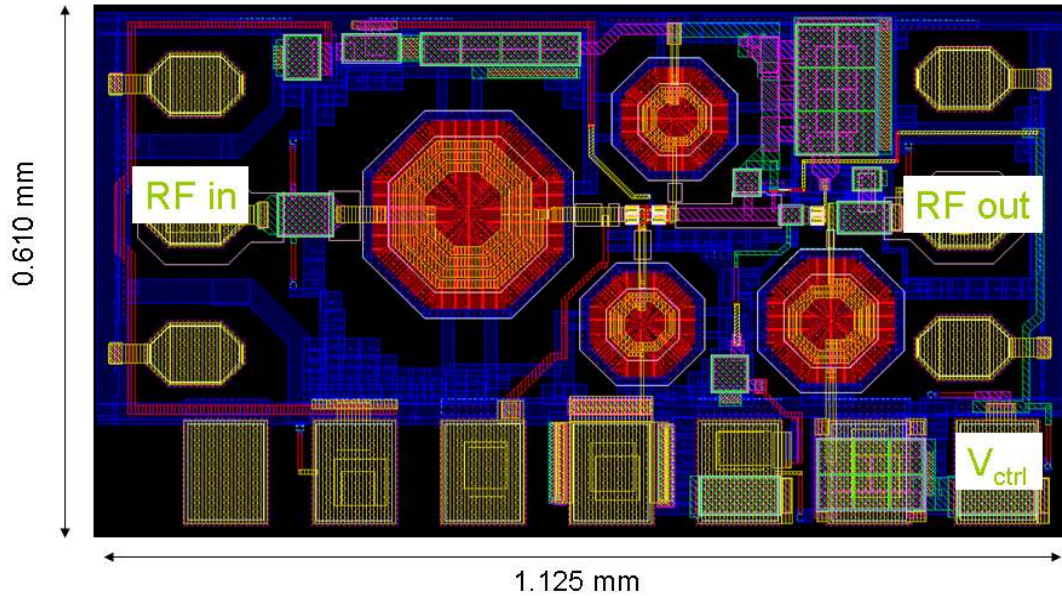


Fig.8.3. Layout of the 5.9 GHz LNA to demonstrate the proposed VGLNA.

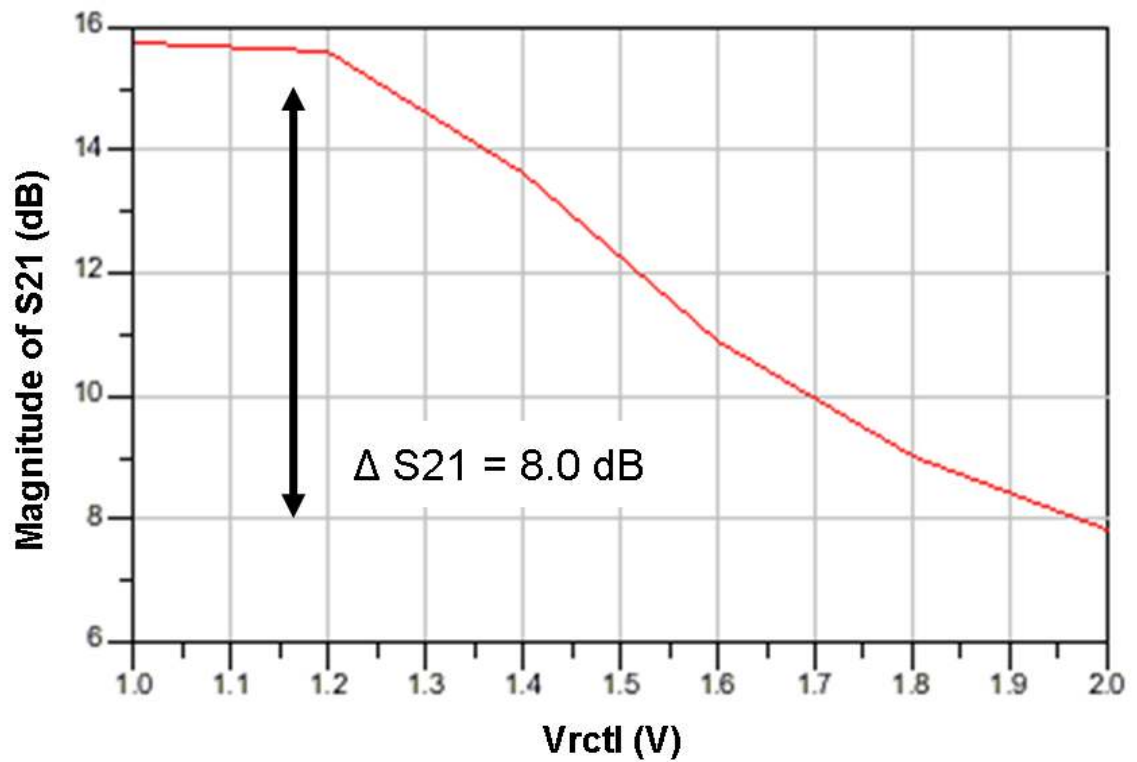


Fig.8.4. Change in Magnitude of S21 at 5.9 GHz for different values of Vctrl

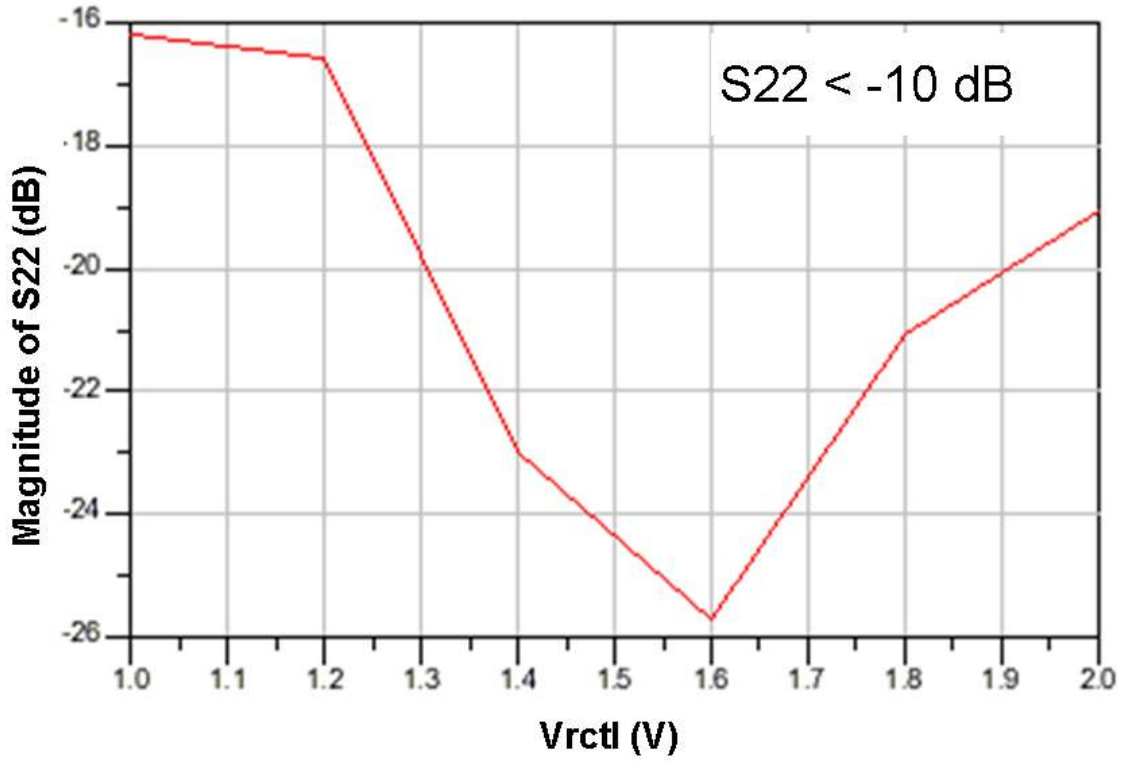


Fig.8.5. Change in Magnitude of S22 at 5.9 GHz for different values of V_{ctrl}

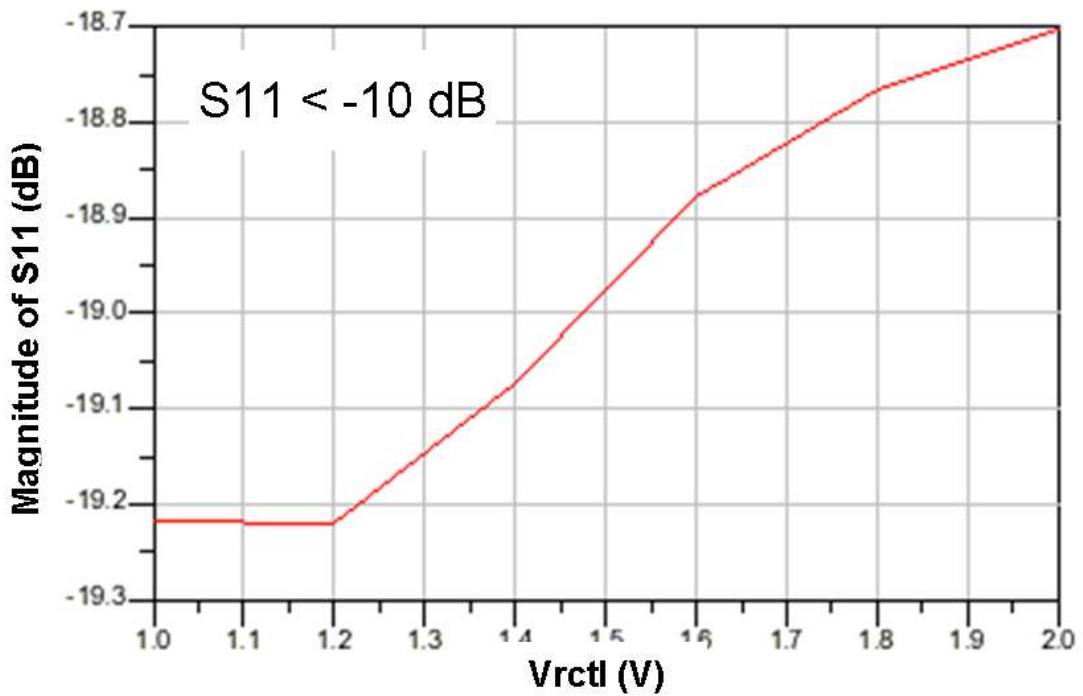


Fig.8.6. Change in Magnitude of S11 at 5.9 GHz for different values of V_{ctrl}

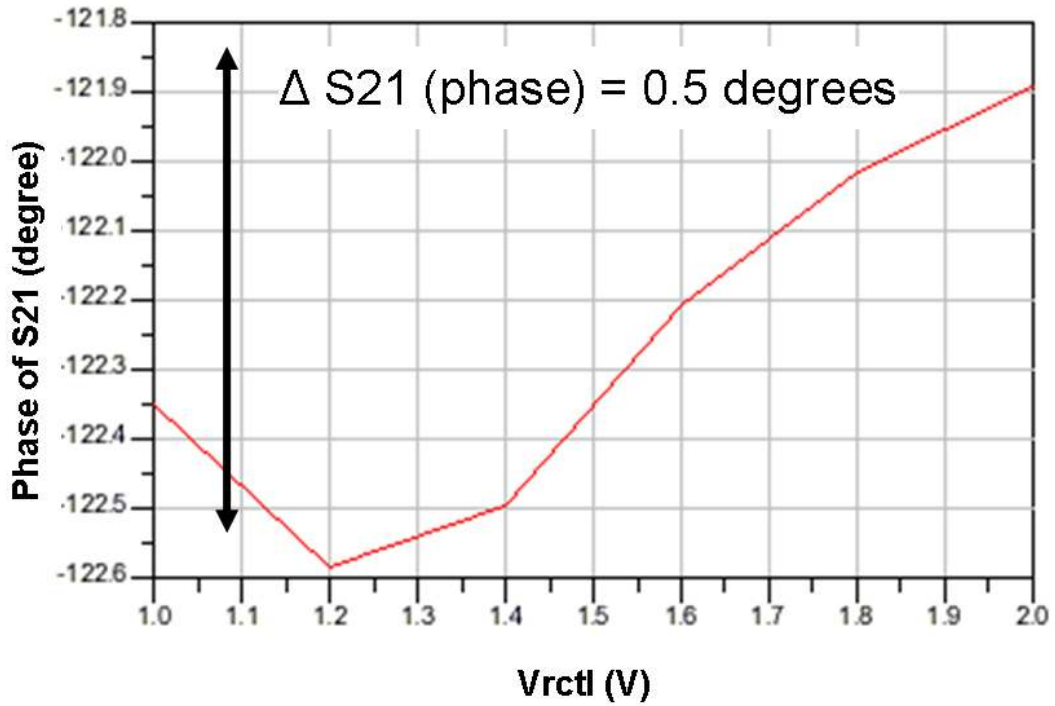


Fig.8.7. Change in phase of S21 at 5.9 GHz for different values of V_{ctrl}

8.2.2 Measurement Results

The fabricated chip prototype (Fig. 8.8) was measured and obtained results are shown in Fig. 8.9 – 8.12. Measurements are little deviated from simulations; the frequency of operation is shifted from 5.9 GHz to 5.2 GHz. But it is important to note that the measured results are quite accurate to show the concept of the proposed VGLNA as a working chip.

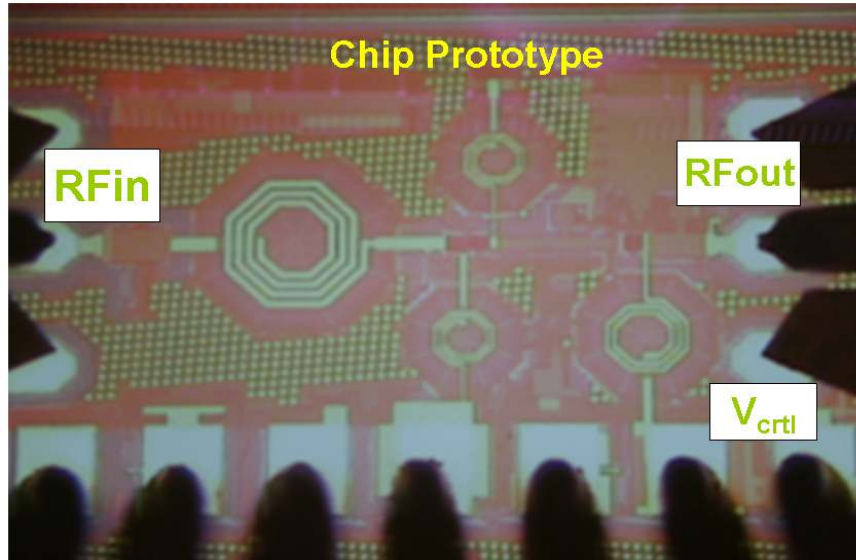


Fig.8.8. Chip prototype to demonstrate the proposed VGLNA.

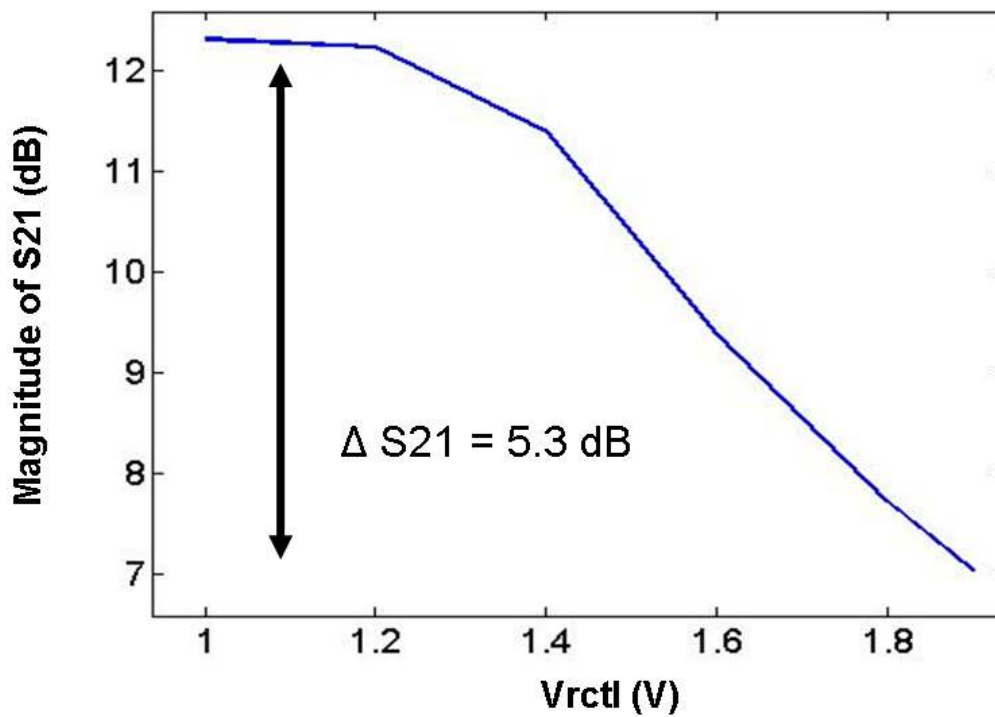


Fig.8.9. Measured change in magnitude of S₂₁ of the VGLNA for different values of V_{ctrl}

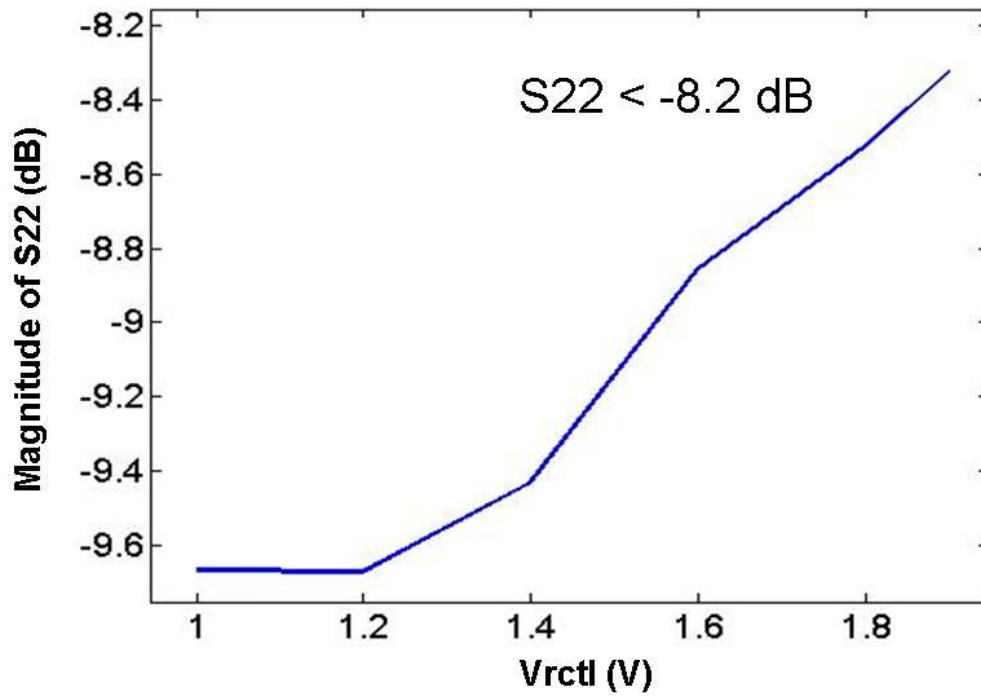


Fig.8.10. Measured change in magnitude of S22 of the VGLNA for different values of V_{ctrl}

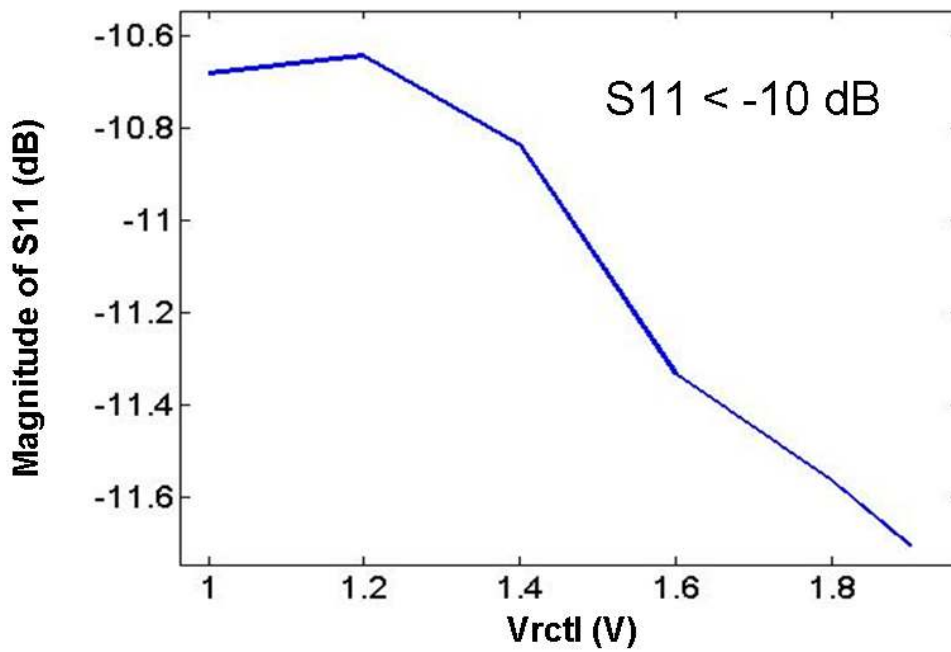


Fig.8.11. Measured change in magnitude of S11 of the VGLNA for different values of V_{ctrl}

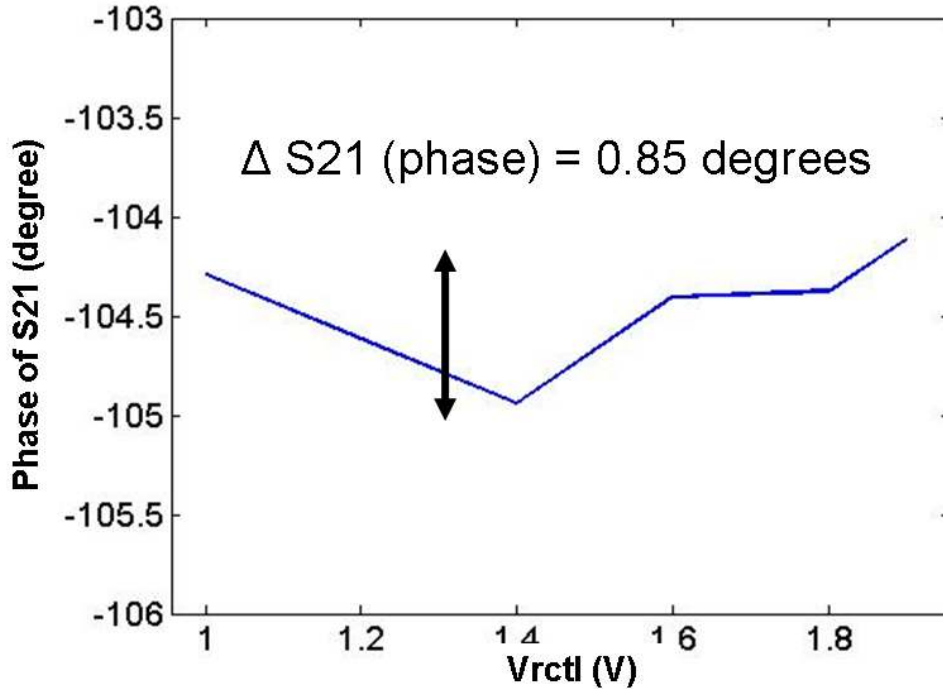


Fig.8.12. Measured change in *phase* of S21 of the VGLNA for different values of V_{ctrl}

Based on the above results it can be concluded that the proposed design of the LNA enables variable-gain capability, but at the same time maintains good input/output matching. In addition, this design also enables gain variation while maintaining relative-constant phase of the signal.

8.3 Summary

A novel variable gain RF amplifier is proposed for developing self-healing RF systems in which the gain of the RF amplifier needs to be changed for healing/correction purposes. The proposed RF amplifier is capable of maintaining relative constant phase of the received signal. Also, this amplifier maintains the good input and output matching of the RF amplifier.

(This page is intentionally left blank)

CHAPTER 9

FUTURE WORK AND PAPERS PUBLISHED

This thesis proposes a multifaceted production test and post-manufacture yield enhancement framework for RF systems. In this thesis, several low-cost test methodologies and self-healing methodologies are developed and demonstrated to reduce the overall manufacturing cost of deep sub-micron RF systems. The test and yield improvement methodologies developed in this thesis can be extended for other RF circuits as well. One such example is RF antenna.

(This part of the chapter is under review)

Fig. 9.1. Self-Healing Antenna Based on Resonance Test Method.

In this thesis, self-healing methodology is proposed and demonstrated using RF LNAs, as a future work, self-healing of RF power amplifiers can also be explored. Also, in this thesis self-healing of RF down-conversion mixers is proposed, the proposed self healing methodology can also be explored for RF Up-conversion mixers.

9.1 Papers Published

The following lists the journal, conference and workshop publications that have resulted from this research

9.1.1 Journal Publications

- 1) **A. Goyal**, M. Swaminathan, A. Chatterjee "Low-Frequency and Low-Cost Test Methodology for Integrated RF Substrates", IEEE Transaction Advanced Packaging, Volume 33, Issue 3, 2010, pp(s) 669-680
- 2) **A. Goyal**, M. Swaminathan, A. Chatterjee, "Low-Cost Specification Based Testing of RF Amplifier Circuits using Oscillation Principles", Journal of Electronic Testing Theory and Applications (JETTA), Volume 26, Issue 1, 2010, pp 13-24

9.1.2 Conference Publications

- 1) **A. Goyal**, M. Swaminathan, " Low-Cost One-port Approach for Testing Integrated RF Substrates," IEEE Proc. Asian Test Symposium, Nov. 2008, pp (s): 49-54 (*nominated for the best paper award*)
- 2) **A. Goyal**, M. Swaminathan; C. Ward; G. White; A. Chatterjee, "A Novel Method for Testing Integrated RF Substrate", Proc. IEEE Asia Pacific Microwave Conference (APMC), Dec 2007, pp (s): 277 – 280
- 3) **A. Goyal**, M. Swaminathan, "A Low-Cost Test Method for Embedded RF Passive Circuits using Two-Tone Input Signals," Proc. IEEE Wireless and Microwave Technology Conference (WAMICON), April 2009, pp (s): 1-4
- 4) **A. Goyal**, M. Swaminathan, "A Low Cost Method for Testing Integrated RF Substrates," Proc. IEEE International Microwave Symposium (IMS), June 2008, pp (s): 378-381

- 5) **A. Goyal**, M. Swaminathan, "A Low Cost Method for Testing Embedded Passive Circuits Based on Oscillation Principles," Proc. IEEE Electrical Design of Advance Packaging and Systems (EDAPS), Dec 2008, pp (s): 194 - 197
- 6) **A. Goyal**, M. Swaminathan, A. Chatterjee , "Low-Frequency Test Method for Integrated RF Substrates", Proc. IEEE Electronic Components and Technology Conference (ECTC), May 2009, pp (s): 489 - 496
- 7) **A. Goyal**, M. Swaminathan; "A Low-Cost Test Approach for Embedded RF Passive Circuits," Proc. IEEE International Mixed-Signals, Sensors, and Systems Test Workshop (IMST3W), June 2008, pp (s): 1 - 5
- 8) **A. Goyal**, M. Swaminathan, A. Chatterjee "A Novel Self-Healing Methodology for RF Amplifier Circuits Based on Oscillation Principles", IEEE Design Automation & Test in Europe (DATE), April 2009. pp(s) : 159 – 165
- 9) **A. Goyal**, M. Swaminathan, A. Chatterjee "Self-calibrating RF Down-Conversion Mixers", IEEE Proc. Asian Test Symposium, Nov. 2009, pp (s): 149-154
- 10) A. Chatterjee,, D. Han, V. Natarajan, S. Devarakond, S. Sen, H. Choi, R. Senguttuvan, S. Bhattacharya, **A. Goyal**, D. Lee, M. Swaminathan, "Iterative Built-in Testing and Tuning of Mixed-Signal/RF Systems", Invited Paper, International Conference on Computer Design, Oct 2009 , pp (s): 319-326
- 11) **A. Goyal**, M. Swaminathan, A. Chatterjee, "RF Substrate yield improvement using package-chip co-design and on-chip calibration ," Proc. IEEE Electrical Design of Advance Packaging and Systems (EDAPS), Dec 2010, pp (s): 1-4

9.1.3 Patents/Invention Disclosures

- 1) **A. Goyal**, M. Swaminathan, "A Low Frequency Low Cost Testing Methodology for Multi-Gigahertz RF Embedded Passive Filters via Inclusion into RF Oscillator Circuits," provisional application filed for GTRC ID 4427, Feb 2008 in the USPTO
- 2) **A. Goyal**, M. Swaminathan, A. Chatterjee, "Low-Cost Testing Methodology for Multi-Gigahertz RF Embedded Passive Filters via Insertion into Feedback Network of Amplifier Circuits," provisional application filed for GTRC ID 4327, Nov 2007 in the USPTO
- 3) **A. Goyal**, M. Swaminathan, "Low-Cost Testing Methodology for Multi-Gigahertz RF Embedded Passive Filters based on Regression Analysis," provisional application filed for GTRC ID 4324, Oct 2007 in the USPTO.

(This page is intentionally left blank)

References

- [1] www.darpa.org (Broad Agency Announcement, DARPA-BAA-08-40, May 19, 2008).
- [2] R. GOERING AND R. WILSON, "Yield, packages hang up design below 100 nm," EE Times, Mar. 31, 2003 [Online]. Available: <http://www.eetimes.com>
- [3] T. NAJIBI, "How designers can increase parametric yield," EE Times, Nov. 21, 2003 [Online]. Available: <http://www.eetimes.com>
- [4] ITRS public document "International Technology Roadmap for Semiconductors - 2007 Edition".
- [5] JOE KELLY, "Advanced production testing of RF, SoC, and SiP devices," Artech House, Boston, 2007.
- [6] M. SLAMANI, "Reducing high-speed/RF test cost - guaranteed by design or guaranteed to fail?," IEEE International Test Conference, Austin, TX, USA, 2006, pp. 1.
- [7] S. OZEV, C. OLGAARD, AND A. ORGILOGLU, "Testability implications in low-cost integrated radio transceivers: a Bluetooth case study," Proc. Int. Test Conference, pp. 965-974, 2001.
- [8] R.R. TUMMALA, M. SWAMINATHAN, "Introduction of System-On-Package (SOP)," McGrawHill, New York, 2008.
- [9] TUMMALA, R.R., "SOP: what is it and why? A new microsystem-integration technology paradigm-Moore's law for system integration of miniaturized convergent systems of the next decade", IEEE Transactions on Advanced Packaging, Volume 27, Issue 2, May 2004 Page(s):241 - 249
- [10] PINEL, S.; LIM, K.; DEJEAN, R. G.; LI, L.; LEE, C-H.; MAENG, M.; DAVIS, M.F.; TENTZERIS, M.; LASKAR, J, "System-on-Package (SOP) Architectures for

- compact and low cost RF Front-end modules”, in IEEE European Microwave Conference, Oct. 2003 pp. (s):307 – 310.
- [11] CHANG-HO LEE; SUTONO, A.; SANGWOO HAN; KYUTAE LIM; PINEL, S.; TENTZERIS, E.M.; LASKAR, J., “A compact LTCC-based Ku-band transmitter module”, IEEE Trans. Advanced Packaging, Volume 25, Issue 3, Aug. 2002 Page(s):374 – 384.
- [12] PARK, Y.H; KIM, H.R; OH, K.J; CHO, Y.H; KIM, B.S, “LTCC quad band GSM RF transceiver using integrated passive matching network”, IEEE Proc. The European Conference on Wireless Technology, Oct 3-4, 2005, pp 407-410.
- [13] J. B. BROCKMAN and S. W. DIRECTOR, “Predictive subset testing: optimization IC parametric performance testing for quality, cost, and yield,” IEEE Trans. Semi. Manufacturing, vol. 2, no. 3, pp. 104-113, Aug. 1989.
- [14] L. MILOR and A. L. S. VINCENNELLI, “Minimizing production test time to defect faults in analog circuits,” IEEE Trans. on Computer-Aided Design of Integrated Circuits and Systems, vol. 13, pp. 796-813, June 1994.
- [15] “IEEE standard test access port and boundary-scan architecture”, IEEE Std 1149.1-2001.
- [16] “IEEE standard for a mixed-signal test bus”, IEEE Std 1149.4-1999.
- [17] S. SUNTER, "The P1149.4 Mixed Signal Test Bus: costs and benefits," IEEE Proceedings International Test Conference, Oct. 1995 Page(s):444 – 450.
- [18] K. ARABI, "Mixed-signal BIST: fact or fiction", IEEE Proceedings International Test Conference, Oct. 2002 Page(s):1200.
- [19] B. DUFORT and G. W. ROBERTS, “On-chip analog signal generation for mixed-signal built-in self-test,” IEEE Trans. Solid-State Circuits, vol. 34, pp. 318–330, Mar. 1999.

- [20] M. MENDEZ-RIVERA, J. SILVA-MARTINEZ, E. SÁNCHEZ-SINENCIO, “On-chip spectrum analyzer for built-in testing analog ICs,” Proceedings of International Symposium. on Circuits and Systems., 2002, vol. 5 , pp. 61-64.
- [21] A. HAJJAR and G. W. ROBERTS, “A high speed and area efficient on-chip analog waveform extractor”, Proc. Int’l Test Conf., 1998, pp. 688–697.
- [22] M. BURNS and G. W. ROBERTS, An Introduction to Mixed-Signal IC Test and Measurement. Oxford, U.K.: Oxford Univ. Press, 2001.
- [23] YEN-CHIH HUANG; HSIEH-HUNG HSIEH; LIANG-HUNG LU, “A Low-Noise Amplifier with Integrated Current and Power Sensors for RF BIST Applications,” IEEE Proc.VLSI Test Symposium, May 2007 Page(s):401 – 408.
- [24] J. S. DAVIS, D. C.KEEZER, O. LIBOIRON-LADOUCEUR, AND K. BERGMAN, “Application and demonstration of a digital test core: Optoelectronic test bed and wafer-level prober,” IEEE Proceedings International Test Conference, 2003, pp. 166–174.
- [25] D. C. KEEZER, D. MINIER, AND M. C. CARON, “A production-oriented multiplexing system for testing above 2.5 Gbps,” IEEE Proceedings International Test Conference, 2003, pp. 191–200.
- [26] P. VARIYAM, S. CHERUBAL, AND A. CHATTERJEE, “Prediction of analog performance parameters using fast transient testing,” IEEE Trans. Computer- Aided Design, vol. 21, pp. 349–361, 1992.
- [27] P. VARIYAM AND A. CHATTERJEE, “Enhancing test effectiveness for analog circuits using synthesized measurements,” in Proc. VLSI Test Symp., Apr. 1998, pp. 132–137.
- [28] P. VARIYAM AND A. CHATTERJEE, “Specification driven test generation for analog circuits,” IEEE Trans. Computer-Aided Design, vol. 19, pp. 1189–1201, Oct. 2000.

- [29] P. VARIYAM AND A. CHATTERJEE, "Test generation for comprehensive testing of linear analog circuits using transient response sampling," in Proc. Int. Conf. Computer-Aided Design, Nov. 1997, pp. 382–385.
- [30] R. VOORAKARANAM AND A. CHATTERJEE, "Test generation for accurate prediction of analog specifications," in Proc. VLSI Test Symp., Apr. 2000, pp. 137–142.
- [31] J. H. FRIEDMAN, "Multivariate adaptive regression splines," The Annals of Statistics, vol. 19, no. 1, pp. 1–141, 1991.
- [32] R. VOORAKARANAM, S. CHERUBAL, AND A. CHATTERJEE, "A signature test framework for rapid production testing of RF circuits," in Proc. Design Automation and Test in Europe, Mar. 2002.
- [33] G. SRINIVASAN, S. BHATTACHARYA, S. CHERUBAL AND A. CHATTERJEE, "Efficient Test Strategy for TMDA Power Amplifiers Using Transient Current Measurements: Uses and Benefits," Proc. Design Automation and Test in Europe, 2004.
- [34] S. S. AKBAY AND A. CHATTERJEE, "Feature extraction based built-in alternate test of RF components using a noise reference," in Proc. VTS, Apr. 2004, pp. 273–278.
- [35] AKBAY, S.S.; HALDER, A.; CHATTERJEE, A.; KEEZER, D.;"Low-cost test of embedded RF/analog/mixed-signal circuits in SOPs", IEEE Transactions on Advanced Packaging, Volume 27, Issue 2, May 2004 Page(s):352 – 363.
- [36] S.BHATTACHARYA AND A.CHATTERJEE, "Use of Embedded Sensors for Built-In-Test of RF Circuits", Intl. Test Conference, Charlotte, NC, October 2004, pp. 801-809.
- [37] D.HAN, S. AKBAY, S.BHATTACHARYA, AND A. CHATTERJEE, "Robust built-in alternate test of RF ICs using envelope," International Mixed-Signal Test Workshop, June 2005.

- [38] SENGUTTUVAN, R., BHATTACHARYA, S., CHATTERJEE, A., "Test Method for Measuring Bit Error Rate of Pulsed Transceivers in the Presence of Narrow-band Interferers", IEEE Transactions on Microwave Theory and Techniques , Vol 55, Issue 9, Sep 2007, pp 1942-1950.
- [39] C. ZHANG, R. GHARPUREY, J. ABRAHAM., "Built-In Test of RF Mixers Using RF Amplitude Detectors", IEEE Proc. International Symposium on Quality Electronic Design, 2007, pp 273-278.
- [40] ARABI, K.; KAMINSKA, B., "Oscillation-test methodology for low-cost testing of active analog filters", IEEE Transactions on Instrumentation and Measurement, Volume 48, Issue 4, Aug. 1999 Page(s):798 – 806.
- [41] HUERTAS, G.; VAZQUEZ, D.; RUEDA, A.; HUERTAS, J.L.; "Practical oscillation-based test in analog integrated filters: experimental results," IEEE International Workshop on Test and Applications, 2002.
- [42] R.W. RHEA, Oscillator Design and Computer Simulation, New Jersey: Prentice Hall, 1990.
- [43] RAGHUNATHAN, A.; HONG JOONG SHIN; ABRAHAM, J.A., "Prediction of analog performance parameters using oscillation based test" Proceedings. 22nd IEEE VLSI Test Symposium (VTS), April 2004 Page(s):377 – 382.
- [44] ARABI, K.; KAMINSKA, B., "Design for testability of embedded integrated operational amplifiers", IEEE Journal of Solid-State Circuits, Volume 33, Issue 4, April 1998 Page(s):573 – 581.
- [45] HUERTAS, G.; HUERTAS, J.L., "Oscillation-Based Test in Data Converters: On-Line Monitoring", 4th IEEE International Symposium on Electronic Design, Test and Applications (DELTA), Jan. 2008 Page(s):322 – 325.
- [46] SUENAGA, K.; ISERN, E.; PICOS, R.; BOTA, S.; ROCA, M.; GARCIA-MORENO, E., "Predictive Oscillation Based Test of CMOS circuits" Proceedings.

- 6th IEEE International Caribbean Conference on Devices, Circuits and Systems, April 2006 Page(s):55 – 60.
- [47] SUENAGA, K.; ISERN, E.; PICOS, R.; BOTA, S.; ROCA, M.; GARCIA-MORENO, E., "Application of Predictive Oscillation-Based Test to a CMOS OpAmp", IEEE Transactions on Instrumentation and Measurement, Volume: 59 , Issue: 8, pp(s): 2076 – 2082, August 2010.
- [48] ARABI, K.; IHS, H.; DUFAZA, C.; KAMINSKA, B., "Dynamic digital integrated circuit testing using oscillation-test method", Electronics Letters Volume 34, Issue 8, April 1998 Page(s):762 – 764.
- [49] J. LI, J. YEH, R. HUANG, AND C. WU, "A built-in self-repair design for RAMs with 2-D redundancy," IEEE Trans. VLSI Systems, vol. 13, no. 6, pp. 742-745, June 2005.
- [50] T. CHEN AND G. SUNADA, "Design of a self-testing and self-repairing structure for highly hierarchical ultra-large capacity memory chips," IEEE Trans. VLSI Systems, vol. 1, no. 2, pp. 88-97, June 1993.
- [51] J. FATTARUSO, S. KIRIAKI, M. WIT, AND G. WARWAR, "Self-calibration techniques for a second-order multibit sigma-delta modulator," IEEE Journal of Solid-State Circuits, vol. 28. no. 12, pp. 1216-1223, 1993.
- [52] K. HAGARAJ, "Area-efficient self-calibration techniques for pipe-lined algorithmic A/D converters," IEEE Trans. Circuits and Systems-II: Analog and Digital Processing, vol. 43, no. 7, pp.540-544, 1996.
- [53] S. BANDI AND P. R. MUKUND, "A compensation technique for transistor mismatch in current mirrors," In Proc. System-On-Chip Conf., 2003, pp. 320-323.
- [54] W. WOO, M. MILLER, AND J. KENNEY, "A hybrid digital/RF envelope predistortion linearization system for power amplifiers," IEEE Trans. on Microwave Theory and Techniques, vol. 53, no. 1, pp. 229-237, 2005.

- [55] J.K. CAVERS AND M.W. LIAO, "Adaptive compensation for imbalance and offset losses in direct conversion transceivers," IEEE Trans. Vehicular Technology, vol. 42, no. 4, pp. 581-588, Nov. 1993.
- [56] M. ELMALA AND S. EMBABI, "A self-calibration technique for mismatches in image-reject receivers," In . IEEE Proc. Custom Int. Circuits Conf., 2002, pp. 251-254.
- [57] M. FAULKNER, T. MATTSON, and W. YATES, "Automatic adjustment of quadrature modulators," Electronic Letter, vol. 27, no. 3, pp. 214-216, 1991.
- [58] SENGUTTUVAN R., CHATTERJEE, A., "Alternate Diagnostic Testing and Compensation of Transmitter Performance using Response Detection", Proceedings of 25th IEEE VLSI Test Symposium, Berkeley, California, May 2007, pp. 395-400.
- [59] T. DAS, A. GOPALAN, C. WASHBURN, AND P.R. MUKUND, "Self-calibration of input-match in RF front-end circuitry," IEEE Trans. Circuits and Systems, vol. 52, no. 12, pp. 821-825, Dec. 2005.
- [60] D. HAN, B. S. KIM, A. CHATTERJEE, "DSP Driven Self-Tuning of RF Circuits for Process-Induced Performance Variability ", Transactions on Very Large Scale Integration (VLSI) Systems. pp (accepted).
- [61] JAYARAMAN, K.; KHAN, Q.; CHI, B; BEATTIE, W.; WANG. Z; CHIANG, P.; "A self-healing 2.4GHz LNA with on-chip S11/S21 measurement/calibration for in-situ PVT compensation", in Proc. IEEE Radio Frequency Integrated Circuits Symposium (RFIC), May 2010 , pp (s): 311 – 314.
- [62] MARSHALL, J.; CHONG, F.C.; MODLIN, D.; WESTBROOK, S.; "CAD-Based Net Capacitance Testing of Unpopulated MCM Substrate," IEEE Trans, on Components, packaging, and manufacturing technology -part B: Advanced Packaging, Vol. 17, No. 1, February 1994.

- [63] ECONOMIKOS, L.; MORRISON, T.; CRNIC, F., "Electrical test of multichip substrates" IEEE Trans, on Components, packaging, and manufacturing technology - part B: Advanced Packaging, Vol. 17, No. 1, February 1994.
- [64] M. BRUNNER, R. SCHMID, R. SCHMITT, M. STURN, and O. GESSNER, "Electron-beam MCM testing and probing," IEEE Transactions on Components, Packaging, and Manufacturing Technology, Feb. 1994. Volume 17, Page(s). 62–68.
- [65] HALPERIN, A.; DISTEFANO, T.H.; SHINWU CHIANG;, "Latent open testing of electronic packaging", IEEE Proceedings Multi-Chip Module Conference, March 1994 Page(s):83 – 88.
- [66] B. KIM, M. SWAMINATHAN, A. CHATTERJEE, D. SCHIMMEL, "A Novel Test Technique for MCM Substrates", IEEE Transactions on Components, Packaging, and Manufacturing Technology, 1997, Volume 20, Issue 1, Feb. 1997 Page(s):2 – 12.
- [67] HEEBYUNG YOON; JUNWEI HOU; CHATTERJEE, A.; SWAMINATHAN, M., "Fault detection and automated fault diagnosis for embedded integrated electrical passives", Proc. IEEE International Conference on Computer Design (ICCD), Oct. 1998, pp. 588 – 593.
- [68] ROBERT G, ROGER, "Low Phase Noise Microwave Oscillator Design," Artech House, 1991.
- [69] B. RAZAVI, "RF Microelectronics," Prentice Hall PTR, NJ, 1998.
- [70] D. M. POZAR, "Microwave Engineering," McGraw Hill, Second Edition 2002.
- [71] <http://www.agilent.com>, date August 21, 2008.
- [72] <http://cascademicrotech.com>, date May 21, 2008.
- [73] <http://www.nova-eng.com>, date August 21, 2008.
- [74] STRATIGOPOULOS, H.-G.D.; MAKRIS, Y., "Nonlinear Decision Boundaries for Testing Analog Circuits," IEEE Trans. Computer-Aided Design, Volume 24, Issue 11, Nov 2005, pp. 1760-1773.

- [75] C. ZHANG; R. GHARPUREY; J. A. ABRAHAM," Low Cost RF Receiver Parameter Measurement with On-Chip Amplitude Detectors" IEEE VLSI Test Symposim (VTS) 2008, pp: 203 – 208, April 2008.
- [76] GOYAL, A; SWAMINATHAN, M; CHATTERJEE, A, "Low-Cost pecification Based Testing of RF Amplifier Circuits using Oscillation Principles", Journal of Electronic Testing Theory and Applications (JETTA), Volume 26, Issue 1, pp 13-24, Feb 2010
- [77] S. ELLOUZ, P. GAMAND, C. KELMA, B. VANDEWIELLE, B. ALLARD, "Combining Internal Probing with Artificial Neural Networks for Optimal RFIC Testing", in Proc. IEEE International Test Conference, Oct. 2006. pp :1 – 9.
- [78] M. L. EDWARDS and J. H. SINSKY, "A new criterion for linear 2-port stability using geometrically derived parameters", IEEE Transactions on Microwave Theory and Techniques, Vol. 40, No. 12, pp. 2303-2311, Dec.1992.
- [79] HAIDER, A.; BHATTACHARYA, S.; CHATTERJEE, A., "Automatic multitone alternate test-generaton for rf circuits using behavioral models" IEEE Proceedings International Test Conference, 2003. ITC 2003.
- [80] R. MUKHOPADHYAY, Y. PARK, S.W. YOON, C.-H. LEE, S. NUTTINCK, J.D.CRESSLER, and J. LASKAR, "Active-Inductor-based Low-Power Broadband Harmonic VCO in SiGe Technology for Wideband and Multi-Standard Applications, Technical Digest of the 2005 IEEE MTT-S International Microwave Symposium, pp. 580-583, 2005.
- [81] PAPPU, A.M.; XUAN ZHANG; HARRISON, A.V.; APSEL, A.B.;"Process-Invariant Current Source Design: Methodology and Examples",IEEE Journal of Solid-State Circuits,Volume 42, Issue 10, pp (s):2293 - 2302 Oct. 2007